UNIVERSITÀ
DEGLI STUDI
DI PADOVA

Università degli Studi di Padova

Dipartimento di Ingegneria Civile, Edile e Ambientale

Corso di Laurea Magistrale in Ingegneria Civile

Behaviour of an MBT waste in monotonic triaxial shear test

Relatore

Prof. Paolo Carrubba

Correlatore

Prof William Powrie

Laureanda

Alessandra Bortoluzzi

N° matricola 1039711

Anno Accademico 2013 / 2014

Alla mia famiglia,

Contents

Index of Tables

Index of Figures

Chapter 1

Introduction

One of the most discussed issue of our society is certainly the management of the solid waste, whose amount increases each year and it is strictly connected with the wealth growth of a country. Every year the European Union produces 3 billion of tonnes of waste; which means about 6 tonnes of solid waste for every man, woman and child, according with the Eurostat statistics. The two most used management method are the incineration and the disposal in landfill. This latter solution is widely the most used not only in Italy but also in the whole EU, although the percentage of recycled MSW is now increasing thanks to modern targets set by EU Landfill Directive (EC, 1999).

The landfilling option implies many environmental problems, like the underground water contamination by leachate and the release into the air of methane. In order to reduce the polluting potential of MSW, the EU Landfill Directive obliges the Member State to reduce the amount of biodegradable waste they landfill to 35% of 1995 levels by 2016. Many European countries (Germany, Austria, United Kingdom, and Italy) have chosen mechanical-biological pre-treatment (MBT) as a technology for treating MSW in order toto arrive at the targets set out. MBT normally involves sorting to remove recyclable materials, particle size reduction and partial biodegradation by anaerobic digestion and/or aerobic composting processes. A large number of new waste treatment facilities have been commissioned over recent years and the role of MBT in waste management is expected to become more popular in the short term.

The mechanical-biological treatment induces huge changes in MSW matrix structure and fibrous content and, consequently, in his mechanical behaviour. The removal of sheet, stick and string-like reinforcement induced by this treatment has produced a new concern regarding a potential loss of strength compared with untreated waste. In addition, the gradual increase in mobilized strength over strains commonly associated with unprocessed municipal solid waste may not occur with treated wastes because of its completely different structure. The importance of studying this new type of waste is

became prior in order to design safe landfills, reducing the risk of waste slope instabilities and landslides. The heterogeneous nature of waste and, in particular, its changing composition are the main problem source regarding the determination of its strength parameters. One of the aspect more difficult to study is the waste behaviour in fully saturated conditions; this is due to the difficulty of preventing anaerobic gas production within the specimens over the considerable length of time needed to carry out the shear tests, used to determine its strength parameters.

1.1 Aims and objectives

In this research, consolidated drained triaxial tests were carried out in fully saturated condition in order to investigate MBT waste behaviour. A digital image analysis technique is also used to describe the locally strain fields and to localize potential failure surface. The specimens were prior consolidated under a vertical stress of 1000 kPa using a modified oedometric equipment. The data are compared with an MBT study (Bhandari, 2012) previously carried out at the University of Southampton using partly saturated samples.

The main aims of this research are to:

- Identify stress-strain-strength characteristics of treated 0-10 mm New Earth Solutions (NES) MBT using triaxial equipment;
- Identify the impact of fully saturated condition on the shear strength of the MBT;
- Investigate the potential for localized failure surfaces to develop.

The objectives of this research are to understand:

- The changes in the mechanical strength of the MBT waste, as a result of MBT process;
- The influence of field conditions (moisture content) on the mechanical behaviour of the MBT waste;
- The impact of radial stress on the shear strength and on the strain field shown by the MBT waste samples.

1.2 Organisation of thesis

This thesis consists of seven chapters, as follows:

1. Chapter 1 summarises the context and the methodology, and defines the aim and objectives of this research work.
2. Chapter 2 presents the EU Landfill directive and its impact on the modern waste management in Europe.
3. Chapter 3 presents the background of this research in detail.
4. Chapter 4 presents a new image-based surface deformation measurement system for triaxial samples for the detailed monitoring of cylindrical triaxial samples to understand the local phenomena.
5. Chapter 5 presents the characterisation of the MBT waste used in this research and the methodology including description of the equipment and sample preparation method.
6. Chapter 6 examines the strength and deformation characteristics of MBT specimen in triaxial compression at effective cell pressure of 25 and 200 kPa.
7. Chapter 7 presents the conclusion achieved from this study.

Chapter 2

Regulation

The EU landfill directive (EC, 1999) represented a big step for the EU waste policy. It marked a decisive shift from landfill towards the EU's new waste hierarchy, which prioritises waste prevention, followed by re-use, recycling and recovery, trying to avoid landfilling wherever possible (Figure 1).

Figure 1 Waste hierarchy

This choice was made in order to control of the growing problem of landfill's environmental impact; in fact, the notably emissions of methane and other gases, the pollution of groundwater, surface water and soil were no longer acceptable and the need of a common EU policy was clearly evident. On that basis, the Landfill Directive set the targets for progressively reducing the amount of biodegradable municipal waste (BMW) landfilled in the period to 2016. According with this Directive the Member State must reduce the amount of BMW going to landfill:

- To 75% of the total amount of biodegradable municipal waste generated in 1995 by 2006;
- To 50% of 1995 levels by 2009;
- To 35% of 1995 levels by 2016.

Landfilling municipal waste has been the predominant option in the EU zone for several years but this is changing. In 1995, 62% of municipal waste was landfilled on average and in 2007, it had fallen to 42%. Nevertheless, landfilling has been and will continue to play a significant role in the waste management in the EU (Figure 2).

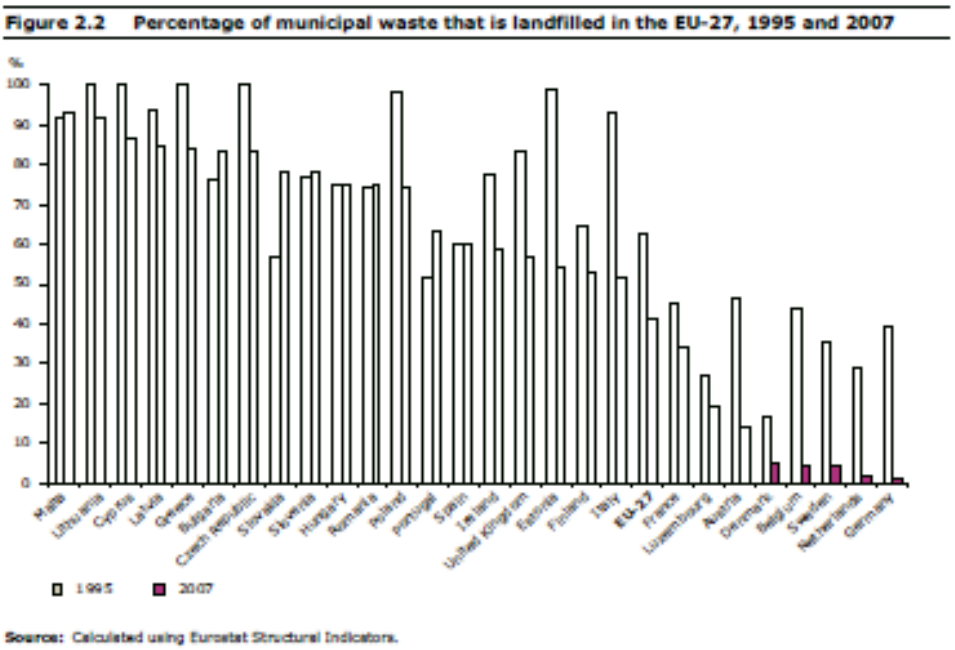

Figure 2 Percentage of municipal waste that it is landfilled in the EU. 1995 and 2007

For that reason, there are requirements to be fulfilled in order to improve the design and management of existing landfill sites and reduce their negative environmental impact. The knowledge of the processes occurring within the landfill and the mechanism controlling them is needed to achieve these objectives. The respect of the EU directive has induced the use of new waste treatment options in order to reduce the environmental impact of waste landfilled. The strategies usually used include a combination of recycling, incineration and mechanical biological treatment.

Incineration capacity has increased significantly, as governments have tightened emissions standard, although the rate of growth has varied widely in European countries. In Germany and in the Flemish region of Belgium, dedicated incineration capacity now accounts for around 35% of municipal waste generated. In other areas, however, several factors have slowed the shift to incineration. These include public opposition, largely based on worries about the environmental and health impact of emissions and difficulties integrating waste incineration into

existing power and heating system (Finland). For these reasons, incineration capacity stands at around 15% of municipal waste in Italy and less than 10% in Finland and Hungary.

Separate collection of biodegradable municipal waste fractions (mainly paper and cardboard, packing waste, and food and garden waste) in increasingly used to divert biodegradable waste from landfill. Obviously, there are considerable variation in the amounts of waste collected separately in the EU region.

Since 1999, capacity at composting and anaerobic digestion plants has increased mainfold in Finland, Germany, Hungary and Italy. Germany has the largest composting capacity per capita, followed by Italy, Finland and the Flemish region; capacity in Hungary and Estonia is considerable lower. Separate collection schemes have struggled to keep up with the increased processing capacity.

The mechanical-biological treatment is usually used to reduce the volume and the organic content and it is considered as an alternative option to incineration to treat mixed municipal waste in Estonia, the Flemish Region, United Kingdom, Germany and Italy. Mechanical-biological treatment is a pre-treatment method, whereby mixed household waste is mechanically separated into a high caloric refuse-derived fuel product and a residue, which is first digested or composted and then sent for landfilling or to dedicated incinerators. In fact, the quality of biologically treated waste fraction is usually poor and therefore it is landfilled or, rarely, used as low quality compost. Capacity for mechanical-biological treatment has doubled or tripled in some countries, with Italy having by far the largest treatment capacity at 240 kilograms per capita (EEA Report, 2009). Obviously, these processes imply the creation of a new kind of waste with completely different characteristics from the MSW produced in the past.

2.1 Mechanical Biological Treatment of Municipal Solid Waste (MBT)

MBT is a generic term for an integration of several processes commonly found in other waste management technologies such as Materials Recovery Facilities (MRFs), sorting and composting or anaerobic digestion plant. MBT compliments, but does not replaced other waste management technologies such as recycling and

composting, respecting the waste management hierarchy introduced by the EU Landfill Directive. The typical aims of MBT plants include the:

- Pre-treatment of waste going to landfill;
- Diversion of non-biodegradable and biodegradable MSW going to landfill through the mechanical sorting of MSW into materials for recycling and/or energy as refuse derived fuel (RDF);
- Diversion of biodegradable MSW going to the landfill by:
    - Reducing the dry mass of Biodegradable Municipal Waste (BMW) prior to landfill;
    - Reducing the biodegradability of BMW prior to landfill;
- Stabilisation into a compost-like output for use on land;
- Conversion into a combustible biogas for energy recover; and/or
- Drying materials to produce a high calorific organic rich fraction for use as RDF.

2.2 Waste Preparation

Residual waste requires preparation before biological treatment or sorting of materials can be achieved. Initial waste preparation may take the form of a simple removal of contrary subject, such as mattresses, carpets or other bulky wastes, which could cause problems with processing equipment down-stream. Further mechanical waste preparation techniques may be used which aim to prepare the materials to subsequent stages. The objective of these techniques is to split open refuse bags; thereby liberating materials inside; and to shred and homogenise the waste into smaller particle sizes suitable for a variety of separation processes, or subsequent biological treatment depending on MBT process employed.

A summary of different techniques used for waste preparation is provided in Table 1.

Technique	Principle	Key Concerns
Hammer Mill	Material significantly reduced in size by swinging steel hammers.	Wear on hammers, pulverising and loss of glass/aggregates, exclusion of pressurised containers.

Shredder	Rotating knives or hooks rotate at slow speed with high torque. The shearing action tears or cuts most materials.	Large, strong object can be physically damage, exclusion of pressurised containers.
Rotating Drum	Materials is lifted up the sides of a rotating drum and then dropped back into the centre. Uses gravity to tumble, mix and homogenise the wastes. Dense, abrasive items such as glass or metal will help break down softer materials, resulting in considerable size reduction of paper and other biodegradable materials.	Gentle action
Ball Mill	Rotating drum using heavy balls to break up and to pulverise the waste.	Wear on balls, pulverising and loss of glass/aggregates
Wet rotating drum with knives	Waste is wetted, forming heavy lumps, which break against the knives when tumbled in the drum.	Relatively low size reduction. Potential for damage from large contraries.
Bag Splitter	A gentler shredder used to split plastic bags whilst leaving the majority of waste intact.	Not size reduction may be damaged by large strong objects.

Table 1 Waste preparation technique

2.3 Waste Separation

A common aspect of many MBT plant used for MSW management is the sorting of mixed waste into different fractions using mechanical means. The sorting of material may be achieved before or after biological treatment. No sorting is required if the objective of the MBT process is to pre-treat all the residual MSW to produce a stabilised output for disposal to landfill.

Sorting the waste allows an MBT process to separate different materials, which are suitable for different end uses. Potential end uses include material recycling, biological treatment, energy recovery through the production of RDF, and landfill. A variety of different techniques can be employed, and most MBT facilities use a

series of several different techniques in combination to achieve specific end use requirements for different materials.

Separation technologies exploit varying properties of the different materials in the waste. There properties include the size and the shape of different objects, their density, weight, magnetism and electrical conductivity. A summary of the different options for waste separation is shown in Table 2.

Separation Technique	**Separation Property**	**Materials targeted**	**Key Concerns**
Trommels and Screens	Size	Oversize (paper, plastic) Small (organics, glass, fines)	Air containment and cleaning
Manual Separation	Visual examination	Plastics, contaminants, oversize	Ethics of role, Health & Safety issues
Magnetic separation	Magnetic properties	Ferrous metals	Proven technique
Eddy Current Separation	Electrical conductivity	Non-ferrous metals	Proven technique
Wet Separation Technology	Differential densities	Floats (plastics, paper) Sinks (stones, glass)	Produces wet waste streams
Air Classification	Weight	Light (plastics, paper) Heavy (stones, glass)	Air cleaning
Ballistic Separation	Density and Elasticity	Light (plastics, paper) Heavy (stones, glass)	Rates of throughput
Optical Separation	Diffraction	Specific plastic polymers	Rates of throughput

Table 2 Waste separation techniques

2.4 Biological Treatment

The biological element of an MBT process can take place prior to or after mechanical sorting of the waste. In some processes, all the residual MSW is biologically treated to produce a stabilised output for disposal to landfill and no sorting is required. The biological processes used are either:

- Aerobic Bio-drying;
- Aerobic In-vessel composting
- Anaerobic digestion

2.5 New Earth's mechanical biological treatment

The New Earth process for the treatment of residual waste utilises mechanical biological treatment and, as usual, it is composed by two different stages.

In the mechanical stage, the waste is liberated and separated so elements such as plastics and metals can be extracted for recycling, a refuse-derived fuel (RDF) is produced for use in renewable energy schemes and the organic part of waste is removed for onward processing. In the biological stage, that organic waste is composted in a controlled environment to produce a useful land remediation, compost-like, product called *nutri-9*.

New Earth's mechanical biological treatment (MBT) facilities incorporate a waste sorting capability to separate the incoming mixed residual wastes into different fractions for further treatment or recovery. Separation of the different fractions is achieved by the use of shredding, particle size screening, ballistic and air separation technology, near-infra red optical recognition, magnets and eddy-current separators.

Recyclables in the form of ferrous and non-ferrous metals and polymers of rigid plastics are recovered at different stages in the process.

A fine material fraction is first separated from the mixed waste using a vibrating screen. The organic-rich fine fraction is transferred to the bio-stabilisation halls for biological treatment, where it is aerobically composted under carefully controlled and continuously monitored conditions over a period of up to six weeks. Conditions of optimise biological degradation in the enclosed bio-stabilisation halls are maintained through agitation (or turning), ventilation and irrigation. This achieves process losses and produces a stabilised material that yields a compost-like-output called *nutri-9*. A further screening is used to achieve two residue types with different particle size (0-20 mm and 0-10 mm). In this research, the 0-10 mm MBT waste is used in order to study its mechanical behaviour using triaxial test in fully saturated conditions (Figure 3).

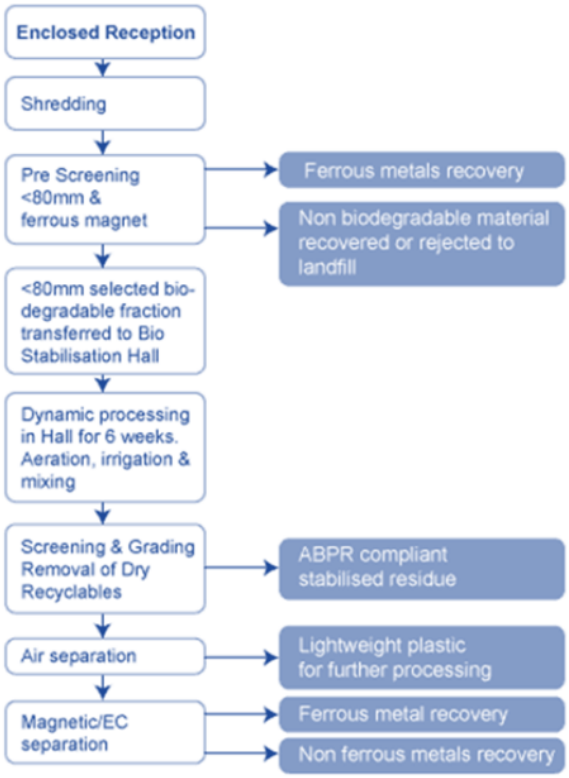

Figure 3 MBT treatment method for the MBT waste used.

The material resulting from the process is less active than MSW but still has some pollution potential (Siddiqui, 2009). The composted material standard (PAS100, 2011) requires the total glass, metal, plastic or any other non-stone fragment larger than 2 mm content to be less than 0.25% of the total mass, with a maximum plastic content of not more than 0.12%. It seems that MBT residues are unlikely to satisfy this requirement for use as a compost. It is therefore likely that these and similar residues will end up being disposed of to landfill.

Chapter 3

Literature Review

Waste is a three-phase material, comprising of: a solid phase, a liquid phase and a gas phase, whose proportions are variable. The solid phase could be split in three components: inert solid fraction, compressible solid fraction and decomposable solid fraction. The liquid phase is mostly generated by the decomposition of the biodegradable fraction but it also comprises the water percolated from precipitations. The gaseous phase is composed of air and organic or nitrogenous gases, produced by the decomposition of the organic fraction. The overall behaviour of waste depends on each component and on their interactions. Another important characteristic of waste is the decomposition of the organic matter, which is the cause of the evolving nature of its behaviour. For these reasons, the geotechnical study of waste is far more complicated than the study of the soil characteristics; even now, the mechanical behaviour of waste as geotechnical material is not completely known although its knowledge is fundamental in order to design safer landfill, avoiding failures and landslides and preventing environmental disaster.

3.1 Waste classification system

To evaluate the waste geo mechanical behaviour and its changing with time, its properties should be well understood and most importantly systemised in a way to ensure comparison between MSW with different age, origin, pre-treatment and geographic reason (Langer et al., 2005). A complete characterisation of wastes may be very challenging and even impossible in view of the extreme heterogeneity of the MSW and their variations with time; however, knowledge of "basic behaviour" and key engineering properties will be significant importance. A waste classification system is essential for development of a unified waste mechanics

framework, which will provide better understanding about waste fill behaviour as a result of time dependant processes (Dixon and Langer, 2006).

3.1.1 Classification system for municipal solid wastes (MSW)

Although classification system for MSW have been proposed by a large number of authors, they often focus on different attributes and generally relate to different types of waste and in a result, the most of the cases they are incomparable to different types of waste and in a result, the most of the cases they are incomparable with each other. There is currently no system that links the mechanical and flow properties of waste with the structure, the combination of the geometry and interconnectivity between the pores. Nevertheless, the classification system suggested by numerous authors are listed and discussed hereafter.

3.1.1.1 Siegel et al. (1990)

They proposed a simple classification system based on material type. They distinguished a number of categories and reported the minimum and the maximum percentages of each as well as the moisture content and the dry unit weight.

- Metal
- Wood
- Soil
- Paper
- Glass
- Rock and brick
- Rubber and plastic
- Miscellaneous

About 95% by wet mass of their sample was placed in the soil group.

This classification system is too simple; there is no apparent difference between some of the material groups: the “soil” category takes up to 95% by wet mass but the nature of that material is not entirely clear (e.g. a degradation residue or mineral soils from the daily cover). Similarly, it is not clear what the content of

"miscellaneous" group is. The materials were not characterised by particle size and shape, neither were their degradability nor mechanical properties taken into account. Thus, while given some information about the waste materials, the classification system is imprecise and incomplete (Siddiqui, 2011).

3.1.1.2 Landva and Clark (1990)

They placed the emphasis on the degree of degradation, which could cause geotechnical properties to vary with time. They distinguished between the following classes of materials:

1. Organic (O)
   a. Putrescible (OP): food, garden and animal waste, and materials contaminated with these wastes
   b. Non-Putrescible (ON): paper, wood, textiles, leather, plastic and rubber, paint, oil, grease, chemicals, organic sludge.

2. Inorganic (I)
   a. Degradable (ID): metals (corrodible)
   b. Non-Degradable (IN): glass and ceramics, mineral soil and rubble, tailings and slimes, ash, concrete and masonry (construction debris)

Landva and Clark (1990) emphasised the importance of the particle shape in a combination with some of the material components from the last three categories (ON, ID and IN) and their possible effect on the geotechnical behaviour of the waste fill: hollow containers (e.g. boxes, cans and bottles); platy or elongated items (e.g. beams, sheets and plates); and bulky items (e.g. furniture, appliances and vehicle bodies). They stated that the visual examination alone is not satisfactory for geotechnical classification; it should be enhanced by parameters such as: water content, organic content, specific gravity and particle size, although they were not included in their categorization.

The classification system provided by Landva and Clark (1990) is useful but not complete; they introduced some important criteria such as material type, degradability and shape, although not very precisely. They carried out tests on unit weight, permeability and settlement but these properties were not included in their classification (Siddiqui, 2011).

3.1.1.3 Grisolia et al (1995)

They extended the classification proposed by Landva and Clark (1990) and focused on the effects of each material class on the settlement and strength behaviour of a landfill. They recognised the importance of the materials deformability for the entire waste behaviour and adopted three broad categories.

1. Class A
   Inert, stable elements, unlikely to deform or degrade and their intrinsic strength and deformability characteristics do not affect the overall waste behaviour:
   - Soils
   - Metals
   - Glass
   - Ceramics
   - Construction debris
   - Ash
   - Wood

2. Class B
   Highly deformable elements, which undergo a large initial settlement due to substantial modification of the initial shape; some of them may exhibit creep:
   - Paper
   - Cardboard
   - Textiles
   - Leather
   - Plastics and rubber
   - Tyres

3. Class C
   Readily biodegradable elements causing volume loss and gas and leachate production:
   - Food waste
   - Garden waste
   - Animal waste
   - Under sieve (particle passing a 20 mm sieve)

They also included parameters, such as size, shape and "assortments" and they explain, in more details, the importance of the water content and of the dry mass for bulk density calculations. Based on their criteria, the authors plotted data for MSW from different regions in the United Stated and City of Rome in ternary diagrams and related them to the mechanical behaviour, e.g. settlement (Figure 4). In that way a comparison between the properties of different wastes was presented in a simple manner.

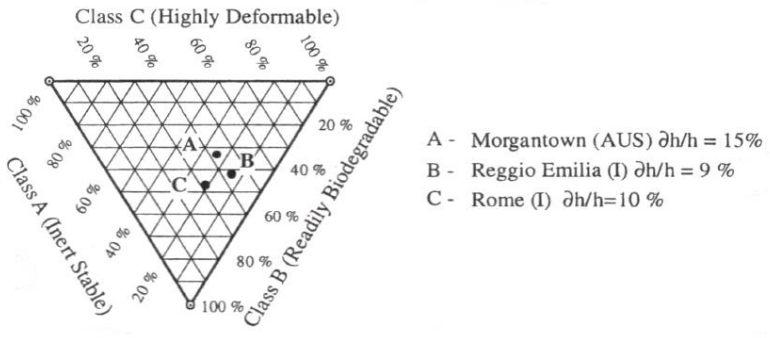

Figure 4 MSW composition and settlement for some observed landfills after Grisolia et al. (1995)

Grisolia et al. (1995) developed a useful classification framework but still there are some omissions: the importance of particle shape was mentioned but not included in the framework; there is no clear distinction between the "undersieve" from class C and the "soil" group from class A, considering that soils could have size of <20 mm and both groups will overlap partially; the distinction between biodegradable from group C and deformable waste from group B is a bit misleading: the degradable wastes will be probably highly compressible and should be placed in both categories (Siddiqui, 2011).

3.1.1.4 Kolsch (1995)

He carried out tensile strength tests on a variety of wastes, showing that fibre-like materials acted to reinforce the waste mass. Four different types of waste sample were used:

- Fresh waste (untreated, without separation of the organic content)
- Residual waste (the same as the fresh waste but the organic components were separated)
- Rotted 18 (pre-treated anaerobically for 18 months)
- Site-old (five years old, excavated from a landfill site.

The materials of each type of waste were categorised into three main groups:

1. Material type (only for particles greater than 40 mm):
    - Paper and cardboard
    - Smooth synthetics (foil, rubber, leather, textiles)
    - Hard synthetics (plastic, hard leather)
    - Metals
    - Minerals (glass, ceramics, soil)
    - Wood
    - Organics (bio-waste, grass and leaves)

2. Particle size (fraction were distinguished by sieving):
    - $<$ 8 mm
    - 8-40 mm
    - 40-120 mm
    - $>$ 120 mm (particles from $>$120 mm were manually separated into 500 mm and 1000 mm)

3. Dimensionality of particles:
    - Zero dimensional (D0) (grain, the finest size fraction)
    - One-dimensional (D1) (fibres, one sized long and two of them short)
    - Two-dimensional (D2) (foils, flat with two long sides and one short)
    - Three-dimensional (D3) (box, three sides long)

    The D0 fraction was reported as comprised by the sizes $<$ 40 mm exclusively.

Kolsch (1995) introduced the most complete criteria in terms of dimensionality of the waste materials. They compared samples differing by treatment history, age and organic content, which is step forward to a classification framework comparable for various types of waste. At the same time, information about the biodegradability of the wastes was not included in this classification system; also, components with a particle size under 40 mm were not categorised by material groups, which may lead to significant differences when assessing the mechanical behaviour.

3.1.1.5 Dixon and Langer (2006)

They proposed a comprehensive classification system, drawing on the previous work of other authors mentioned above, in an attempt to create a universal system

that would facilitate the estimation of both compressibility and shear strength. They summarised the following requirements needed to classify waste:

1. A distinction between the material groups with dominant groupings established; information is required on the proportion (e.g. by weight) of different size components of each material group.

2. Knowledge of component to distinguish between soil-like (three-dimensional) and non-soil-like (two dimensional, e.g. sheet) components. This allows classification of components in relation to their potential for influencing mechanical behaviour of the waste mass (e.g. compressibility, shear and tensile strength).

3. Grading by size for each group of components.

4. An assessment of component compressibility and hence the potential for components to change shape during placement and/or burial.

5. An assessment of degradation potential for both organic and inorganic components.

Dixon and Langer (2006) proposed a procedure for waste classification (Figure 5) and gave details for each element as follows:

1. *Material type description*
   The importance of distinguish major material groups was emphasised due to the waste components variation; it was also explained that the major obstacles for comparison between previous studies of different authors on waste classification was the lack of unified material groups.

2. *Mechanical properties of components in the material groups*
   It was suggested that the waste components need to be categorised upon delivery to the landfill due to change in their mechanical properties, shape and size, because of compaction, overburden stress and decomposition. It was pointed out that with time some components may change their groups within the framework. As important mechanical properties were suggested:
   - Shear strength
   - Tensile strength
   - Compressive strength
   - Elongation at break

- Modulus of elasticity

Dixon and Langer (2006) indicated the need to be determined the effect of each material group, in a combination with shape and particle size, on the waste mechanical properties. In that way, long-term predictions of the entire waste fill behaviour and changes will be possible. In addition, it was emphasised that the suggested categories should be appropriate for every type of waste.

3. *Shape-related subdivisions of components*

   Two main shape-related groups were suggested, using partially the description of Kolsch (1995):

   a. Reinforcing components
      One and two dimensional, such as sheets of paper, plastic, bags etc.; the size of the reinforcing elements should exceed the nominal diameter of the surrounding "regularly shaped" three-dimensional particles (matrix).
   b. Three-dimensional
      - Compressible components:
        - High compressibility (putrescible materials, plastic packing) They may crush or shear even at the deposition;
        - Low compressibility (beverage cans)
        - They may remain unchanged before a certain stress threshold;

      - Incompressible elements (bricks, pieces of metal)

        They will not compress even subjected to a maximum overburden stress.

Dixon and Langer (2006) emphasised the importance of the compressibility subdivision for estimation of changes in volume and other mechanical properties as a result of placement activities and overburden stress. It was stressed on the importance of distinguishing between high and low compressible elements for assessment of the short and long-term behaviour of the components in response to increasing overburden stress and creep.

4. *Size of components*

   The information of grading was reported to have a key importance for the waste classification. The combination of material groups with size grading would provide essential data about the distribution by mass of the shape related sub-divisions. This is useful for estimation of the mass distribution within the shape related subdivisions: the overall percentage of reinforcing, compressible and incompressible materials and initial estimation of the waste fill behaviour can be made. Using experimental data from Kolsch (1995) the following grading bands were suggested: <8 mm, 8-40 mm, 40-120 mm, 120-500 mm, 500-1000 mm and >1000 mm.

   Depending on the type of waste, the material groups are expected to vary within the size ranges, e.g. heavy components (glass, stones, etc.) will be dominant in the range 40-120 mm as well as reinforcing components such as paper and plastics.

5. *Degradation potential*

   This is also an important element of the waste classification as information on the degradation potential would ensure estimation of the approximate time related changes in the material components, which on the other hand will help to modify the classification system. A distinction was suggested between short term, medium term and long-term degradation, which was related to the material groups (kitchen waste degrades more rapidly than the paper).

The mechanical properties, shape and size of particles will vary with time due to compaction, burial, deformability and/or degradation of the materials, therefore the authors suggested that there should be a possibility to change categories of the components at different time periods.

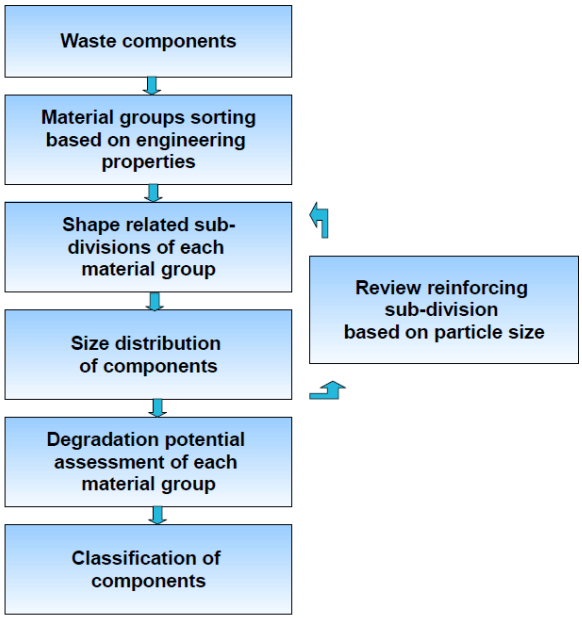

Figure 5 Procedure and application of the proposed classification framework by Dixon and Langer (2009)

3.1.2 Studies on properties of Mechanically-biologically pretreated (MBT) wastes

Although the classification system suggested by Dixon and Langer (2006) is an important step forward for improved prediction and management of the waste bodies in landfills, in the last decade the legislation system in Europe has been significantly modified and since 2006 much waste has been mechanically and biologically pre-treated (MBT) prior to disposal. Inevitably, this will cause changes in the composition, properties and the amount of wastes going to landfills and these changes will probably alter the waste geotechnical properties (Velkushanova et al. 2009; Hall et al. 2006).

In the last few years, different authors have tried to describe properties of MBT waste and predict their behaviour in the context of sustainable landfilling.

Munnich et al. (2005) also analysed two MBT samples; the first one (denoted Bu<60) had maximum particle size of 60 mm and had been anaerobically treated; the second one (Pi<30) has been only aerobically treated and had a maximum particle size of 30 mm. The authors determined the optimal density and moisture content by Proctor tests for both materials (

Table 3), as well as their particle size distribution.

Material	Proctor density, Mg/m3	Water content, %
Pi<30	1.20	26
Bu<60	0.87	33

Table 3 Proctor density and Water content after Munnich (2005)

The higher density of Pi<30 was explained with its larger content of inert materials such as glass, sand and ashes. Additionally, it was examined the settlement and density changes as a function of vertical load and horizontal hydraulic conductivity.

Kuehle-Weidmeier (2004) suggested that in terms of biodegradability, the pre-treated wastes are comparable to MSW that have been buried in a landfill for more than 50 years, without formation of low degradable ones. They stressed the importance of reducing the calorific value, in the MBT residue, by sieving it to <60 mm. Also was noted that the density of samples with larger particles is much lower than for finer ones. They carried out particle size distribution analyses and separated the waste into three fractions: 0-20 mm, 20-40 mm, 40-60 mm. the dominant fraction was the finest (0-20 mm), followed by 20-40 mm. from a mechanical point of view, Kuehle-Weidmeier considered that the MBT is a much finer and homogeneous material then the untreated waste which is why its geo-mechanical and hydraulic properties can be described in a better way using the conventional soil mechanics. However, some of their statements needed further experimental confirmation. The suggested impact of the treatment process on some of the waste geotechnical properties is given in Table 4.

Property/influence	Mechanical treatment (ps<60mm)	Biological treatment	Mechanical and biological treatment
Water permeability	-	-	Decrease
Angle of shear	No change	Increase	Increase
Cohesion	No change	No change	No change
Angle of tensile	Extreme reduction	No change	Extreme reduction

Oedometric modulus	Increase	-	Increase
Subsidence	Decrease	Decrease	Huge decrease
Mass reduction	25-50%	15-30%	40-70%

Table 4 Effect of MBT processing on some waste particles, Kuehle-Weidmeier

Bauer et al. (2005) investigated the influence of the hydraulic conditions on landfill stability by direct shear tests to check the effect of water saturation on the strength of MBT waste. They used a residue with a nominal particle size distribution and material type.

Zardava et al. (2011) described the moisture retention characteristics, Siddiqui (2011) observed the settlement behaviour and gas potential of two MBT samples coming from different resources, while Fernando (2010) used computer tomography imaging analysis in the attempt to understand the structure formation and pores interconnectivity in MBT waste as a porous media.

However, currently there is no such a comprehensive MBT classification system as was previously provided for untreated MSW and since the MBT processing is becoming more and more popular, there is a dearth of knowledge to relate the properties of this residue to their short and long-term behaviour prediction in landfills.

3.2 Waste structure

Waste is a heterogeneous material constituted by different components such as degradable material, paper, cardboard, textile, finer particles, glass, metals, plastic, wood, vegetable reside and inert. Moreover, it is a developing material because of the change of its nature with time due to the presence of different kind of substances, which could be classified as rapidly, moderately and slowly biodegradable. Microscopically, this material could be considered as an ensemble of solid components, randomly disposed, a liquid phase and a gas phase (Figure 6). The spaces between these solid components are known as voids, and their volume can significantly change due to different causes, like consolidation or biodegradation.

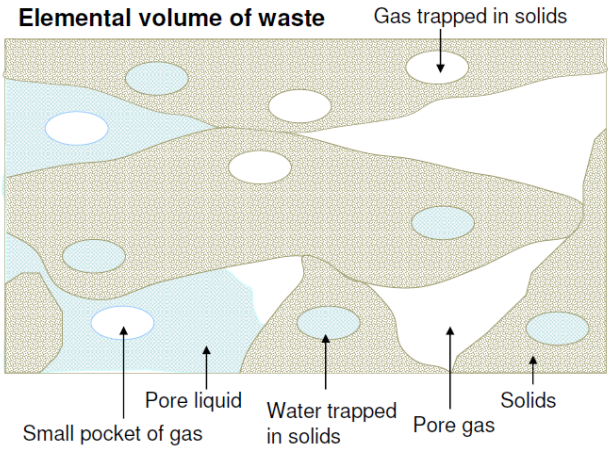

Figure 6 Schematic conceptual model of waste structure

Jessberger et al. (1995) considered MSW as a compound material consisting of a basic matrix of granular materials and a fibre matrix of one and two-dimensional particles which increase the strength of the material by providing reinforcement (Figure 7).

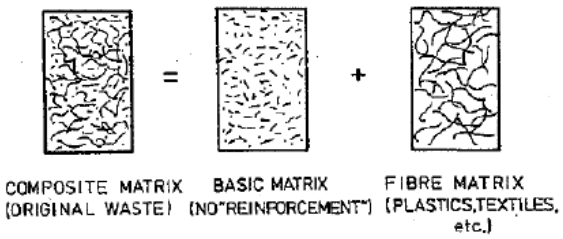

Figure 7 Waste as a compound matrix with non-reinforced basic matrix and a fibre compound matrix (Jessberger, 1995)

The model for waste proposed is similar to reinforced sand with randomly distributed reinforcing elements, mostly fibres. Sand can be consider as the basic matrix. There are differences between the two materials, for instance soil particles are denser and harder than most of the materials found in waste. Reinforcements in waste are mainly two dimension particles whereas the reinforcing particles added into soils are typically fibres. Reinforced soil can help to better understand

the waste behaviour, however, comparison of the two materials need to be treated with care due to the difference in properties.

3.3 Settlement mechanisms in landfills

The factors controlling the landfill settlement are many and often influence each other: waste composition, initial density or void ratio, content of degradable materials, operational practices (fill height and time for placement, stress history, leachate level and fluctuations) and environmental factors, mainly related with biodegradation (moisture content, temperature and gas generation within the landfill). A large proportion of the MSW at placement will have a high void ratio and the voids within and between the individual particles will be reduced as a result of compaction. Hence, the mechanism of waste settlement can be a lot more complex than in soils.

Hudson et al. (2004) carried out experiments, using a large-scale compression cell and describe the mechanism of compressibility in MSW in response of increasing vertical load:

- Particle slip as a result of particle rearrangement (normal compression line)
- Particle distortion at constant volume (unload-reload lines)
- Particle compression as a result of breakage, crushing or rupture of hollow particles (e.g. plastic and glass bottles and cans); liquids or gas topped within these elements could be released and this may also apply to absorbent materials (textiles, paper, etc.)
- Compression of the pore fluid, which is much more significant for gases than for liquids.

The overall effect of these mechanism will be a reduction of the total volume.

Dixon and Jones (2005) expressed the total settlement δ_t as:

$$\delta_t = \delta_p + \delta_s$$

Where δ_p is primary compression and δ_s is secondary compression.

The primary compression includes:

- Physical deformation of particles (distortion, bending, crushing and particle re-orientation)

- Consolidation for saturated waste bodies. The physical compression will occur immediately on application of load and the consolidation will take a few days to a few weeks. For that, the primary compression is qualified as a short-term process, taking a few days to a few weeks (probably depending on the saturation ratio).

The secondary compression comprehends:

- Creep as a time dependent particle distortion, reorientation and ravelling under constant stress;

- Degradation as the main component of secondary compression and total settlement in landfills.

Powrie et al. (2009) suggested another description of the waste settlement mechanism so far and related them to the different stages of settlement:

1. Rearrangement of the solid matrix (sliding, reorientation or distortion of the particles) with increasing vertical stress as in conventional soil mechanics; if the waste is not fully saturated, settlement can occur immediately or in a number of days in saturated conditions.

2. Compression of the pore fluid; if the waste is partially saturated, the air or gas between the pores will be highly compressible;

3. Compression or crushing of the waste particles;

4. Breakage of particles with increasing stress or softening of their contacts on wetting as a result they lose their strength;

5. Degradation as a result of decomposition and physic-chemical processes (corrosion or oxidation);

6. Mechanical creep (continuing settlement at constant effective stress);

7. Ravelling (migration of their particles into larger voids).

These mechanisms will influence the three main phases of settlement in a MSW landfill, as follows:

a. *Immediate compression* as a result of expulsion of gas and liquid from the voids or some hollow particles (plastic bottles or cans); in unsaturated waste, it will be as a result of mechanisms 1,2,3 and 4 mentioned above;

b. *Primary settlement* due to waste consolidation in saturated conditions; mechanism 1 will be dominant, with mechanisms 3 and 4 possibly also playing a part;

c. *Secondary settlement* due to degradation and creep as a result of 5, 6 and 7.

The compressibility of solid particles will be dominant during the first stage (immediate compression) and will play a partial role in the second stage (primary settlement).

3.3.1 Settlement models

A reasonable prediction of settlement is important in estimating landfill capacity, designing final cover grades, gas and leachate extraction system and planning post closure redevelopment projects. Numerous models have been proposed to estimate settlement of the waste in landfills.

3.3.1.1 Consolidation models

These models developed to estimate MSW settlement are based on the consolidation theory of soils. The Sowers (1973) model is simplified one-dimensional model that deals with primary and secondary settlement separately and requires separate equations to estimate waste settlement in both phases. This model assumes that the portion of settlement curve corresponding to the secondary settlement is linear with the logarithm of time as expressed by the equation:

$$\frac{\Delta h_s}{h_{ref}} = C_{\alpha\varepsilon} \log\left(\frac{t}{t_{ref}}\right)$$

With $C_{\alpha\varepsilon} = \frac{C_\alpha}{(1+e_0)}$

Δh_s is the secondary settlement at time t;

h_{ref} is the height of waste upon completion of primary settlements;

t_{ref} is a reference time for secondary settlement;

$C_{\alpha\varepsilon}$ is the coefficient of secondary settlement and

e_0 is the initial void ratio

Based on the field movements, Sowers (1973) recommended values of $C_{\alpha\varepsilon}$ in the range 0.02 to 0.07. A value of 0.02 corresponds to unfavourable conditions to biodegradation, while 0.07 corresponds to favourable condition for biodegradation. The advantages to use this model are its simple formulation and that it involves only few number of model parameters, which can be often determined from simple compression tests. The disadvantages is that it is often difficult to make distinction between primary and secondary settlement, while creep and biodegradation are lumped together. Another problem with this model is that the landfills are usually not saturated; therefore, the classical consolidation model for saturated soils may not be appropriate.

Wall and Zeiss (1995) used one dimensional consolidation equation to model settlement in bioreactor landfill cells. They conducted a lab study and showed that secondary settlement is linear with the logarithm of time. They found one dimensional consolidation theory suitable to simulate the settlements. El Fadel and Al Rashed (1998) demonstrated that a one dimensional consolidation model had a greater application potential for practice.

The behaviour of secondary settlement is complicated due to the combined effects of mechanical creep and biodegradation. Several studies have evaluated a coefficient of secondary settlement ($C_{\alpha\varepsilon}$) describing continuing settlement with time under constant effective stress. Most researchers do not make a clear distinction between creep and biodegradation, and evaluated $C_{\alpha\varepsilon}$ based on the similarity of the time dependant nature of creep and biodegradation induced settlements. $C_{\alpha\varepsilon}$ was determined from the slope of the settlement versus log(time) plot assuming that biodegradation continued with time just like the mechanical creep. This assumption is invalid, as biodegradation cannot continue indefinitely with time. The values of $C_{\alpha\varepsilon}$ reported in the literature mostly include components of both creep and biodegradation (Table 5).

Source	$C_{\alpha\varepsilon}$
Sowers (1973)	0.02 to 0.07
Rao et al. (1977)	0.012 to 0.046
Oweis and Khera (1990)	0.02 to 0.072
Wall and Zeiss (1995)	0.033 to 0.056
Gabr and Valero (1995)	0.015 to 0.023
Green and Jamenjad (1997)	0.01 to 0.08
El Fadel and Al Rashed (1998)	0.01 to 0.016
Landva et al. (2000)	0.01 to 0.016
Machado et al. (2002)	0.012 to 0.016
Hossain et al. (2003)	0.02 to 0.19
Durmusoglu et al. (2006)	0.043 to 0.083
Breither et al. (2008)	0.01 to 0.19
Siddiqui (2011)	0.018 to 0.024 (MBT)

Table 5 Summary of published values of $C_{\alpha\varepsilon}$ for MSW and MBT waste.

Current knowledge regarding settlement characteristics is mainly related to MSW landfills. There are virtually no settlement data for MBT waste landfills. The behaviour of MBT waste will be different from the experiences, which have been gained in the past for MSW landfills, and a clear distinction between the creep and biodegradation components of settlement is needed.

Siddiqui (2011) analysed the settlement characteristics of two different kind of MBT, one treated in Germany and one in UK. He divided the whole settlement into immediate compression, primary settlement (consolidation) and secondary settlement (mechanical creep and biodegradation contribution were identified and quantified separately). The long-term settlement curve for both pre-treated wastes and a traditional raw MSW could be reproduced with a model based on logarithmic law for creep and kinetic model for the biodegradation induced settlement and the primary settlement followed the Terzaghi's theory of one-dimensional consolidation. The long-term secondary settlement of pre-treated waste was much smaller than raw MSW's one, this could be explained by the reduced contribution of the biodegradation in MBT waste.

3.3.1.2 Empirical models

The rheological model (Gipson and Lo, 1961), power creep law model (Edil et al. 1990), logarithmic model (Yen and Scanlon, 1975) and hyperbolic model (Ling et

al., 1998) were mainly designed to predict only the mechanical compression characteristics of soil like materials. Therefore, they are not capable of estimating the settlement of MSW landfills, which results from both mechanical creep and biodegradation. These models do not required separation of settlement into primary and secondary components. They attempt to simulate the settlement of a landfilled waste by a mathematical function involving adjustment of empirical parameters, which are site specific and seldom have a physical significance.

3.3.1.3 Biomechanical models

Edgers et al. (1992) developed a waste settlement model, which takes into consideration the mechanical compression and decomposition through the microbiological processes within the landfill. They expressed biodegradation-induced settlement as a function of the activity of microorganism. The major drawback is that the model incorporates the growth kinetics of a single species of bacterial population (methanogens), and therefore, underestimates the role of hydrolysis, which is the rate limiting step in degradation. Another limitation is that there is no accurate method available to predict the critical time at which the settlement rate starts to increase due to biological activity.

Park and Lee (1997) defined the concept of settlement that occurs due to the decomposition of biodegradable refuse using first order kinetics as follows:

$$\varepsilon_b = \varepsilon_{bt}(1 - e^{-k_b t})$$

Where ε_b is the settlement strain due to biodegradation at a time t since the start of degradation, ε_{bt} is the total amount of settlement strain resulting from biodegradation and k_b is a first order degradation rate constant. This model does not on its own account for mechanical compression during or immediately after waste placement although it handles the biodegradation-induced settlement well.

Elagroudy et al. (2008) confirmed the applicability of the previous equation to wastes of different composition, with or without the addition of sewage sludge, in different operational conditions.

The landfill degradation and transport (LDAT) model developed by the University of Southampton (UK) incorporate microbial kinetics activity of leachate and gas production and their transport in addition to the consolidation

of MSW. The advanced model, HBM (Hydro-Bio-Mechanical model, Mc Dougall (2007)) is a coupled framework for the integrated analysis of the landfilled MSW. Machado et al. (2002) proposed an advanced constitutive model to simulate the mechanical behaviour of MSW based on laboratory experiments. They combined a mechanical creep component together with biodegradation-induced settlement related to gas generation.

Despite the fact that these models take into account most of the mechanisms, the requirement for a large number of parameters makes them at present difficult to implement in practice. At present, due to the simplicity and familiarity of a consolidation based approach to practicing engineers, Sowers method is the most widely used for long term settlement prediction. Models incorporating separately mechanical creep and biodegradation are generally not available.

3.4 Hydraulic properties of MSW in landfills

The knowledge of the hydraulic behaviour of waste is correlated with the determination of leachate collection and distribution rates and volumes; hydraulic conductivity is the key in order to manage the problem of leachate. The hydraulic behaviour of MSW depends mainly on the pore size and geometry, which varies with the size and shape of particles. The drainable porosity is linked with the void space available for water movement through the saturated waste. Previous research has demonstrated that the hydraulic conductivity of MSW is controlled by vertical stress, through its impact on waste compression and density.

Powrie and Beaven (1999) carried out tests on municipal solid waste in a large-scale compression and reported a decrease in hydraulic conductivity as a function of applied stress and density. Reddy et al. (2009) showed that the hydraulic permeability of MSW could be influenced by vertical stress, which was attributed to the increase in density, leading to low void ratio. Other factors influencing the hydraulic conductivity are the gas entrapped in the waste (Hudson et al. 2004) and the presence of plastic sheet fragments in the waste (Xie et al., 2006). Table 6 summarises the hydraulic permeability values obtained by previous study on MSW.

Reference	Hydraulic conductivity (m/s)	Dry density (kg/m3)
	Laboratory tests	
Bleiker et al. (1995)	$1x10^{-6} – 5x10^{-9}$	500 – 1200
Chen and Chynoweth (1995)	$9.6x10^{-4} – 4.7x10^{-7}$	160 – 480
Powrie and Beaven (1999)	$1.5x10^{-4} – 3.7x10^{-6}$	390 – 720
Durmusoglu et al. (2006)	$1.2x10^{-4} – 4.7x10^{-6}$	N/A
Olivier and Gourc (2007)	$1x10^{-4} – 1x10^{-6}$	490 – 710
Reddy et al. (2009)	$2x10^{-5} – 7.8x10^{-7}$	320 – 960
Staub et al. (2009)	$7.4x10^{-5} – 4.6x10^{-6}$	370 – 530
Stoltz et al. (2010)	$1x10^{-4} – 1.1x10^{-5}$	600 – 900
	Field test	
Oweis et al. (1990)	$2.4x10^{-5} – 9.4x10^{-6}$	680
Landva and Clark (1990)	$4x10^{-4} – 1x10^{-5}$	1000 - 1400
Jain et al. (2006)	$6.1x10^{-7} – 5.4x10^{-8}$	N/A
Machado et al. (2010)	$1x10^{-5} – 1x10^{-8}$	N/A

Table 6 Summary of the reported values of hydraulic conductivity of MSW

The hydraulic conductivity may also depend on the degradation of waste causing a possible change in the composition and size of the waste particles. Powrie and Beaven (1999) analysed hydraulic conductivity of fresh, processed and aged waste and showed that differences in the values of hydraulic conductivity resulting from particle size reduction and waste degradation are less significant than the effects of stress and compression.

Hossain et al. (2009) investigated the change in hydraulic conductivity of MSW at different staged of biodegradation in a laboratory bioreactor. They reported a decrease in hydraulic conductivity from 8.8 x 10^{-5} m/s to $1.3x10^{-5}$ m/s, which was attributed to a decrease in particle size.

Several authors have studied the decrease in hydraulic conductivity of MBT waste as a function of density, as summarised in Table 7. These values are nearly of the same order of magnitude to those obtained for MSW and as such indicate a comparable hydraulic conductivity.

Reference	Hydraulic conductivity (m/s)	Density (kg/m3)
Bidilingmaier et al. (1999)	$1x10^{-4} – 1x10^{-7}$	600-900 (dry)

Bauer et al. (2006)	$1x10^{-5}$ – $1x10^{-7}$	850-1200
Kuehle-Weidmeier (2004)	$3x10^{-6}$ – $6x10^{-9}$	690-920 (dry)
Xie et al. (2001)	$2x10^{-7}$ – $6.3x10^{-8}$	800-1100 (dry)

Table 7 Summary of the reported values of hydraulic conductivity of MBT.

Siddiqui (2011) analysed the settlement of MBT waste divided into immediate compression, primary settlement (consolidation) and secondary settlement. The contribution on mechanical creep and biodegradation to secondary settlement were identified separately and mechanical creep was found to be more significant of the two. This was possible because was used two different reactor, in one of theme the microbial activity has been suppressed and the onset of methanogenesis stopped. The two reactor were operated at 50 kPa load until about 10 months, and then at 150 kPa. He measured the hydraulic conductivity and the bulk density at each load stage; he found that the hydraulic conductivity decreases with increasing of stress and waste density (Table 8). The drainable porosity was reduced to about 15-17% at an applied stress of 50 kPa and to less than 5% at 150 kPa. The hydraulic conductivity of pre-treated wastes and raw MSW are similar for the given range of dry density.

Applied stress (kPa)	**Hydraulic conductivity (m/s)**	**Density (kg/m3)**
Microbial activity suppressed reactor (UK MBT)		
Initial (no load)	$8.12x10^{-6}$ – $7.52x10^{-6}$	679
50 kPa	$6.26x10^{-6}$ – $6.9x10^{-6}$	940
150 kPa	$7.59x10^{-7}$ – $8.48x10^{-7}$	1120
MBT mixed with leachate reactor		
Initial (no load)	$7.21x10^{-6}$ – $7.01x10^{-6}$	685
50 kPa	$6.09x10^{-6}$ – $5.78x10^{-6}$	949
150 kPa	$6.97x10^{-7}$	1091

Table 8 Hydraulic conductivity and density for the UK MBT waste (Siddiqui, 2011)

3.5 Shear strength of waste and concepts

The geotechnical design of landfill requests the knowledge of the mechanic characteristic of waste disposed, in particular its deformability and compressibility but also its shear strength. The knowledge of this last parameter is fundamental in order to verify the structures used to retain the material landfilled, avoiding any instability and failure.

The behaviour of MSW is quite different from what obtained for other geo-materials, mostly because of the completely different structure and its changing with time due to the biodegradation and creep. One of the most different characteristics in the absence of any strength peak, even under high deviatoric stress values (Figure 8). MSW samples usually present strain hardening even under high strain level and a failure criterion is difficult to set. As the main component of this material is organic matter and because of the biodegradation effect, strength is a function of time.

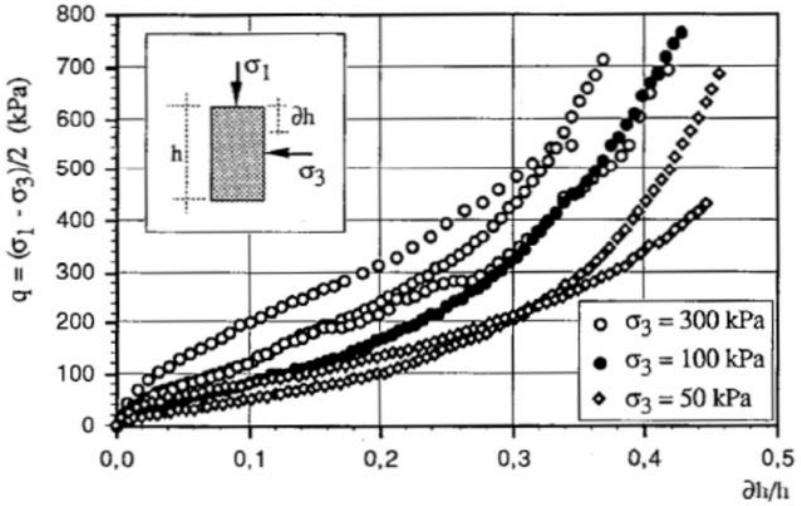

Figure 8 Triaxial tests result for MSW (Grisolia et al. 1992, Gasparini et al. 1993)

This particularity is usually associated with some waste features, which represent a singularity comparing with the ordinary geo-material as soil:

- Different relationship used to evaluate effective stress in porous media than the Terzaghi's one, which consider the contact between two solid particles on a statistical plane of area;

- Presence of fibrous elements which affects the waste strength, inducing an increasing and an anisotropic behaviour due to the orientation of the fibres;

- Excessive compressibility of waste, which induces the presence of large strain.

Skempton proved that the original relationship for effective stress in porous media proposed by Terzaghi could be replaced by the following equation:

$$\sigma' = \sigma - (1 - a)u_w$$

Which consider the contact between two solid particles. The a parameter is defined as the ratio of the statistical contact area between two solid particles and the total cross section area in a plane parallel to the contact (Figure 9). Than he improved this equation proposing the following expressions for effective stress in fully saturated materials in the case of shear strength and volume change:

$$\sigma' = \sigma - (1 - \frac{a \tan \psi}{\tan \phi'})u_w$$

$$\sigma' = \sigma - (1 - \frac{C_S}{C})u_w$$

Where:

ψ is the angle of intrinsic friction

ϕ' is the angle of shearing resistance

C_S is the average compressibility of the particles

C is the overall compressibility of the porous materials

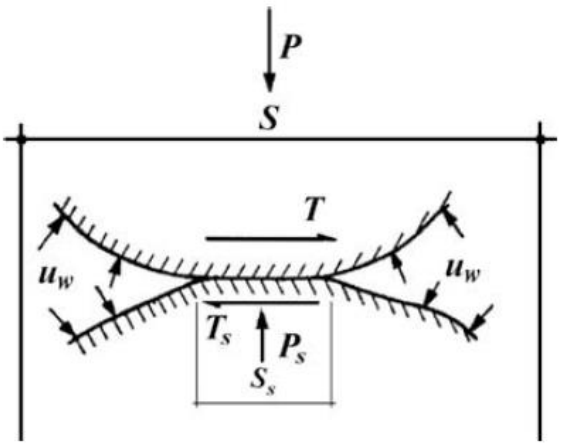

Figure 9 Particle arrangement in a porous geo-material and their connection points after Skempton (1961)

The estimation of parameters such as "a" and ψ is not an easy task because of the fact that waste is composed by several types of components. The parameters C_S and C have a clear physical significance which facilitates data interpretation. In fact, this second equation seems to be more useful to estimate the effective stress in MSW.

Powrie et al. (1999) using a large compression cell with nominal size of 3 m height and 2 m diameter carried out a set of compression tests on MSW materials and measured the average particle compressibility and the overall compressibility of three types of waste: raw, pulverized and aged wastes. The results show that the overall compressibility and the average compressibility of waste particles decrease with the level of confining stress. The waste overall compressibility seems to be unaffected by the type of waste, but the solid particle compressibility seems to reduce with the age of waste.

In the case of partly saturated samples, another expression has been formulated. This situation can happen very often because of the difficult to carry on geotechnical tests on fully saturated sample without methanogenesis, which destroys the waste internal structure affecting the results. The intergranular effective stress depends on air pressure (u_a) and on water pressure (u_w) within the voids and on the ration of water and total surface, χ:

$$\sigma' = \sigma - u_a + \chi(u_w - u_a)$$

Several researchers have tried to explain the strength of waste providing some models, which describes the different stages of its behaviour. Two of the most discussed and known are the models formulate by Kolsch (1995) and Powrie et al. (1999); both of theme speak about the importance of the fibrous content reinforcement and its contribution to the waste strength.

3.5.1 Kolsch (1995)

Kolsch has elaborated a theory to explain this additional force assuming that the waste shear strength has two major resistance component: friction and tension.

Frictional forces is guaranteed by the contact between grains, which compose the matrix of waste. Tensile force is linked with fibrous elements contained in the waste and it is strongly influenced by the orientation of these to the shear surface. This consideration implies the anisotropy in shear resistance of MSW.

Kolsch describes the mobilization of the shear strength in a reinforced soil using four phases (Figure 10):

Phase 1 The strength is due only to the friction force generated between grains because the tensile one is not yet mobilized (the fibres are not strained)

Phase 2 The strength is due both to friction and tension. In particular, the tension force increases with increasing of displacements until it reaches its maximum.

Phase 3 The shear strength is also made up by friction and tension. As a result of slipping and tearing of the reinforcements, there is a tension decay.

Phase 4 Under large displacements, the shear strength is purely frictional.

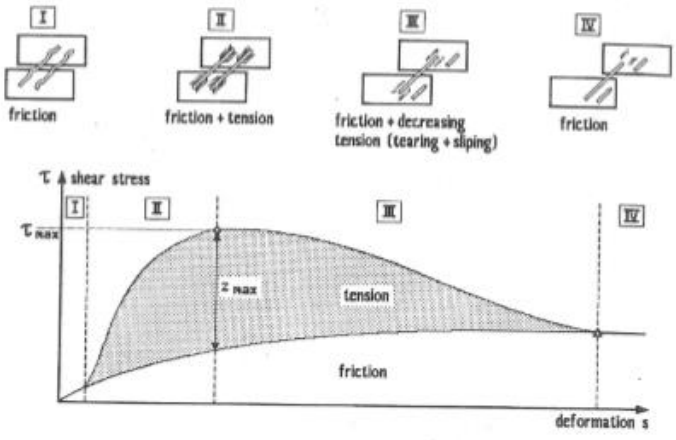

Figure 10 Behaviour of the reinforcement during the shear stage (Kolsch, 1995)

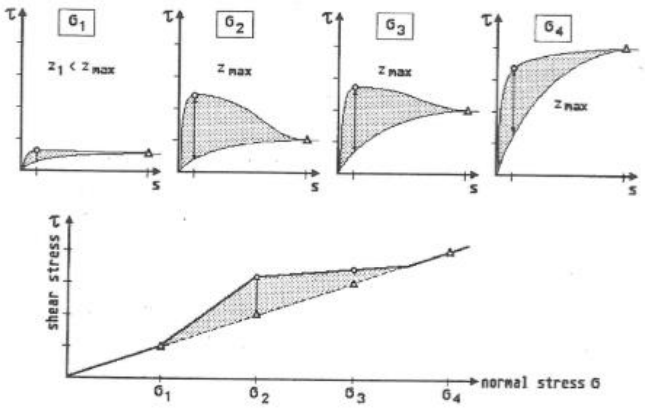

Figure 11 Behaviour of the reinforcement with the normal stress (Kolsch, 1995)

Kolsch has provided also a mechanical model to better understand the relationship between normal and shear stresses and the influence of fibrous constituents on it.

As we can see in the Figure 11, there is not a significant reinforcing effect under low and high normal stress. Nevertheless, the reinforcing effect become more important under intermediate stresses. These observations can be explained with the need of a minimum of confining pressure to prevent pull-out of reinforcing elements and the presence of a maximum beyond which the mobilization of tensile force decreases.

For these reasons, Kolsch has suggested the use of a bi-linear envelope to describe the relationship between shear and normal stresses. At low normal stress values (<100 kPa), the friction angle is supposed higher than one obtained at superior normal stresses.

3.5.2 Powrie et al. (1999)

Powrie et al. (1999) examined the validity of the Mohr-Coulomb failure criteria for waste and argued that the use of cohesion and angle of friction are inappropriate for waste because of the following facts:

1. Cohesion is due only to the reinforcing effect; in fact, as discussed by Kolsch (1995), at low confining stresses the reinforcing effect is negligible.
2. Talking about friction angle is not correct regarding waste because it represents both the frictional and tensile components. Powrie et al. (1999) suggested that it would be better to use the name of "angle of shearing resistance".
3. Angle of shearing resistance under higher stresses cannot be applied under the lower normal stress due to the relationship between the reinforcing effect tension and normal stress.

3.5.3 Major factors affecting the shear stress of waste

As we said previously the MSW is a very heterogeneous material, whose characteristics change with time. It is important to analyse how these characteristics can affect the strength behaviour of waste.

1. *Reinforcement content*
   Several studies show that the inclusion of the reinforcements has a positive impact in increasing the strength of the material.

   Fucale et al. (2007) carried out direct shear tests on MBT waste with different percentages of reinforcing content, under 200 kPa normal stress. There is a clear evidence that the waste components larger than 8 mm have the ability to increase the shear strength of the material (Figure 12). The material with the lower reinforcing content (matrix 2, red line) has a higher strength than the material with 20% reinforcement (matrix 1, green line). The basic matrix (blue line) shows higher stiffness and lower strength with displacement. These results clearly show that a greater amount of reinforcements than an optimum reduces the shear strength.

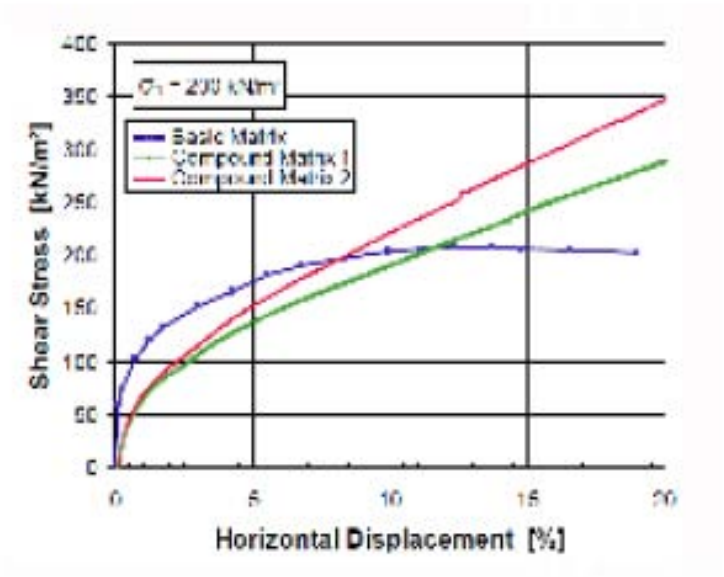

Figure 12 Direct shear results for an MBT waste with different composition (Fucale, 2007)

2. Waste basic matrix

In order to investigate how the basic matrix can affect the shear strength many studies have been carried out using reinforced sand instead of waste. Santoni et al. (2001) used 1% by mass of 51 mm fibres in unconfined compression tests using sand as the matrix. In these test, the silt content was varied from 1% to 12%. The results showed that the maximum strength was achieved with 1% silt content but the strength with a silt content of 8% was still greater than silt free material (Figure 13). However increasing the silt content to 12% did not conduce to an improvement of its mechanical characteristics. It can be possible to say that the basic matrix has an important impact on the shear strength characteristics. This would suggest that the shear strength of waste might change over time due to the biological activities.

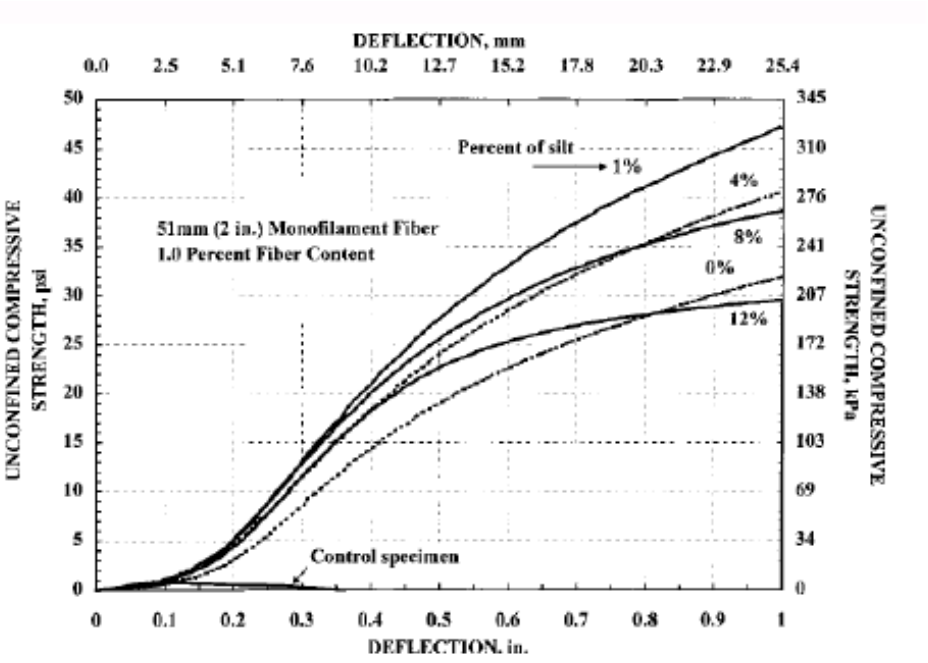

Figure 13 Shear strength of a reinforced sand using different silt content (Santoni et al., 2001)

3. *Decomposition*

As we said previously, waste can change its composition with time, due to the biological and chemical degradation of its particles. Several studies are carried out in order to investigate the influence of degradation on the mechanical behaviour of waste (Kavazanjian, 2001); they suggest that degraded waste shows a similar shear strength comparing with fresh waste. However, degradation of the waste is likely to change the properties of the material:

- Due to the breakdown of the organic material, a finer matrix material can be expected in aged waste compared with raw MSW;

- Although reinforcing materials such as flexible and stiff plastics are unlikely to be significantly affected by decomposition, other reinforcing materials such as paper and wood are likely to be weakened or removed by biodegradation;

- Heating during aerobic degradation may lead to increase brittleness and reduce strength in some plastics.

The shear behaviour of waste and the effect of degradation on it was investigated by Kuehle-Weidmeier (2006). The average friction angle of the

aged waste was the same as fresh waste. The cohesion of aged waste was lower than the fresh MSW but the difference is less than 10% so is unlikely to be significant (Table 9).

Waste type	**Average friction angle °**	**Cohesion (kN/m2)**
Fresh MSW	29	50
Old MSW	29	46

Table 9 Shear strength properties of fresh and old MSW (Kuehle-Weidmeier, 2006)

Waste composition is highly dependent on social and economic conditions in the collection area, which may change over time. For examples, significant increase in rates of recycling over the last decade have changed the composition of residual waste. The results obtained from fresh and old waste samples are not easy to compare due to the heterogeneous nature of waste.

It is clear that properties of the waste are likely to change with degradation, but it is difficult to get some conclusions on the level of the degradation and its impact on the shear strength from the available data.

4. Particle size

Many researchers have studied reinforcement particle size and its impact on strength. Jessberger (1995) conducted large (540 mm diameter) uniaxial compression tests on two different waste types: as-received MSW and the MSW fraction passing a 120 mm sieve (85% MSW is smaller than 120 mm). The compression testing results showed that the sample with <120 mm material failed with a peak at 20% strain. The MSW sample increased its compressive strength with strain without reaching a peak or a failure in contrast to the sieved sample (Figure 14).

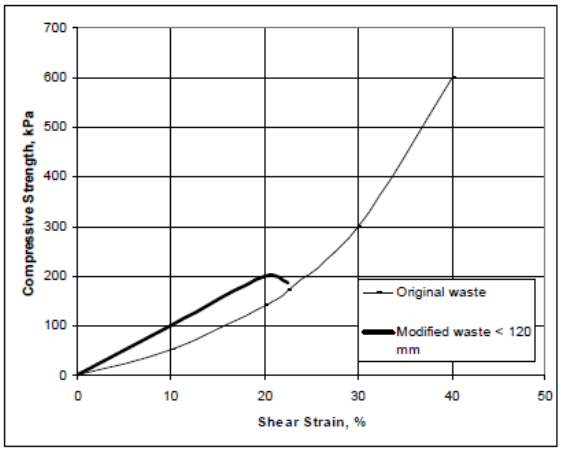

Figure 14 Unconfined compression test on as-received MSW and <120 mm sieved MSW (Jessberger et al., 1995)

Consoli et al. (2007) used a ring shear apparatus to investigate the residual strength of reinforced sand at large shear strains. Sand with an effective diameter (D_{10}) of 0.16 mm was used with 0.023 mm diameter polypropylene fibres of 6,12 and 24 mm length. The fibre content was 0.5% by dry soil mass. The displacement rate was 0.17 mm/min in all tests. The results of these tests indicate that:

- Fibre length has a strong influence in increasing the residual strength. The sand with 6 mm fibres showed a slight increase in residual strength compared with the unreinforced material. Sand reinforced with 12 and 24 mm fibres showed the same residual strength and, in both cases, higher than that achieved by the sand reinforced with 6 mm fibres.

- Under lower normal stresses such as 20 kPa and 100 kPa, the shear strength were not much different in reinforced sand samples regardless of the reinforcement length.

- At higher normal stresses higher differences in shear strength can be observed

After about 3000% strain, the length of the fibres was measured and it was found that it was 4-6 mm each case. This indicates that the fibres less long than these values tend to fail by pullout rather than elongation or breakage.

It can be assumed there is a minimum length for the fibres to act as reinforcement in order to provide the tensile strength and it seems that reinforcement length has an influence on the shear strength.

5. *Orientation of reinforcement*

The impact of reinforcement orientation on the strength of reinforced soils and waste has been investigated in order to improve the knowledge of the anisotropy on MSW in shear resistance and compressibility. Rajan t al. (1996) explained that the tensile stress in the fibre could be split in two components, normal and tangential to the shear plane.

Jewell and Wroth (1987) carried out direct shear tests using reinforced sand; they obtained that the highest reinforcement impact can be achieved when the reinforcement was oriented at 30° vertical to the shear plane. Reinforcement have an adverse impact on the strength when the reinforcement is in compression (Figure 15).

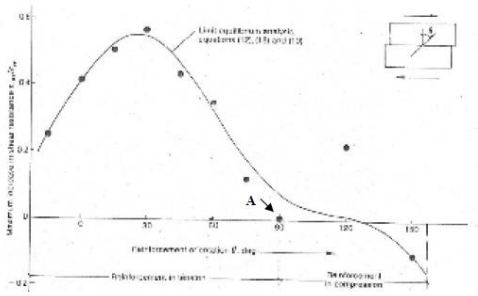

Figure 15 the impact of fibre orientation on shear strength of a reinforced sand (Jewell and Wroth et al. 1987)

Zekkos (2013) investigated the effect of reinforcement orientation in MSW using different sample of the same waste composition and compaction effort using a 300 mm size direct shear device; the only difference was the orientation of the fibres (vertical and horizontal considering the shear plane). Representative results of shear stress as a function on horizontal displacement for two pairs of direct shear specimens with different waste composition and at two different confining pressures are shown in Figure 16. The specimens that have the same testing conditions but different orientation of fibrous waste constituents show different shear response.

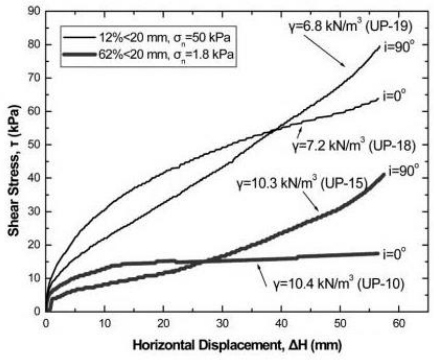

Figure 16 Effect of fibrous waste orientation with respect to the shear surface in direct shear (Zekkos et al, 2010)

This direct shear data clearly indicate that the shear resistance of MSW is anisotropic and significantly affected by the relative orientation of the fibrous constituents to the horizontal shear surface. The improvement of shear resistance of a fibre reinforced soil was a function of the type of fibre and their orientation compared to the shearing plane.

Test by Athanasopoulos et al. (2008) on mixtures of waste constituents and daily soil cover from a landfill in Greece, highlighted the significant effect of anisotropy. The shear resistance was found to be significantly affected by the orientation angle, *i*, between the fibrous waste and the horizontal shear surface, as shown in Figure 17.

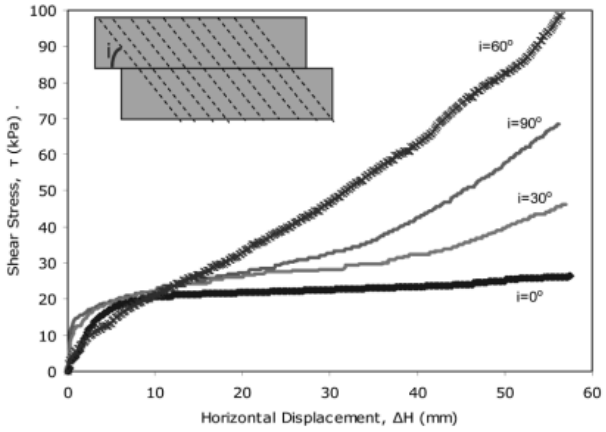

Figure 17 Stress-displacement response for specimens with plastic reinforcement at varying fibre orientation angle for an MSW (Athanaspoulos et al., 2008)

6. *Interface frictional properties of reinforcement*
   Several studies (Michalowski and Cermak, 2003) have demonstrated that reinforcement with high interface friction is likely to increase the shear strength of the material more than low friction reinforcement.

7. *Normal stress*
   Kolsch (1995) introduced a model to explain how the normal stress can influence the shear resistance of the waste as discussed previously.

   Borgatto et al. (2009) conducted a direct shear testing programme using a 300 mm shear box on MBT waste (0-60 mm). In order to investigate the impact of reinforcement, the MBT waste was modified elimination the soft plastic and then direct shear tests were conducted on both as-received and modified samples under 25 and 300 kPa normal stresses. The 25 kPa test showed that the original MBT material had a higher shear strength than modified MBT (Figure 18). On increasing the normal stress, the impact of the soft plastic was reduced, complying with the behaviour suggested by Kolsch (1995) at higher stresses (Figure 19).

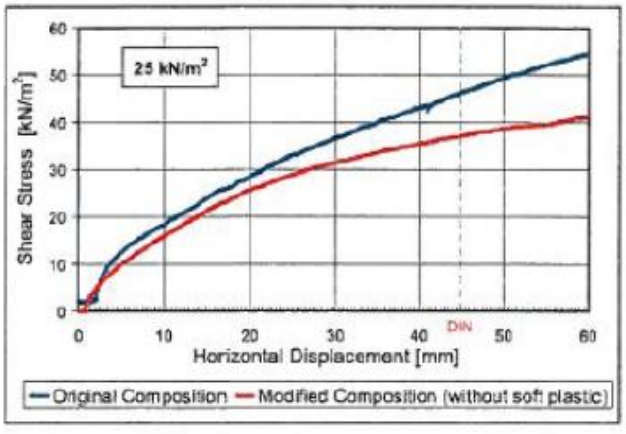

Figure 18 Shear displacement under 25 kPa using a 300 mm shear box (Borgatto et al., 2009)

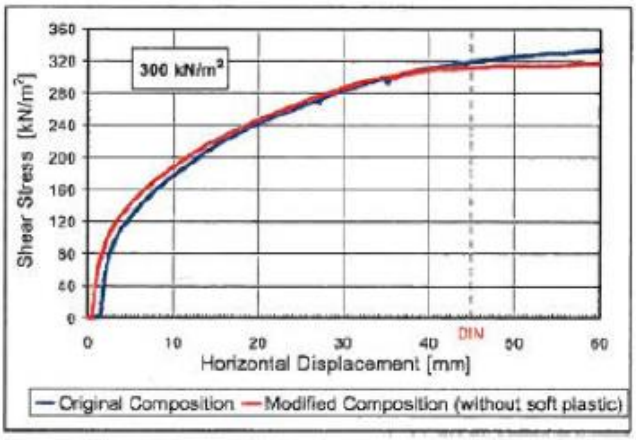

Figure 19 Shear displacement under 300 kPa using a 300 mm shear box (Borgatto et al., 2009)

8. Reinforcement stiffness

Jewell and Wroth (1987) highlighted that the higher stiffness of the reinforcing induces a greater contribution to the shear strength (Figure 20).

Shewbridge and Sitar (1989, 1996) suggested that the reinforcement increase the strain hardening of the material and the reinforcement stiffness increased the shear zone thickness while increasing the shear stress of the material.

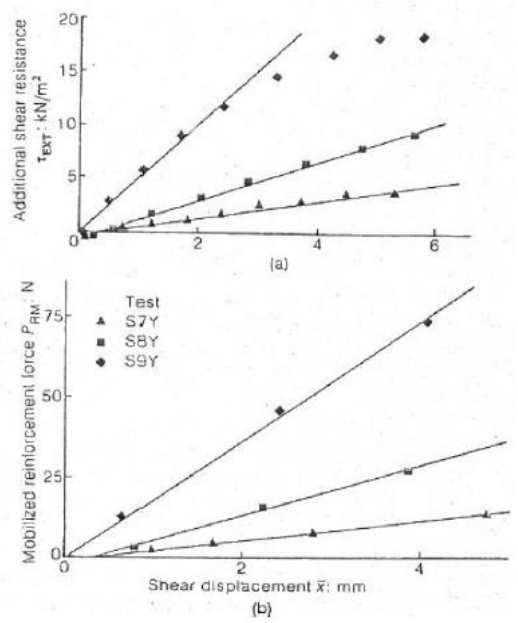

Figure 20 Shear strength change with stiffness of the reinforcements (Jewell and Wroth, 1987) (stiffness S7Y - 0.107 kN, S8Y - 0.387 kN, S9Y - 105 kN)

3.5.4 Geotechnical tests used for Municipal Solid Waste

In order to investigate the mechanical behaviour of waste as geomaterial, the most common practice is laboratory testing; usually direct shear or triaxial compressions test are used to determine shear parameters. However, the different material structure and behaviour of waste requires the use of large scale of testing device. Other tests could be the unconfined compression test, which is less common, and the ring shear test in order to study the residual strength.

3.5.3.1 Direct shear equipment

Direct shear tests are used to determine the shear behaviour, which is described by the angle of internal friction and cohesion according with Kolsch approach. Powrie provides another point of view saying that cohesion and angle of friction are inappropriate in order to describe waste's behaviour. The waste is a loose material so there is not cohesion at low confining stresses and it is due only to the reinforcing effect. So he suggests to define only the angle of shearing resistance φ' with a zero value cohesion. Another aspect of direct shear apparatus is that the mobilized shear strength depends on the orientation of the layered fibrous components to the failure plane, which is forced into a specific direction. Therefore, the results cannot be easily transferred in situ conditions.

Thomas et al. (1999) conducted direct shear tests on MSW using a 1 m x 1 m shear box and displacement rate of 3mm/min. The sample with higher content of reinforcements such as plastic, paper, textile and wood showed lower stress ratio than the normal one (Table 10). This must be due to a higher then optimum fibre content.

Sample	**Normal stress (kPa)**	**Stress ratio at 180 mm displacement**
As-received MSW	50	0.986 and 1.222
	100	0.835
Reinforced MSW	75	0.795

Table 10 Summarised Shear Stress Ratio

Kolsch (2009) highlighted the shear strength continuing to rise with larger displacement until the end of the test using a direct shear box (Figure 21).

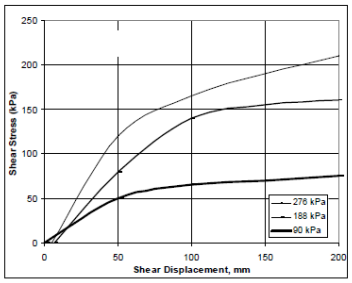

Figure 21 Direct shear results for MSW (Kolsch, 2009)

Maher (2009) conducted a direct shear test programme on pre-treated MSW using a shear box with dimensions of 400 x 250 mm. The waste was shredded and aerobically treated in windrows. The tests were conducted under normal stresses of 25, 50, 75, 100 kPa. At about 45 mm displacement, the direct shear curves at the two highest normal loads (100 kPa and 75 kPa) have achieved clear peak strengths while the 50 kPa direct shear test has shown a constant shear resistance(Figure 22). However, the direct shear result at 25 kPa showed that the shear strength is still slightly increasing after 45 mm displacement.

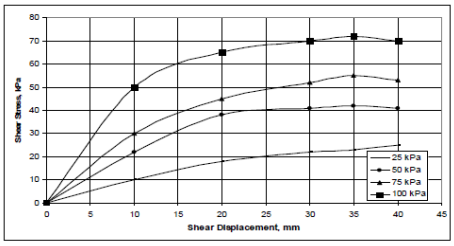

Figure 22 Shear strength plot for pre-treated MSW using 400 x 250 mm shear box (Maher, 2009)

The direct shear results showed suggest the following consideration:

- Reduction of the particle size may aid the achievement of a peak or constant shear stress with larger displacement (it is possible to observe a failure in waste);

- Under high normal stresses, peak strength or failure is more likely to be observed.

3.5.3.2 Triaxial equipment

To avoid the problem of the forced shear plane, the triaxial shear testing can be used; another advantage of this test is the possibility to control the drainage

within the specimens. However, a large scale triaxial cell is requested for the determination of strength parameters and the investigation of stress-strain response of waste; in fact, the standard triaxial cell may be not able to reach the axial deformation required to mobilize the whole strength. Then, the reduced size of triaxial cell could be too restrictive for MBT residues. The triaxial compression test is composed of two phases; in the first phase, the consolidation of specimens takes place. It could be reached using an isotropic ($Ko = 1$) or anisotropic compression. During the second phase, a deviator stress is applied to the consolidated sample until the failure is reached or until the stress ratio reaches a constant value. The second part of the test can be carried out in drained (CD) or undrained (CU) conditions. The undrained shear test analyses the variation of pore pressure so it could be very interesting in order to investigate the behaviour of the waste exposed to static or dynamic force in saturated conditions. Indeed, in the developing countries, where the landfills are not covered, the high water content causes a high initial saturation state, which could increase the level of leachate and, especially, compromise the slope stability. In these cases, the analysis of the dissipation of excess pore pressure and of the resulting decrease of effective stress is necessary. The drained triaxial test lets to control the drainage so the development of effective stress during the test and the volume changes can be investigate.

Triaxial tests on waste (Kavazanjian, 2001 and Grisolia et al. 1995) have shown that it can withstand very high strains without reaching failure as can be seen in Figure 8. The reinforcements within waste may be elongating, providing a tensile component of strength without failing within the strain limits of the test. The higher tensile forces in the reinforcements can explain the increasing stiffness at higher displacement.

Zekkos et al. (2007) conducted triaxial tests on waste samples with different fibrous content (Figure 23). They obtained that the specimens with fibres length < 20 mm (A3-L2) reached a peak shear stress conditions at an axial strain of about 22% and then exhibited a post-peak reduction in shear resistance. When fibrous length was > 20 mm the samples (A3-7L with $62\% < 20$ mm) the specimen exhibited a lower stiffness initially, but at larger strains showed a progressive upward curvature without reaching a peak shear stress. Similarly specimen included $14\% < 20$ mm (A3-12L) material by weight, exhibited a more pronounced upward curvature.

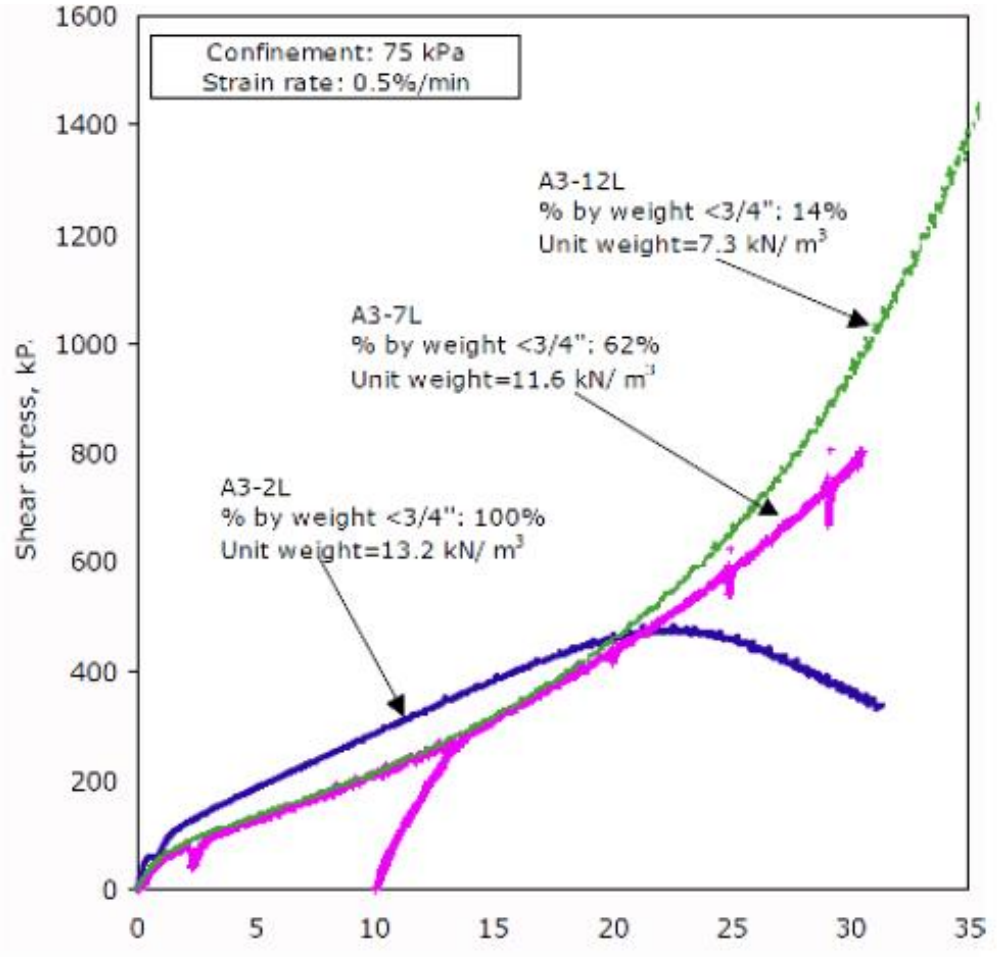

Figure 23 The effects of reinforcement content on shear stress and axial strain on 300 mm dia. triaxial tests on MSW (Zekkos et al., 2007)

Shariatmadari, Lemos Machado, Noorzad, Karimpour-Fard (2009) have evaluated the mechanical behaviour of MSW materials using a large triaxial test apparatus. The shear/strain curves obtained from CD triaxial tests are shown in Figure 24 and Figure 25; they are obtained for two level of confining pressure (50 and 300 kPa) and for various values of fibre content.

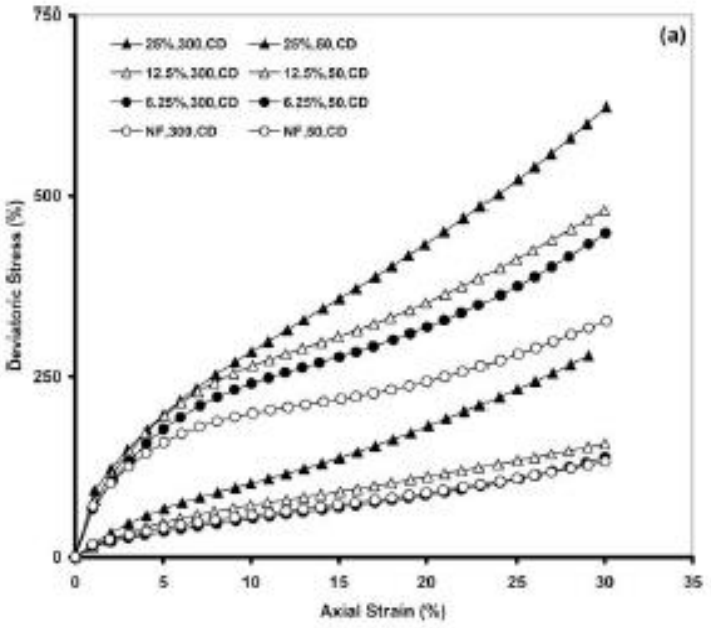

Figure 24 CD triaxial test results at confining pressure of 50 and 300 kPa (deviatoric stress) (Shariatmadari et al., 2009)

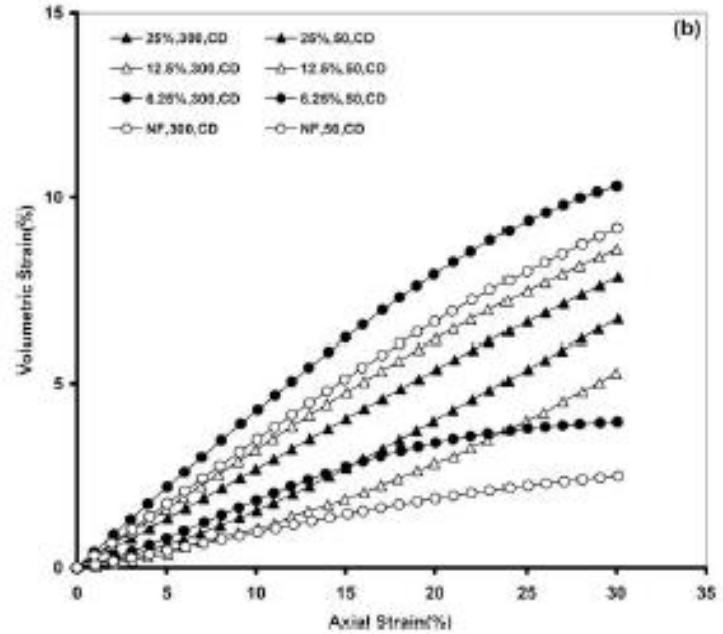

Figure 25 Cd triaxial test results at confining pressure of 50 and 300 kPa (volumetric strain) (Shariatmadari et al., 2009)

The figures show as the shear strength increases with strains and does not reach either a peak or a steady state. Greater values of strains are necessary to mobilize the whole strength of the specimens. Due to this condition some authors have suggested that the design of new landfills and the verify of their stability should be carried out considering the strength that can be mobilized at an accettable value of strain. Another consideration is that the upward concavity is clearer when

the value of fibre content is high. That fact has led Kolsch to assume that the increase of mobilized shear strength with strain could be due to the reinforcing effect of fibers within the waste. Then the samples show a compressive behaviour with a high reduction of volume. At low confining pressure, the specimen with highest fibre content shows the greatest value of volume strain, wich is almost double than the NF one.

3.5.3.3 Bhandari and Powrie (2013)

In order to analyse the behavior of MBT waste Bhandari and Powrie (2012) have carried out a series of monotonic triaxial shear tests on overconsolidated specimens and on lightly consolidated specimens. Two kind of material were examined, the first (full fraction) was composed by the fraction of MBT waste passing a 10 mm sieve and the other (fine fraction) was composed by the friction of MBT waste passing a 2.8 mm sieve. The particles passing through the 2.8 mm sieve are generally three dimensional, therefore they cannot be considered as reinforcing elements. Thus, the investigation of the effect of potential reinforcing elements on the stress-strain-strength characteristics is possible, comparing the results obtained for the two kind of specimens. The samples (71 mm in diameter) were prepared at the as-received moisture content through compression in four layer using a modified oedometer apparatus; higher density specimens were prepared using a vertical stress of 1070 kPa and lower density specimens by compressing each layer to a vertical stress of 100 kPa. Both fractions compressed significantly in response to the increase in vertical stress (Figure 26). The bulk and dry densities of each specimen are given in Table 11. The use of not fully saturated specimens was due to the difficulty of preventing anaerobic gas production within the specimen over the time needed to carry out the shear tests.

Physical property	**High density specimen**		**Low density specime**	
	Full	**Fine**	**Full**	**Fine**
Bulk density (Mg/m3)	1.33-1.37	1.30-1.32	0.96	0.93
Dry density	0.86-0.89	0.78-0.79	0.58	0.49

Table 11 Densities of MBT waste specimens (Bhandari and Powrie, 2013)

The triaxial tests were carried out on overconsolidated sample at different values of cell pressure (25-50-100-200 kPa) and on lightly consolidated specimens at a cell pressure of 100 kPa. Once the consolidation was ended, the samples were sheared in drained condition and the volume changes were recorded. The rate of shearing (expressed in terms of the rate of axial compression as a proportion of the initial specimen height) was 4%/hour for overconsoliated specimens and 6%/hour for lightly consolidated specimens. Shearing was continued until the stress ratio had reached a constant value or had started to decrease. The tests were carried oit in a strain-controlled triaxial apparatus comprising a transparent celle fitted with three external digital cameras. The digital cameras were used to capture images of the deformating specimens at various stages of each test; these images were then used to determine a detailed displacement fields using a novel digital image analysis technique. The results are shown in the following figures (Figure 27, Figure 28).

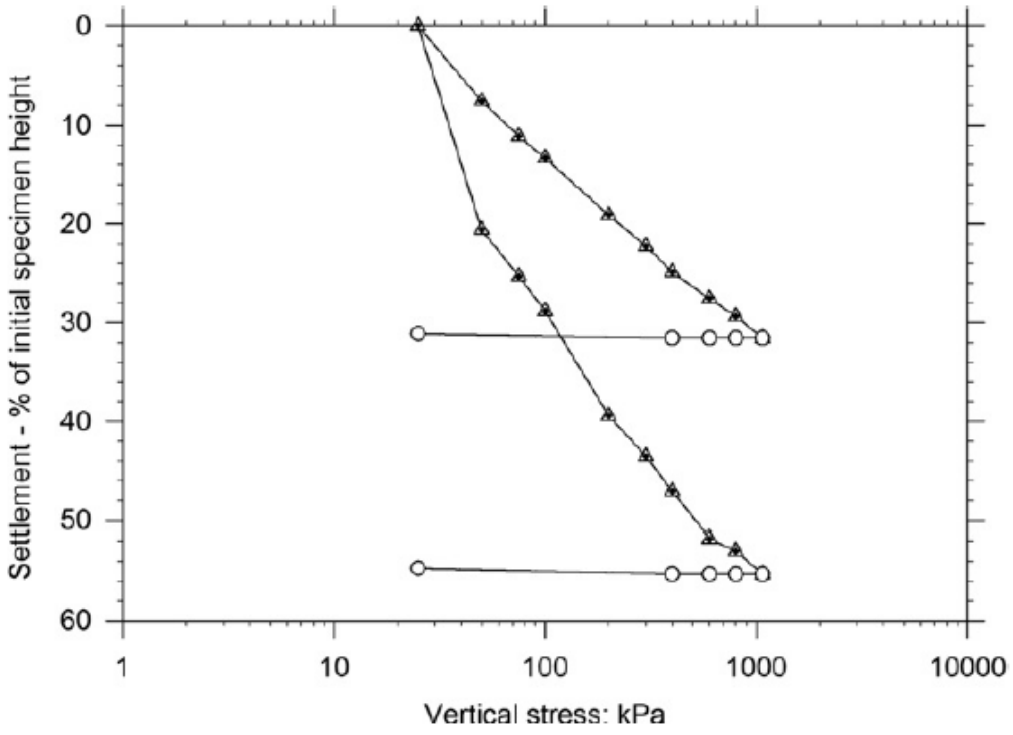

Figure 26 Normalized one-dimensional compression curves: full and fine fraction (Bhandari and Powrie, 2013)

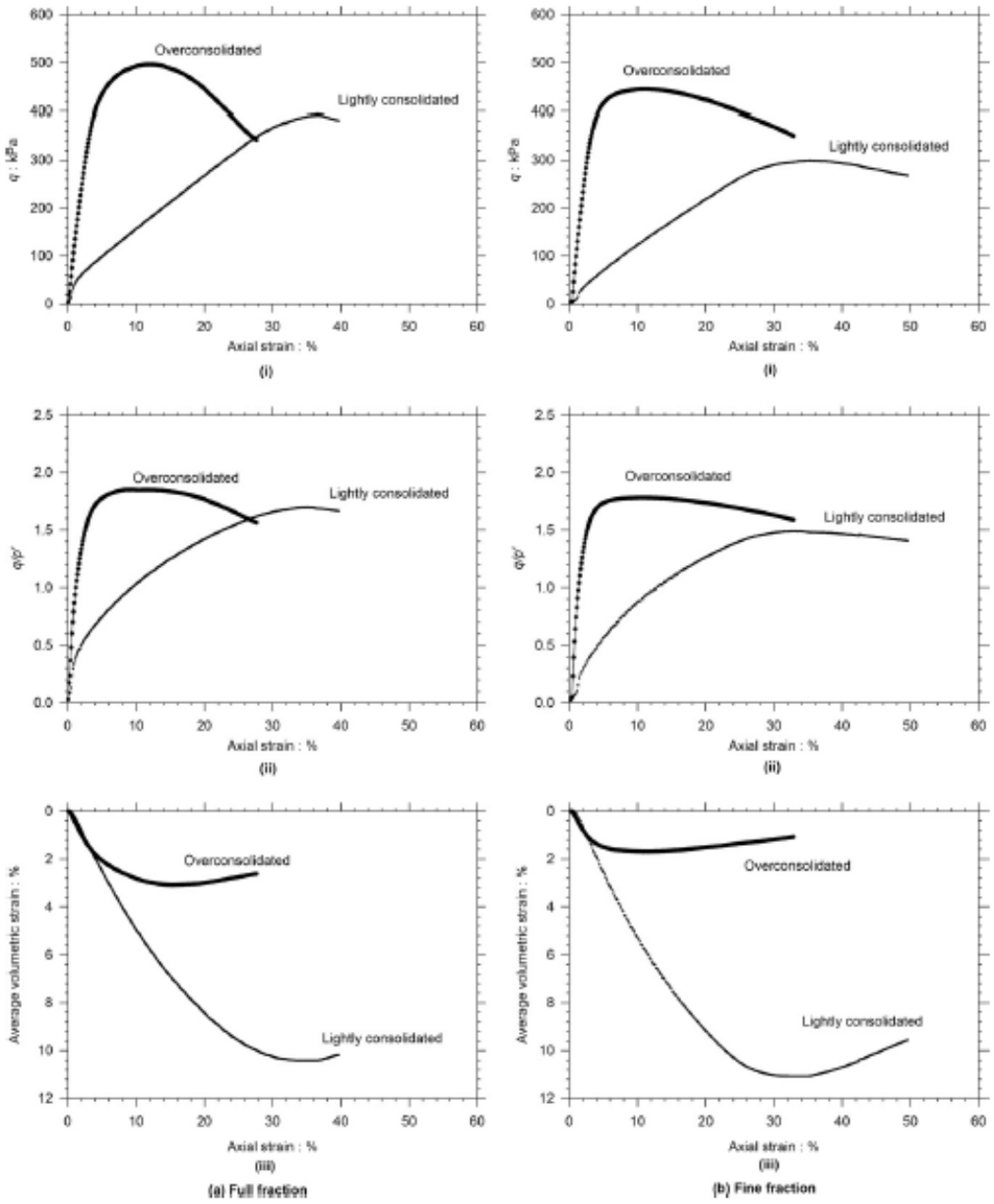

Figure 27 Triaxial test results on over-consolidated and lightly consolidated specimens using a cell pressure of 100 kPa (Bhandari and Powrie, 2013)

Both lightly consolidated specimens underwent substantial volumetric compression (11%) with increasing axial strain, up to an axial strain of about 30%. In terms of deviator stress, a clear peak is reached at an axial strain of about 35%. For the overconsolidated specimens, the maximum volumetric compression was much smaller. The deviator stress peaked was reached at a smaller axial strain. Moreover, the steady state stress ratio achieved was very similar to that

achieved by the corresponding lightly consolidated specimen, after a much greater axial strain.

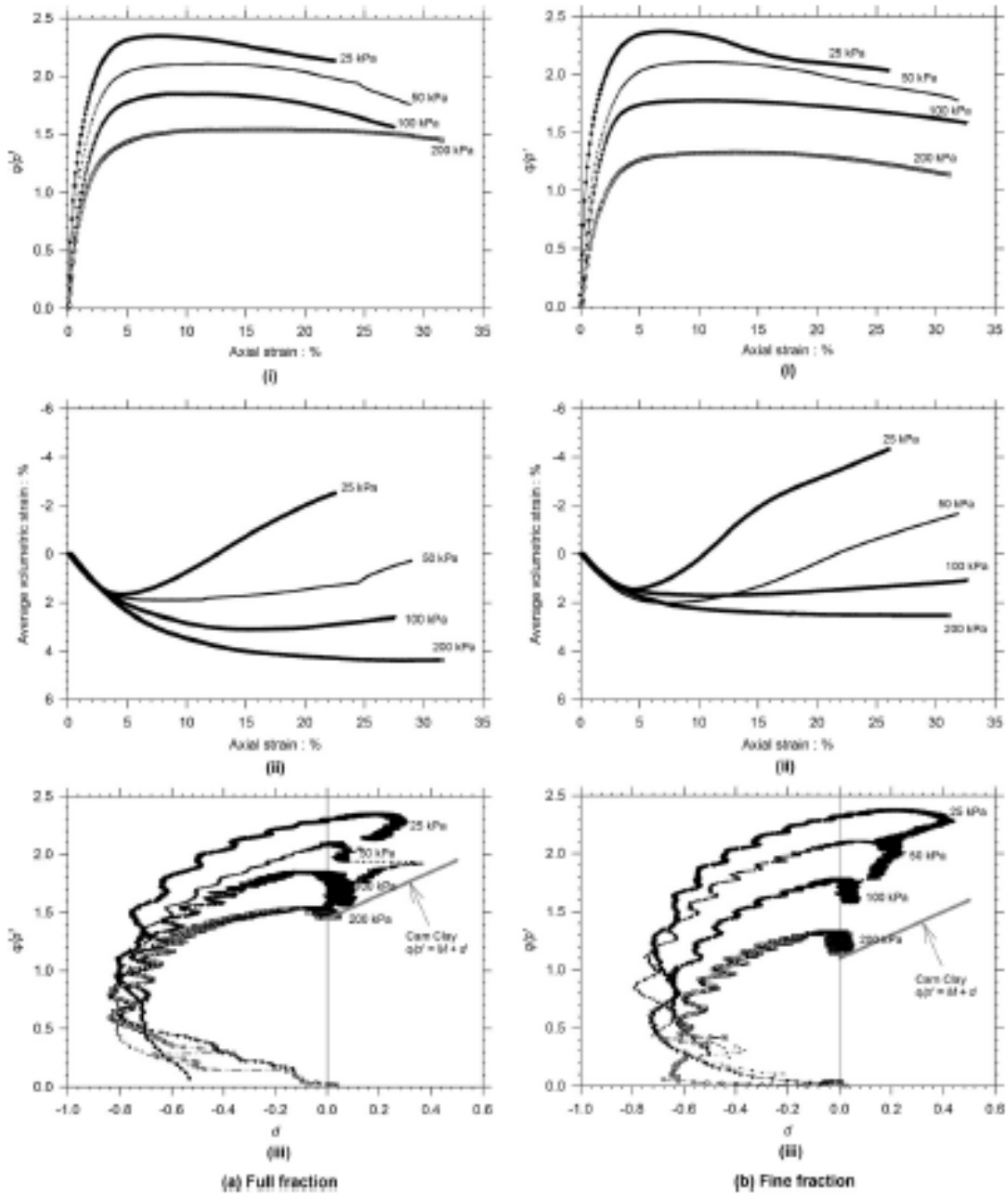

Figure 28 (i) Stress ratio (q/p') plotted against axial strain, (ii) average volumetric strain plotted against axial strain and (iii) stress ratio plotted against rate of dilation d measured for high density specimens (Bhandari and Powrie, 2013)

The experiments reveal that MBT waste is a strong material compared to MSW; in fact, the MBT waste mobilizes its strength rapidly with strains (Table 12). Unlike what happens with MSW specimens, the large scale triaxial test provides a sufficient sample deformation in order to reach a peak deviatoric stress condition. The value of peak stress ratio increases with the reduction of confining pressure as we can see in the first figures. The second figures show that the most dilative behaviour occurred when the specimen was exposed to low confining pressures. However, the values of volume strain are smaller than MSW ones because the MBT process greatly reduces the compressible components; so the compression is mostly due to the reduction of voids within the specimens. The effect of reinforcing elements is clearer when the confining pressure is high; this fact is due to the need for a minimun confining pressure to prevent the pull-out of reinforcing elements. The form of the stress-strain curves indicates that it is quite possible to define stress dependent strength envelopes, rather than adopting a strain-based criterion as has been proposed for unprocessed MSW. However, the specimens tested must be a high enough density, and/or the element test must be continued to a large (~50%) axial strain.

Specimen state	**Fraction**	**Cell Pressure (kPa)**	**Peak stress ratio achieved**	**Axial strain at the peak stress ratio (%)**	**Angle of shear resistance at peak (°)**
Overconsolidated	Full	25	2.34	7.4	57.4
		50	2.11	11.5	51.3
		100	1.85	9.2	45
		200	1.54	16.2	37.8
	Fine	25	2.37	7.3	58.2
		50	2.10	10.6	51.3
		100	1.78	10.8	43.4
		200	1.32	13	32.9

Table 12 Locations of peak stress ratios with respect to axial strain (Bhandari and Powrie, 2013)

The last figures show the stress ratio (q/p') plotted against the rate of dilation d which is defined as the negative of the rate of increase of average volumetric strain ε_{vol} with triaxial shear strain ε_q:

$$\varepsilon_q = 2(\varepsilon_a + \varepsilon_r)/3$$

$$d = -\frac{\delta\varepsilon_{vol}}{\delta\varepsilon_q}$$

The results highlight that the stress ratio associated with a specific value of dilation d is much greater than that indicated by the stress dilation relationship given by Cam Clay:

$$\frac{q'}{p'} = M + d$$

Where M is the value of critical stress ratio and it should be the same for every specimen if they are made from the same material. In fact, M is function of the material's characteristics only and it is not influenced by the confining pressure. In this experiment the critical stress ratio M is defined by the tests carried out using a cell pressure of 200 kPa because the specimens show a more uniform deformation and the dilation has zero value at the end of test. The other specimens tested at low cell pressures were still dilating when the tests were over (Figure 29).

Bhandari and Powrie suggested that the greater value of stress ratio comparing with what predicted by Cam Clay was likely due to the not full saturation of specimens. The generation of suctions within the smaller voids which are not filled by water may be the cause of the high apparent angles of shearing resistance and the stress ratios achieved by the samples tested at low effective cell pressure.

In order to investigate if the not complete saturation condition of samples is the real cause of the greater value of stress ratio, the test could be repeated using fully saturated specimens made by the same MBT waste. With the purpose of suppressing microbial activity and preventing the onset of methanogenesis, it is requested to mix MBT waste with an acid solution, made by 10 g of both acetic acid and propionic acid per litre of water (pH of about 4.5).

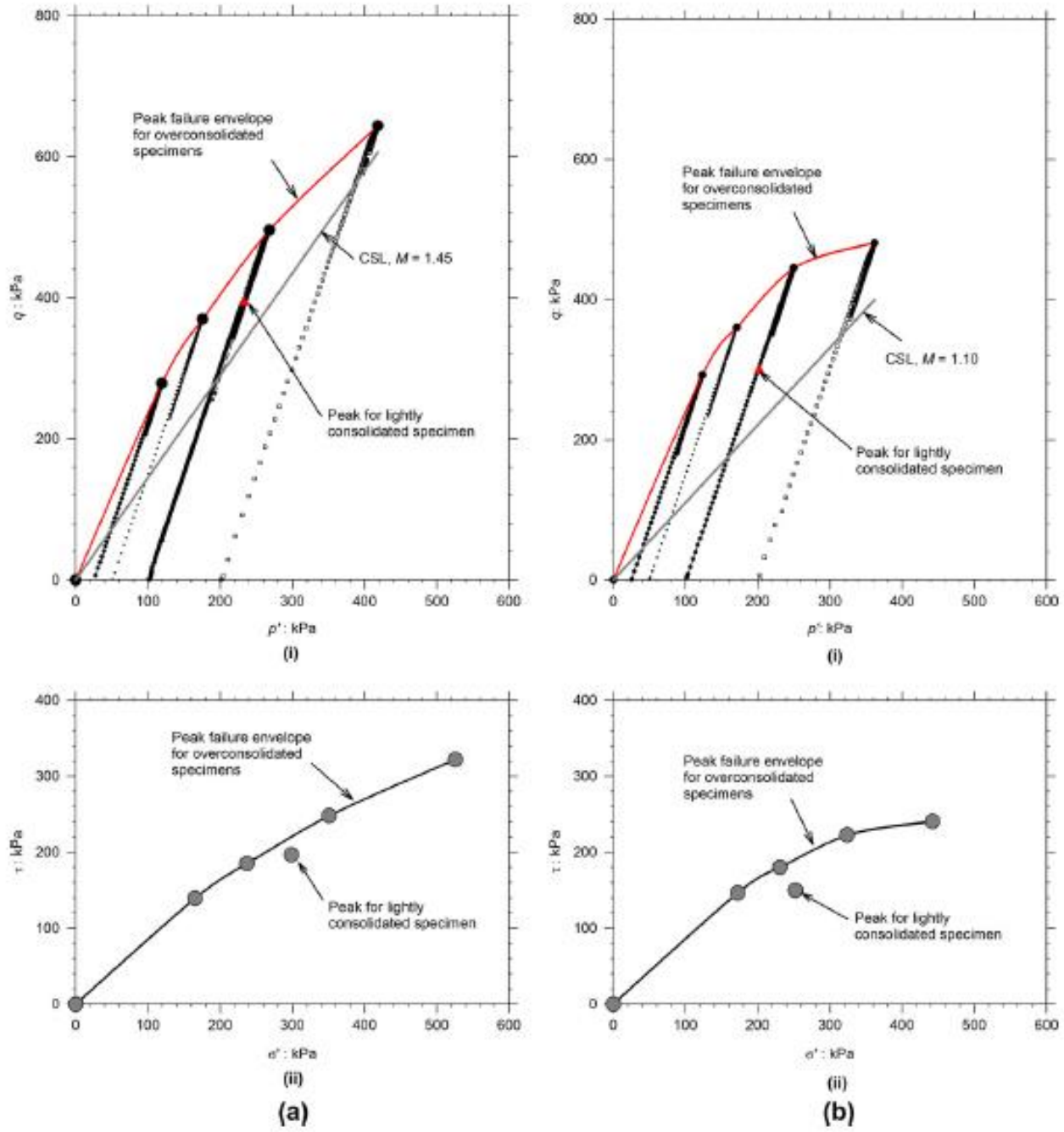

Figure 29 Peak strength failure envelopes for overconsolidated and lightly consolidated specimens (a) full fraction (b) fine fraction (Bhandari and Powrie, 2013)

Chapter 4

Digital image-based deformation measurement system for triaxial test

In recent years, there has been a rapid increase in the use of digital cameras to monitor the deformation of soils in centrifuge model and laboratory small-scale model tests. This is mainly due to there being no need for any contact with soil specimen, and to the increasing availability of inexpensive digital cameras. Furthermore, by employing suitable digital image correlation techniques, effectively continuous information about deformations at both the full field and local micro-scale is possible. Most analyses of the triaxial compression test assume that the soil specimen deforms as a right circular cylinder. In practice, the continuous strain fields associated with this assumed mode of deformation is frequently interrupted by the development of a failure surface, where the displacements concentrate. The measurement of specimen deformation using digital cameras overcomes this problem, but it is complicated by the distortion of the image of the specimen due to the refraction at the interfaces between the cell fluid, the cell wall and the atmosphere.

4.1 Camera calibration

Camera calibration in the context of three dimensional machine vision is the process of determining the internal camera geometric and optical characteristics (intrinsic parameters) and the 3-D position and orientation of the camera frame relative to a certain world coordinate system. Physical camera parameters are commonly divided into extrinsic and intrinsic parameters. The *pinhole camera model* is based on the principle of collinearity, where each point in the object space

is projected by a straight line through the projection centre into the image plane (Figure 30).

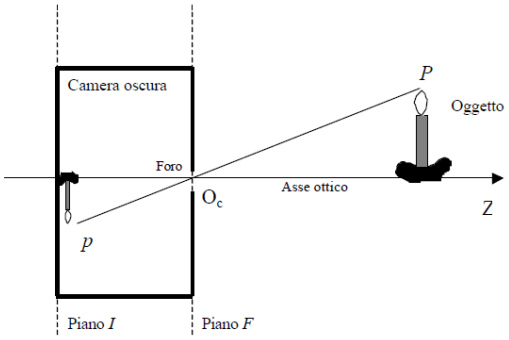

Figure 30 Pinhole camera model.

The origin of the camera coordinate system is in the projection centre at the location (X_0, Y_0, Z_0) with respect to the object coordinate system, and the z-axis of the camera frame is perpendicular to the image plane (Figure 31).

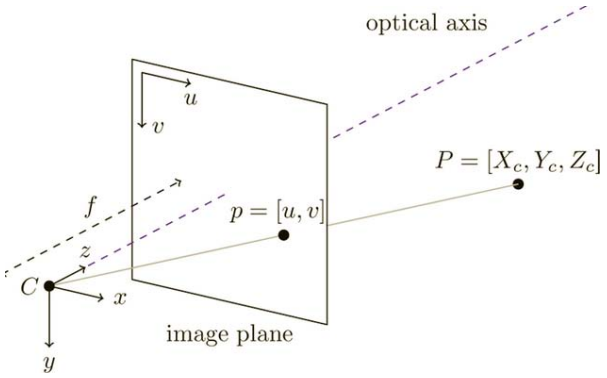

Figure 31 The coordinate system involved in camera calibration.

The rotation is represented using Euler angles ω, φ and κ that define a sequence of three elementary rotations around x, y and z axis respectively.

In order to express an arbitrary object point P at location (Xi, Yi, Zi) in image coordinate we first need to transform it to camera coordinate (xi, yi, zi). This transformation consists of a translation and a rotation, and it can be performed by using the following matrix equation:

$$\begin{bmatrix} x_i \\ y_i \\ z_i \end{bmatrix} = \begin{bmatrix} m_{11} & m_{12} & m_{13} \\ m_{21} & m_{22} & m_{23} \\ m_{31} & m_{32} & m_{33} \end{bmatrix}$$

Where:

$m_{12} = \sin\omega \sin\varphi \cos\kappa - \cos\omega \sin\kappa$ $\qquad$ $m_{11} = cos\varphi cos\kappa$

$m_{22} = sin\omega sin\varphi sin\kappa + cos\omega cos\kappa$ $\quad$ $m_{21} = cos\varphi sin\kappa$

$m_{13} = cos\omega sin\varphi cos\kappa + sin\omega sin\kappa$ $\quad$ $m_{31} = -sin\varphi$

$m_{23} = cos\omega sin\varphi sin\kappa - sin\omega cos\kappa$ $\quad$ $m_{32} = sin\omega cos\varphi$

$m_{33} = cos\omega cos\varphi$

Extrinsic parameters are needed to transform object coordinates to a camera centred coordinate frame. The intrinsic parameters are:

- The effective focal length (f_0) which is the distance between the focal points of a lens (that is, the point at which the lens will focus parallel rays of light) to the centre point of the lens;
- The image centre c_c (u_0,v_0);
- The scale factor (s_u)

Here, as usual in computer vision literature, the origin of the mage coordinate system is in the upper left corner of the image array. The unit of the image coordinated is pixels, and therefore coefficients D_u and D_v are needed to change the metric units to pixels. These coefficients can be typically obtained from the data sheets of the camera and framegrabber. In fact, their precise values are not necessary, because they are linearly dependent on the focal length f and the scale factor s_u. By using the *pinhole model*, the projection of the point (xi, yi, zi) to the image plane is expressed as:

$$\begin{bmatrix} \tilde{u}_i \\ \tilde{v}_i \end{bmatrix} = \frac{f}{z_i} \begin{bmatrix} x_i \\ y_i \end{bmatrix}$$

The corresponding image coordinates (u'_i, v'_i) in pixels are obtained from the projection $(\tilde{u}_i, \tilde{v}_i)$ by applying the following transformation:

$$\begin{bmatrix} \tilde{u}_i \\ \tilde{v}_i \end{bmatrix} = \begin{bmatrix} D_u s_u \tilde{u}_i \\ D_v \tilde{v}_i \end{bmatrix} + \begin{bmatrix} u_0 \\ v_0 \end{bmatrix}$$

The pinhole model is only an approximation of the real camera projection. It is a useful model that enables simple mathematical formulation for the relationship between object and image coordinates. Usually, the pinhole model is a basis that is extended with some correction for the systematically distorted image coordinates. The most commonly used correction is for the radial lens distortion that causes the actual image point to be displaced radially in the image plane. The radial distortion can be approximated using the following expression:

$$\begin{bmatrix} \delta u_i^{(t)} \\ \delta v_i^{(t)} \end{bmatrix} = \begin{bmatrix} \tilde{u}_i(k_1 r_i^2 + k_2 r_i^4 + \cdots) \\ \tilde{v}_i(k_1 r_i^2 + k_2 r_i^4 + \cdots) \end{bmatrix}$$

Where k_1, k_2 are coefficients for radial distortion, and $r_i = \sqrt{\tilde{u}_i^{\,2} + \tilde{v}_i^{\,2}}$. Typically, one or two coefficients are enough to compensate for the distortion.

Centres of curvature of lens surfaces are not always strictly collinear. This introduces another common distortion type, decentring distortion, which has both a radial and tangential component. The expression for the tangential distortion is often written in the following form:

$$\begin{bmatrix} \delta u_i^{(r)} \\ \delta v_i^{(r)} \end{bmatrix} = \begin{bmatrix} 2p_1 \tilde{u}_i \tilde{v}_i + p_2(r_i^2 + 2\tilde{u}_i^{\,2}) \\ p_1\left(r_i^2 + 2\tilde{v}_i^{\,2}\right) + 2p_2 \tilde{u}_i \tilde{v}_i \end{bmatrix}$$

Where $p_1$and p_2 are coefficients for tangential distortions.

A proper camera model for accurate calibration can be derived by combining the pinhole model with the correction for the radial and tangential distortion components:

$$\begin{bmatrix} u_i \\ v_i \end{bmatrix} = \begin{bmatrix} D_u s_u(\tilde{u}_i + \delta u_i^{(t)} + \delta u_i^{(r)}) \\ D_v(\tilde{v}_i + \delta v_i^{(t)} + \delta v_i^{(r)}) \end{bmatrix} + \begin{bmatrix} u_0 \\ v_0 \end{bmatrix}$$

In this model the set of intrinsic parameters (f, s_u, u_0, v_0) is enhanced with the distortion coefficients $k_1, \ldots, k_n, p_1$and p_2. These parameters are also known as physical camera parameters, since they have a certain physical meaning. Generally, the objective of the explicit camera calibration procedure is to determine optimal values for these parameters based on image observation of a known 2-D or 3-D target. In the case of self-calibration, the coordinates of the target points are also included in the set of unknown parameters.

4.1.1 Linear parameter estimation

The direct linear transformation (DLT) was originally developed by Abdel-Aziz and Karara. The DLT method is based on the pinhole camera model and it ignores the nonlinear and tangential distortion components. The calibration procedure consists in two steps. In the first step the linear transformation from the object coordinates (X_i, Y_i, Z_i) to the image coordinates (u_i,v_i) is solved. Using a

homogeneous 3 x 4 matrix representation for matrix **A** the following equation can be written:

$$\begin{bmatrix} u_i w_i \\ v_i w_i \\ w_i \end{bmatrix} = \begin{bmatrix} a_{11} & a_{12} & a_{13} & a_{14} \\ a_{21} & a_{22} & a_{23} & a_{24} \\ a_{31} & a_{32} & a_{33} & a_{34} \end{bmatrix} \begin{bmatrix} X_i \\ Y_i \\ Z_i \\ 1 \end{bmatrix}$$

We can solve the parameters a_{11},…, a_{34} of the DLT matrix by eliminating w_i. We obtain the following matrix:

$$\boldsymbol{L} = \begin{bmatrix} X_1 & Y_1 & Z_1 & 1 & 0 & 0 & 0 & 0 & -X_1u_1 & -Y_1u_1 & -Z_1u_1 & -u_1 \\ 0 & 0 & 0 & 0 & X_1 & Y_1 & Z_1 & 1 & -X_1v_1 & -Y_1v_1 & -Z_1v_1 & -v_1 \\ \vdots & \vdots & \vdots & \vdots & \vdots & \vdots & \vdots & \vdots & \vdots & \vdots & \vdots & \vdots \\ X_i & Y_i & Z_i & 1 & 0 & 0 & 0 & 0 & -X_iu_i & -Y_iu_i & -Z_iu_i & -u_i \\ 0 & 0 & 0 & 0 & X_i & Y_i & Z_i & 1 & -X_iv_i & -Y_iv_i & -Z_iv_i & -v_i \\ \vdots & \vdots & \vdots & \vdots & \vdots & \vdots & \vdots & \vdots & \vdots & \vdots & \vdots & \vdots \\ X_N & Y_N & Z_N & 1 & 0 & 0 & 0 & 0 & -X_Nu_N & -Y_Nu_N & -Z_Nu_N & -u_N \\ 0 & 0 & 0 & 0 & X_N & Y_N & Z_N & 1 & -X_Nv_N & -Y_Nv_N & -Z_Nv_N & -v_N \end{bmatrix}$$

$$\boldsymbol{a} = \left[a_{11}, a_{12}, a_{13}, a_{14}, a_{21}, a_{22}, a_{23}, a_{24}, a_{31}, a_{32}, a_{33}, a_{34}\right]^T$$

The following matrix equation for N control points is obtained:

$$\boldsymbol{La} = \boldsymbol{0}$$

By replacing the correct image points (u_i,v_i) with observed values (U_i,V_i) we can estimate the parameters a_{11},…, a_{34} in a *least squares fashion*. In order to avoid a trivial solution a_{11},…, $a_{34} = 0$, a proper normalization must be applied. Abdel-Aziz and Karara used the constraint $a_{34} = 1$. Then, the equation can be solved with a pseudo-inverse technique. The problem with this normalization is that a singularity is introduced, if the correct value of a_{34} is close to zero. Instead of $a_{34} = 1$ Faugers and Toscani suggested the constraint $a_{31}^2 + a_{32}^2 + a_{33}^2 = 1$, which is singularity free.

The parameters a_{11},…, a_{34} do not have any physical meaning, and thus the first step where their values are estimated can be also considered as the implicit camera calibration stage. There are techniques for extracting some of the physical camera parameters from DLT matrix, but not many are able to solve all of them. Melen proposed a method based on RQ decomposition where a set of eleven physical camera parameters are extracted from DLT matrix. The decomposition is as follows:

$$\boldsymbol{A} = \lambda \boldsymbol{V^{-1}B^{-1}FMT}$$

Where λ is an overall scaling factor and the matrices $\boldsymbol{M}$ and $\boldsymbol{T}$ define the rotation and translation from the object coordinate system to the camera coordinate system. Matrices $\boldsymbol{V}$, $\boldsymbol{B}$ and $\boldsymbol{F}$ contain the focal length l_0, principal point (u_0,v_0) and coefficients for the linear distortion (b_1, b_2):

$$\boldsymbol{V} = \begin{bmatrix} 1 & 0 & -u_0 \\ 0 & 1 & -v_0 \\ 0 & 0 & 1 \end{bmatrix} \qquad \boldsymbol{B} = \begin{bmatrix} 1+b_1 & b_2 & 0 \\ b_2 & 1-b_1 & 0 \\ 0 & 0 & 1 \end{bmatrix} \qquad \boldsymbol{F} = \begin{bmatrix} f & 0 & 0 \\ 0 & f & 0 \\ 0 & 0 & 1 \end{bmatrix}$$

The linear distortion correction is used here to compensate for the vertical hortogonality errors of the image coordinate axes.

4.1.2 Non-linear estimation

Since no iterations are required, direct methods are computationally fast. However, they have at least the following two disadvantages. First, lens distortion cannot be incorporated, and therefore, distortion effects are not generally corrected. The second disadvantage of linear methods is more difficult to be fixed. Since, sue to the objective to construct a non-iterative algorithm, the actual constraints in the intermediate parameters are not considered. Consequently, in the presence of noise, the intermediate solution does not satisfy the constraints, and the accuracy of the final solution is relatively poor. Due to these difficulties, he calibration results obtained are not accurate enough.

With real cameras the image observation are always contaminated by noise. As we know, there are various error components incorporated in the measurement process; if the systematic parts of measurement error are compensated for, it is convenient to assume that the error is white Gaussian noise. Then, the best estimate for the camera parameters can be obtained by minimizing the residual between the model (u_i,v_i) and N observations point (U_i,V_i), where $i = 1, \dots, N$. In the case of Gaussian noise, the objective function is expressed as a sum of squared residuals:

$$F = \sum_{i=0}^{N} (U_i - u_i)^2 + \sum_{i=0}^{N} (V_i - v_i)^2$$

The *least squares estimation* technique can be used to minimize the previous equation. Due to the non-linear nature of the camera model, simultaneous

estimation of the parameters involves applying an iterative algorithm. However, values the optimization without proper initial parameter may stick in a local minimum and thereby cause the calibration to fail. This problem can be avoided by using the parameters from the DLT method as the initial values for the optimization. A global minimum of the previous equation is then usually achieved after few iterations.

Two coefficients for both radial and tangential distortion is normally enough; and the linear distortion in modern CCD arrays is typically negligible. Thus, parameters b_1 and b_2 can be usually left out, and totally eight intrinsic parameters are then estimated.

4.2 Bhandari et al.'s image-based deformation measurement technique for Triaxial Tests

Bhandari et al. (2012) has developed a new image-based technique for triaxial tests on soils using three digital cameras placed on radii interval of 120° viewed on plan outside the transparent cell. This technique permits to obtain the local strain field using images of the deforming cylindrical soil specimen taken at various instants. These images are compare to detect displacements by searching a matched point from on image to another. The technique involves the following main steps:

- *Pre-processing*
  The establishment of measurement points marked on the membrane, which wraps the specimen surface and the determination of their positions in the captured image;

- *Processing*
  The determination of the movements of the measurement points between pairs of successive images using a digital image correlation program;

- *Post-processing*
  The calculation of strain fields.

4.2.1 Determination of measurement points in image

Measurement points are established on the surface of the specimen at equal intervals on the circumferential and vertical axis, with a spacing dependent on the level of analysis detail required. Figure 32 shows the coordinate system adopted for representing points in the image plane (assumed to be in front of the outer cell wall) and on the specimen surface.

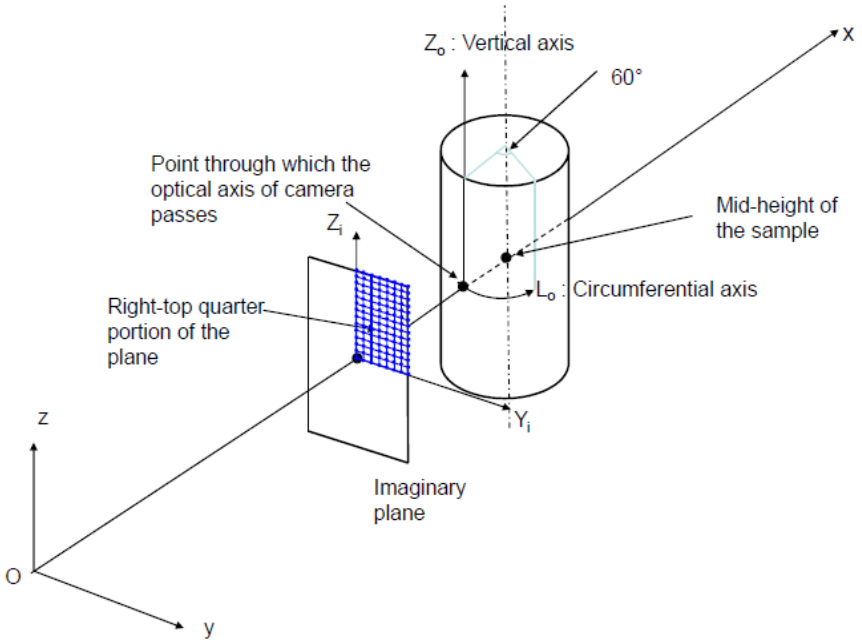

Figure 32 Coordinate axes, specimen and the image plane in front of the triaxial cell.

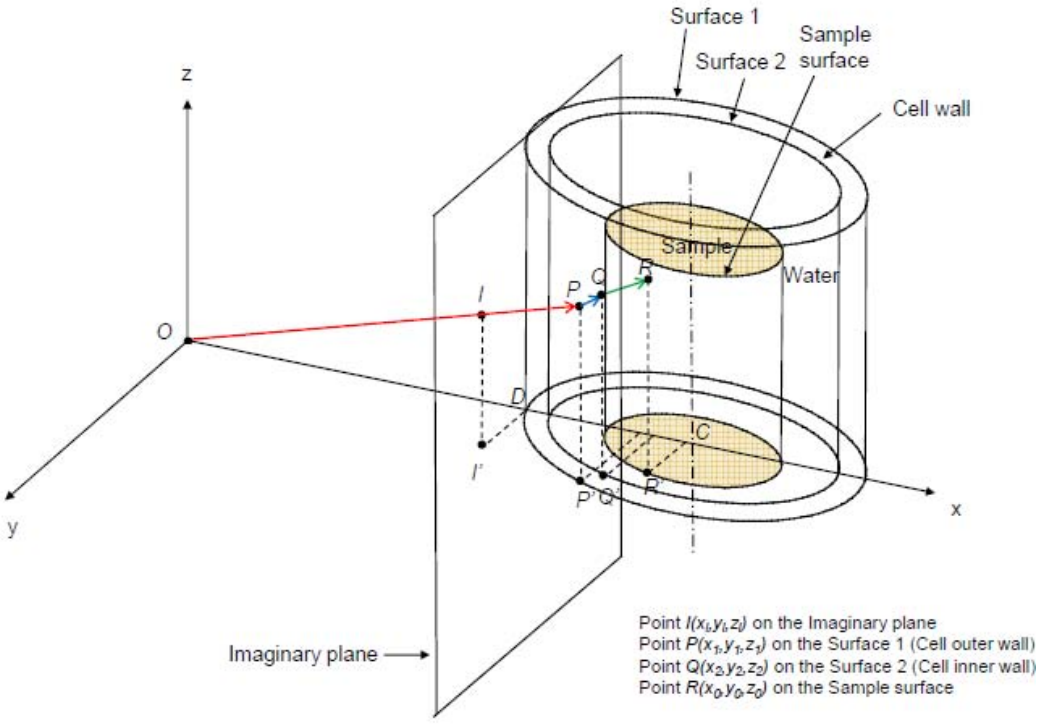

Figure 33 Schematic representation of the ray tracing technique for an individual ray (3D view).

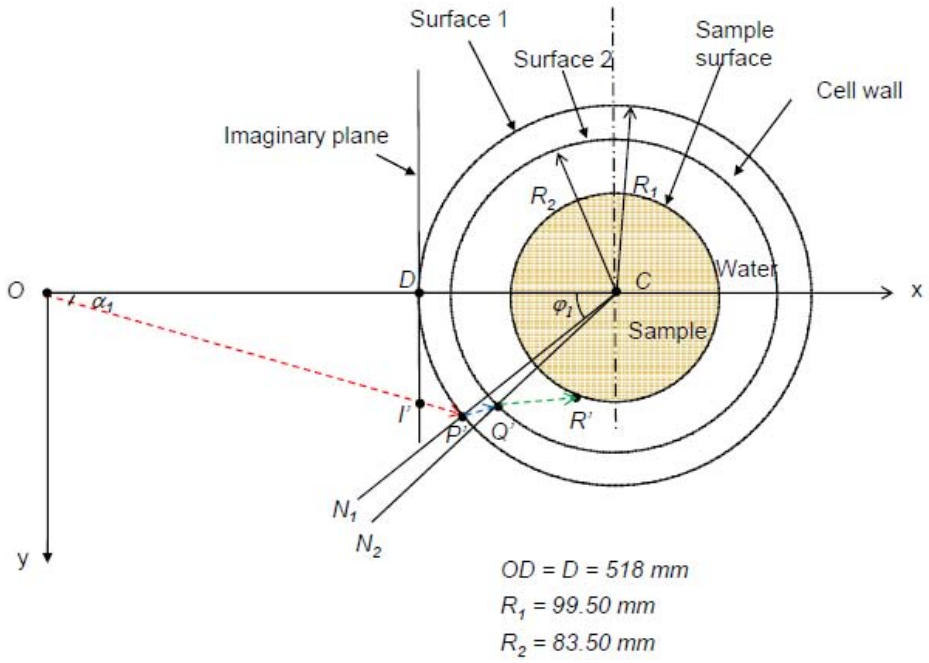

Figure 34 Schematic representation of the ray tracing technique for an individual ray (plan view).

Due to the refraction effects, these points will appear to be irregularly spaced. In fact, there is a passage from the cylindrical coordinate system (θ, r) to the state plane coordinate system of the image plane (Y_i, Z_i). Bhandari et al. (2013) used a *ray tracing technique* to determine the locations of the measurement points in the image plane. Ray tracing involves tracing the path of each ray of light backward from the camera focus and through the image point (in the image plane) to the specimen surface. It is not possible to ray trace the measurement points in the reverse direction (from the specimen surface toward the camera focus), as an infinite number of rays are possible.

4.2.2 Ray tracing

Figure 33 shows an isometric view of a transparent triaxial cell filled with water and a specimen placed inside. The cell outer and inner walls are designated as surface 1 and surface 2, respectively. The axes x, y and z originating from the focus of the camera O are also shown. The x-axis passes normal to the image plane at the mid height of the specimen and intersects the longitudinal axis of the specimen at C. The x-axis is the optical axis of the camera, and the camera is at O facing toward the cell. Ray tracing follows the paths of all rays backward from O through points in the image plane to the specimen surface, in order to determine their locations on the specimen surface. The deviation of the ray at the cell's outer wall (air-cell interface) and inner wall (at the cell-water interface) is governed by the refraction law of Snell. Although ray tracing is conceptually simple, its execution in 3D space is not easy; the problem can be simplified by considering the projections of the incident and refracted rays on the horizontal and vertical planes at each interface.

Exploiting the symmetry of the problem, points representing a quarter-portion of the image plane are ray traced Bhandari (2013) developed a function in MATLAB to ray trace the points located at desired intervals in the quarter image plane shown onto the specimens. In order to cover the 40 mm wide x 80 mm high portion of the image plane at a grid spacing of 0.1 mm (for example), 400 x 800 = 320000 passes through the algorithm are required.

4.2.3 Interpolation of ray traced data

To determine the locations of the measurement points on the image plane using the ray tracing data, a bi-linear interpolation algorithm was developed by Bhandari (2013). This algorithm finds four ray-traced points (Figure 35) to the left and right above and below the measurement points in its close neighbourhood, the locations of which in the image plane are already known from the ray tracing process.

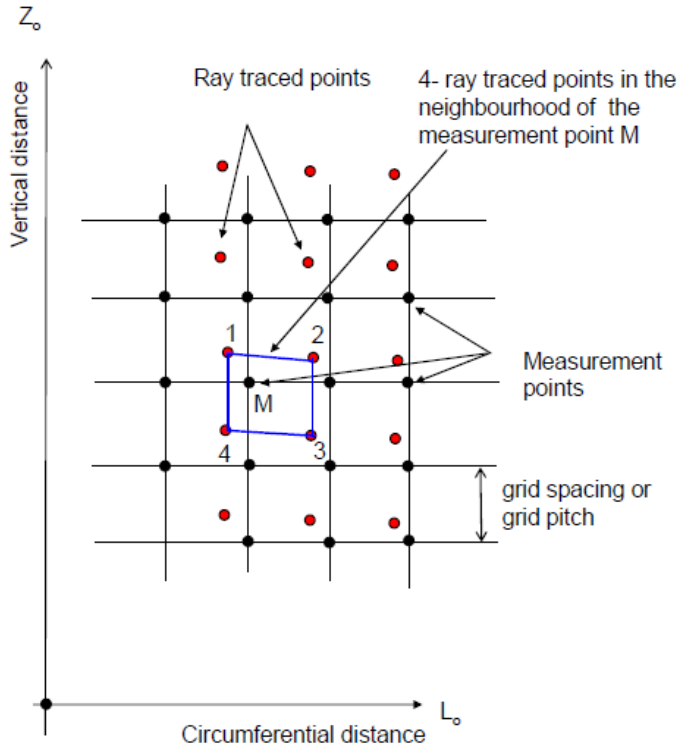

Figure 35 Measurement points and ray traced points on the surface of the unwrapped specimen.

4.2.4 Camera calibration and determination of measurement points in image

The locations of the measurement points were then determined in the actual image (within the camera, in pixel coordinates) using a *pinhole camera model*, establishing a link between the positions of object points and those of their corresponding image points. Camera parameters (i.e. focal length) are obtained

by calibrating the camera using the Camera Calibration Toolbox for MATLAB, using a planar check board as a calibration pattern at different orientations about the image plane position and keeping the camera stationary. The principal point is assumed to be at the image centre, and the lens distortion is assumed insignificant.

4.2.5 Determination of scaling factors

The image scale varies across an image. Therefore, scaling factors (horizontal and vertical) must be applied to components of displacement vectors at the measurement points determined using the digital image correlation technique described later. The scaling factors are obtained by dividing the spacing of measurement points on the specimen surface by the spacing of measurement points on the image plane. Ideally, the scaling factors should be determined over an infinitesimal distance, but this is not feasible. As a result, the scaling factors depend on the chosen spacing of measurement points. To determine the proper scaling factors, a grid spacing of 5 mm or less is adequate.

4.2.6 Digital image correlation

4.2.6.1Principle of matching

The technique of displacement measurement using image analysis involves capturing images of the specimen undergoing shear deformation at various stages of loading. The images are then analysed using a numerical matching technique to identify the most similar patterns in the subsequent images (Figure 36).

An area with multiple pixel points is used to perform the matching process. This area, usually called *subset*, has a unique light density (gray level) distribution inside the subset itself. The basic assumptions are that the patters is approximately constant between successive images and that the local textural information is unique. Figure 37 shows the part of the digital images before and after deformation. The displacement of the subset on the image before deformation

is found in the image after deformation by searching the area of the same light intensity distribution with the subset. Once the location of this subset in the deformed image is found, the displacement of this subset can be determined. If no feature is observed on the surface object, an artificial random pattern must be applied, which can be produced by spraying paint.

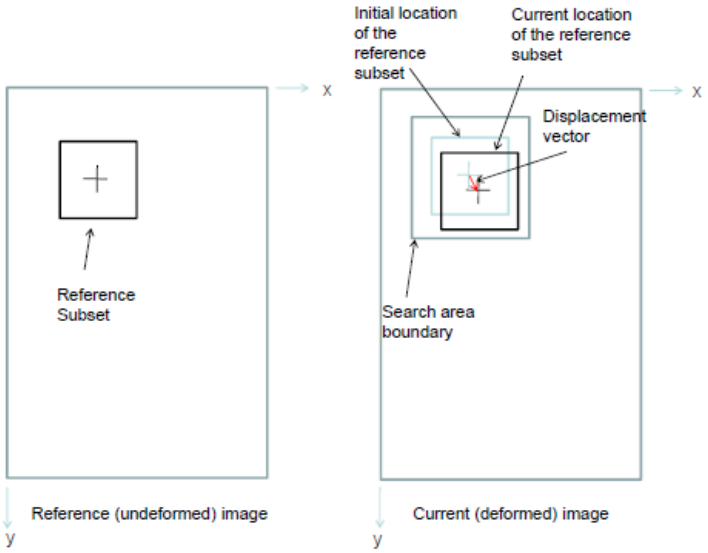

Figure 36 Principle of digital image correlations.

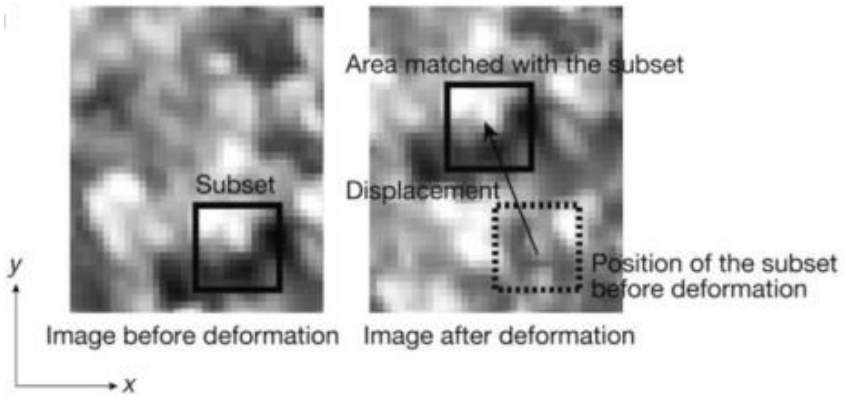

Figure 37 Matching the subset before and after deformation

The matching algorithm compares the image subsets in the reference (undeformed) image to the image subsets in the current (deformed) image. For an example, an image subset **t** from the reference image (template) of size N x N pixels and an image subset **s** from the current image size M x M pixels can be compared by computing the normalized cross correlation coefficient:

$$C_n(u,v) = \frac{\sum_{x=1}^{N}\sum_{y=1}^{N}(t(x,y)-\bar{t})(s(u+x,v+y)-\bar{s}_{u,v})}{\sqrt{\sum_{x=1}^{N}\sum_{y=1}^{N}(t(x,y)-\bar{t})^2}\sqrt{\sum_{x=1}^{N}\sum_{y=1}^{N}(s(u+x,v+y)-\bar{s}_{u,v})^2}}$$

The indices u and v are valid in the range {1,…,M-N} and the elements of t and s refer to grey level intensity values. $\bar{t}$ represents the arithmetic mean of the gray level of reference subset and $\bar{s}_{u,v}$ represents the arithmetic mean of the gray level of the current image subset underneath the reference subset, the left corner of which lies on pixel (u,v). Therefore, displacement components are obtained by searching the best set of displacements after deformation (u,v) which maximize $C_n(u,v)$. A MATLAB executable interface function implementation of this correlation coefficient is used in the form of a dynamic link library of OpenCV, the open source computer vision library available at http://SourceForge.net/projects/opencvlibrary. This function is computationally efficient compared with the built-in function "normxcorr2" in MATLAB.

4.2.6.2 Sub-pixel interpolation

The pixel points within the subset usually locate among the pixels on the deformed image. In addition, the subset can be deformed along with the deformation of the object surface. In a digital image, gray values can exist on discrete pixel points. In order to calculate the correlation on the position among pixel points and to allow the deformation of the subset, therefore, the values of gray level among the pixel points are required.

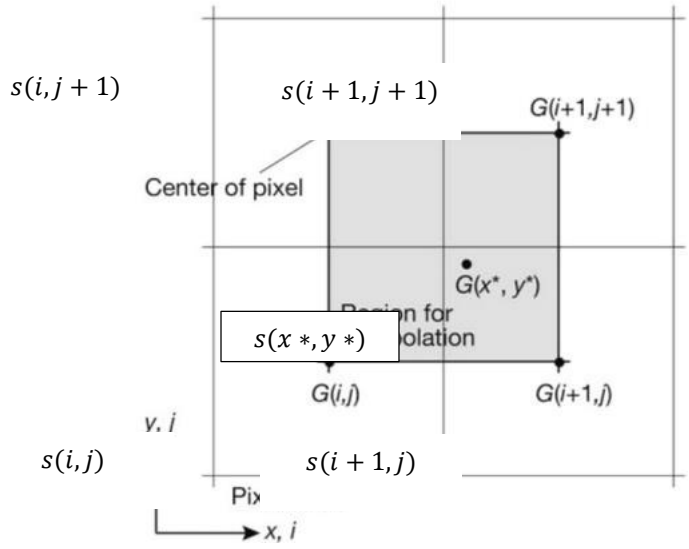

Figure 38 Pixel points and interpolating region for bilinear interpolation

The simplest approach to obtain the value of gray level among the pixels is a bilinear interpolation. Figure 38 shows the neighbouring four pixel points. It is assumed that the gray level of the pixel is the value at the centre of the pixel. In this figure, four squares represent the four pixel, and $s(i,j)$, $s(i+1,j)$, $s(i,j+1)$, $s(i+1,j+1)$ express the gray levels at the center points of the pixels. Here,(i,j), $(i+1,j)$, $(i,j+1)$, $(i+1,j+1)$are the integer pixel position. The gray level $s(x*,y*)$ at the point $(x+u,y+v)$ among the integer pixel points is obtained as:

$$s(x*,y*) = a_{00} + a_{10}u' + a_{01}v' + a_{11}u'v'$$

Where u' and v' are te distance along the x and y from (i,j) to $(x+u,y+v)$, that is, $u' = x* - i$ and $v' = y* - j$, and they lie in the rage of $0 \leq u' < 1$ and $0 \leq v' < 1$. a_{00}, a_{10}, a_{01}, a_{11} are the coefficients on the bilinear interpolation function. These coefficients can be determined from the gray levels at the integer pixel point as:

$$a_{00} = s(i,j)$$

$$a_{10} = s(i+1,j) - a_{00}$$

$$a_{01} = s(i,j+1) - a_{00}$$

$$a_{11} = s(i+1,j+1) - a_{00} - a_{10} - a_{01}$$

Various interpolation methods other than the bilinear interpolation, such as bi-cubic interpolation and spline interpolation, have long been used. However, is is noted that the gray level obtained at a fractional pixel point by any interpolation technique is essentially not an actual value but just an interpolated and deduced value. Figure 39 shows a discrete 10 x 10 pixels region of an original image and the interpolated results by bilinear interpolation and bi-cubic interpolation. It is observed that continuous light intensity distribution is obtained by interpolation.

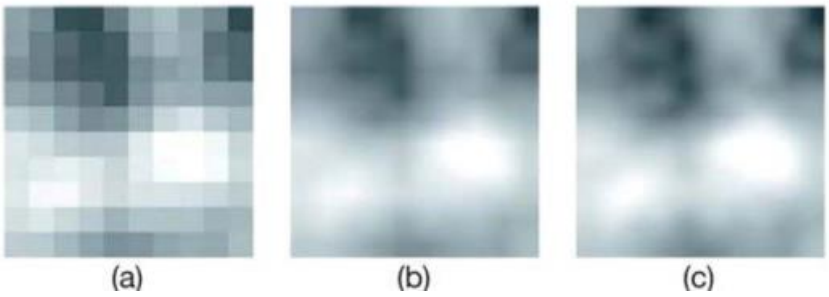

Figure 39 10 x 10 region (a) bilinear interpolation (b) bi-cubic interpolation (c)

In order to estimate the displacement vector to a sub-pixel resolution, Bhandari et al. (2013) fit a *bi-cubic interpolation function* evaluated at 1/100th pixel intervals to the region close to the correlation peak. With added computational cost, this interval could be reduced further to improve the resolution of the calculation.

4.2.7 Calculation of strain fields

During shearing, images of the specimen are captured at close intervals and analysed incrementally. The measurement points are typically at a 5 mm grid spacing, and the values of the displacement components obtained are small in comparison with this. Small strain theory is therefore used in the calculation of strain components.

Having determined the displacements components in both the x (circumferential) and y (vertical) directions at each measurement point, the region was divided into quadrilateral elements.

4.2.7.1 Determination of strains

A bilinear quadrilateral and its eight nodal degrees of freedom are shown in Figure 40.

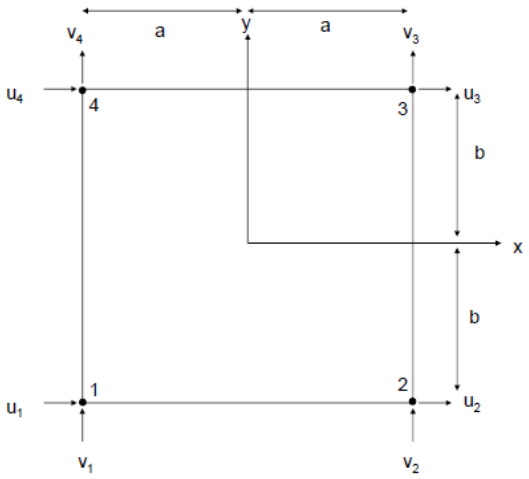

Figure 40 Four-nodded quadrilateral element; x and y represent the circumferential and vertical directions.

The displacement functions u and v can be represented as:

$$u = u_1N_1 + u_2N_2 + u_3N_3 + u_4N_4$$

$$v = v_1N_1 + v_2N_2 + v_3N_3 + v_4N_4$$

$$\begin{Bmatrix} u \\ v \end{Bmatrix} = \begin{bmatrix} N_1 & 0 & N_2 & 0 & N_3 & 0 & N_4 & 0 \\ 0 & N_1 & 0 & N_2 & 0 & N_3 & 0 & N_4 \end{bmatrix} \begin{Bmatrix} u_1 & v_1 \\ u_2 & v_2 \\ u_3 & v_3 \\ u_4 & v_4 \end{Bmatrix}$$

Where $N_1, N_2,\ N_3,\ N_4$ are shape functions that describe the variation of the displacement within an element, defined as follows:

$$N_1 = \frac{(a-x)(b-y)}{4ab}$$

$$N_2 = \frac{(a+x)(b-y)}{4ab}$$

$$N_3 = \frac{(a+x)(b+y)}{4ab}$$

$$N_4 = \frac{(a-x)(b+y)}{4ab}$$

And $u_1, v_1, u_2,\ v_2,\ u_3,\ v_3,\ u_4,\ v_4$ represents the circumferential and vertical displacement components (x,y) at the four nodes (1,2,3 and 4).

Following soil mechanics convention, whereby compression is positive and the strain is calculated as:

$$\varepsilon = \begin{bmatrix} \frac{\partial}{\partial x} & 0 \\ 0 & \frac{\partial}{\partial y} \\ \frac{\partial}{\partial y} & \frac{\partial}{\partial x} \end{bmatrix} \begin{Bmatrix} u \\ v \end{Bmatrix}$$

$$\varepsilon = -[\boldsymbol{B}]d$$

$$\varepsilon = \{\varepsilon_x \quad \varepsilon_y \quad \varepsilon_z\}^T$$

$$[\boldsymbol{B}] = \frac{1}{4ab} \begin{bmatrix} -(b-y) & 0 & (b-y) & 0 & (b+y) & 0 & -(b+y) & 0 \\ 0 & -(a-x) & 0 & -(a+x) & 0 & (a+x) & 0 & (a-x) \\ -(a-x) & -(b-y) & -(a+x) & (b-y) & (a+x) & (b+y) & (a-x) & -(b+y) \end{bmatrix}$$

$$d = \{u_1 \quad v_1 \quad u_2 \quad v_2 \quad u_3 \quad v_3 \quad u_4 \quad v_4\}^T$$

The principal strains are:

$$\varepsilon_1 = \frac{(\varepsilon_x + \varepsilon_y)}{2} + \sqrt{\frac{1}{4}(\varepsilon_x - \varepsilon_y)^2 + \left(\frac{\gamma_{xy}}{2}\right)^2}$$

$$\varepsilon_3 = \frac{(\varepsilon_x + \varepsilon_y)}{2} - \sqrt{\frac{1}{4}(\varepsilon_x - \varepsilon_y)^2 + \left(\frac{\gamma_{xy}}{2}\right)^2}$$

The maximum shear strain is:

$$\gamma_{max} = \varepsilon_1 + \varepsilon_3$$

The volumetric strain is:

$$\varepsilon_{vol} = \varepsilon_1 + 2\varepsilon_3 = \varepsilon_x + 2\varepsilon_y$$

Strain in the radial direction is assumed to be equal to the strain in the circumferential direction.

Chapter 5

Material and methods

MBT residue is finer and more heterogeneous in composition and structure than row or shredded MSW. The MBT waste tested was a fraction passing a 10 mm sieve of the output from the New Earth Solutions MBT plant, Dorset, England. The first stage of processing involved mechanical sorting to extract recyclable materials. The remaining waste was shredded and screened, and further ferrous metal extracted. The waste was then composted in forced aerated windrows, regularly wetted and turned, in a fully enclosed hall for a period of six weeks, the composted material was then screened down to 10 mm to remove any remaining dry recyclables.

5.1 Determination of the moisture content

The MBT used was recovered in a double black plastic bag in a room without any temperature control. It is easy to understand that these conditions should affect the moisture content of the material. In fact, the values obtained were quite different from what expected to find comparing with previous study on the same material (Fernando, 2012; Velkushanova et al., 2009).

Six samples of MBT were oven dried at 70° C to determine the moisture content. The dried samples were allowed to cool at room temperature and the mass was determined at 24 hour intervals. When weight difference between two consecutive readings was constant or less than 1% of the original mass, it was considered that the waste had achieved a dry state. The moisture content was expressed as the ratio of the mass of water to the mass of waste solids:

$$w = \frac{m_{wet} - m_{dry}}{m_{wet}}$$

The moisture contents obtained are summarized in the following Table 13:

	1	**2**	**3**	**4**	**5**
Mass of wet MBT (g)	12.3	13.1	13.3	13.44	30.85
Mass of dry MBT (g)	6.86	7.23	7.43	5.92	7.63
Mass of moisture (g)	5.44	5.87	5.87	4.43	6.02
Moisture content w	79%	81.2%	79%	74.83%	78.89%

Table 13 Moisture content.

5.2 Analysis of 0-10 mm MBT waste

The waste analysis was obtained from the results of previous study where the same MBT was used. The analysis were conducted identifying the waste by material type. Following existing model (Dixon and Langer, 2005; Kolsch, 1995) waste was sorted into the following particles:

- Flexible plastic
- Stiff plastic
- Textile/wool
- Glass
- Ceramic
- Stone
- Metal
- Paper
- Wood
- Bones
- Rubber

The categories of the material listed above give an indication of the mechanical properties (density, brittleness, flexibility) of the various material type. The category defined as "unidentifiable" is composed by particles, which were composites, smeared with soil like material or otherwise visually unidentifiable.

The fraction whose dimensions were less than 63 μm was analysed using a Loss on ignition (LOI) analysis and an X-ray Fluorescence (XRF) Analysis. This last analysis was carried out at the GAU-Radioanalytical Laboratories at the National Oceanography Centre, Southampton (UK). The LOI loss was predominantly

Carbon, Hydrogen and Oxygen. The results are summarised in the following Table 14.

Material	**% of total dry mass**
Waste composition by material type 0-10 mm fraction MBT	
Plastic (flexible)	2
Plastic (stiff)	4
Glass	17
Ceramic	2
Stones	1
Metal	Very small
Paper	Very small
Textiles	Very small
Unidentifiable >5mm	30
Fines <5mm	43

Loss of ignition (LOI) and X-Ray Fluorescence (XRF) analysis of the fraction below 63 µm												
XRF Analysis												
Compound name	SiO_2	TiO_2	Al_2O_3	Fe_2O_3	MnO	MgO	CaO	K_2O	Na_2O	P_2O_5	S	Sum
% of total by weight	23.48	0.366	4.97	2.04	0.062	1.07	10.00	0.80	0.50	1.42	0.10	44.81
Loss-on-ignition (LOI_{450}), % of total by weight												55.79

Table 14 Characterization of MBT waste.

Figure 41 MBT sample (0-10 mm fraction)

5.3 Oedometer test

5.3.1 Sample preparation

The geotechnical analysis of fully saturated sample of waste is very rare, mostly because the difficulty of preventing anaerobic gas production within the specimen over the considerable length of time needed to carry out the geotechnical test. In fact, the contact with water accelerate the biodegradation process, inducing many changes in the waste structure and making the results useless. In this research, the aim of analysing MBT waste sample in fully saturated condition has requested the use of a bacteria inhibitor. Siddiqui (2013) has analysed the effect of biodegradation on settlement and hydraulic properties comparing two different MBT waste, one with suppressed microbial activity and one where the biodegradation was allowed. In order to prevent the onset of methanogenesis, he added 80 litres of leachate mixed with acetic and propionic acid at a concentration of 10 grams per litre to the waste. Inhibition by organic acids accumulation has been demonstrated in numerous studies (Gachet et al, 2003; Bayard et al., 2005; Ivanova et al., 2008). In this research, an acid solution with the same concentration of acetic and propionic acid has been used for the saturation of the MBT waste (pH 4.5).

Figure 42 Mixing procedure

Each sample has been consolidated in four layers so, after weighing 928 g of MBT waste, the full amount was divided into 4 equal sized chunks (232 g) and placed in a container with a lid and cover with the acid solution. In order to have a complete saturation the waste has been mixed with the acid solution using a knife. After reaching a sludge consistency, the waste has been leaved in the sealed container for at least one day (Figure 43).

Figure 43 MBT waste mixed with acid solution three days after the sealing.

5.3.2 Sample consolidation

The oedometer is used to carry out one-dimensional compression tests on saturated samples of Mechanically Biologically Treated waste. The sample is retained in a steel sampler and it is subject to a uniform compressive strain by the application of a vertical load. The sampler was higher than the normal one; in fact, its height was 165 mm in order to retain the whole waste specimen. Two-way vertical drainage is permitted through porous stones at the top and the bottom. The porous discs were placed before in deaired water within a vacuum jar and left there for at least 30 minutes. The vertical stress was applied on a plate which diameter perfectly suits with the sampler; this perfect matching was necessary in order to avoid leak of MBT material during the consolidation, especially under low stresses, when the material is not enough compacted to be

solid. The plate had also two little hole, diametrically opposite, used to let the drained water bleed out. In order to reduce the friction between the plate and the inner wall of the sampler a common grease was applied, especially during the first phase of consolidation, when the higher settlement values were recorded. The bigger dimension of the sampler requested the use of a particular load system where the load sticks were much longer than what used normally (Figure 44).

Figure 44 Oedometer apparatus

The different dimensions have created many instability problems, partly due to the length of the load stick but also to the incompatibility between the load point above the plate and the head of the load stick. In fact, the steel stick was manually cut from a longer piece, therefore its head was not well shaped and the hole above the plate, used as load position, was too large comparing with the diameter of the stick. For these reasons, the load stick has fallen down very often during the test and, when the load was too high, it has bent under the load applied (Figure 45, Figure 46). A bandage has been used in order to connect the three stick and make the system stiffer, but this attempt did not work even if some improvement has

been shown. Therefore, the data obtained from this test are affected by the continuous instability of the machinery and they cannot be considered entirely reliable. However, this modified oedometer has been perfectly useful in order to achieve fully consolidated specimens. The settlements were recorded manually using a stop-watch and a dial gauge.

Figure 45(a) Bended load stick.

Figure 45(b) Bended load stick.

Figure 46 Bended load sticks.

The saturated MBT waste was compacted in four layers increasing loads from 25 kPa to 1000 kPa. The MBT waste, mixed with the acid solution, was liquid; therefore, it was necessary to start loading use a very low normal stress (25 kPa) in order to avoid any material spill.

The content of the first sealed bowl was then decanted into the 70 mm mould and the upper plate sprinkled with grease in order to reduce the friction with the inner wall of the sampler. The sample was placed in the oedometer, registering the initial height. After lifting the load hanger and yoking to position load point within the upper plate, a vertical stress of 25 kPa was applied and the height monitored. The dial gauge readings were taken after 4", 8", 15", 30", 1', 2', 3', 6', 10',15' 30'… until at least 1 hours.

In order to provide an indicative value for the time requested for consolidation, the results obtained by Siddiqui (2013) for the MBT waste, whose microbial activity was inhibited, have been used. Considering the Terzaghi's theory of one-dimensional consolidation, the value of the consolidation coefficient c_v is expressed by the following equation:

$$c_v = \frac{kE'_0}{\gamma_w}$$

Where k is the hydraulic conductivity of the waste,

E'_0 is the constrained modulus $\frac{\Delta\sigma'_v}{\Delta\varepsilon_v}$,

γ_w is the unit weight of water.

The time for completion of primary settlement for one layer is estimated by the following expression:

$$t = \frac{Td^2}{c_v}$$

Where d is the maximum drainage path length, for two-way drainage, the maximum drainage path length d=h/2 for a waste sample of height h.

T is the time factor, which is about 1 when the primary settlement is complete (Powrie, 2004).

The results obtained for two loading stages (50 kPa and 150 kPa) are summarised in the following Table 15:

	50 kPa	**150 kPa**
k (m/s)	4,24E-05	3,6E-06
E'0 (kPa)	203,14	1755,01
γw (kN/m3)	9807	9807
cv (m2/s)	8,78E-07	6,44E-07
d (m)	0,0225	0,021
t (s)	576,4211	684,5303
t (m)	9,607019	11,40884

Table 15 Estimated time for consolidation.

At the light of the first Oedometer results, the time interval requested for the consolidation seemed to be longer than what expected; an interval of one hour has been used; it is considered enough not only to complete the consolidation but also for analysing the secondary settlement.

When the primary consolidation is considered ended the load has been increased to the successive step. The normal stress is doubled each stage (25 kPa, 5 kPa, 125 kPa, 250 kPa, 500 kPa, 1000 kPa). On completion of layer consolidation, the top surface of the material was roughen to minimize artificial internal interface effect (Figure 47) and the next layer was added. The fourth layer has been added in two stages because the reduced height of the mould could not contain the overall wet material. In order to reduce consolidation time, the second part of the 4th layer was added after the consolidation under 25 kPa because the large settlements values permitted to free up enough space. During the consolidation the sample was always maintained wet adding acid solution to the cell and to the top of the mould.

Figure 47 Scrabbled surface between two consecutive layers.

At the end of the consolidation, the samples have been extrude from the sampler and covered using plastic wrap in order to avoid any moisture loss.

5.3.3 Results

The measured data of LVDT and time can be readily be converted to obtain the settlements-log(t) and settlements-$\sqrt{t}$ curves for each layer of the four samples. Each of these curves shows an inflection point so that the time of the end of primary consolidation could be determined using graphical construction method. However, the position of the inflection point becomes more difficult to identify with the increase of normal stress applied. At the higher load, the curves become more flat suggesting that the primary settlements have more or less the same value of the secondary ones. The most of the settlements are achieve during the first load stages, in particular the first one. When the vertical stress of 25 kPa was applied, the height usually reduced of the 15% of the initial value in the first minute, most of all during the first four second. This was mainly due to the high wet condition of the waste, which looked like slurry. The curves obtained for the first load step shows a more identifiable inflection point and the primary consolidation contribute is much more evident than secondary settlement one. Anyway, the curves which shows the settlements plotted against the square root of time is the best choice in order to better distinguish the primary compression from the secondary one, which is only due to the creep phenomena because the biodegradation was suppressed, thanks to the use of the acid solution.

The settlement values recorded cannot be discussed in a specific way because the frequent instability of the load system made impossible to obtain reliable results with continuity. In fact, the dial gauge is sensible enough to perceive even the minimum displacement of the load stick so the results recorded are highly disturbed. The instability problems have occurred especially during the application of the highest normal stresses (250 kPa, 500 kPa and 1000 kPa). In particular, during the consolidation of the last layer of each sample, the load stick bended frequently (Figure 45) making impossible to carry out the test with continuity. However, the data obtained are good enough to say that the MBT waste can be considered completely consolidated at the end of the test.

5.3.3.1 First Sample

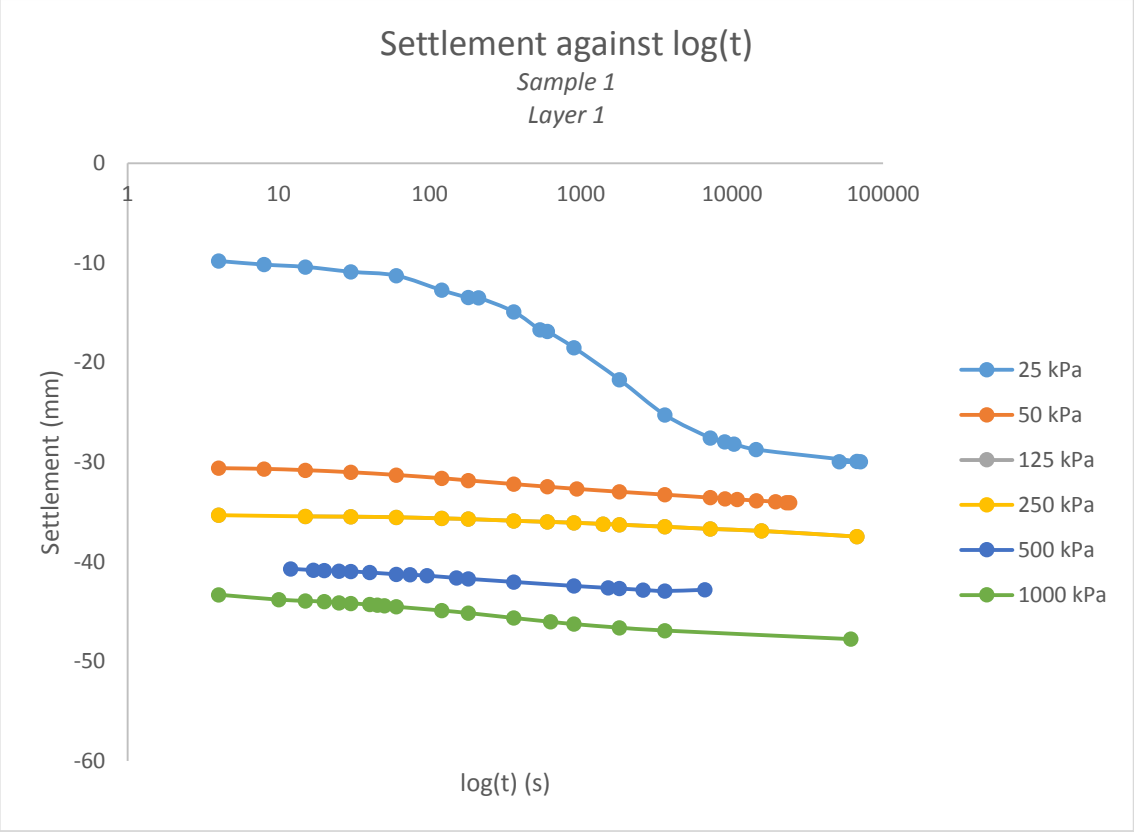

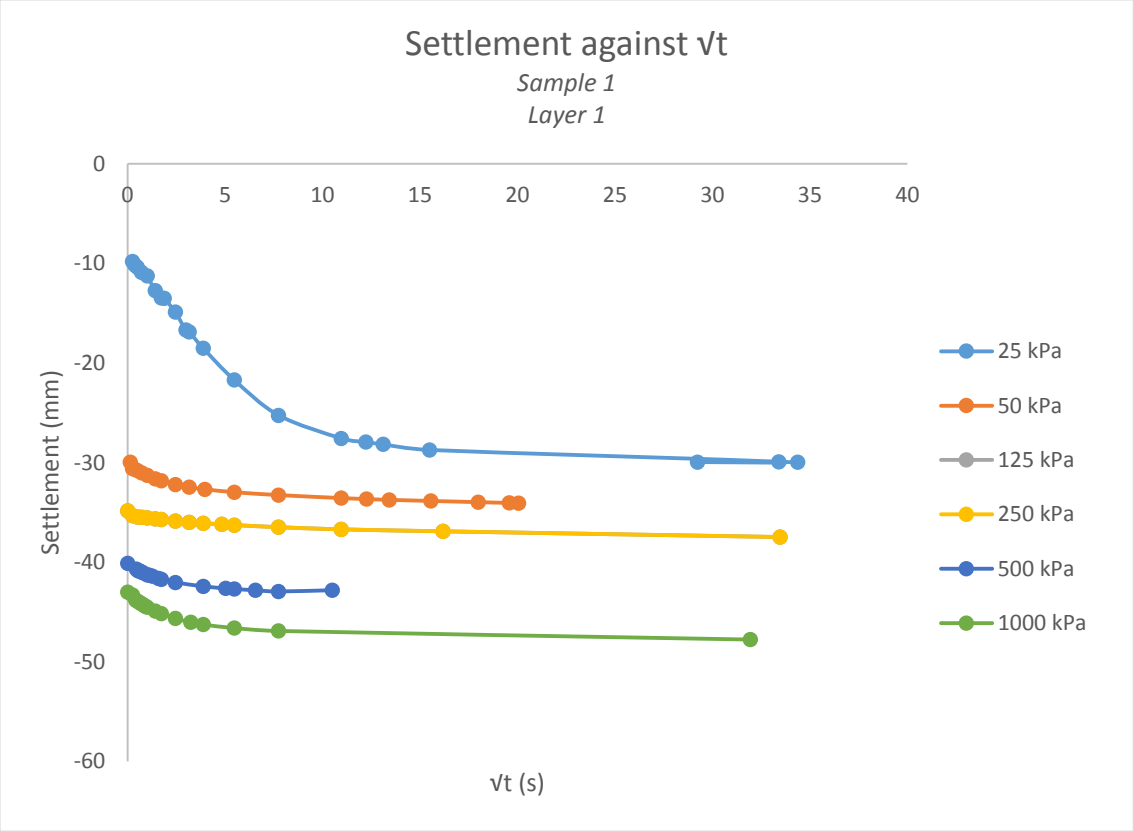

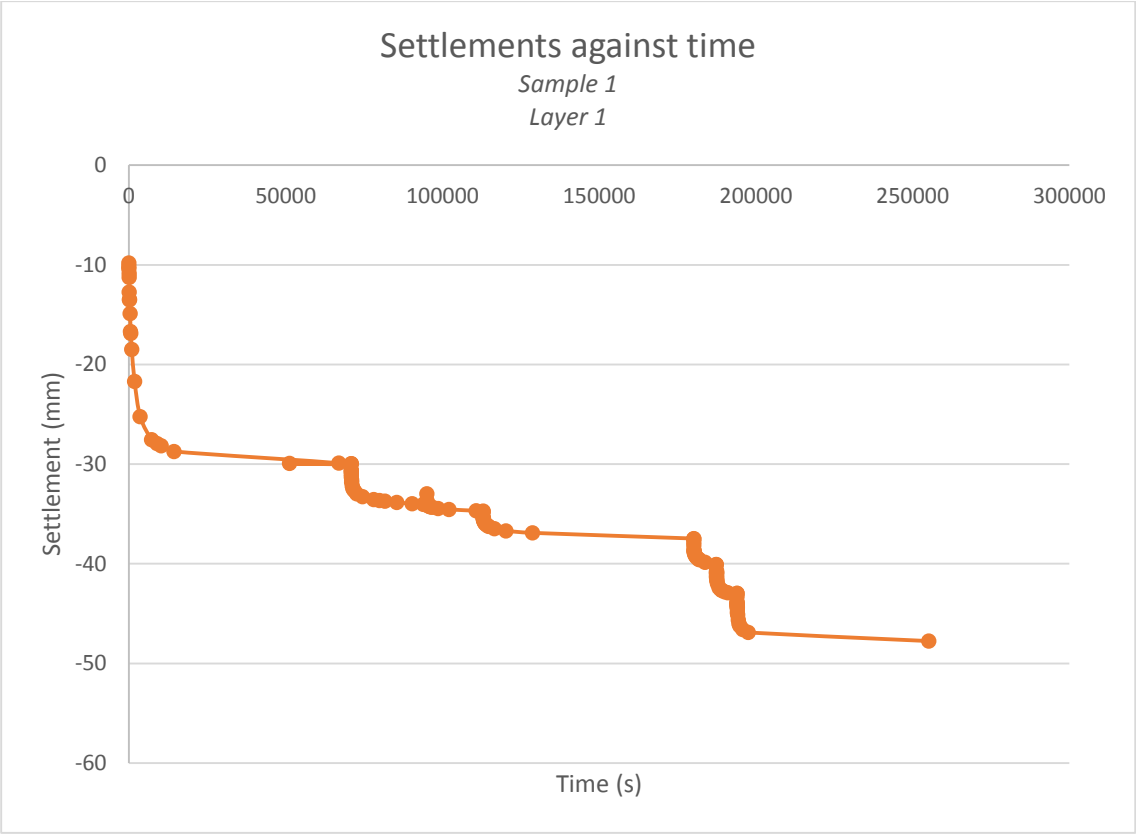

Table 16 Oedometer test results (Sample 1; Layer 1)

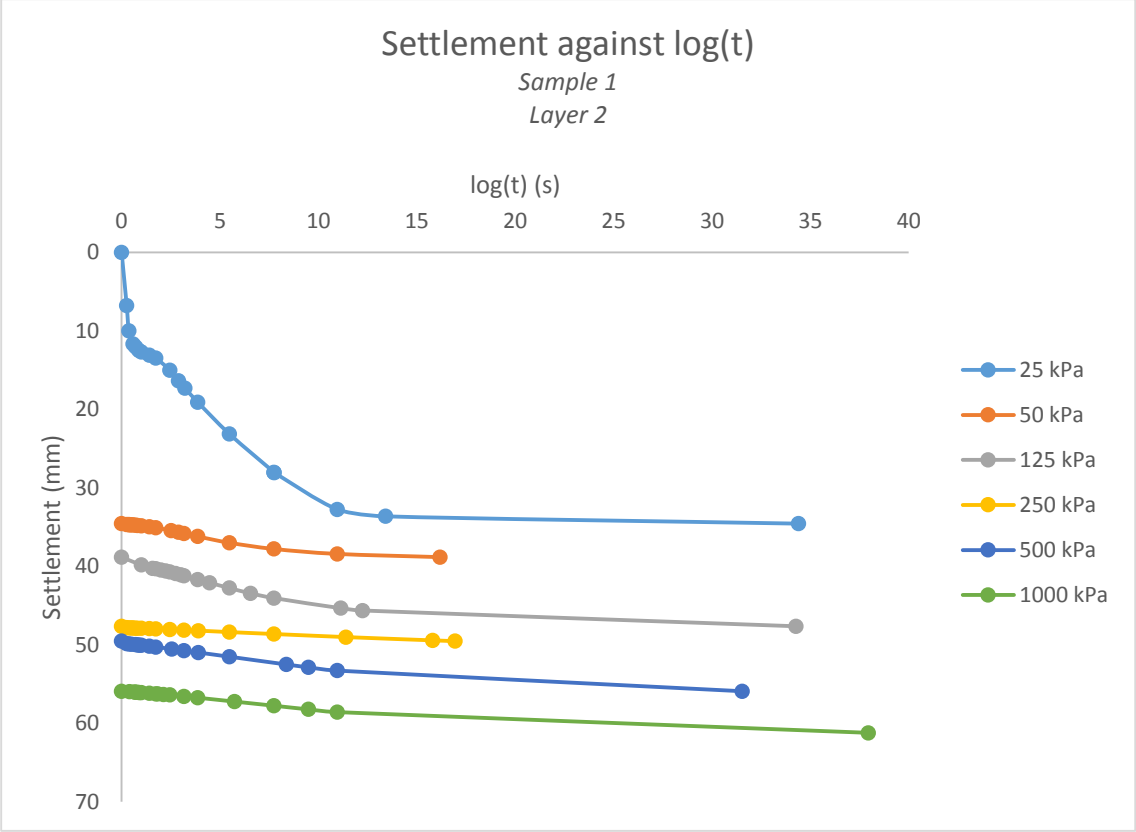

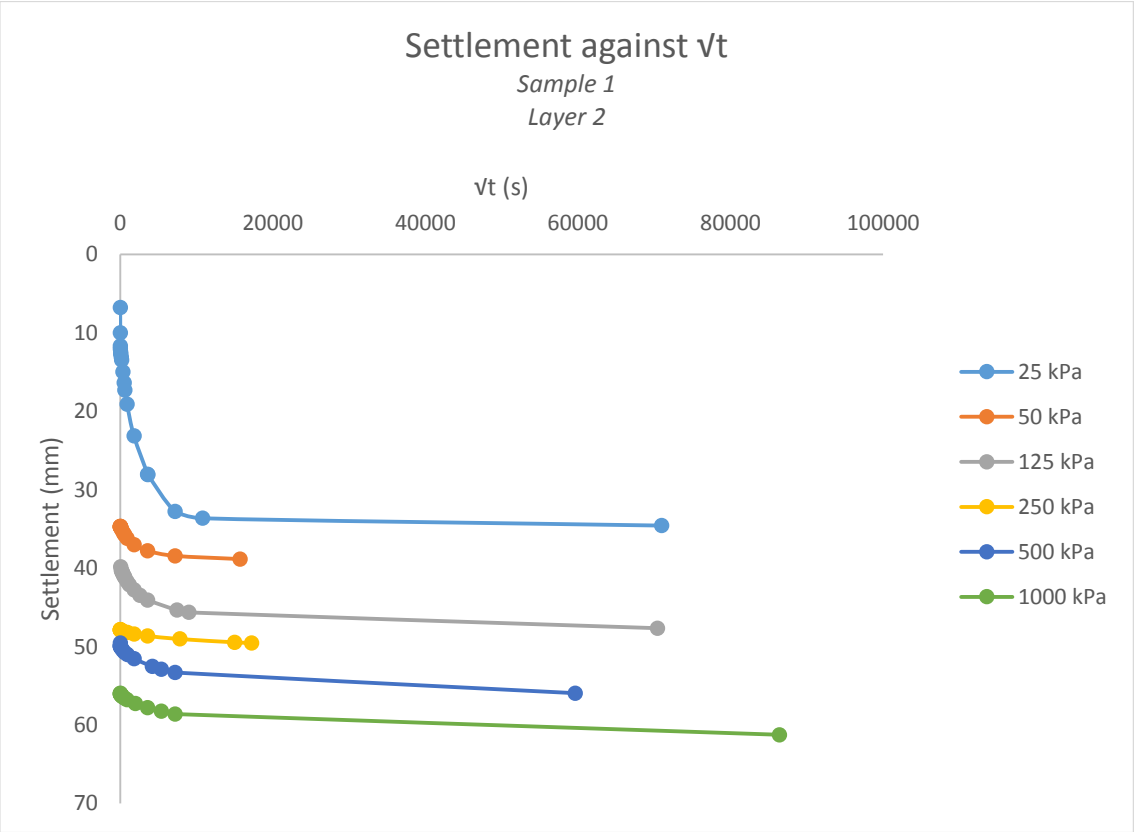

Table 17 Oedometer test results (Sample 1 Layer 2)

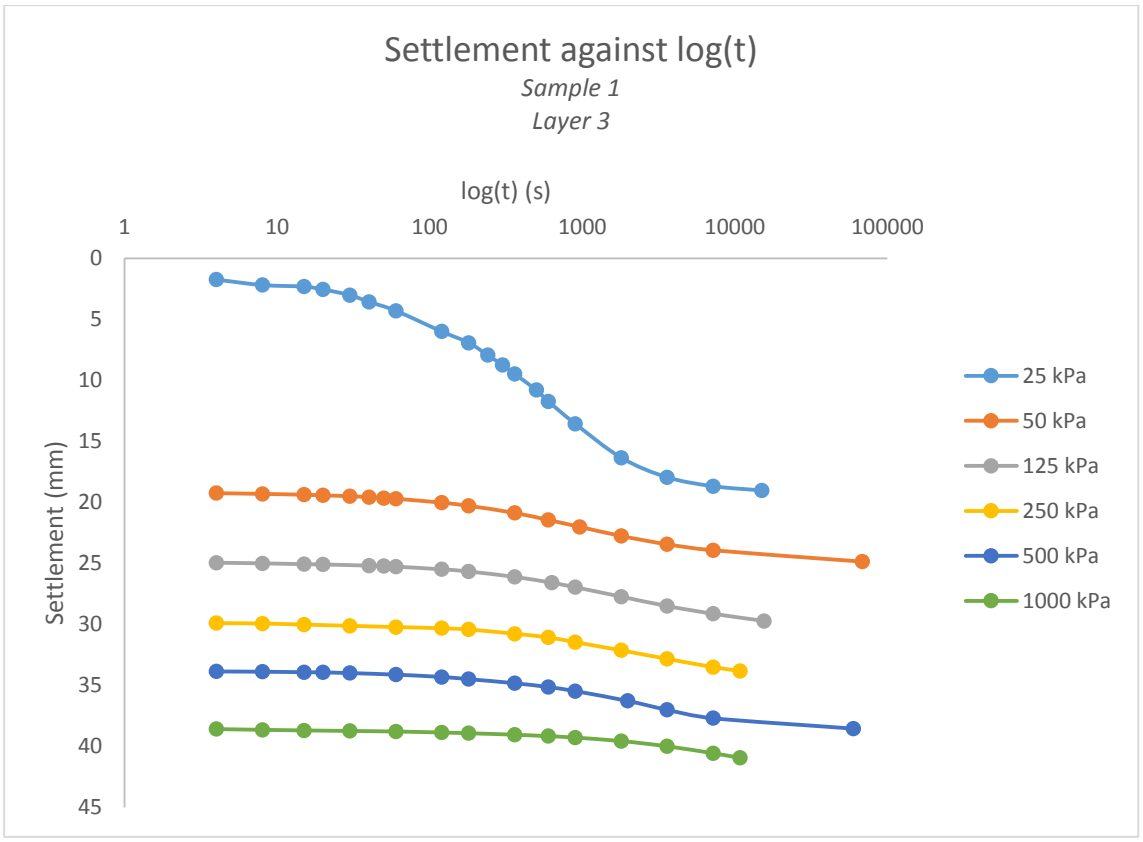
Settlement against log(t)
Sample 1
Layer 3
log(t) (s)
1
10
100
1000
10000
100000
0
5
10
15
20
25
30
35
40
45
Settlement (mm)
25 kPa
50 kPa
125 kPa
250 kPa
500 kPa
1000 kPa

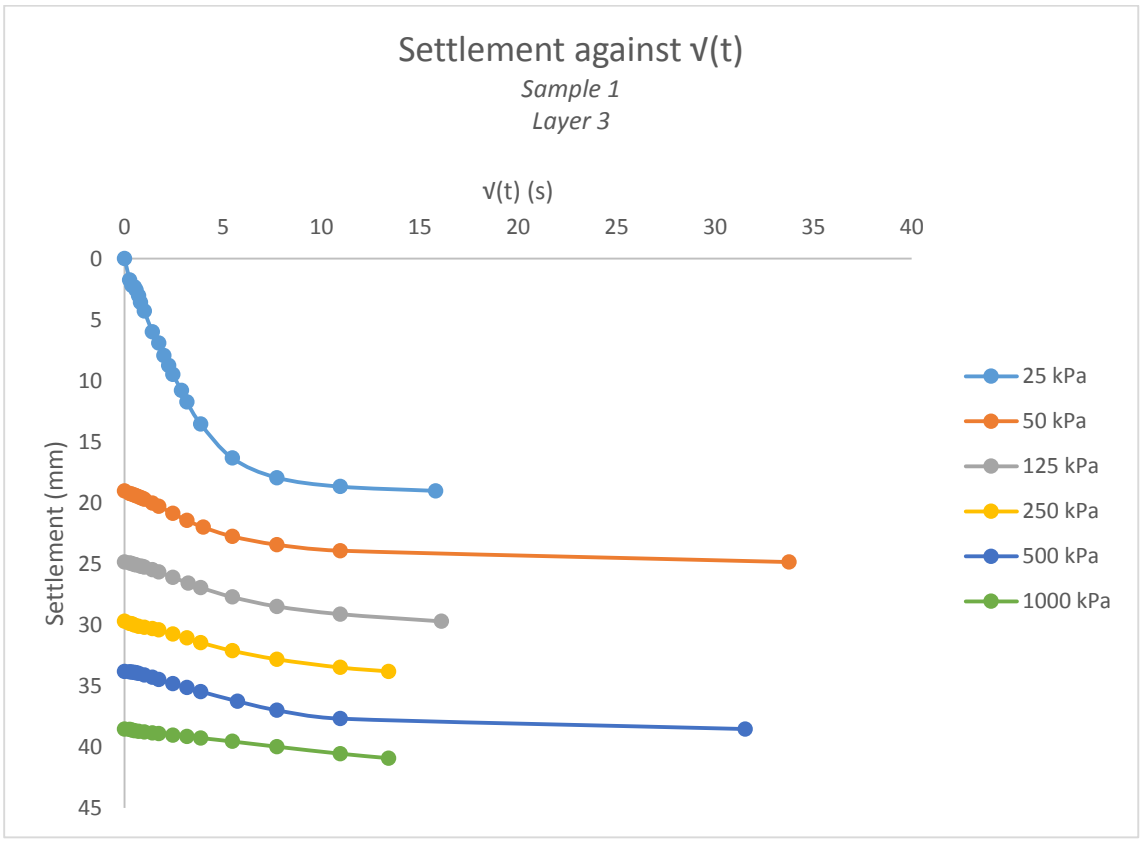
Settlement against √(t)
Sample 1
Layer 3
√(t) (s)
0
5
10
15
20
25
30
35
40
45
Settlement (mm)
25 kPa
50 kPa
125 kPa
250 kPa
500 kPa
1000 kPa

Table 18 Oedometer test results (Sample 1 Layer 3)

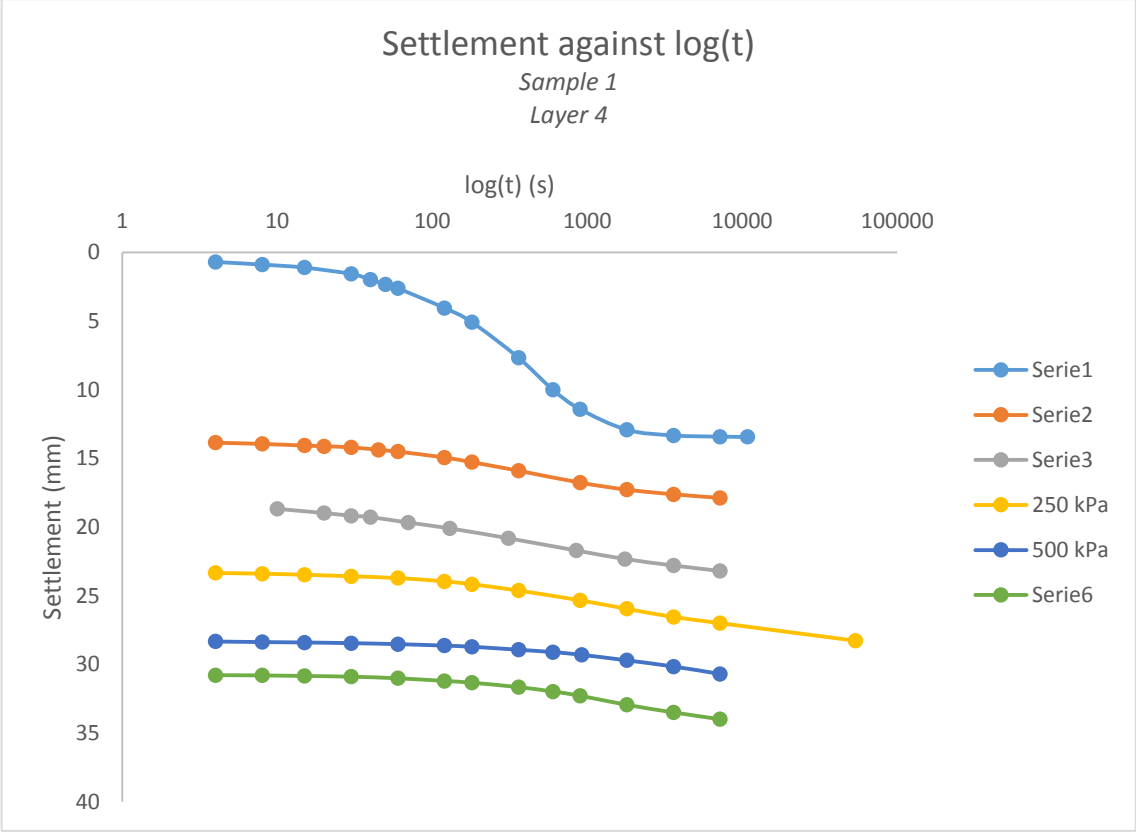

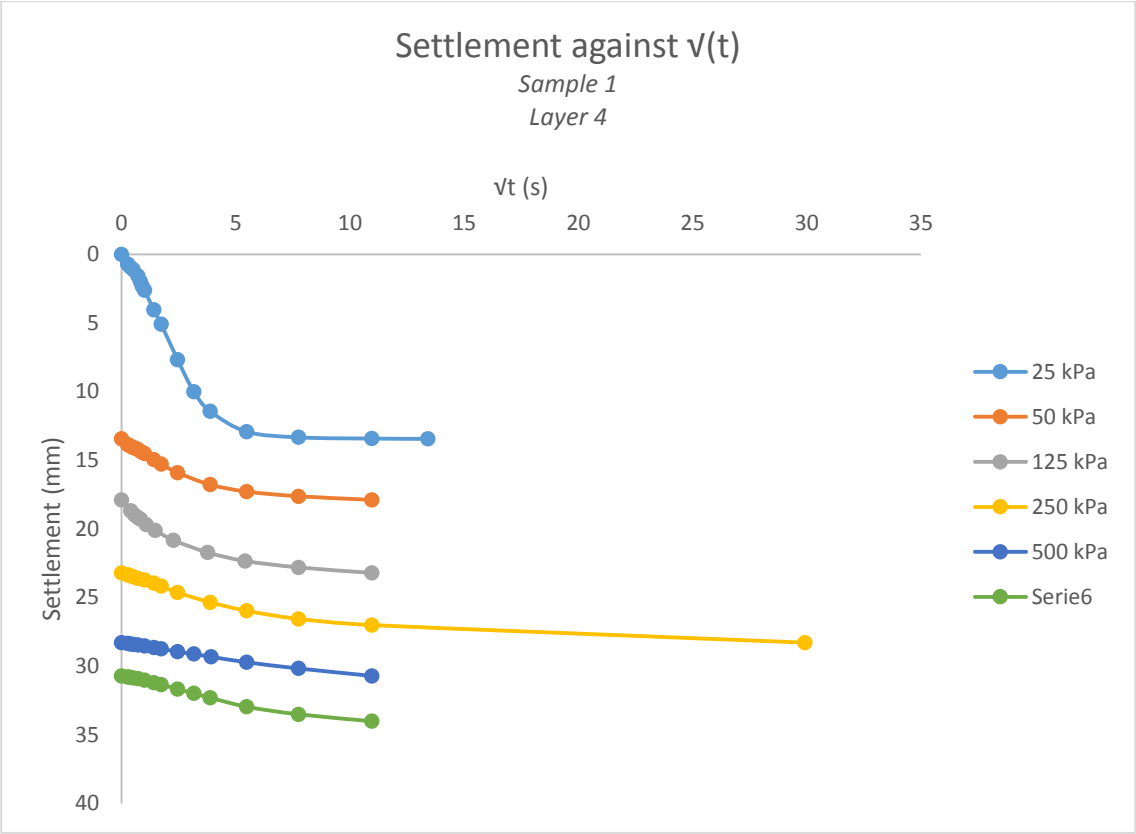

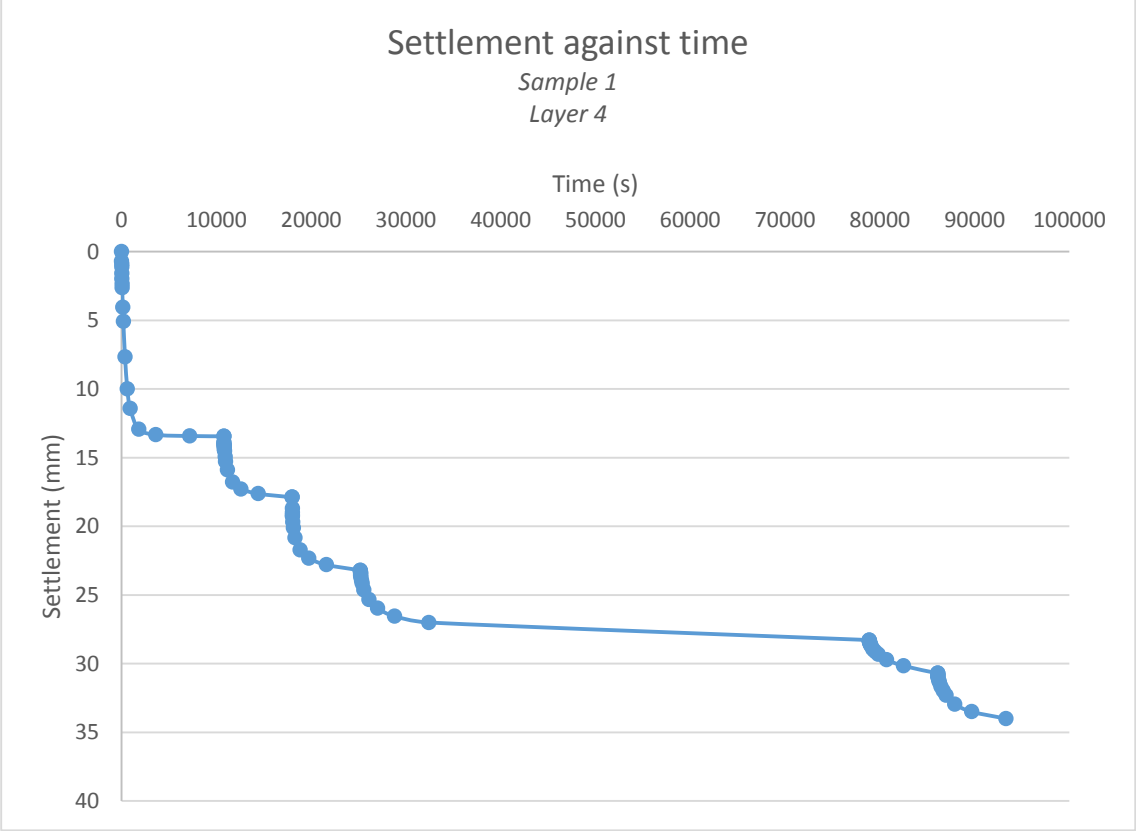

Table 19 Oedometer test results (Sample 1; Layer 4)

5.3.3.2 Second sample

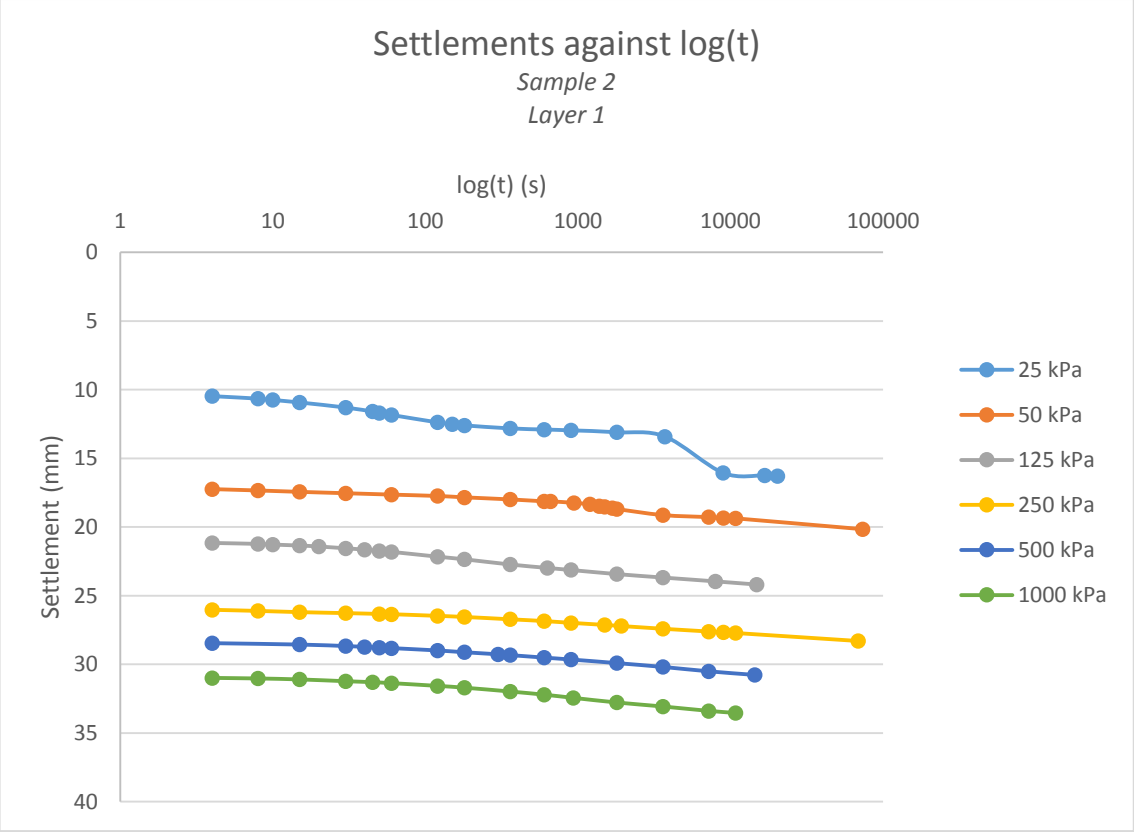

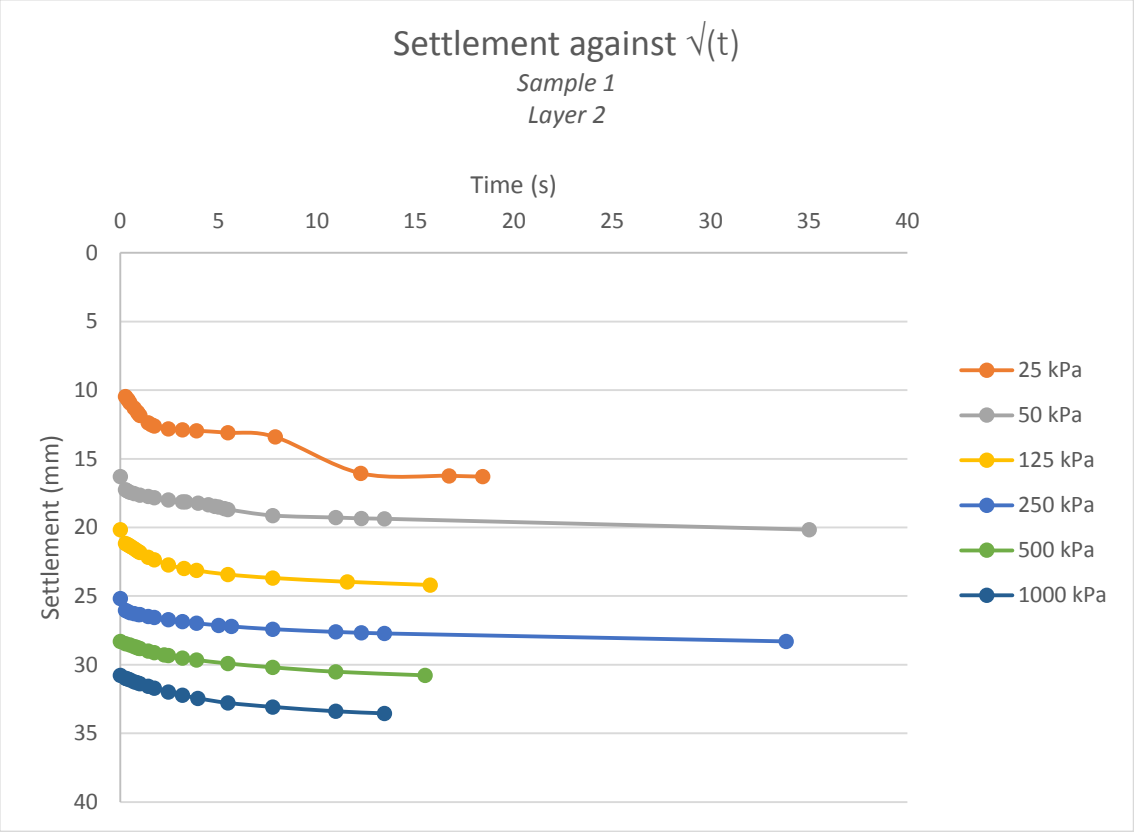

Figure 48 Oedometer test results (Sample 2; Layer 1)

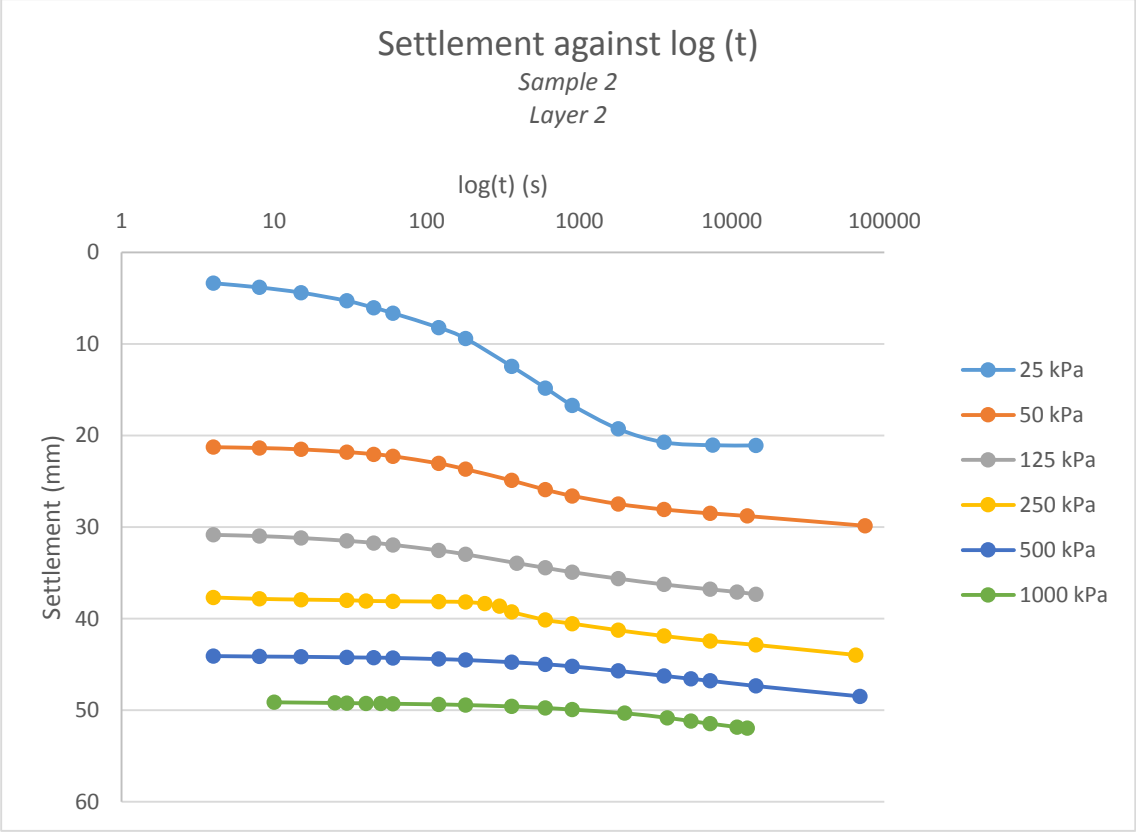

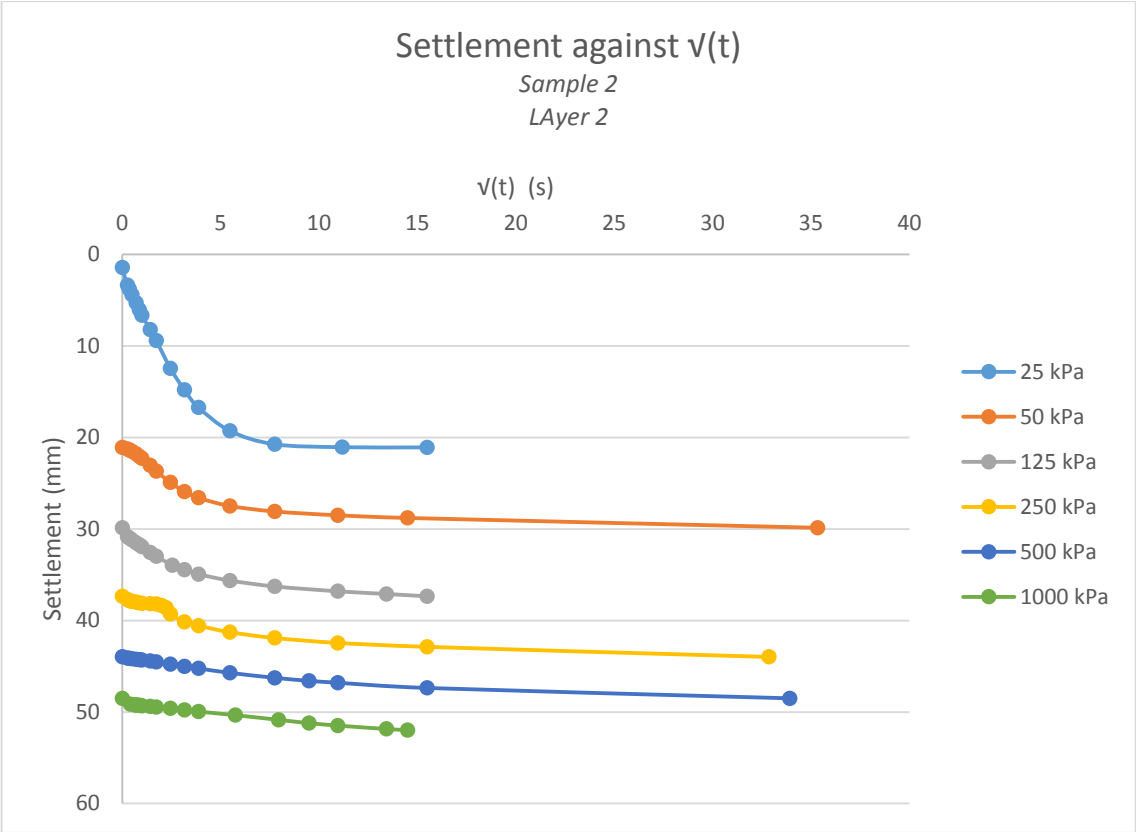

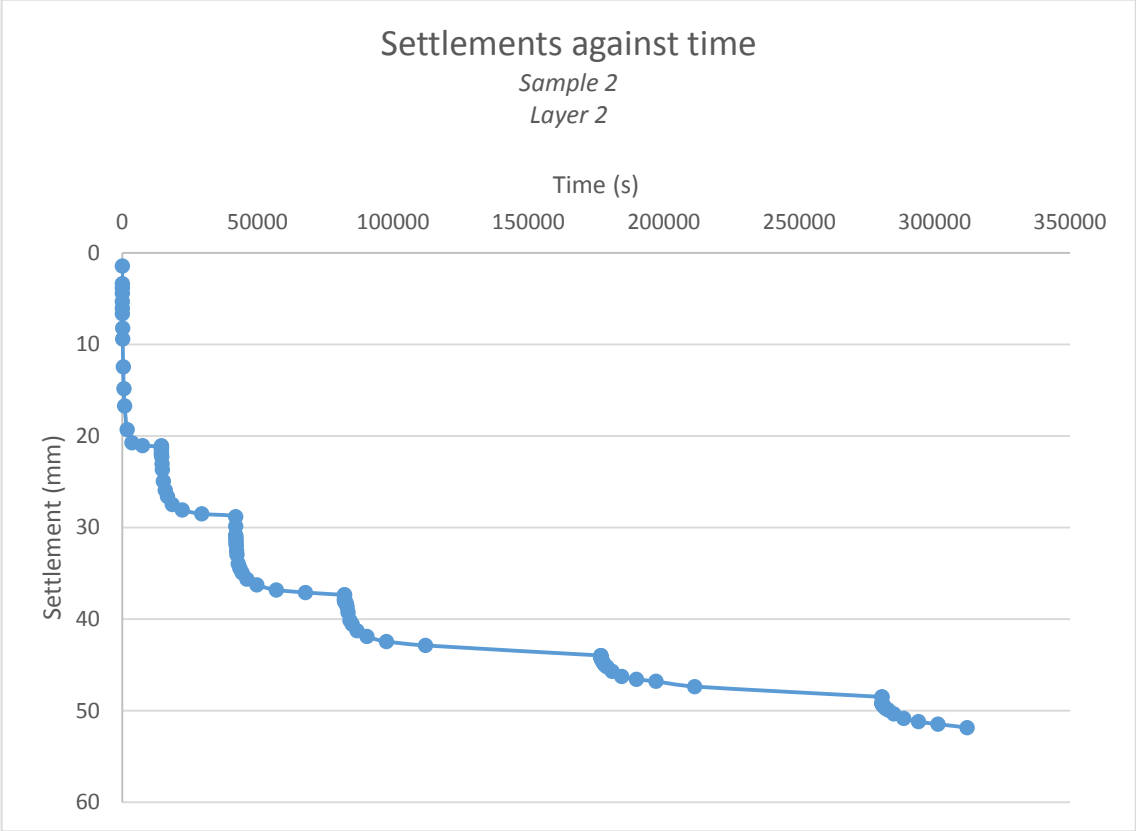

Figure 49 Oedometer test results (Sample 2; Layer 2)

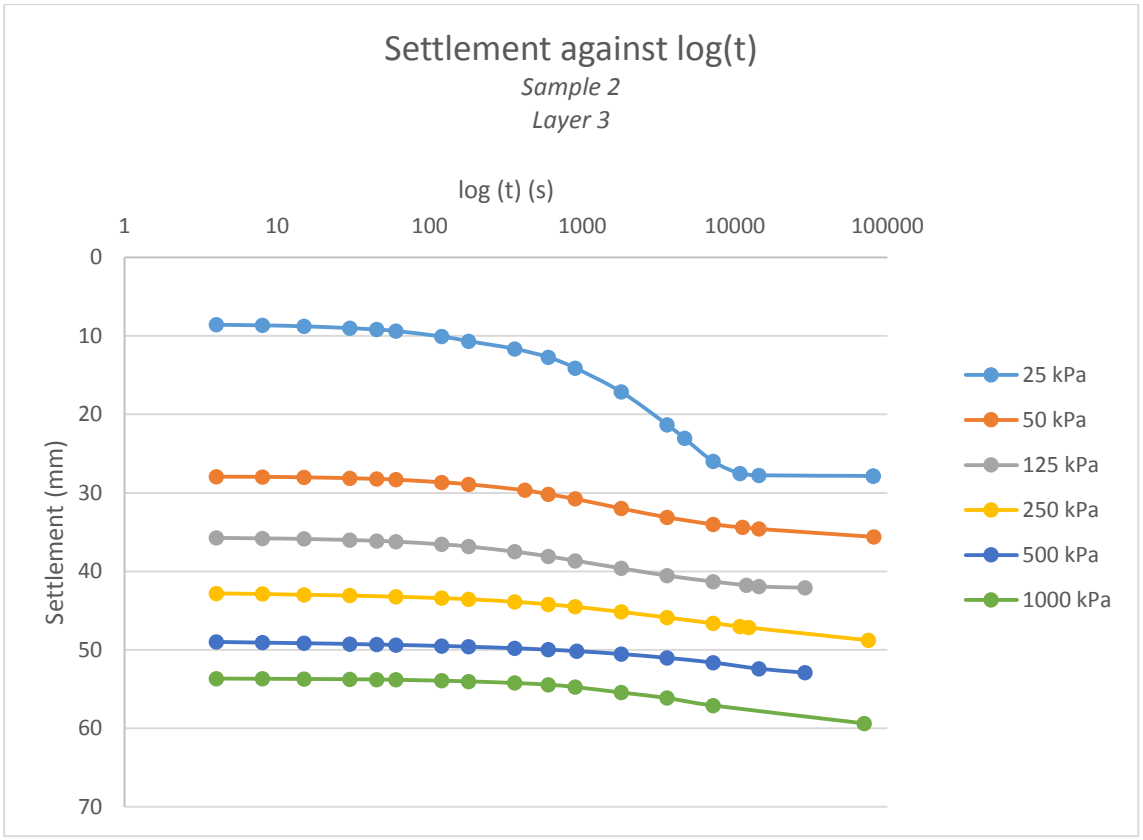
Settlement against log(t)
Sample 2
Layer 3
log (t) (s)
1
10
100
1000
10000
100000
0
10
20
30
40
50
60
70
Settlement (mm)
25 kPa
50 kPa
125 kPa
250 kPa
500 kPa
1000 kPa

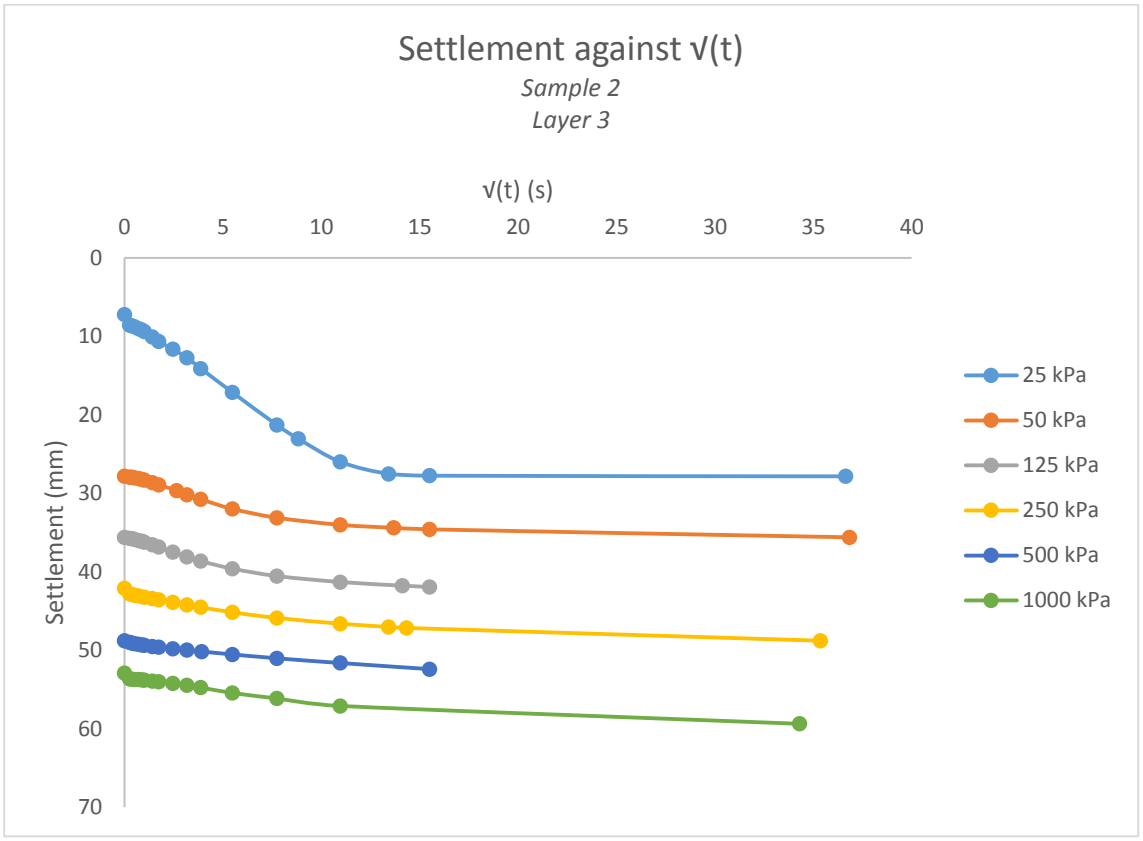
Settlement against √(t)
Sample 2
Layer 3
√(t) (s)
0
5
10
15
20
25
30
35
40
0
10
20
30
40
50
60
70
Settlement (mm)
25 kPa
50 kPa
125 kPa
250 kPa
500 kPa
1000 kPa

Figure 50 Oedometer test results (Sample 2; Layer 3)

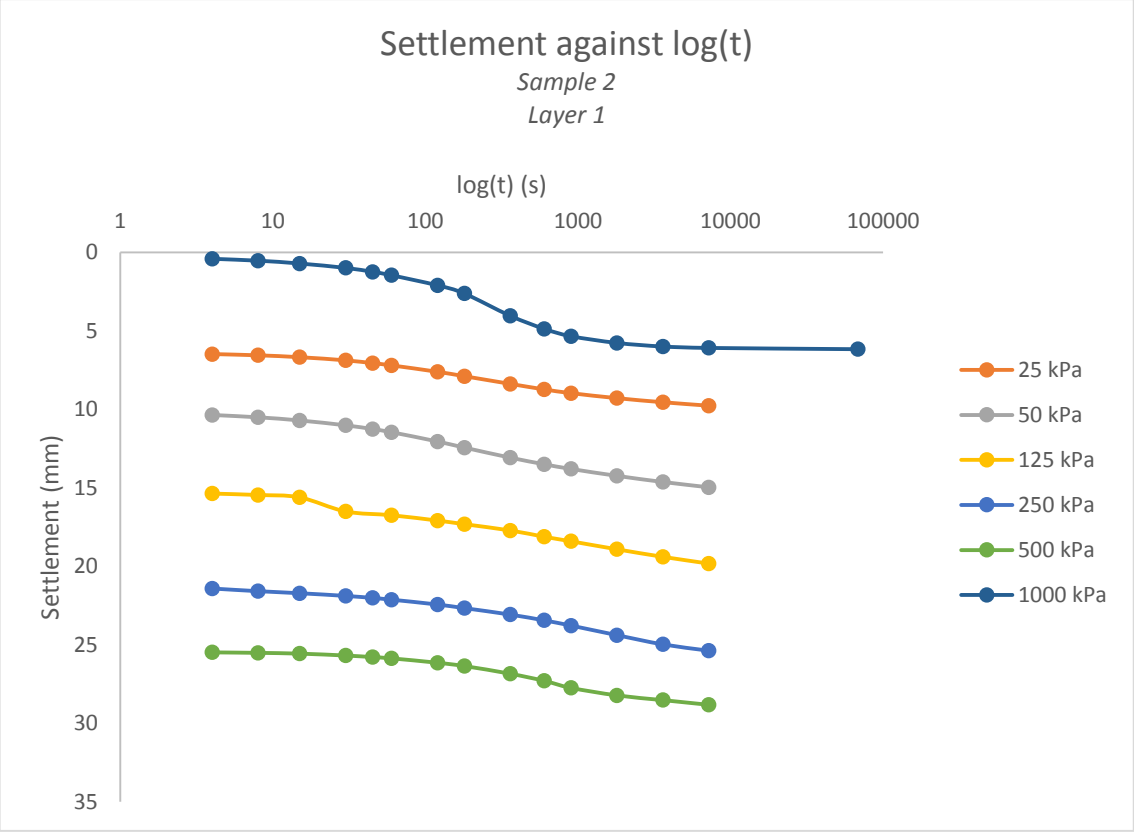

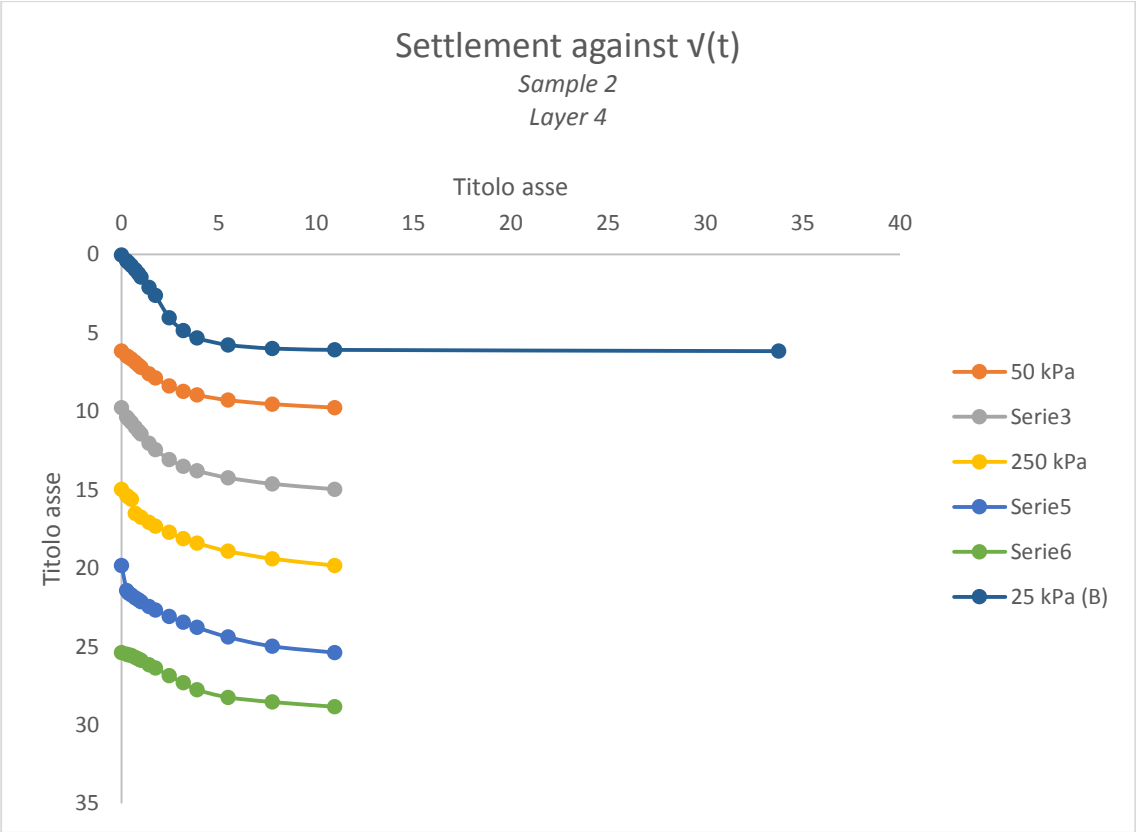

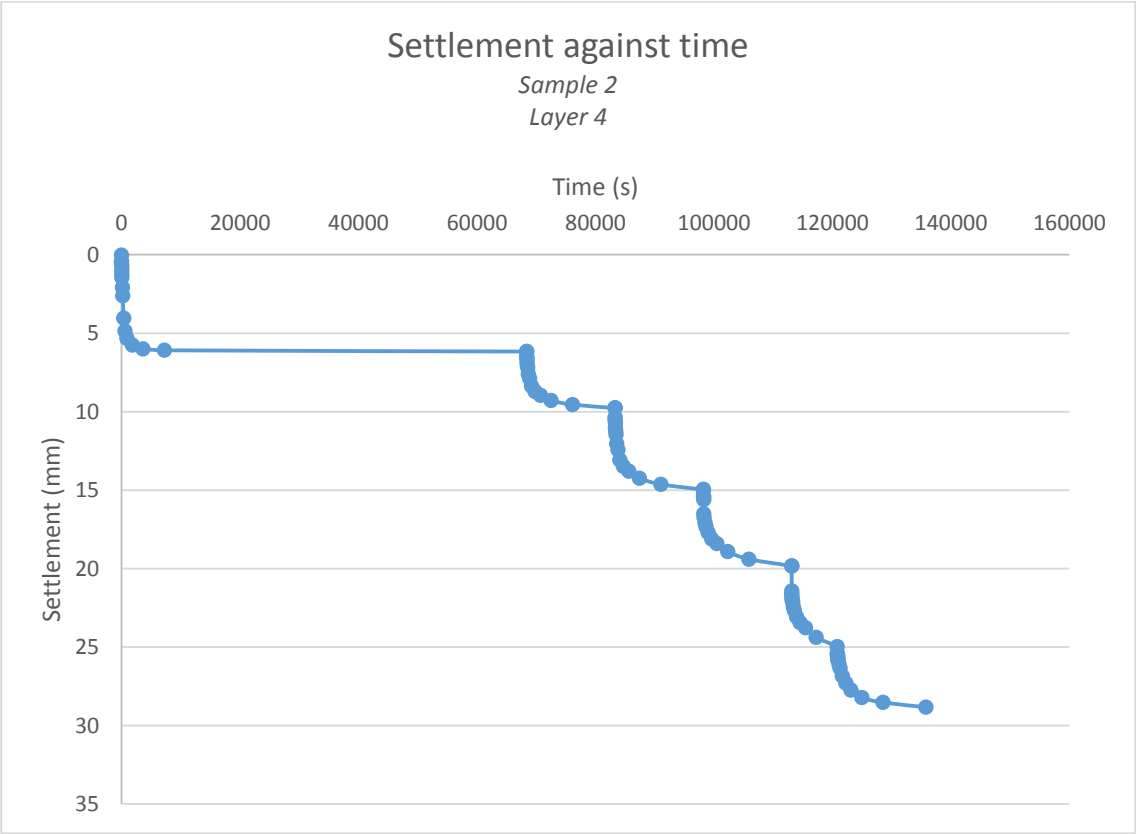

Figure 51 Oedometer test results (Sample 2; Layer 4)

5.3.3.3 *Third sample*

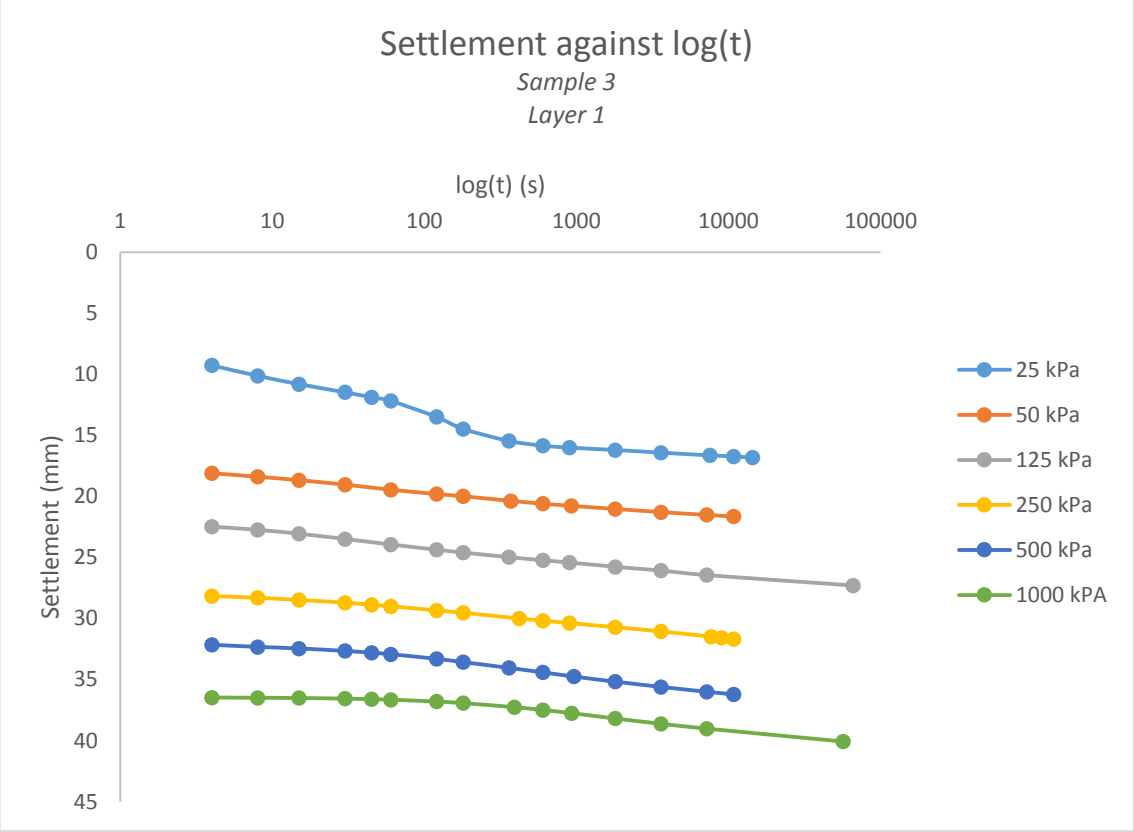

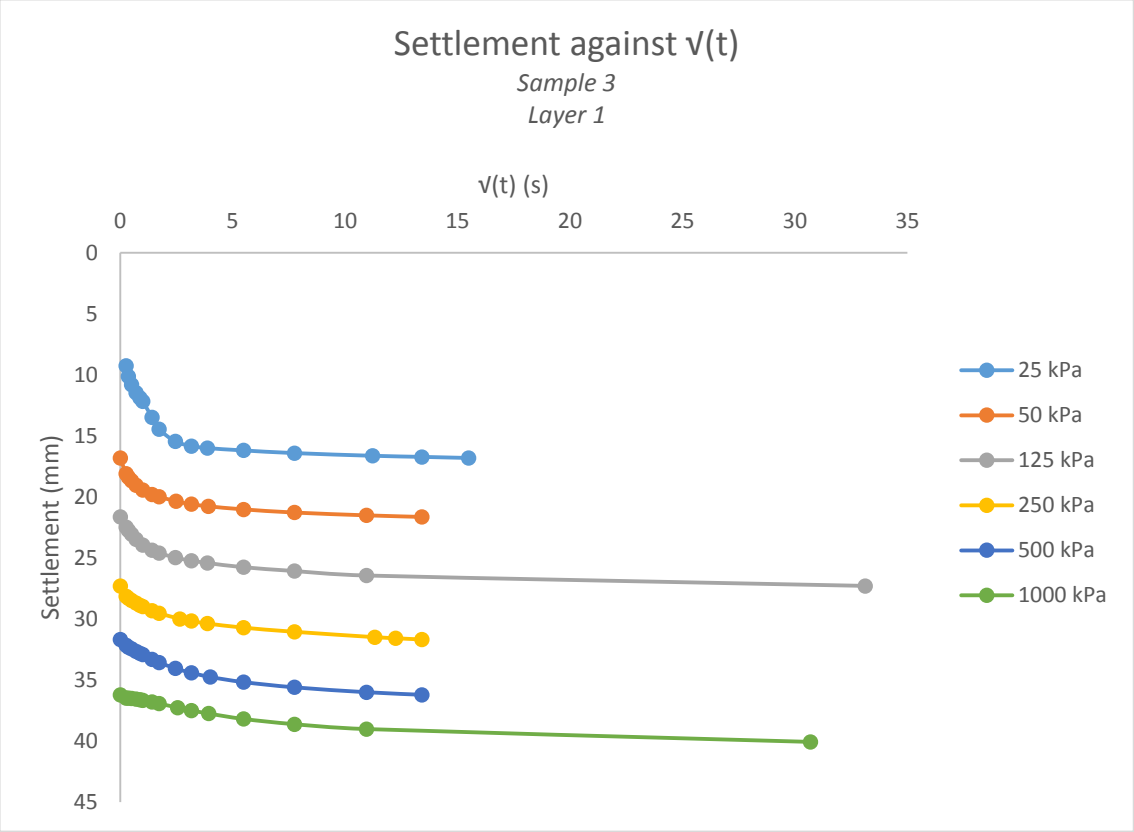

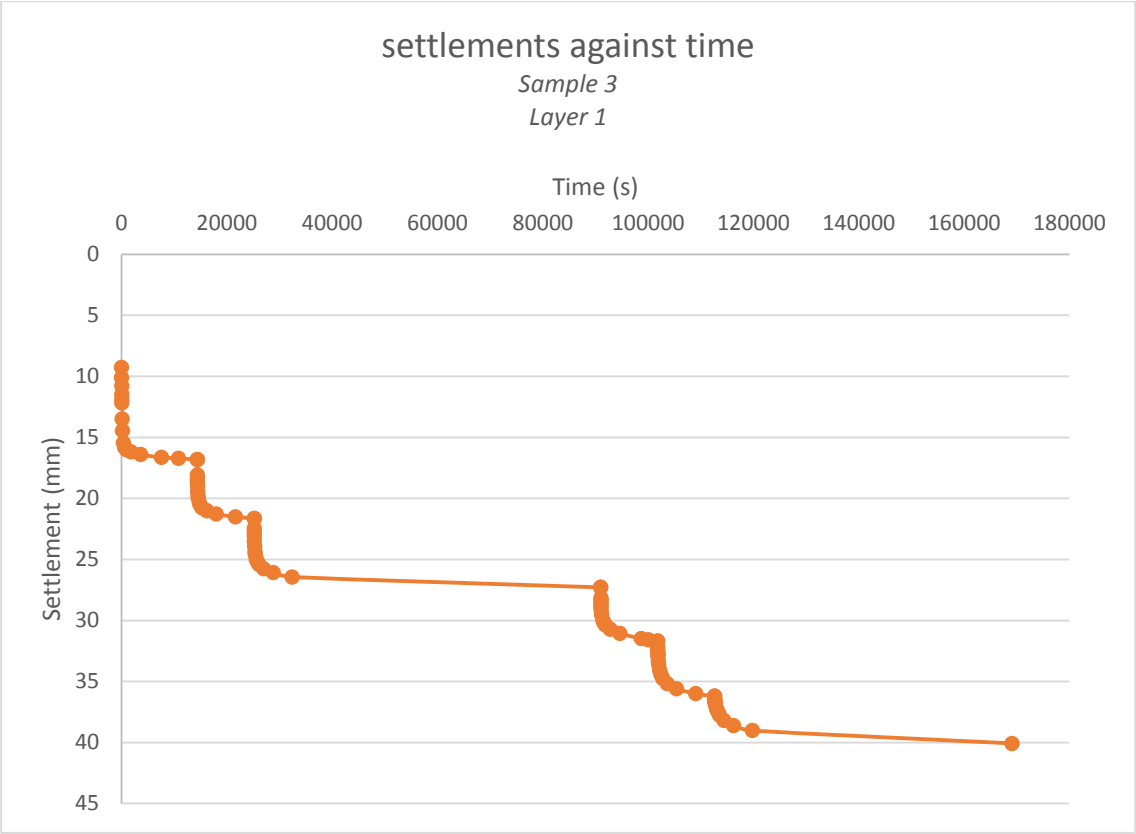

Figure 52 Oedometric test results (Sample 3; Layer 1)

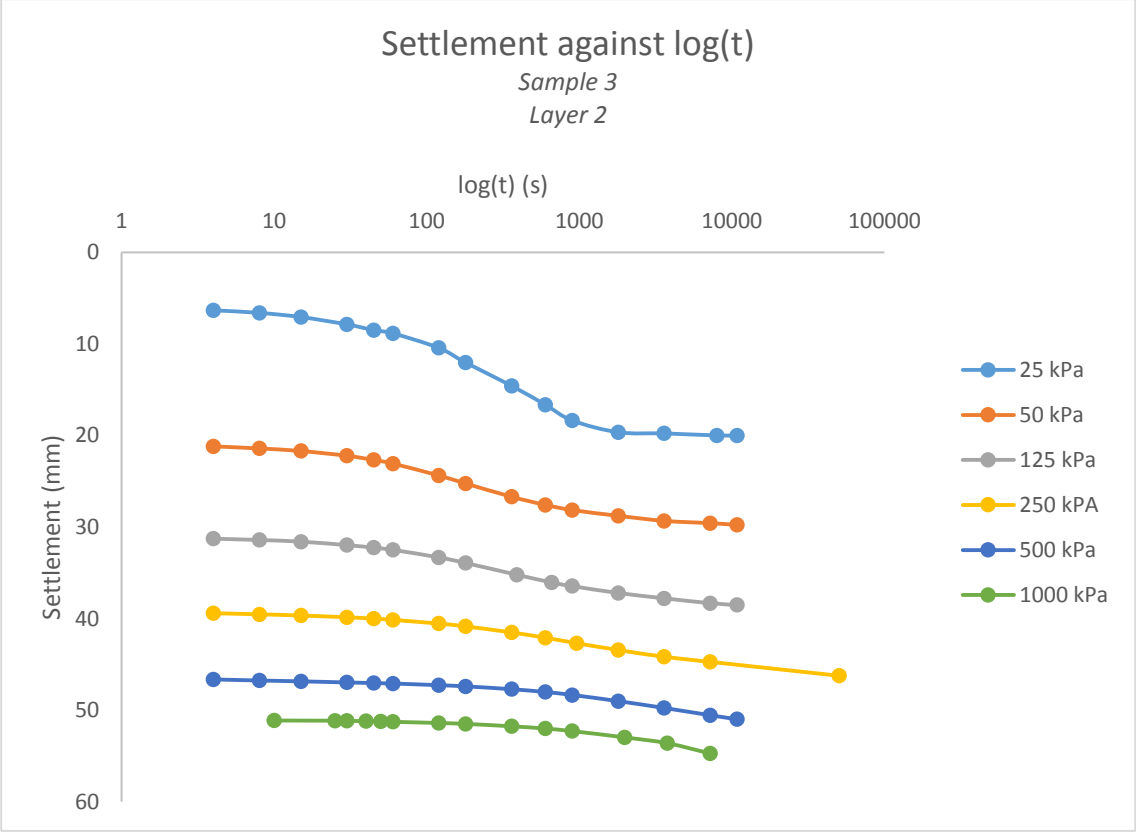

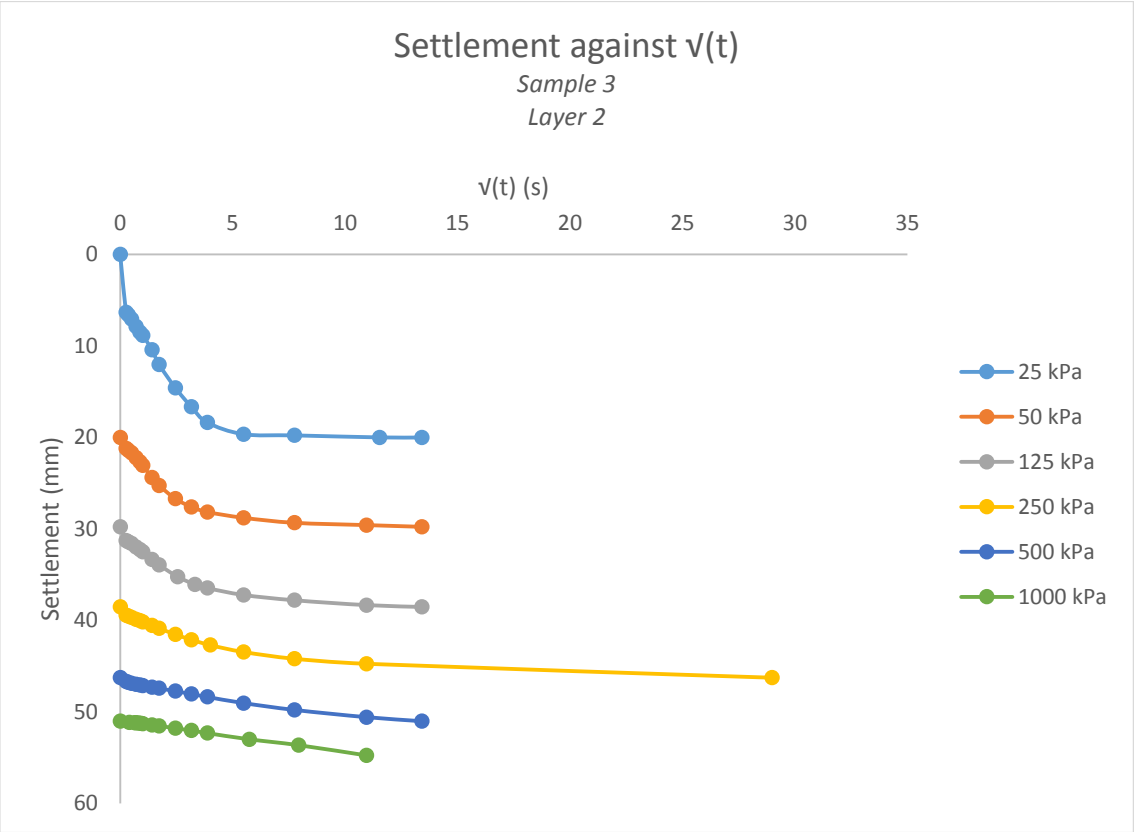

Figure 53 Oedometer test results (Sample 3; Layer 2)

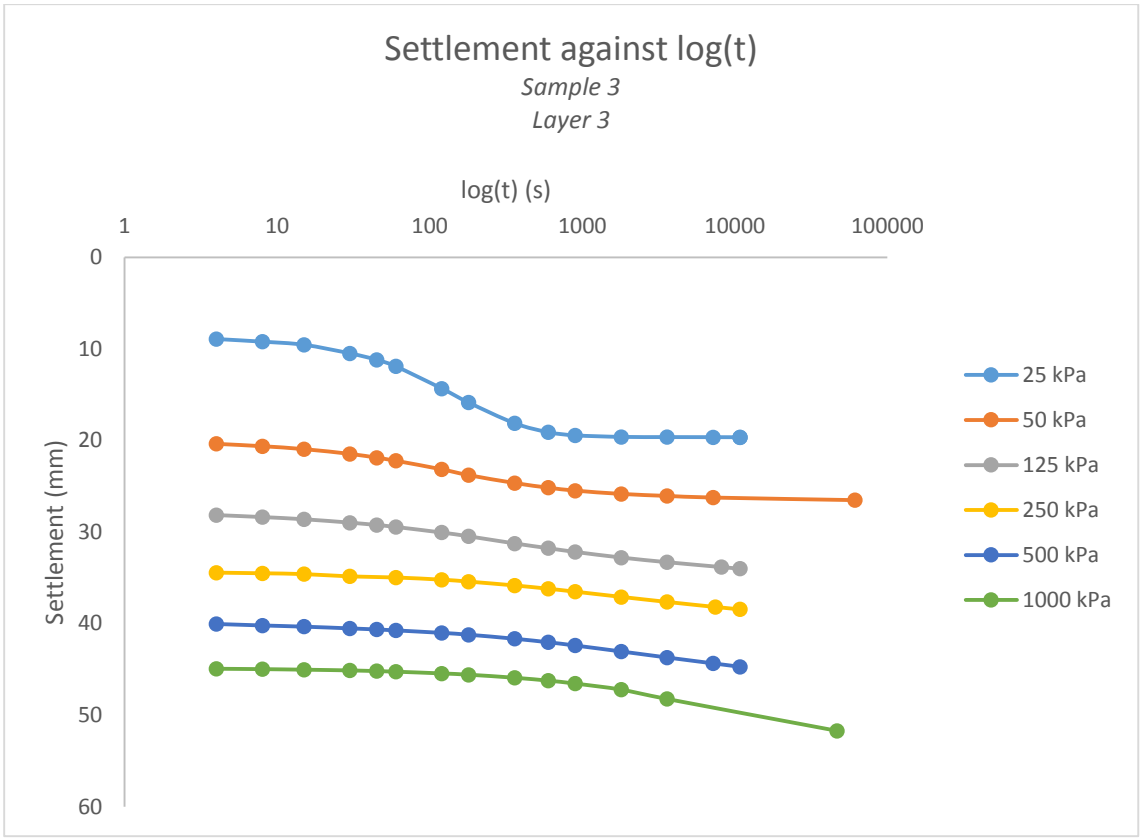
Settlement against log(t)
Sample 3
Layer 3
log(t) (s)
1
10
100
1000
10000
100000
0
10
20
30
40
50
60
Settlement (mm)
25 kPa
50 kPa
125 kPa
250 kPa
500 kPa
1000 kPa

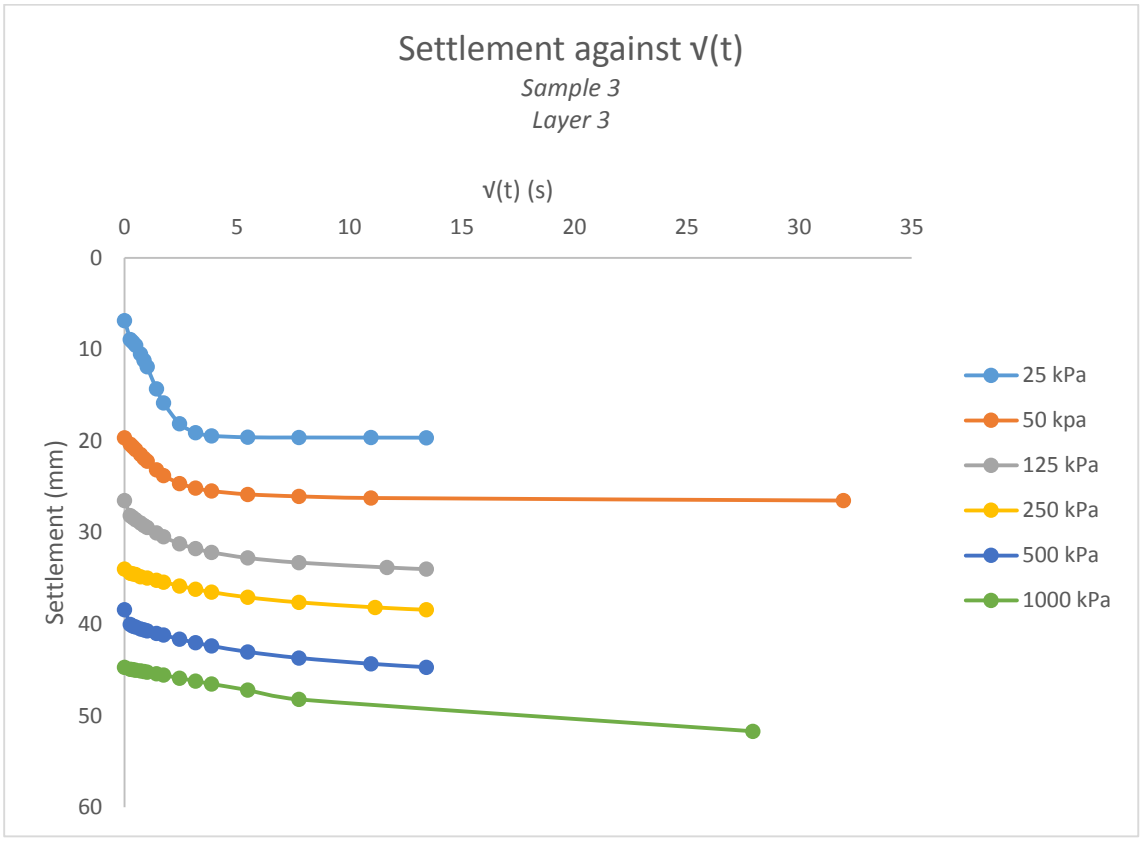
Settlement against √(t)
Sample 3
Layer 3
√(t) (s)
0
5
10
15
20
25
30
35
0
10
20
30
40
50
60
Settlement (mm)
25 kPa
50 kpa
125 kPa
250 kPa
500 kPa
1000 kPa

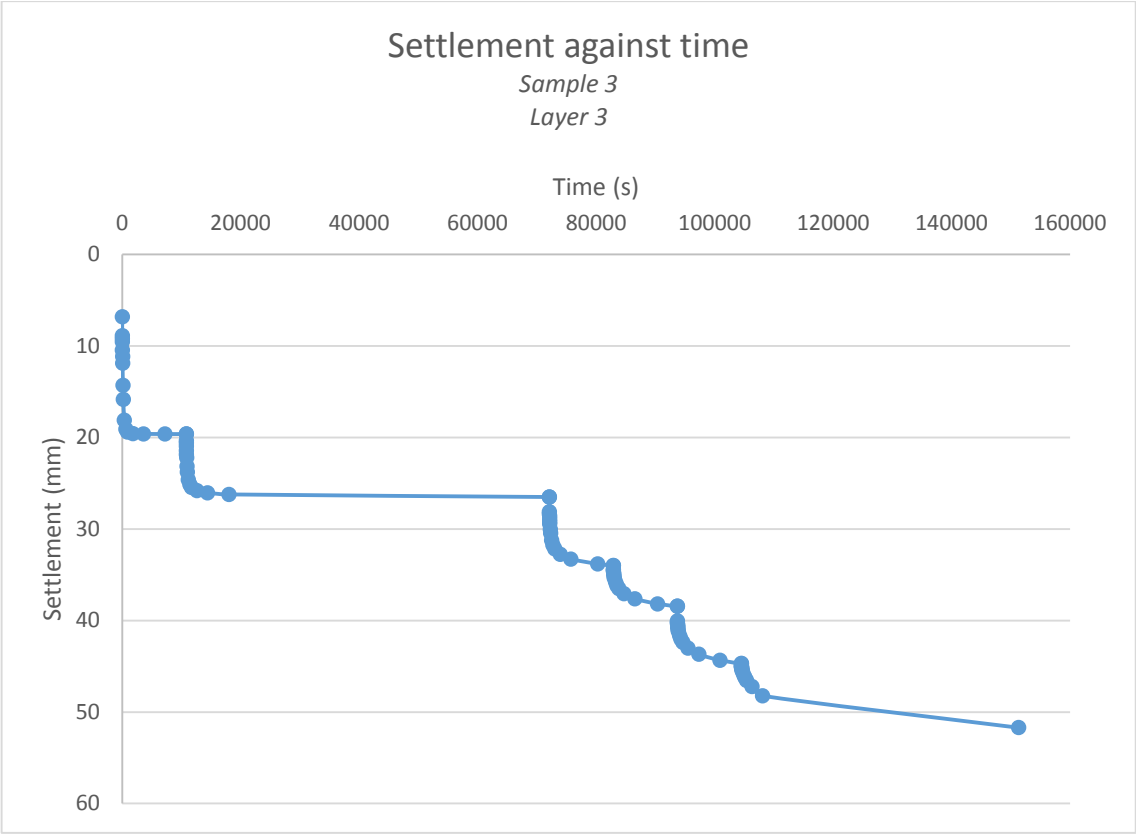

Figure 54 Oedometer test results (Sample 3; Layer 3)

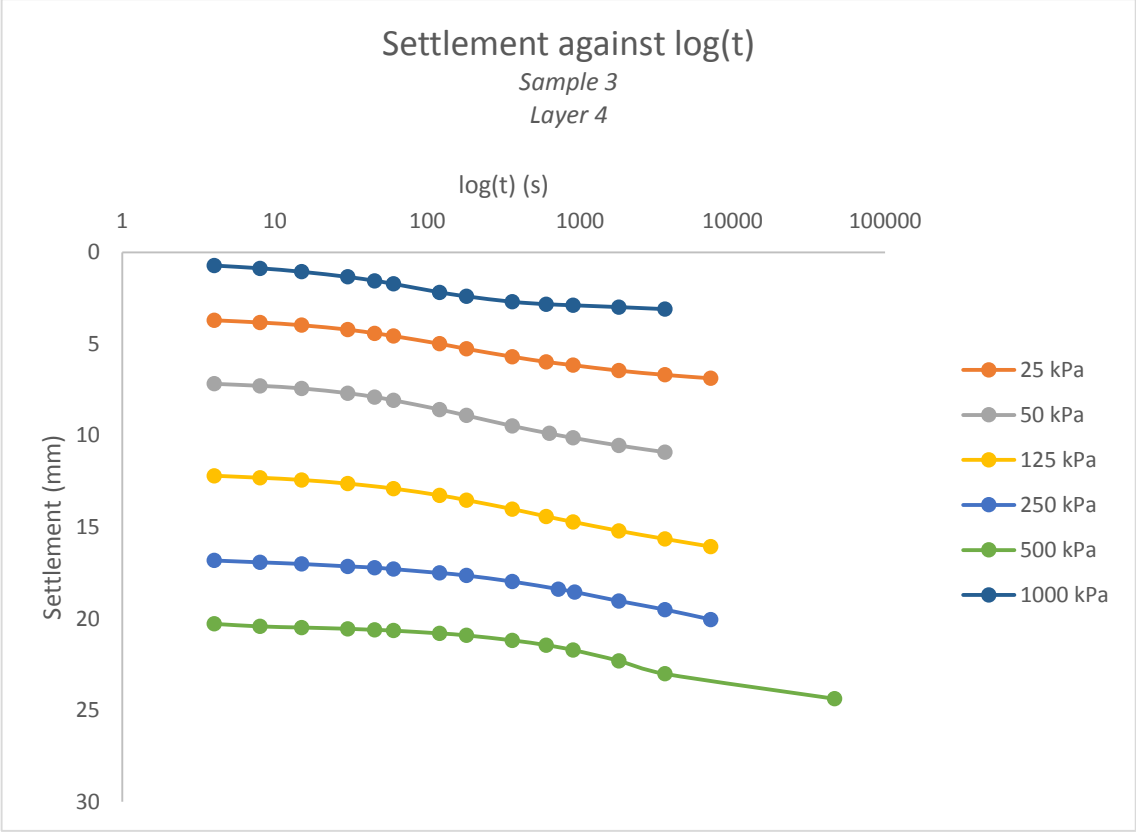

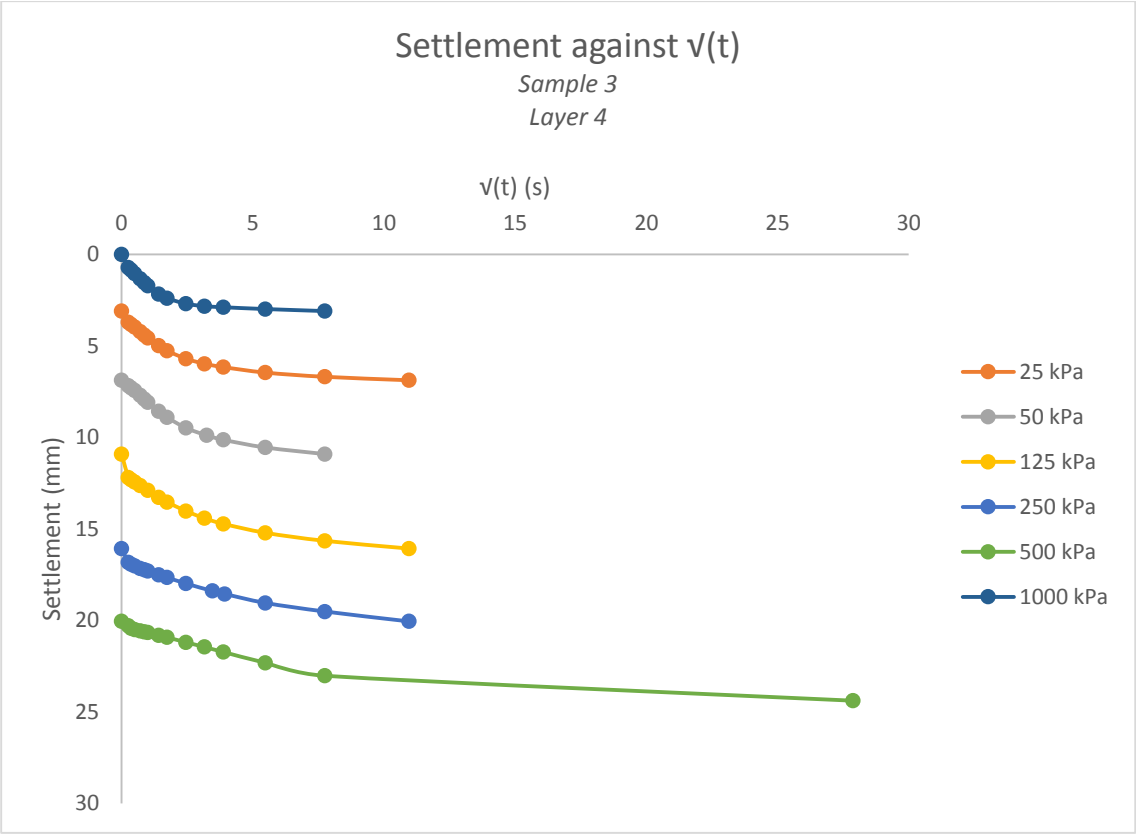
Settlement against √(t)
Sample 3
Layer 4
√(t) (s)
0
5
10
15
20
25
30
Settlement (mm)
0
5
10
15
20
25
30
25 kPa
50 kPa
125 kPa
250 kPa
500 kPa
1000 kPa

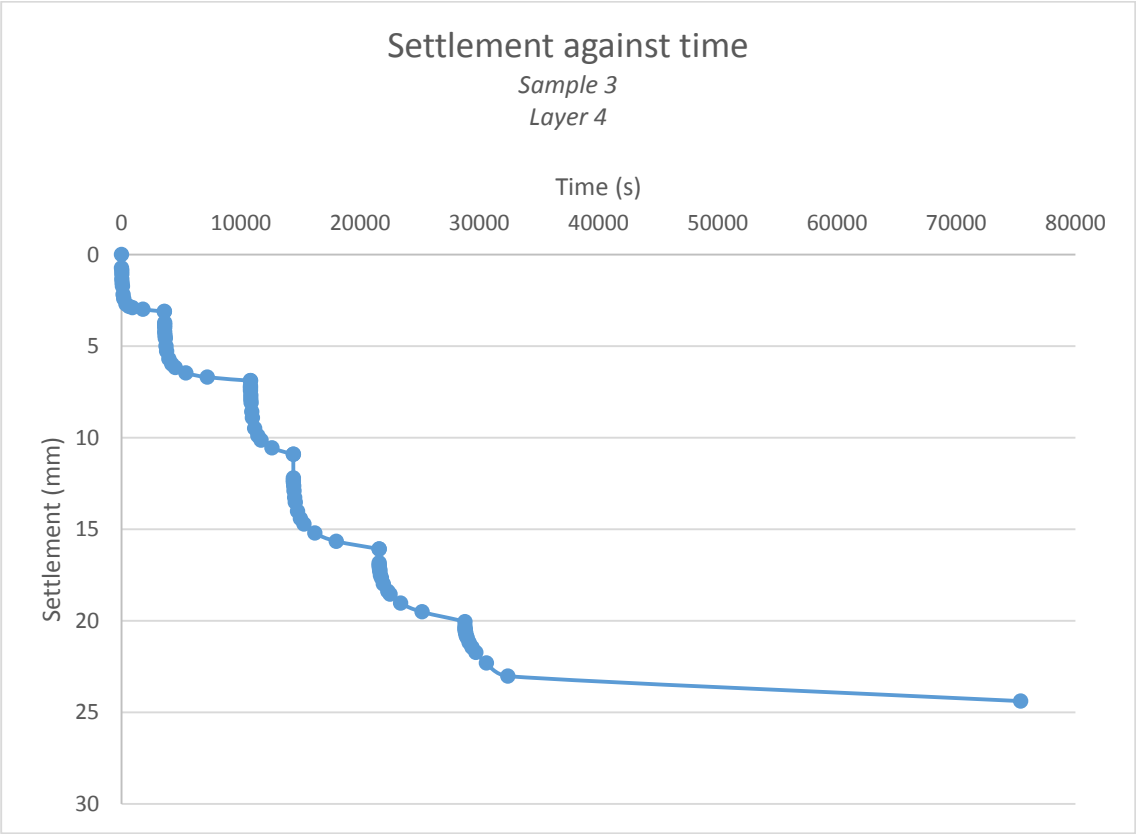
Settlement against time
Sample 3
Layer 4
Time (s)
0
10000
20000
30000
40000
50000
60000
70000
80000
Settlement (mm)
0
5
10
15
20
25
30

5.3.3.4 *Fourth sample*

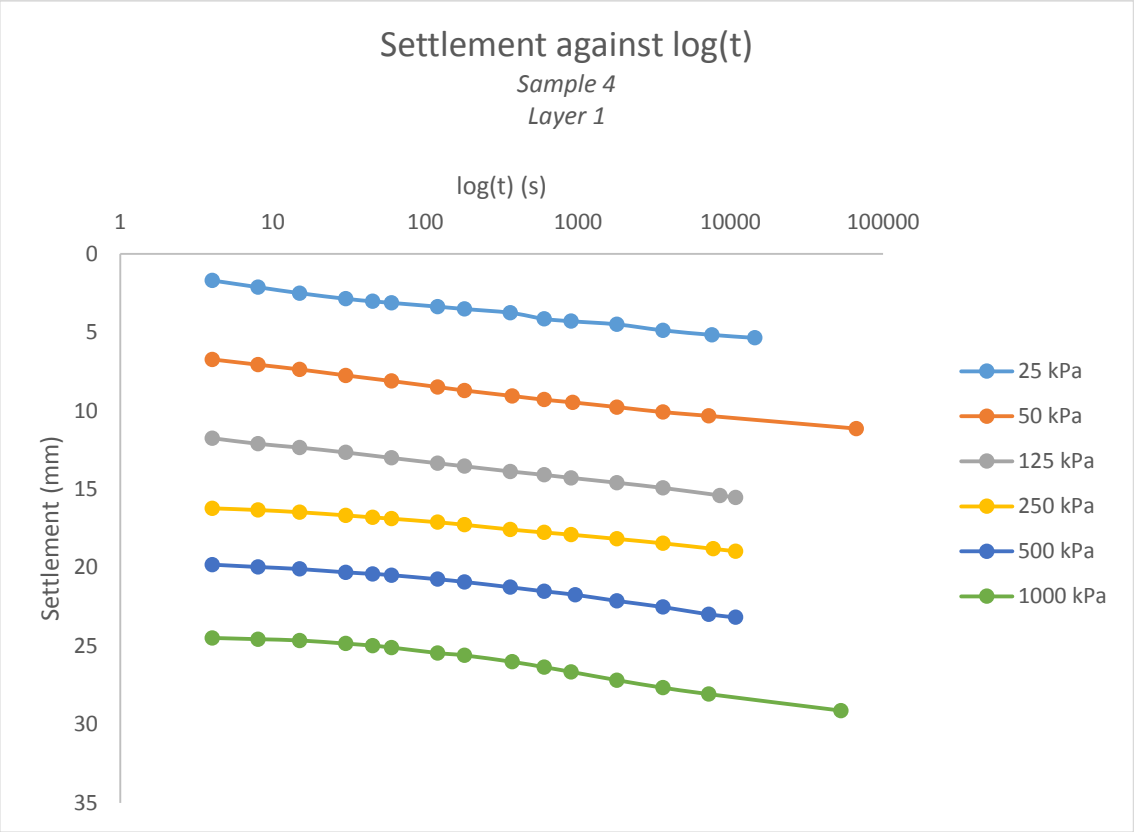

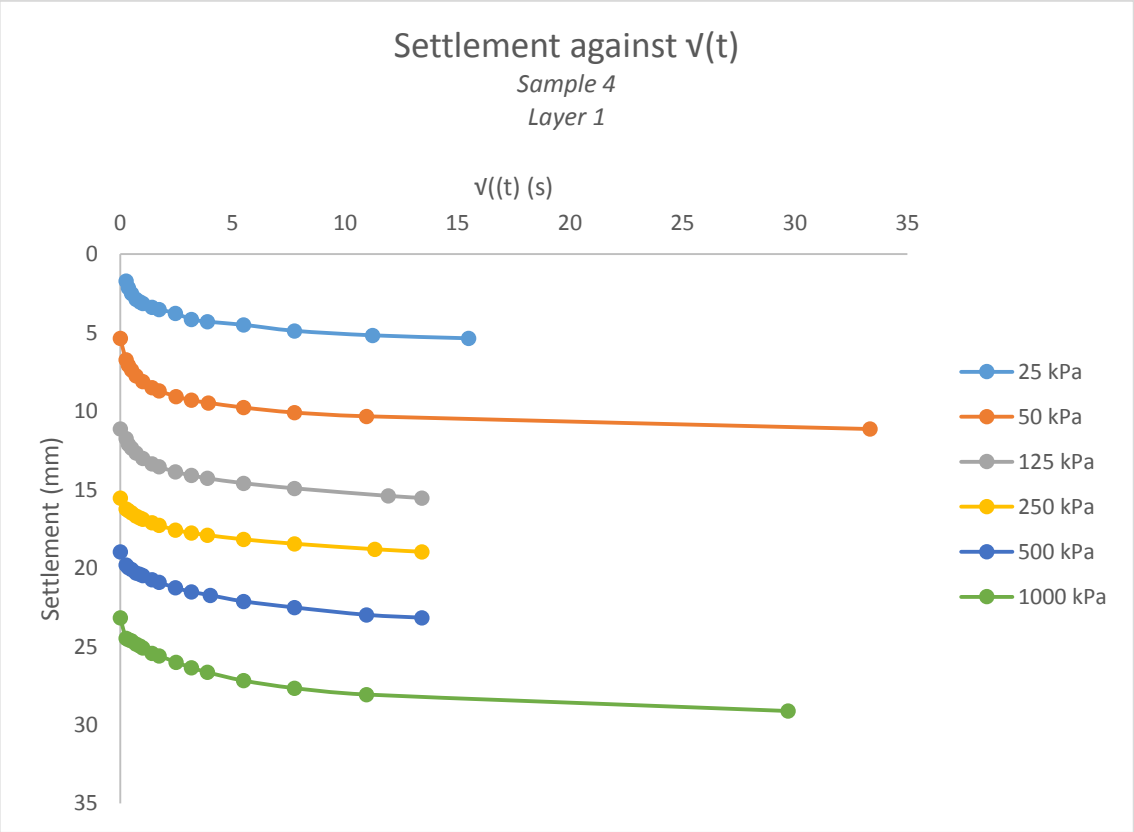

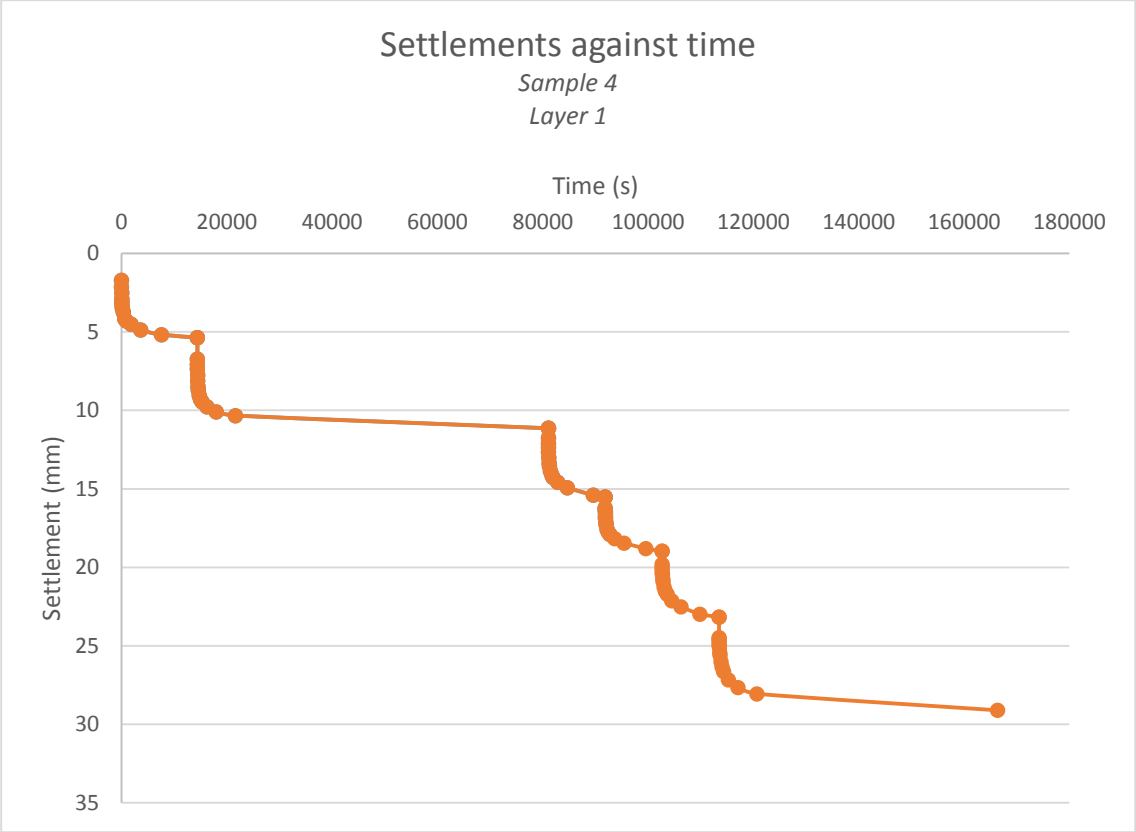

Figure 55 Oedometer test results (Sample 4; Layer 1)

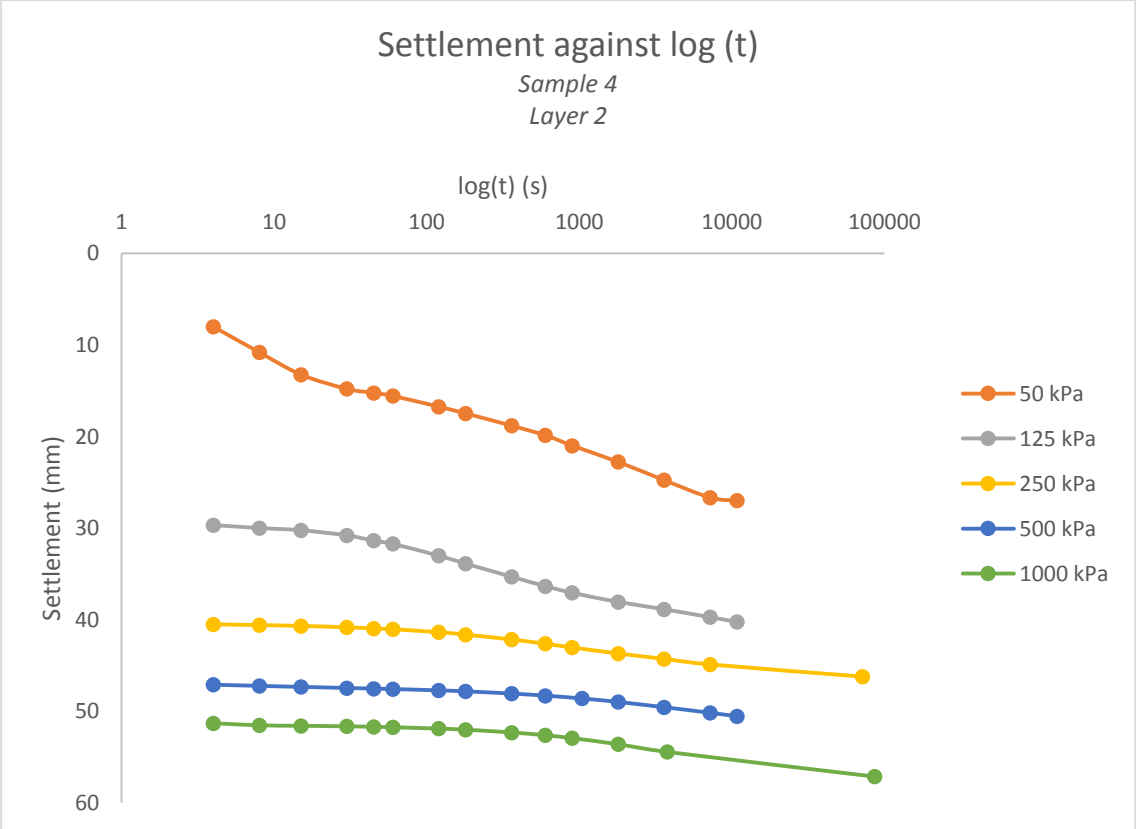

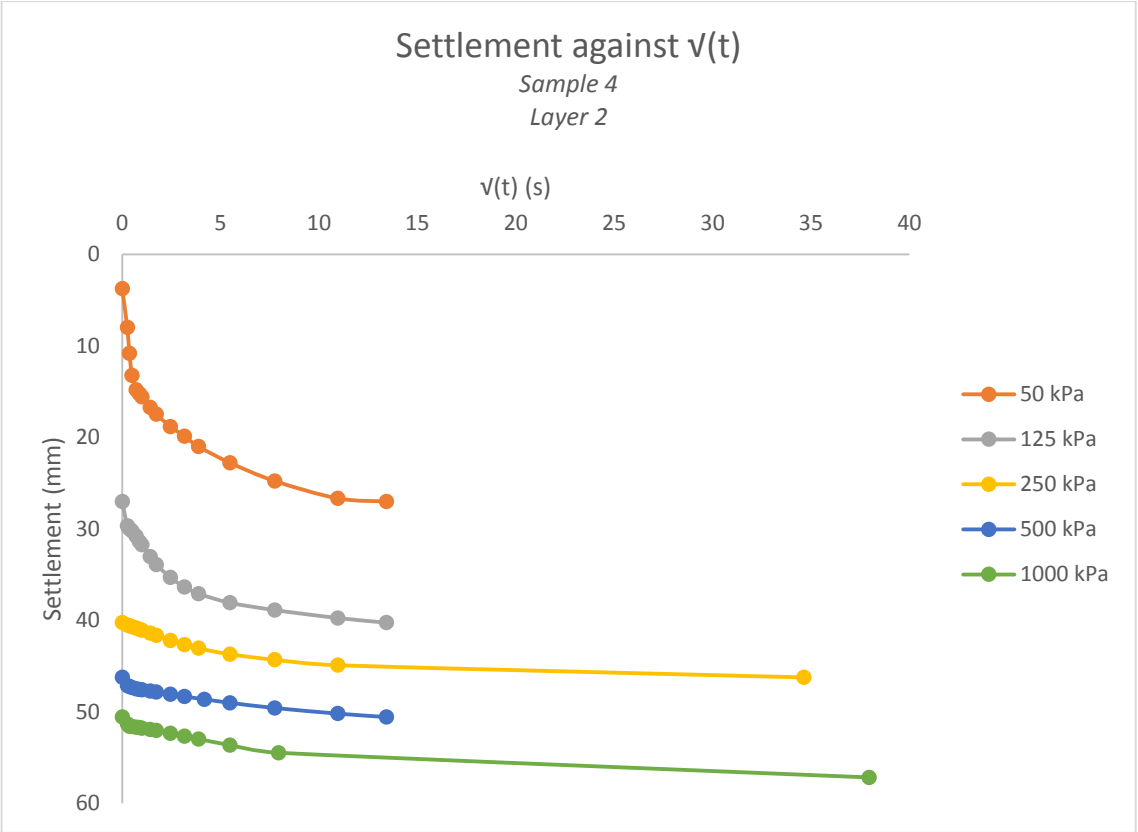

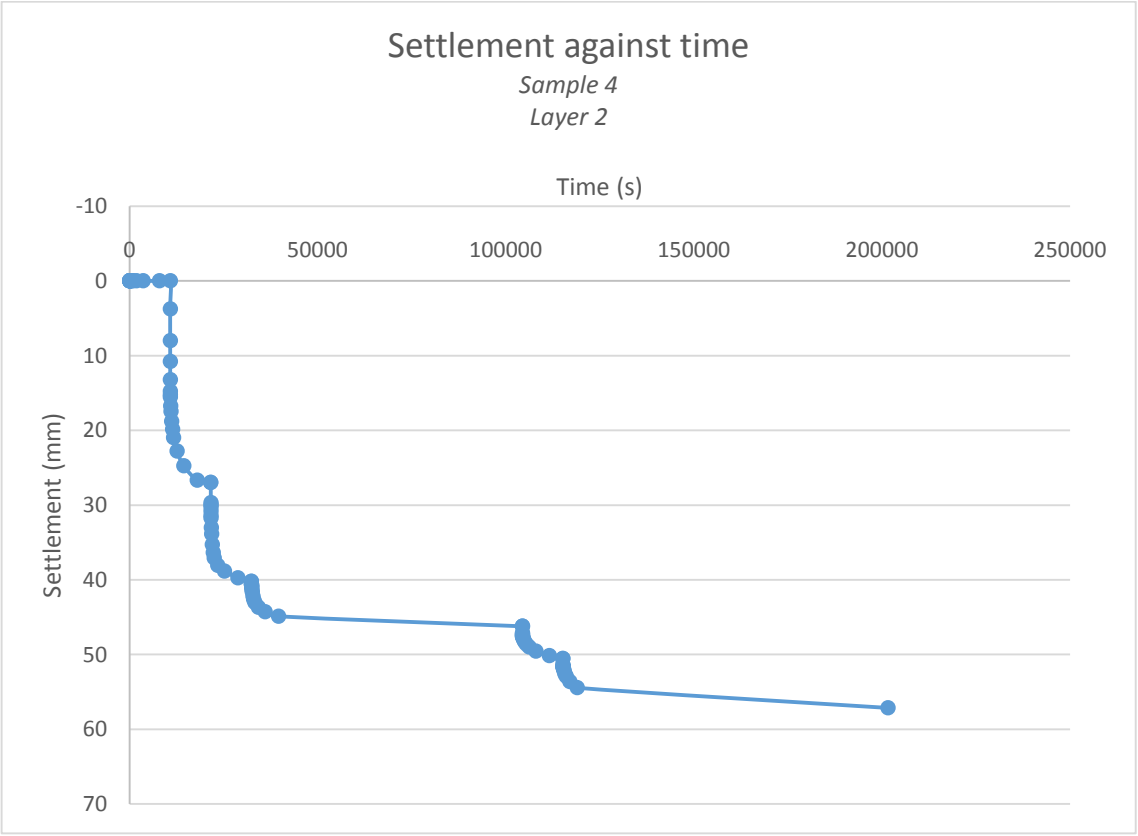

Figure 56 Oedometer test results (Sample 4; Layer 2)

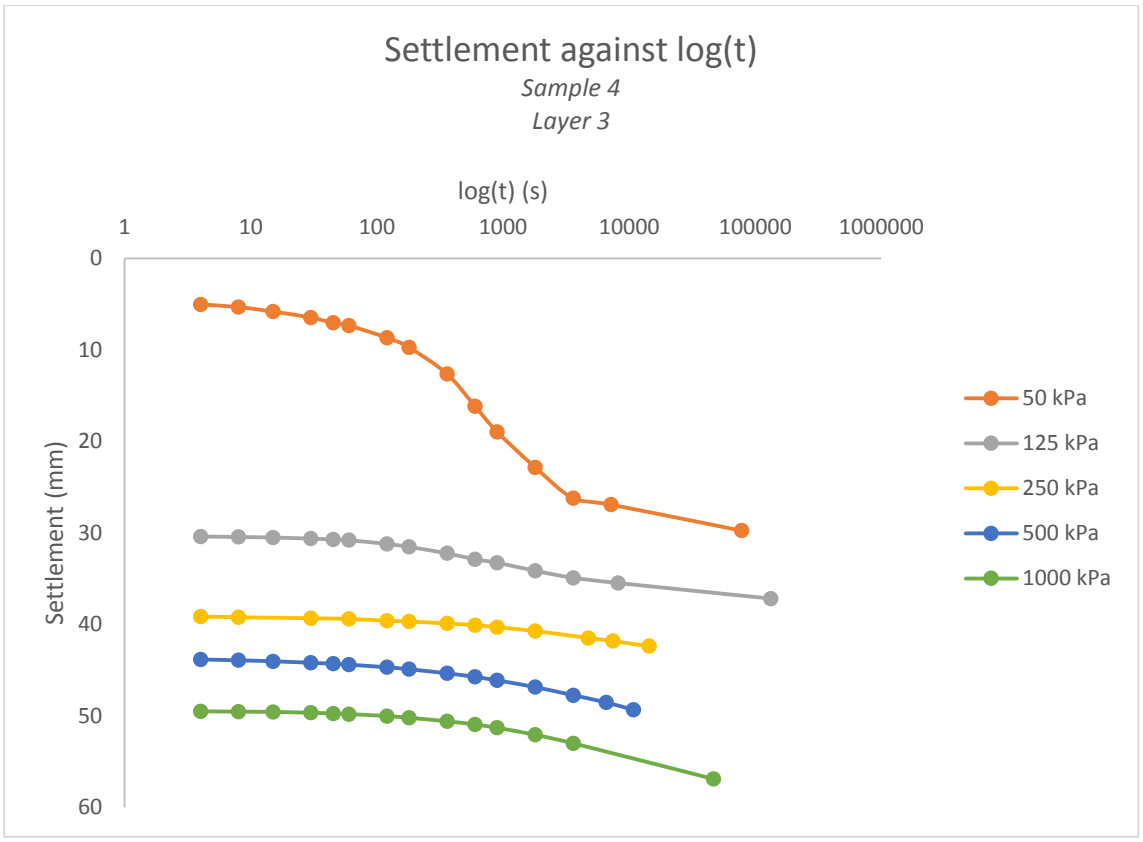
Settlement against log(t)
Sample 4
Layer 3
log(t) (s)
1
10
100
1000
10000
100000
1000000
0
10
20
30
40
50
60
Settlement (mm)
50 kPa
125 kPa
250 kPa
500 kPa
1000 kPa

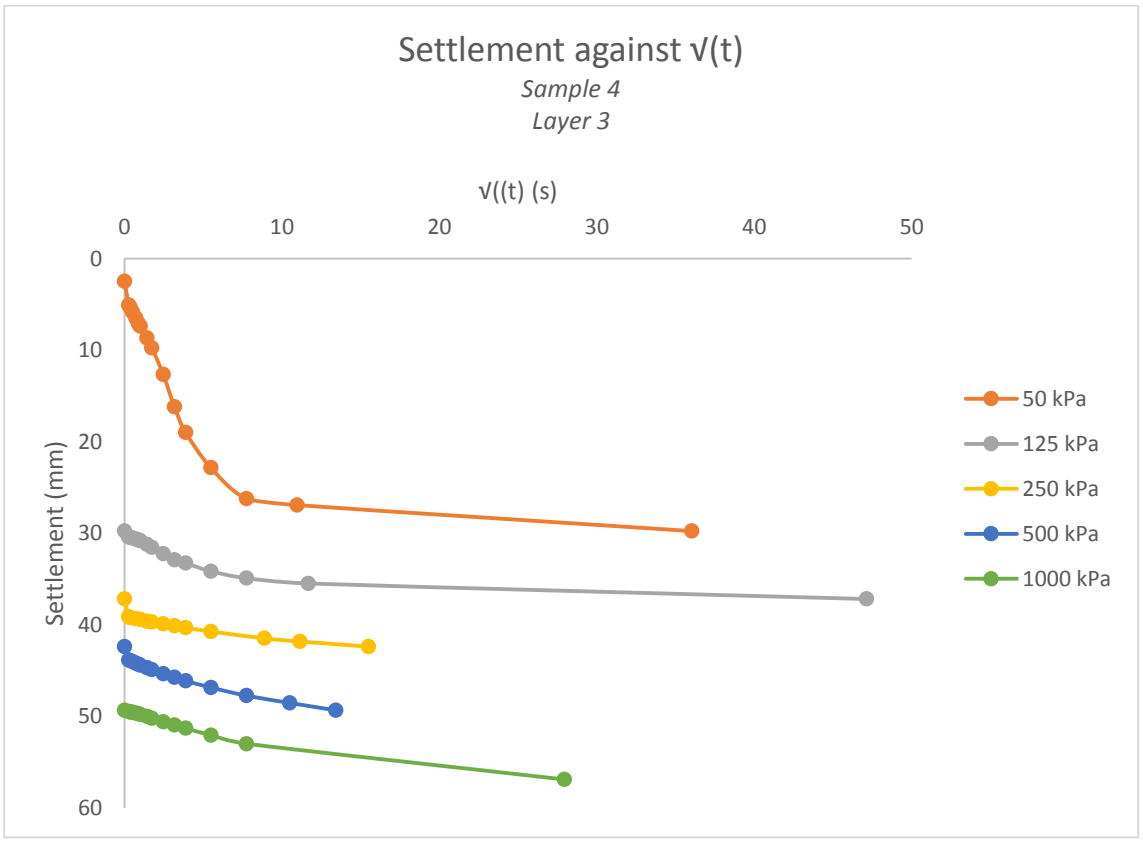
Settlement against √(t)
Sample 4
Layer 3
√((t) (s)
0
10
20
30
40
50
60
Settlement (mm)
50 kPa
125 kPa
250 kPa
500 kPa
1000 kPa

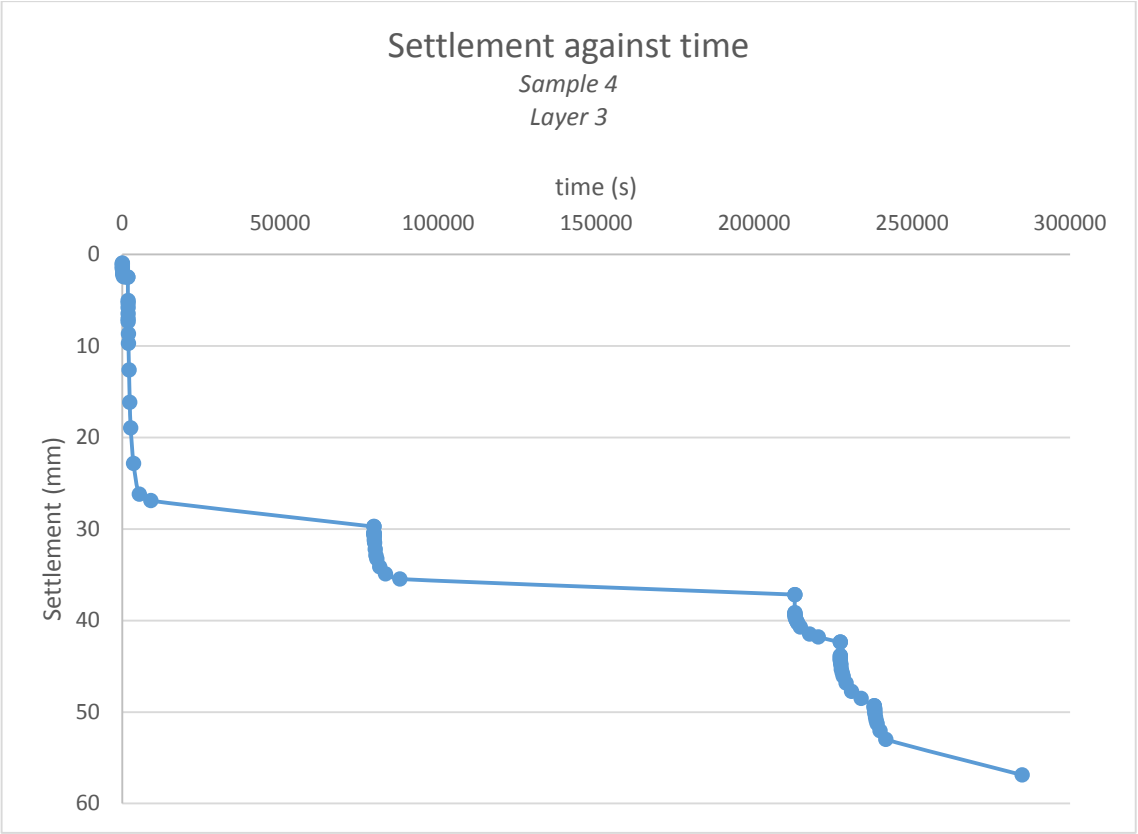

Figure 57 Oedometer test results (Sample 4; Layer 3)

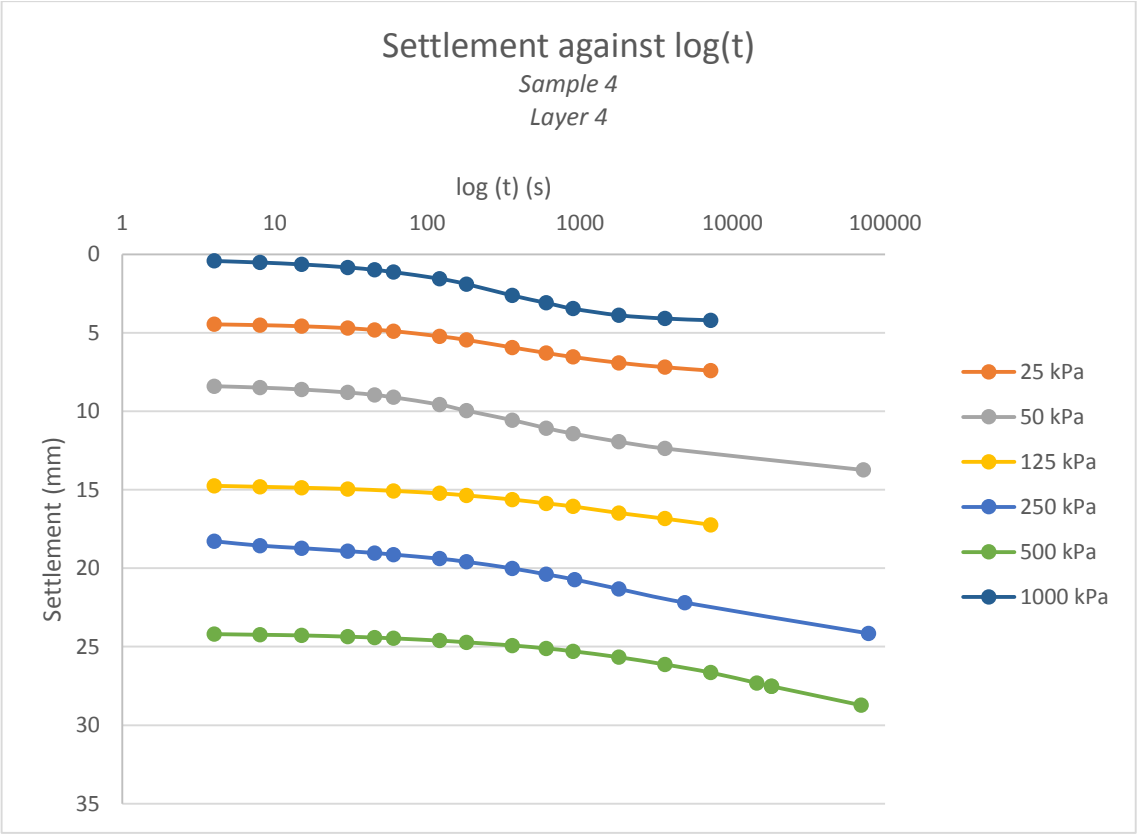

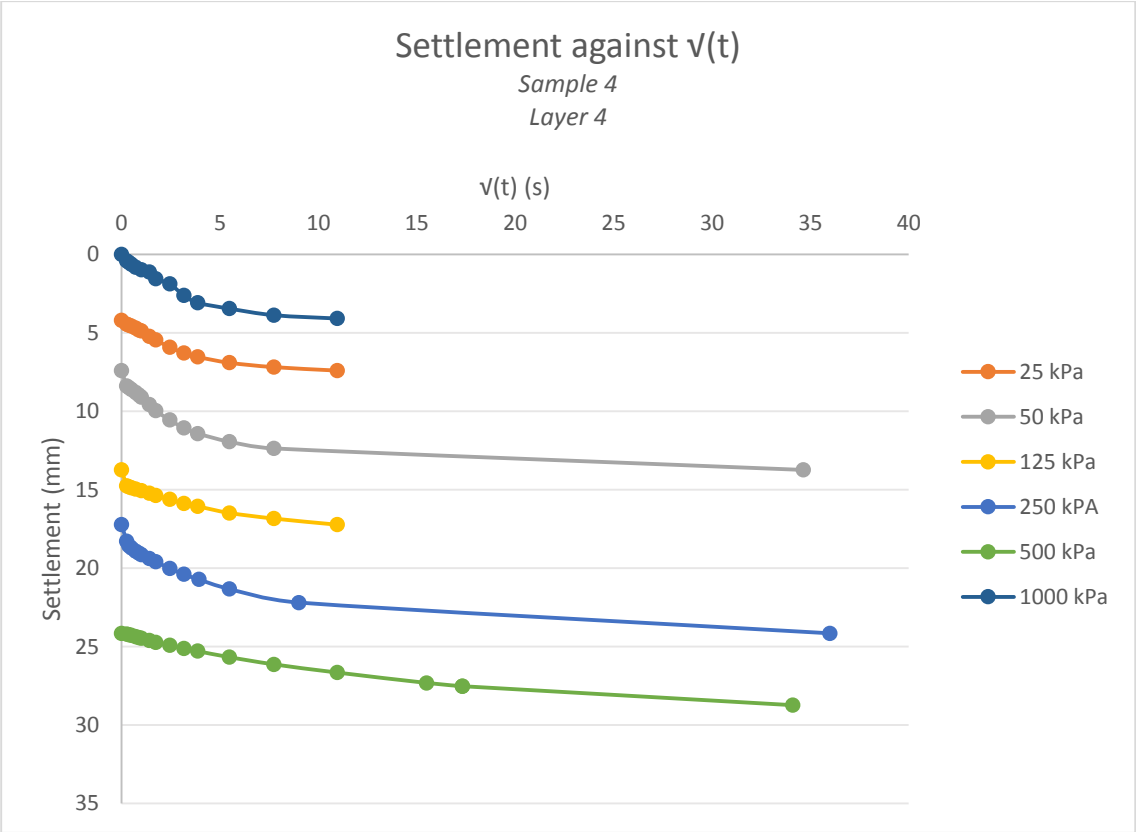

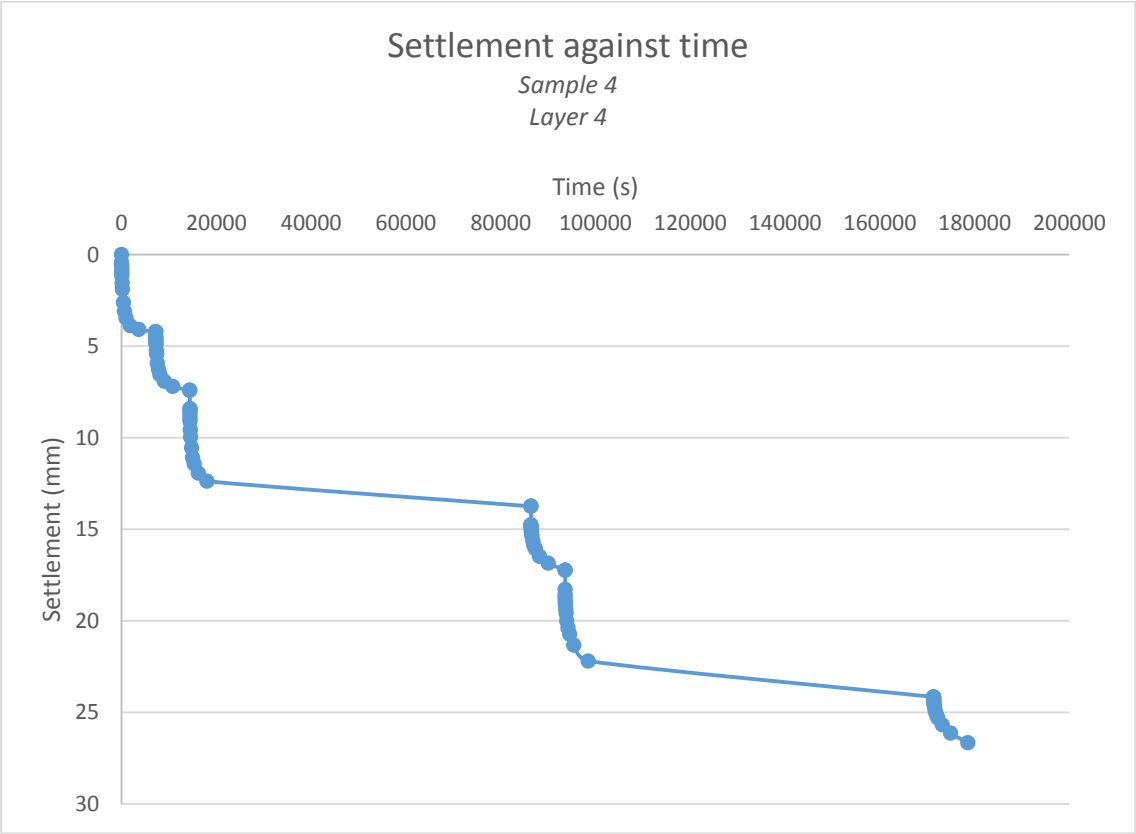

Figure 58 Oedometer test results (Sample 4; Layer 4)

5.3.4 Determination of c_v using graphical approach

The data of the settlement for each load stage were plotted against the square root of time for each layer of the third sample, in order to obtain the value of the consolidation coefficient. Only the third sample has been used because its consolidation was the less affected by the instability of the oedometer apparatus. A best fit straight line was drawn through the initial data points and a horizontal line was then drawn to represent an asymptote based on the final data points. The intersection of these lines gives $\sqrt{t_x}$ and c_v is calculated as (Powrie, 2004):

$$c_v = \frac{3d^2}{4t_x}$$

The values of the average of c_v and T after 1 hour for each load stage of each sample layer are summarised in Table 20.

Parameter	**25 kPa**	**50 kPa**	**125 kPa**	**250kPa**	**500 kPa**	**1000 kPa**
$\sqrt{t_x}$ **(minute)$^{1/2}$**	3	3,5	3,75	4	4,5	5
t_x **(seconds)**	540	735	843,75	960	1215	1500
d (m)	0,0315	0,02491	0,026	0,024	0,0215	0,0195
c_v **(m2/s)**	1,3781E-06	6,33E-07	6,01E-07	4,5E-07	2,85E-07	1,9E-07
T (after 1 hours)	5	3,673469	3,2	2,8125	2,222222	1,8

Table 20 Results of consolidation analysis using graphical approach

The values of T after 1 hour are greater than one, so it is possible to say that the sample is completely consolidated after this range of time. The value of the consolidation coefficient for the load stage of 50 kPa is quite similar of what obtained by Siddiqui (2013) $c_v = 6.87 \times 10^{-7}$ m^2/s.

5.3.5 Secondary settlement

The choice to extend the time of the oedometer test has permitted to analyse not only the consolidation settlement but also the secondary settlement. As said before, the secondary settlement are only due to the mechanical creep only, because the biologically activity was inhibited over the entire duration of the tests.

The portion of the curve corresponding to the secondary settlement has been considered linear with the logarithm of time as expressed by the equation:

$$\frac{\Delta h_s}{h_{ref}} = C_{\alpha\varepsilon} \log\left(\frac{t}{t_{ref}}\right)$$

With:

Δh_s is the secondary settlement at time t;

h_{ref} is the height of waste upon completion of primary settlements;

t_{ref} is a reference time for secondary settlement;

$C_{\alpha\varepsilon}$ is the coefficient of secondary settlement.

$C_{\alpha\varepsilon}$ describes the change in strain relative to the logarithm to the base 10 of time. It can be determined from the slope of the graph of settlement data plotted against $\log_{10}$ (time).

In order to analyse the relationship between the coefficient of secondary settlement and the applied stress, the average of $C_{\alpha\varepsilon}$ has been calculated for each normal stress considering each layer of the sample. As done before, the only third sample has been used to analyse this material characteristics because the results obtained are more reliable than what obtained for the other samples. The results are summarised in the Table 21.

Cα	**Layer 1**	**Layer 2**	**Layer 3**	**Layer 4**	**Cα (average)**
25 kPa	0,01015	0,004081	0,002752	0,010215	*0,0068*
50 kPa	0,014857	0,010356	0,005796	0,010486	*0,010374*
125 kPa	0,016736	0,011868	0,026011	0,021975	*0,019147*
250 kPa	0,026629	0,020205	0,031339	0,028232	*0,026601*
500 kPa	0,027599	0,030309	0,046009	0,038544	*0,035615*
1000 kPa	0,030918	0,028219	0,07913	0,032728	*0,042749*

Table 21 Creep settlement parameters.

There is an increase of the creep parameter with increasing values of the applied normal stress, even significant comparing the values obtained for 25 kPa and 1000 kPa. This difference can be probably due to the different density of the sample

layer at the different load stages. However, the results cannot be considered completely reliable due to the instability phenomena described before. In fact, it is likely that the settlement records include the load stick movements due to the load applied, in particular at high stresses like 500 kPa and 1000 kPa.

The results can be compared with those obtained by Siddiqui (2009), at least considering the increment of $C_{\alpha\varepsilon}$ with the applied normal stress:

MBT	Bulk unit weight (kN/m³)	$C_{\alpha\varepsilon}$
UK MBT		
Biologically activity inhibited MBT (50 kPa)	9.4	0.024
Biologically activity inhibited MBT (150 kPa)	11.2	0.021
Normal MBT (150 kPa)	10.9	0.021
German MBT		
Biologically activity inhibited MBT (50 kPa)	9.9	0.020
Biologically activity inhibited MBT (150 kPa)	11.4	0.018
Normal MBT (150 kPa)	11.5	0.019

Table 22 Creep settlement parameters for the UK and German MBT wastes (Siddiqui, 2013)

5.3.6 Compression curve

The one-dimensional compression characteristics for one layer of the fourth sample up to a vertical stress of 1000 kPa are shown in Figure 59. The MBT waste compressed significantly in response to the increase of the vertical stress, more or less $\sim$ 60% of the initial height. The settlement percentage is higher than what obtained by Bhandari (2013) for the overconsolidated 0-10 mm MBT waste sample; on the contrary, it seems to be more similar to the value obtained for the fine fraction (0-2,8 mm). However, Bhandari's MBT waste samples were prepared at the as-received moisture content of 33.7%, even lower than the moisture content measured for the MBT waste material used for this research. The fully saturated condition is likely the main cause for the high settlement recorded, in particular under the lower vertical stress when the material was very wet and the percentage

of liquid within the sample was high. The rebound on unloading was not very relevant but not even negligible as reported by Bhandari (2013). The probable cause is still the presence of the acid solution within the voids, which offer a sort of resistance to deformation once the specimen is unloaded.

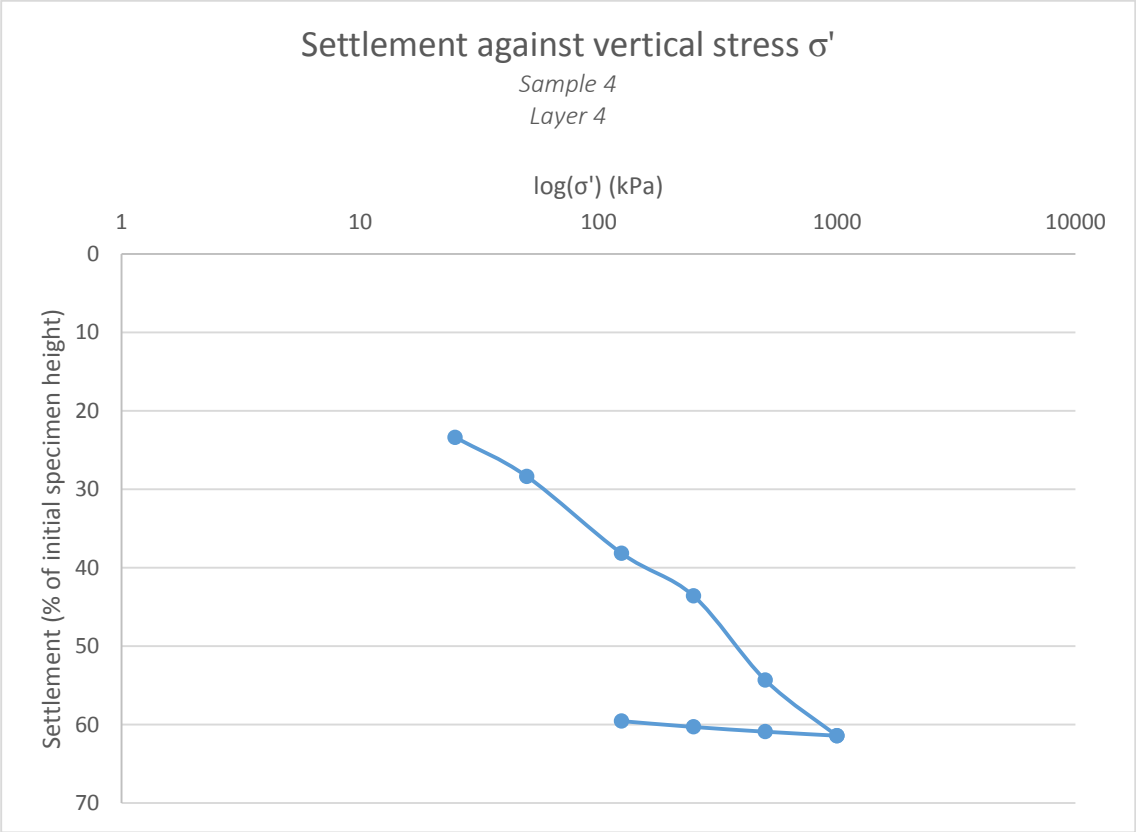

Figure 59 One-dimensional compression curve (0-10 mm)

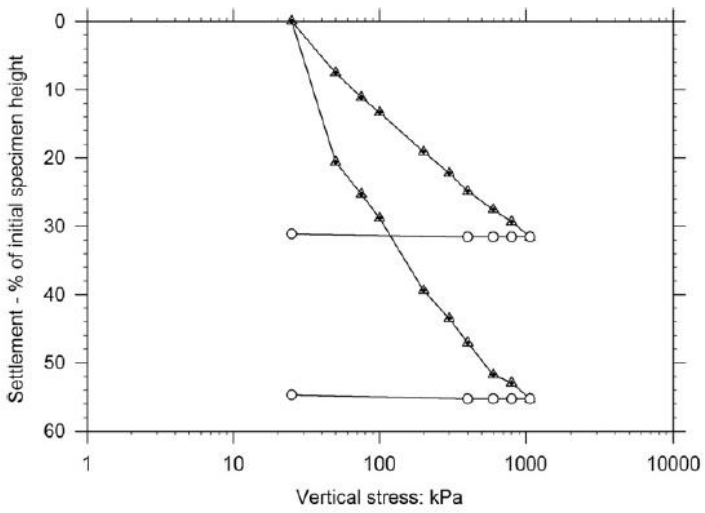

Figure 60 Normalized one-dimensional compression curves: full and fine fractions (Bhandari et al., 2013)

The bulk and dry densities are given in the following Table 23.

Physical property	**Sample 1**	**Sample 2**	**Sample 3**	**Sample 4**
Bulk density (Mg/m^3)	1.39	1.42	1.43	1.43
Dry density (Mg/m^3)	0.786	0.83	1.02	1.00

Table 23 Densities of MBT waste specimens.

When extruded, the samples were very compacted. Figure 61 shows a picture of an overconsolidated specimen. The one and two-dimensional particles tended to become oriented horizontally even though they had been randomly placed in the mould prior to the specimen compression.

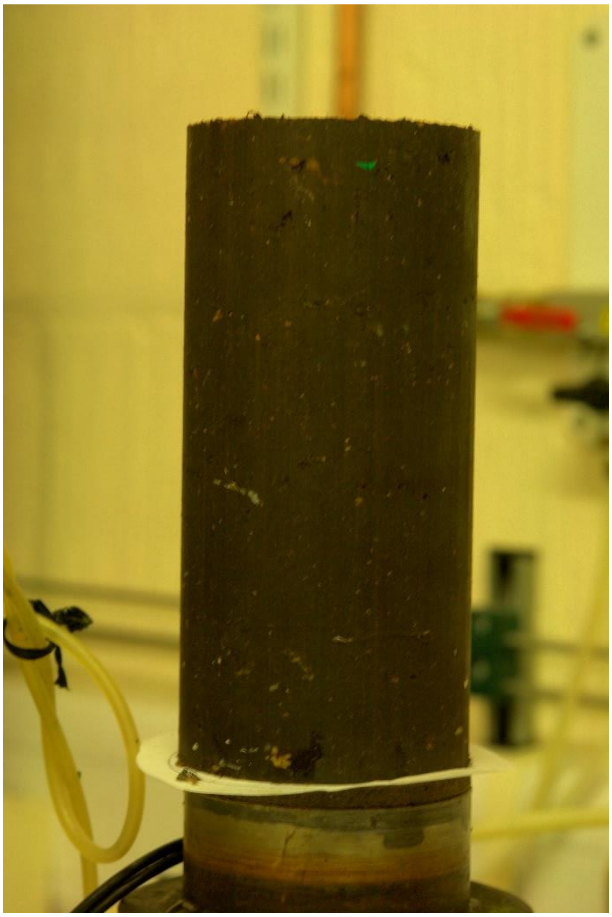

Figure 61 Overconsolidated MBT waste specimen.

5.4 The triaxial apparatus

The triaxial test is widely used in industry to investigate the stress/strain behaviour of soil for design purpose. The tests have been carried out on cylindrical samples 70 mm in diameter and about 150 mm in height. The sample is enclosed by double thin rubber membranes and placed inside the triaxial test, where it can be subjected to an all-around water pressure and to a vertical force acting through a piston.

Triaxial tests were carried out on overconsolidated specimens at the cell pressures of 25 and 200 kPa in order to investigate the mechanical behaviour of the MBT waste in fully saturated conditions. The test are all drained.

The tests were carried out using a strain-controlled triaxial apparatus comprising:

- a transparent triaxial cell;
- an external digital camera;
- an uniform light source;
- a light reflecting surface.

5.4.1 Camera setup

The digital camera was placed in front of the cell, mounted on cantilevers extending from the base of the triaxial platform. Therefore, the whole camera system moved up with the cell base during the shear test. Horizontal and vertical adjustment screw allowed the camera to be set up, with optical axes of the cameras approximately level with the mid height of the specimen. The camera position was adjusted until the offset distances from the edge of the specimen to the edge of the image on each side were approximately equal.

The aspect ratio of images was 3:2 (3888 pixels x 2592 pixels). Because focusing on the specimen through the cell wall is difficult in autofocused mode, images were captured in manual focus mode. The aperture was set to small opening (large F-number), decreasing the amount of light admitted and increasing the depth of field, allowing the whole specimen to appear in focus. In this mode, the shutter speed is automatically adjusted by the camera to obtain the correct exposure according to the brightness of the object.

A lighting arrangement was used to provide uniform illumination to the specimen, enabling clear, high quality images to be captured. The light source was fixed to a yoke clamped onto one of the two vertical posts of the triaxial loading frame.

The digital image correlation technique requires the application of an artificial texture to the membrane via a casual spraying with quick-drying black enamel paint. The spray creates a non-repeating, random arrangement of small dots on the membrane surface.

The digital camera was used to capture images of the deforming specimens at various stages of each test. The images were captured every hour during the test, in order to analyse the local strain field and to identify any strain localization, which might lead to the formation of a shear bands.

The tests were carried out in a constant temperature laboratory maintained at 20 °C.

5.4.2 Sample preparation

After posed the porous stone and the filter paper soaked in the acid solution, the MBT waste sample is placed above the triaxial base platen (Figure 62).

Figure 62 MBT waste specimen placed inside the triaxial apparatus.

In order to facilitate the drainage, an additional lateral filter paper drain was applied over the specimen surface. The use of a lateral filter paper around the sample has the advantage of markedly reducing the time needed for the excess pore water pressure inside the sample to dissipate. This additional drain is then fixed on the top of the specimen with another circular filter paper and, above it, the porous stone. Each filter used for the test was before soaked in the acid solution used during the consolidation of the specimen.

The internal rubber membrane (0.3 mm thick) was rolled over a length of a metal tubing. In order to ensure the contact between the membrane and the tube, it was necessary to create a vacuum. The first membrane was then applied on the specimen and fixed to the base platen. The same operation was done for the external membrane, which had the texture on its surface. The two membrane are then fixed to base platen and to the top cap using four black rubber O-ring, which permit the complete sealing of the specimen. Two layer of membrane each 0.3 mm thick were used in order to avoid that the membrane could be punctured by sharp objects and to avoid the possible ingress of cell water into the specimen.

5.4.3 Triaxial procedure

Once the sample is placed upon the triaxial platen, the triaxial cell was put over the sample, being careful to line up the piston in the cell with the ball bearing on the sample top cap. The cell was then filled with deaerated water mixed with a little bit of bleach. The bleach has been used in order to avoid the growth of algae inside the cell, which affects the picture quality. This phenomenon occurred in the second test at the radial pressure of 25 kPa.

At this point, the top cap valve was closed in order to be able to monitor the real pore pressure inside the specimen. The drainage was allowed only through the base of the specimen, so the drainage path length was the entire length of the specimen.

Once the cell was completely filled, a cell and a back pressure was applied by the GDS pressure/volume controller. The external LVDT was then reset to zero. All instruments were logged via a personal computer using the GDSLAB software and

GDS Ltd data logging system with 16 bit data acquisition. The data were recorded every 10 seconds.

The specimen was then allowed to saturate until the B-Value reached at least a value of 0.92. This value was the maximum which could be achieved; this fact is likely due to the compressibility of the waste particles which prevent the fully saturation. The procedure consists simply of closing the drainage circuit, then increasing the cell pressure by an increment $\Delta\sigma_3$ and measuring almost immediately, through the pressure transducer connected to the drainage circuit, the increment of pore water pressure Δu thus generated. Skempton equation can then be used to calculate the coefficient B of saturation:

$$B = \frac{\Delta u}{\Delta \sigma_3}$$

After the saturation, the sample was allowed to consolidate to a new equilibrium condition. The cell and back volume change were both recorded in order to measure the deformation of the sample during this first phase of the test. The consolidation was considered concluded when the back volume became stable. The measurable volume changes occurred during the isotropic compression of the samples were used to calculate their actual density at the start of the shearing.

Once the specimen was consolidated, it was then sheared using a constant rate of shearing. The drained test had to be carried out slowly enough not to allow significant excess pore water pressure to develop within the sample. The rate testing depends on the permeability, the size of the sample and on the drainage arrangements. In the following table, the shear ratio and the B-Value for each test are summarised (Table 24). During two of the four test carried out the shearing ratio was no more controlled by the personal computer and started to increase, affecting the test results. However, the data obtained from these tests are used only to describe the MBT waste behaviour in an approximate way.

	Test 1* **(25 kPa)**	**Test 2** **(25 kPa)**	**Test 3*** **(200 kPa)**	**Test 4** **(200 kPa)**
Shear ratio (mm/min)	0.0125	0.003	0.0028	0.001
Shear ratio (%/hour)	0.5	0.125	0.112	0.04
B-Value	0.925	0.925	0.9312	0.899

Table 24 Shear rate and B-Value

The axial load was measured by an internal load cell, the global axial displacement by the external LVDT and the volume of the water flowing into or out of the cell and the sample by the GDS pressure/volume controller.

Shearing was continued until the stress ratio reached an approximately constant value or had started to decrease.

Once the test is completed, the camera was calibrated using a planar check board as a calibration pattern at different orientations about the image plane position and keeping the camera stationary (Figure 63).

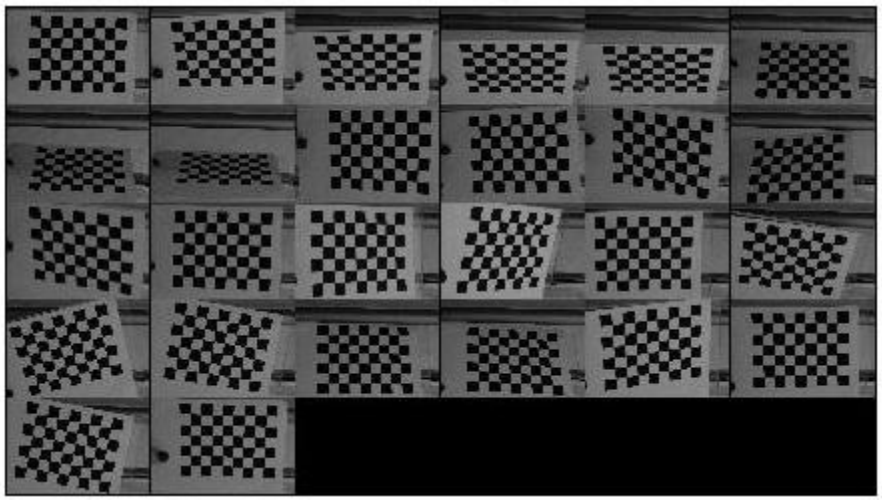

Figure 63 Calibration images.

After the calibration, the sample was removed from the triaxial apparatus and weighed. In order to calculate the moisture content and the dry density, the specimen was then dried in oven at 70 °C.

5.4.4 Description of the parameters

The measured quantities which can be obtained from a triaxial drained test are:

- The cell pressure σ_c (kPa)
- The ram load Q (kN)
- The pore pressure u (kPa), considered as the average of the measures obtained from the transducers at the base and at the top of the sample
- The change in sample height Δh (mm)
- The change in sample volume ΔV

The following step is to convert these measurements to stress, strain and state parameters.

The sample height and volume at the start of the shear test (h_0 andV_0) are not be the same as the height and volume of the sample at the beginning of the test. In fact, the application of the cell pressure induced changes in the sample volume, which could extend or reduce.

$$V_{t0} = V_{ti} - \Delta V_{tc}$$

Where V_{ti} is the volume at the beginning of the test,

ΔV_{tc} is the volume change during the consolidation.

Assuming that the sample deforms isotropically under the cell pressure during the consolidation, the linear strain in all three directions must be the same:

$$\frac{\Delta V_{tc}}{V_{ti}}\frac{1}{3} = \varepsilon_1 = \varepsilon_2 = \varepsilon_3$$

So the sample height at the beginning of shearing can be expressed as:

$$h_0 = h_i(1 - \frac{\Delta V_{tc}}{3V_{ti}})$$

To convert the readings of axial force or ram load Q into deviatoric stress q it is necessary to divide it by the current area of the sample A:

$$V_t = \left(V_{to} - \Delta V_{tq}\right) = A(h_o - \Delta h)$$

Where ΔV_{tQ} is the volume of water expelled during shear.

$$q = \frac{Q}{A} = \frac{Q(h_o - \Delta h)}{V_{to} - \Delta V_{tq}}$$

Another expression can be used using the axial and volumetric strain, ε_a:

$$h_0 - \Delta h = h_0(1 - \frac{\Delta h}{h_0})$$

$$h_0 - \Delta h = (1 - \varepsilon_a)$$

$$V_{to} - \Delta V_{tq} = V_{to}(1 - \frac{\Delta V_{tq}}{V_{to}})$$

$$V_{to} - \Delta V_{tq} = V_{to}(1 - \varepsilon_{vol})$$

Hence:

$$q = \frac{Q}{A_0}\frac{1-\varepsilon_a}{1-\varepsilon_{vol}}$$

The average effective stress p' is defined as:

$$p' = \frac{\sigma'_1 + \sigma'_2 + \sigma'_3}{3}$$

$$p' = \frac{\sigma_a + 2\sigma_c}{3} - u$$

Where the axial stress σ_a is defined as:

$$\sigma_a = q + \sigma_c$$

Hence:

$$p' = \sigma_c + \frac{q}{3} - u$$

The specified volume at the end of the test ν is determined from the dry mass of the sample m_s and its total final volume V_{tf}.

$$V_{tf} = V_{ti} - \Delta V_{tc} - \Delta V_{tq}$$

The specific gravity of the soil particles G_s is known as:

$$G_s = \frac{\rho_s}{\rho_w}$$

Where ρ_s is the soil particles density and ρ_w is the water density.

$$V_s = \frac{m_s}{\rho_s} = \frac{m_s}{G_s\rho_w}$$

Hence:

$$\nu_f = \frac{V_{tf}}{V_s} = \frac{V_{tf}G_s\rho_w}{m_s}$$

The final void ratio e_f can be defined as:

$$e_f = w_f G_s$$

Where w_f is the final water content.

The final specified volume can be rewritten as:

$$\nu_f = \frac{V_{tf}}{V_s} = \frac{V_v + V_s}{V_s} = 1 + e_f = 1 + w_f G_s$$

It can be difficult to remove the sample cleanly from the membrane to measure the dry sample mass so that equation usually gives more reliable result than the other one.

To plot the state path in ν/lnp' space, the specific volume has to be determined at each stage of the test from the total volume of the sample at the start of the shear test V_{t0} and the volume of water expelled since the start of the shear test ΔV_{tq}:

$$\nu = 1 + e = \frac{(V_{t0} - \Delta V_{tq}) G_s \rho_w}{m_s}$$

$$\frac{G_s \rho_w}{m_s} = \frac{\nu_f}{V_{tf}} = \frac{1 + w_f G_s}{V_{tf}}$$

Mohr circles of stress

$$\sigma_1 = \sigma_3 + q$$

The maximum stress ratio τ/σ' mobilised in the sample corresponds to the mobilized angle of shearing ϕ'_{mob}:

$$\phi'_{mob} = \sin^{-1} \frac{\sigma'_1 - \sigma'_3}{\sigma'_1 + \sigma'_3}$$

ϕ'_{mob} is defined by the tangent to the Mohr circle which passes through the origin and it is a measure of the strength used or mobilized to enable the waste to carry the applied stresses.

The shear stress τ can be defined graphically using the Mohr circles as:

$$\tau = \frac{\sigma'_1 - \sigma'_3}{2}$$

The normal effective stress applied on the specimen can be expressed as an average of the principal normal stress σ_1 and σ_3:

$$\sigma' = \frac{\sigma'_1 + \sigma'_3}{2}$$

Mohr circles of strain

In a drained test ε_{vol} is no zero, so the radial strain can be expressed as:

$$\varepsilon_r = \frac{1}{2}(\varepsilon_{vol} - \varepsilon_a)$$

In addition, the maximum shear strain is equal to:

$$\gamma_{max} = \frac{1}{2}(3\varepsilon_a - \varepsilon_{vol})$$

An alternative shear strain parameter which is sometimes used is the triaxial shear strain $\varepsilon_q$and it is defined as:

$$\varepsilon_q = \frac{2}{3}(\varepsilon_a - \varepsilon_r)$$

The rate of dilation d is defined as the negative of the rate on increase of average volumetric strain ε_{vol} with triaxial strain ε_q. It could be defined as:

$$d = -\frac{\delta\varepsilon_{vol}}{\delta\varepsilon_q}$$

The stress ratio q/p' is associated with a given degree of dilation d through the stress-dilatancy relationship given by Cam Clay (Schofield and Wroth, 1968).

$$\frac{q}{p'} = M + d$$

Where M is the value of critical stress ratio and it should be the same for every specimen if they are made from the same material. In fact, M is function of the material's characteristics only and it is not influenced by the confining pressure. In this experiment the critical stress ratio M is defined by the second tests carried out using a cell pressure of 200 kPa because the specimens show a more uniform deformation and the dilation has zero value at the end of test ($M = 1.65$).

Chapter 6

Triaxial compression test results

Four drained triaxial test are carried out in order to investigate the strength characteristics of an MBT waste in fully saturated condition. In particular, the major aim of this research was the study of the different behaviour shown by the MBT waste under different confining pressure. Hence, the specimens have been tested at cell pressures of 25 kPa and 200 kPa in order to better highlight the possible differences. The test characteristics are summarized in the following table:

	Test 1	**Test 2**	**Test 3**	**Test 4**
Sample diameter (mm)	70.51	70.61	70.63	70.66
Sample height (mm)	148.987	151.95	152.71	152.75
B-Skempton value	0.925	0.925	0.9312	0.899
Consolidation type	Isotropic	Isotropic	Isotropic	Isotropic
Shear type	CD-TXC	CD-TXC	CD-TXC	CD-TXC
Strain rate C(%/h)	0.5	0.125	0.112	0.04

Table 25 Triaxial test characteristics.

6.1 Triaxial tests with confining pressure of 25 kPa

The results obtained from the test carried out using a cell pressure of 25 kPa highlights a dilative behaviour and the presence of a strength peak. The Figure 64 and Figure 65 show the deviatoric stress plotted against the axial strain and the stress ratio plotted against the axial strain respectively. They both shows the presence of a peak at an axial strain of about 5%, beyond which the strength of the waste decreases towards a sort of critical value as the strain increases. The steady state stress ratio is achieved after an axial strain of ~20%. This behaviour

is quite different from what observed for the raw MSW where the material resistance usually increases at high axial strain. The peak stress ratio has a value of 2.29 and a residual value of 2.05.

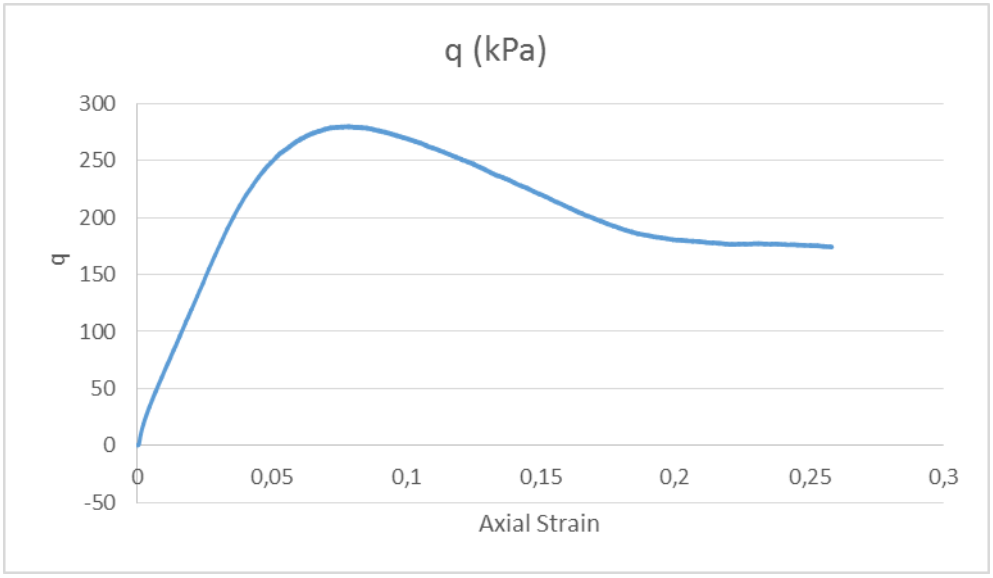

Figure 64 Deviatoric stress plotted against axial strain (Test 2)

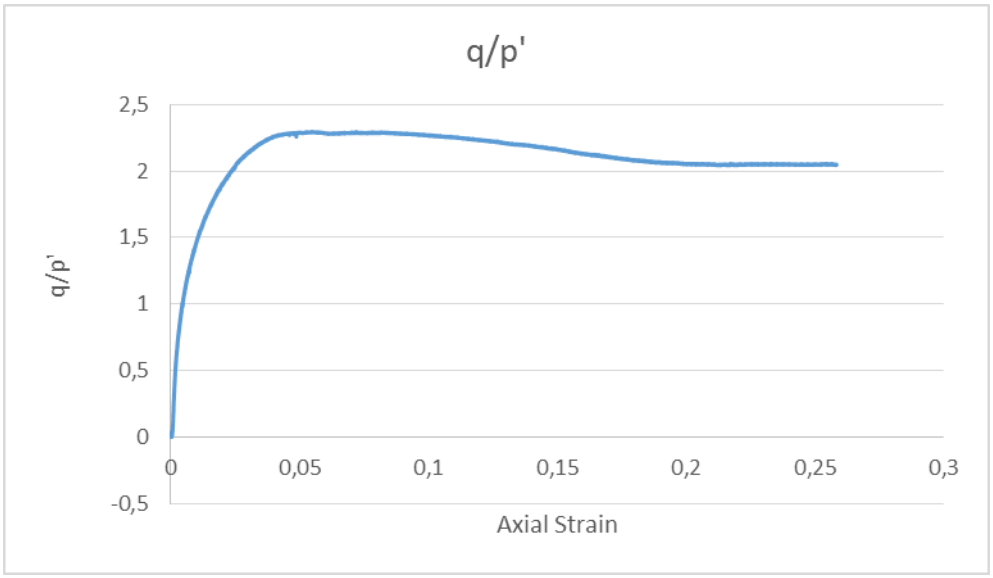

Figure 65 Stress ratio against axial strain (Test 2)

The sample starts to compress at the beginning of the test reaching a volumetric strain value of 1,5% of the total volume at the beginning of the shear stage. After that, the specimen starts to dilate until the end of the test. The final volumetric value is -2.25% of the initial volume. The rate of dilation seems to reduce with the increase of the axial strain. Is it possible to say that the mobilization of the peck stress ratio (Figure 66) is associated with dilation, as could be seen for other compacted geo-material like overconsolidated clay. The peak value of stress ratio is linked to the rate of dilation; in fact, when the rate of dilation is maximum the stress ratio reaches the peak value of 2.29.

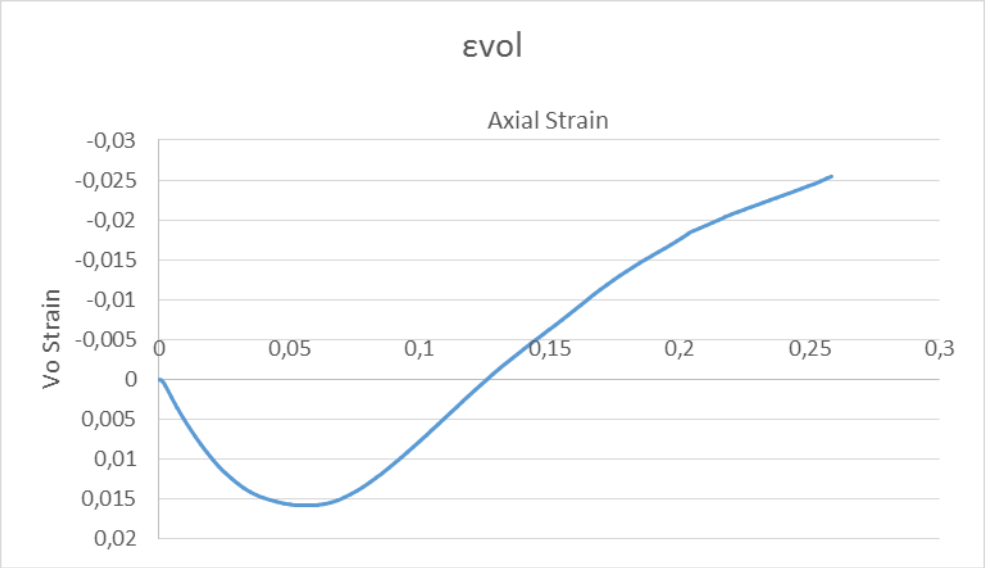

Figure 66 Average volumetric strain plotted against axial strain (Test 2)

The triaxial shear test data is also presented as graphs of mobilized angle of shearing ϕ'_{mob} as a function of the axial strain, as shown in Figure 67. The rate of increase of ϕ'_{mob} reduced with the axial strain until the peak is reached. After that, the mobilized angle starts to reduce and, at the end, it seems to reach a sort of residual value. The angle of shear resistance at peak is 56° and it is reached at an axial strain of 5.48%. The angle of the residual strength has a value of 49°.

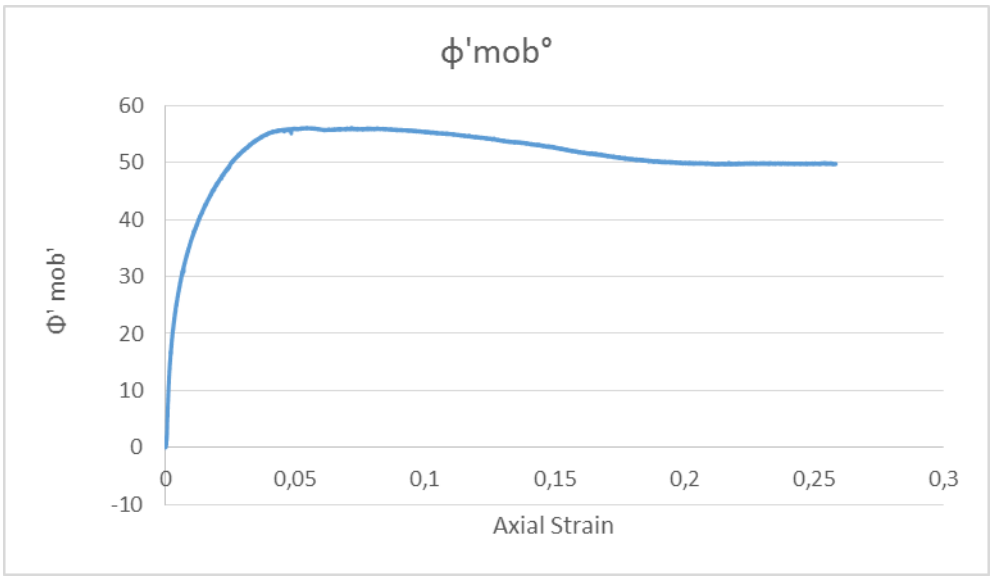

Figure 67 Mobilized angle of shearing against axial strain (Test 2)

The following Figure 68 shows the stress ratio q/p' associated with a given degree of dilation d. At the beginning, the dilation decrease, describing the increase of sample compression at the beginning of the test. After the stress ratio reached a value of 1, the dilation ratio start to increase until a value of 0.28. The peak stress ratio is achieved when the maximum dilation rate is observed. As we can see, the critical state when $q/p' = M$ is not reach and the rate of dilation contribute is still relevant. However, the stress ratio q/p' associated with a given degree of dilation d was much greater than that indicated by the stress-dilatancy relationship given by Cam Clay:

$$\frac{q}{p'} = M + d$$

As the sample is fully saturated, the cause of the high stress ratios and the subsequent angle of shearing could not be the generation of suctions within the smaller voids as supposed by Bhandari et al (2013). The cause has to be reach into the behaviour of the MBT waste material, which seems not to follow the Cam Clay rule. Thus, the higher stress ratio obtained is a subsequence of the dilative behaviour shown at low effective cell pressure.

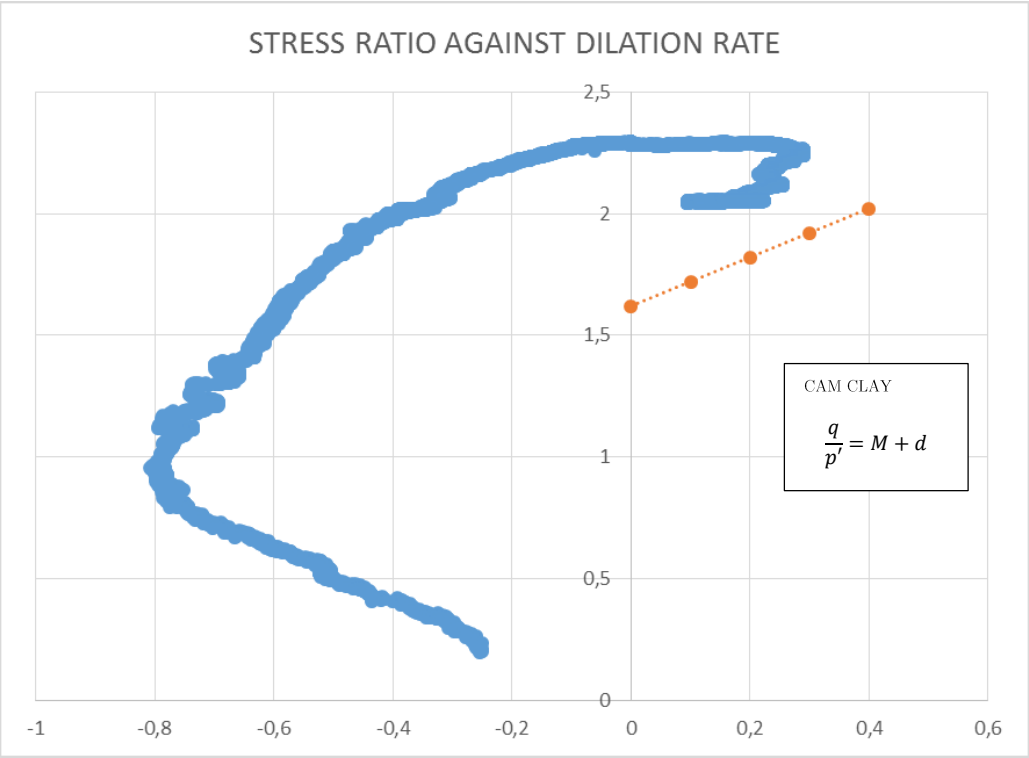

Figure 68 Stress ratio against rate of dilation d (Test 2)

All these consideration can be confirmed by the results obtained for the first test, even if they are affected by the relevant increase of the pore pressure within the sample during the test. In fact, the shear rate increased until a value of 0.5% of the specimen height per hour for a problem of computer control. The increase of the pore pressure has induced a reduction of the effective stress within the sample, making impossible to compare the results with those obtained from the second test.

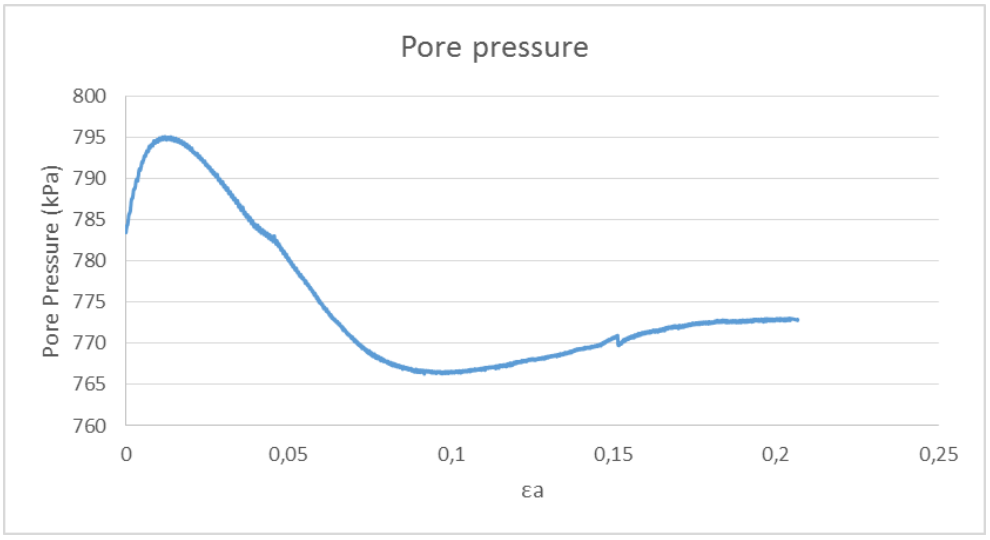

Figure 69 Pore pressure within the sample in the test 1

The graphs obtained are shown in the following figures. The compressive volumetric strain is smaller than what obtained in the second test; this fact can be explained by the impossibility for the water to flow out form the pores and the subsequent increase of its pressure. The peak stress ratio (2.4781) is a little bit higher and it can be explained by the reduced effective stress in the sample. The mobilized angle of shear resistance reaches the peak value of 61°, higher than what obtained in the second test. The graph of the stress ratio plotted against the dilation rate d shows a similar curve, but more shifted to the left part. The rate of dilation reaches a peak value of 0.35, which means that the sample expanded more. As seen previously, the stress ratio is higher than what provided by Cam Clay, validating the assertion that the MBT waste has a dilative behaviour once subjected to low effective stresses.

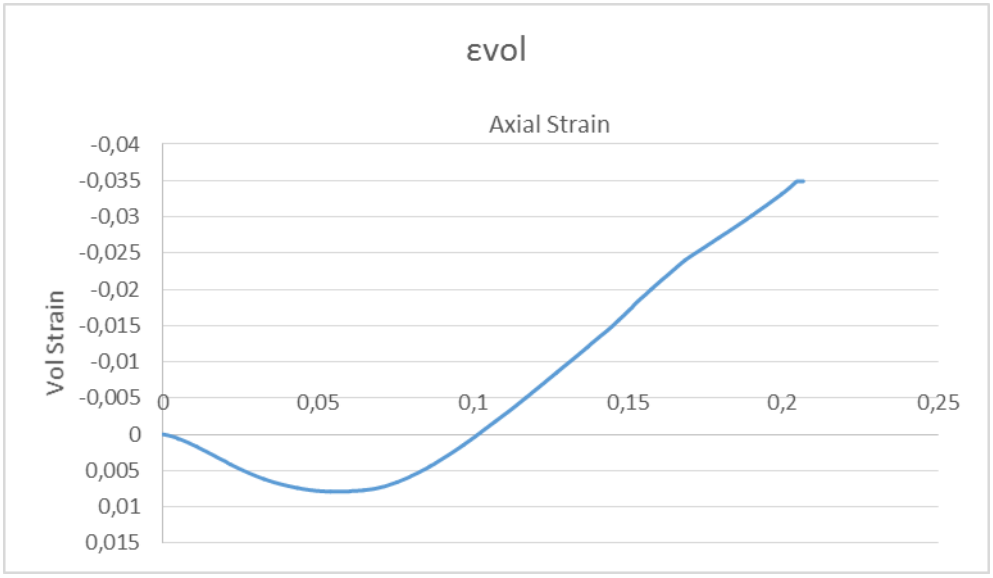

Figure 70 Volumetric strain against axial strain (Test 1)

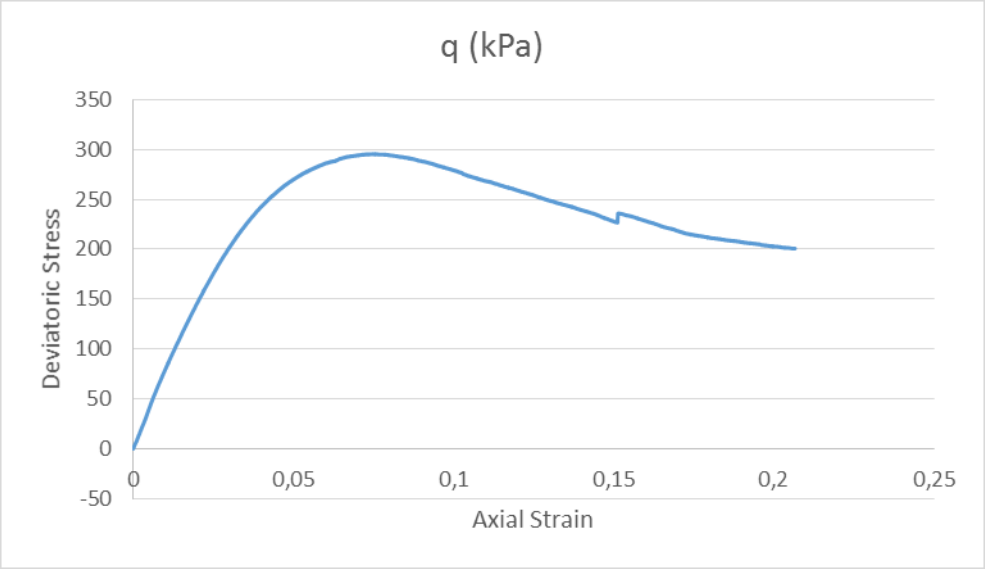

Figure 71 Deviatoric stress against axial strain (Test 1)

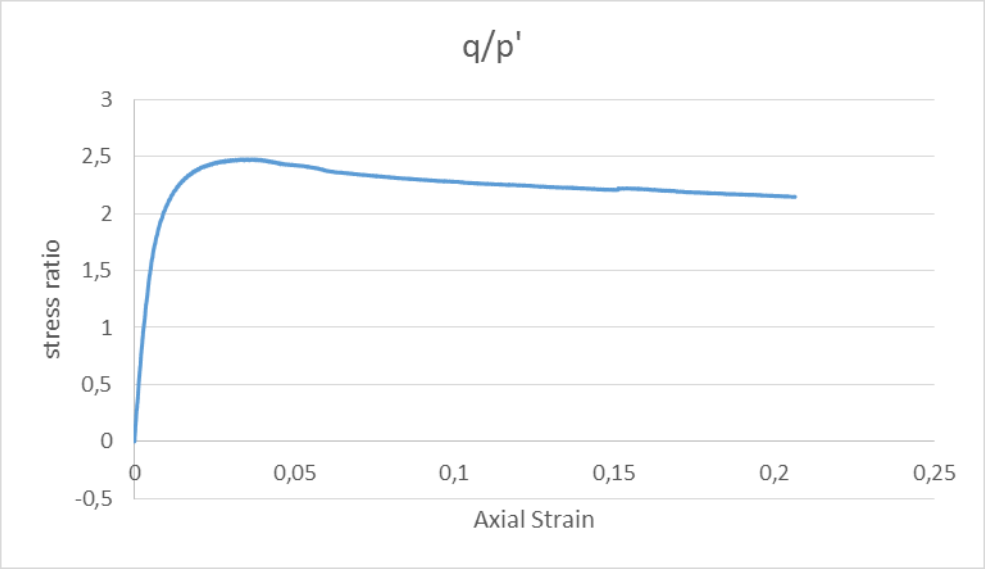

Figure 72 Stress ratio against axial stress

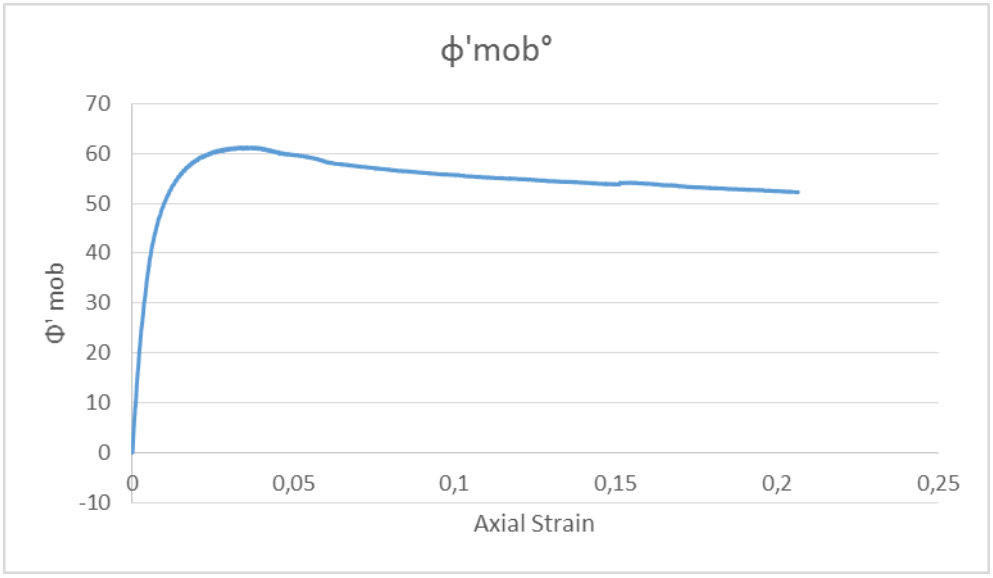

Figure 73 Mobilized angle of shearing against axial strain

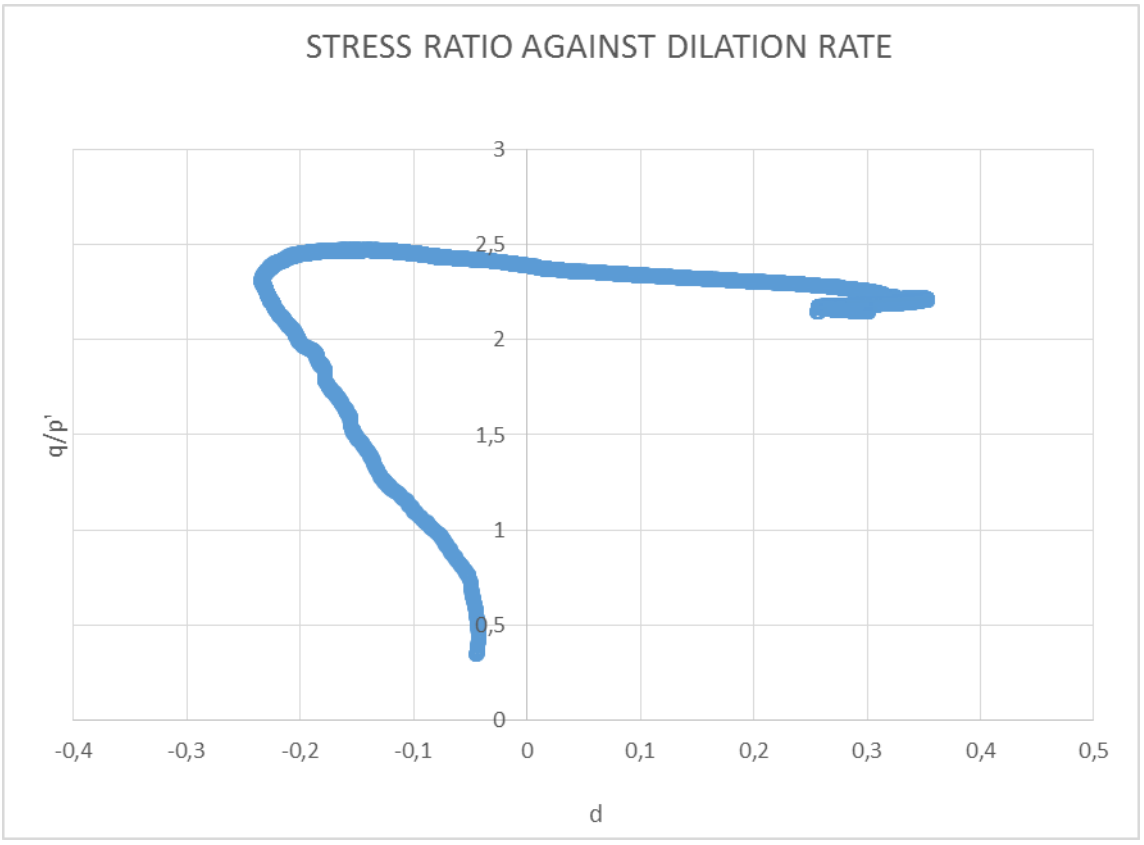

Figure 74 Stress ratio against rate of dilation (Test 1)

6.1.2 Image analysis and deformation pattern

Typical fields of displacement obtained by analysing image pairs taken at various axial strain intervals for the overconsolidated sample tested at a cell pressure of 25 kPa are shown in the following figures. The deformation fields obtained by DIC at an axial strain greater than 20% are beginning to become unreliable, owning to the folding of the membrane.

The local deformation distributions show that the main mode of deformation is one-dimensional compression because the displacement vectors are substantially vertical. However, at high axial strain values, the radial component becomes more relevant even if it does not reach high values. The application of the deviator stress is mainly to compress the specimen on dimensionally. There is almost no lateral expansion at this axial strain values and the main effect of the shearing up to an average axial strain of 10-15% was to increase the density of the specimen. There is no evidence of clear and distinct localized failure. Anyway, the final picture shows a higher concentration of vertical displacement localized on the top of the sample and a tendency to expansion in the bottom.

However, at large strains (in the post peak regime) asymmetric bulging and significant buckling of the specimen occur, as shown in the Figure 79. After an axial strain of approximately 20%, a localization of deformation can clearly be observed looking at the specimen pictures taken during the test. In fact, the top of the sample does not show any lateral expansion, rather than what could be seen on the bottom; the sample seems to split in two part with different deformative behaviour.

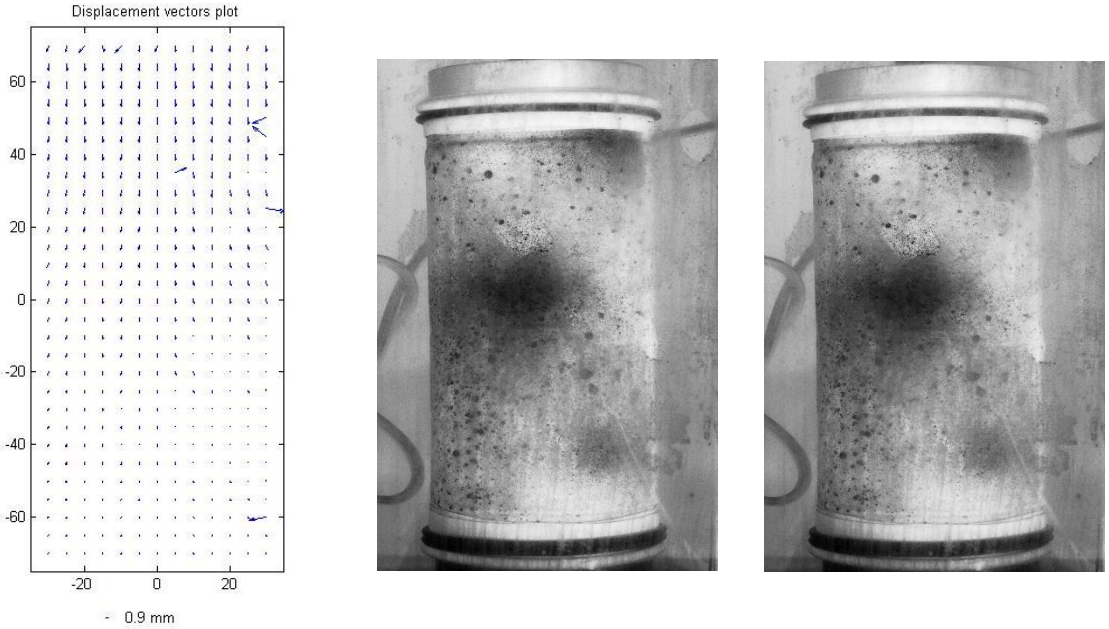

Figure 75 Displacement field at 4-5% axial strain interval (25 kPa).

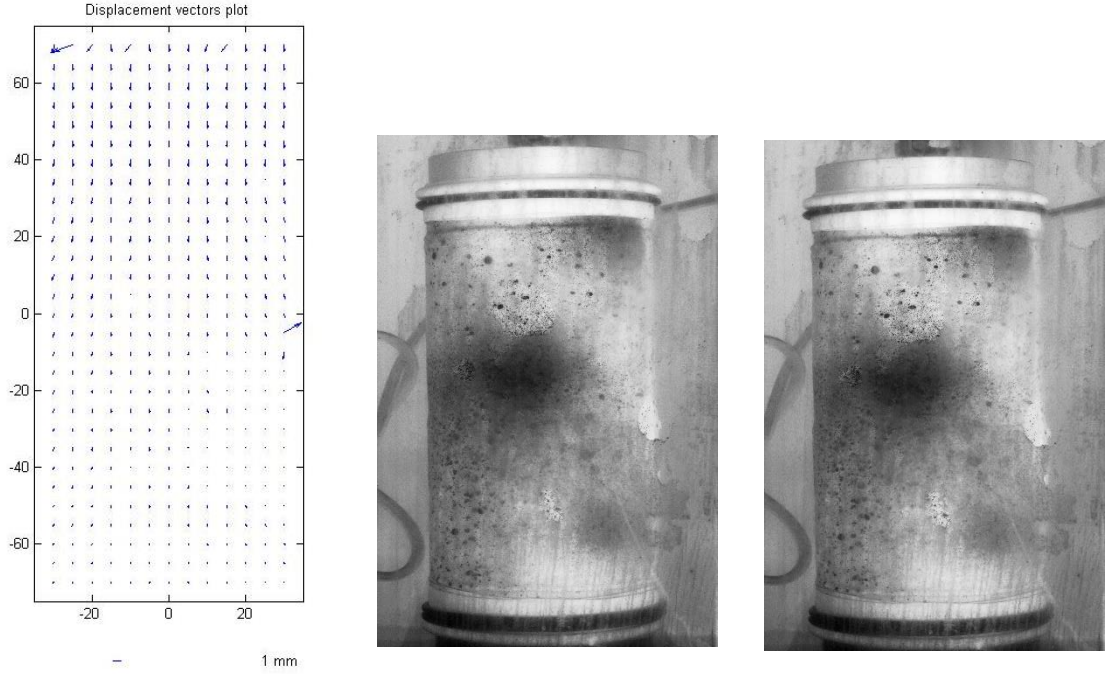

Figure 76 Displacement field at 7-8% axial strain interval (25 kPa).

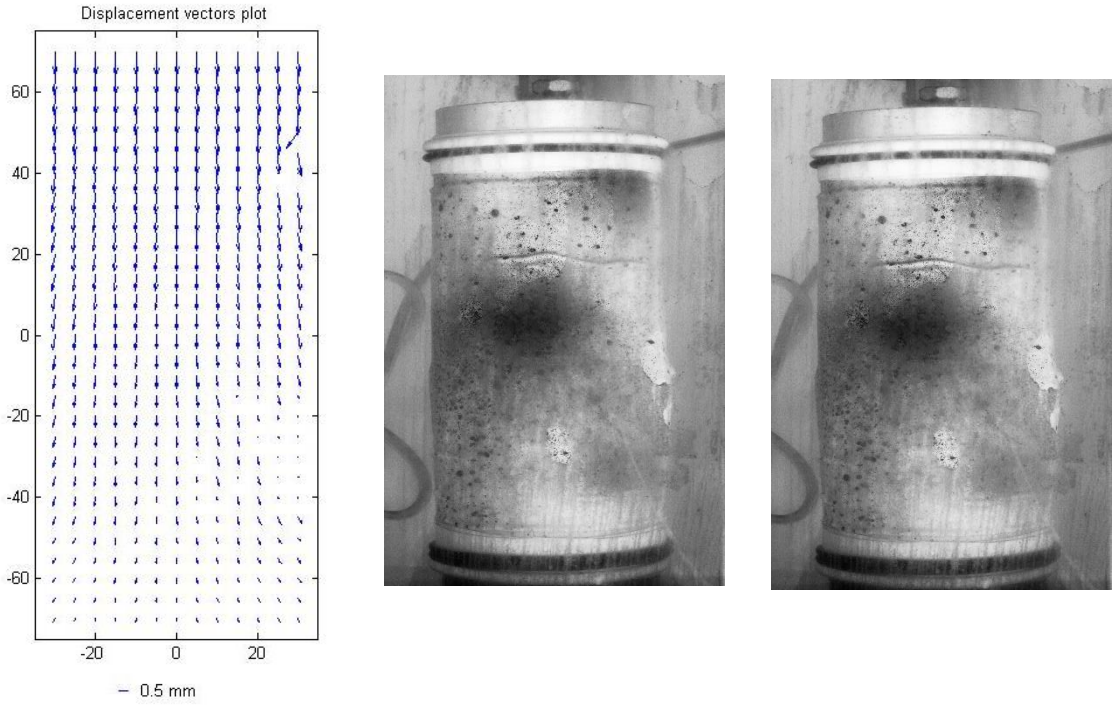

Figure 77 Displacement field at 11-12% axial strain interval (25 kPa).

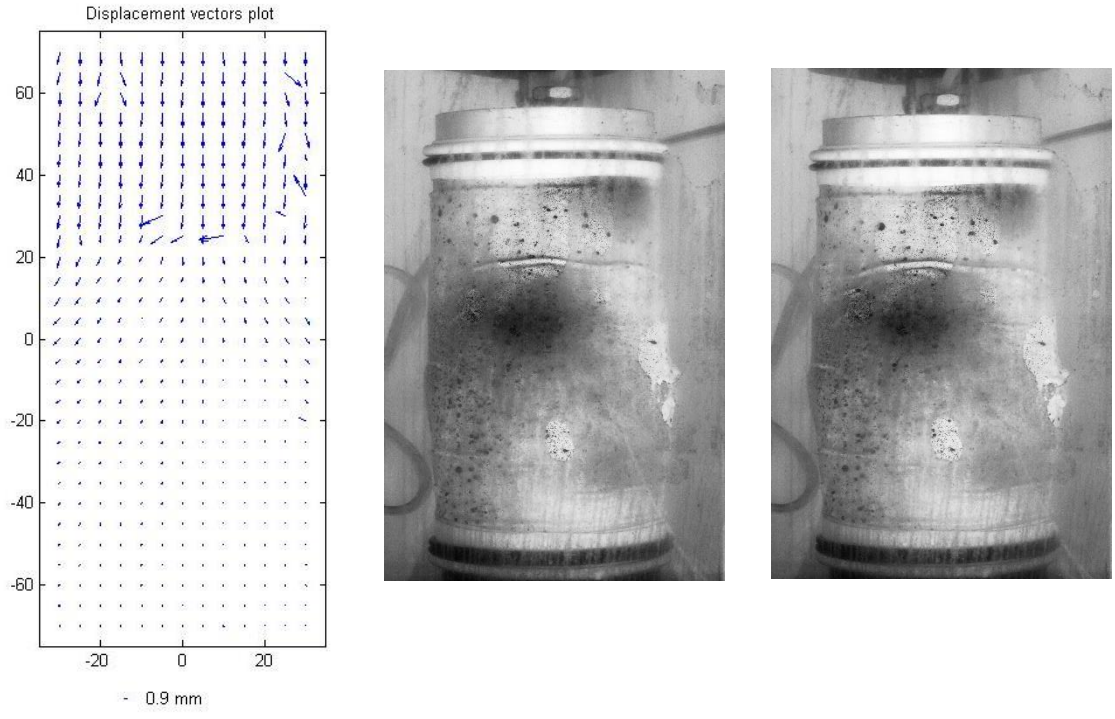

Figure 78 Displacement field at 14-15% axial strain interval (25 kPa).

Figure 79 Specimen at the end of the test at a cell pressure of 25 kPa

Figure 80 Dry and wet specimen after the triaxial test at a cell pressure of 25 kPa

6.2 Triaxial tests with confining pressure of 200 kPa

The results obtained from the test carried out using a cell pressure of 200 kPa shows a compressive behaviour and a logarithmic increase of the strength. The Figure 81 and Figure 82 show the deviatoric stress plotted against the axial strain and the stress ratio plotted against the axial strain respectively. The first graph shows the increase of deviatoric stress which increase until he reaches the peak of ~820 kPa. The stress ratio tends toward a critical value of 1.65. The steady state stress ratio is achieved after an axial strain of ~20%. Then, it is possible to say that the mobilization of peak stress ratio reduces with increasing confining pressure. This behaviour is quite different from what observed for the raw MSW where the material resistance usually increases at high axial strain. The peak stress ratio has a value of 1.76 and a residual value of 1.65. The initial stiffness is much lower than what obtained for the MBT waste specimens tested at the cell pressure of 25 kPa. The results obtained highlight how the cell pressure can affect the behaviour of an MBT waste.

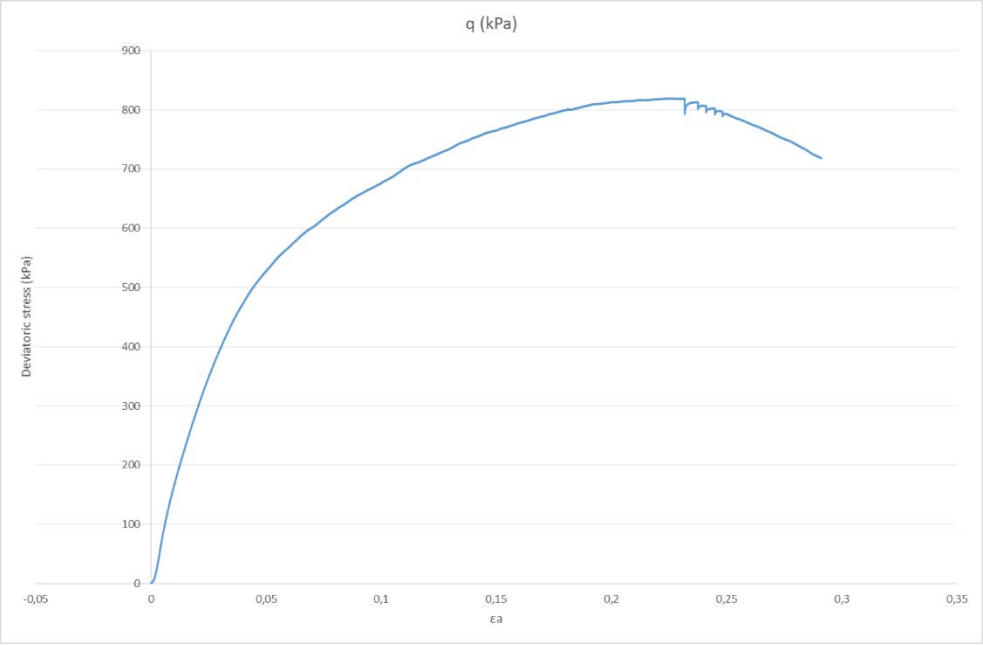

Figure 81 Deviatoric stress against axial strain (Test 4)

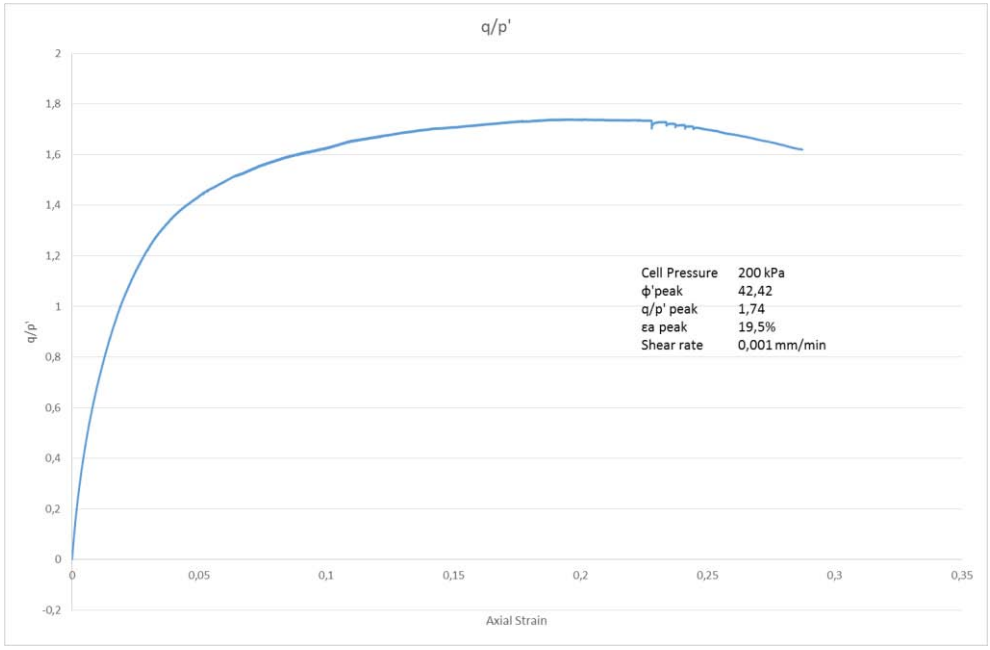

Figure 82 Stress ratio against axial strain (Test 4)

The sample shows a contraction of its volume (Figure 83), with a volumetric strain, which increases following a logarithmic curve. The final volumetric value is ~ 8% of the initial volume at the beginning of the shearing stage. After an axial strain of ~26%, the volumetric strain seems to achieve a steady state without any further increase. This fact is likely due to the reaching of the critical state where the sample deforms without changing its volume.

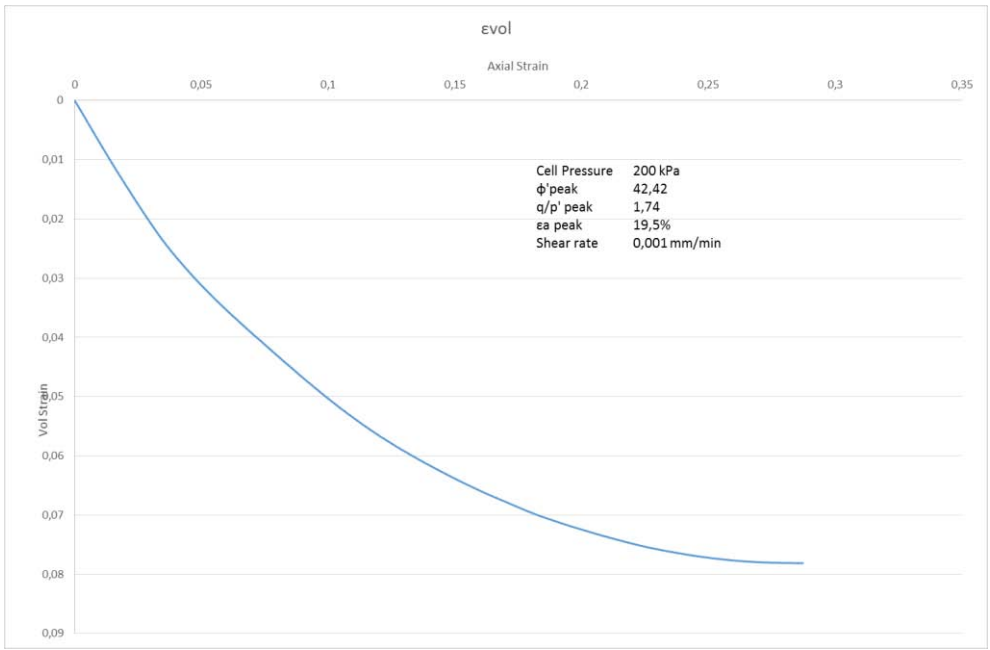

Figure 83 Volumetric strain against axial strain (Test 4)

The triaxial shear test data is also presented as graphs of mobilized angle of shearing ϕ'_{mob} as a function of the axial strain, as shown in Figure 84. The rate of increase of ϕ'_{mob} reduced with the axial strain until the residual value is reached. After that, the mobilized angle starts to reduce and, at the end, it seems to reach a sort of residual value. The angle of the residual strength has a value of 42°, a little bit lower than what obtained in the test at the cell pressure of 25 kPa ($\phi'_{mob} = 49°$). This consideration corroborates the assumption that no residual state is achieved in the tests at lower cell pressure.

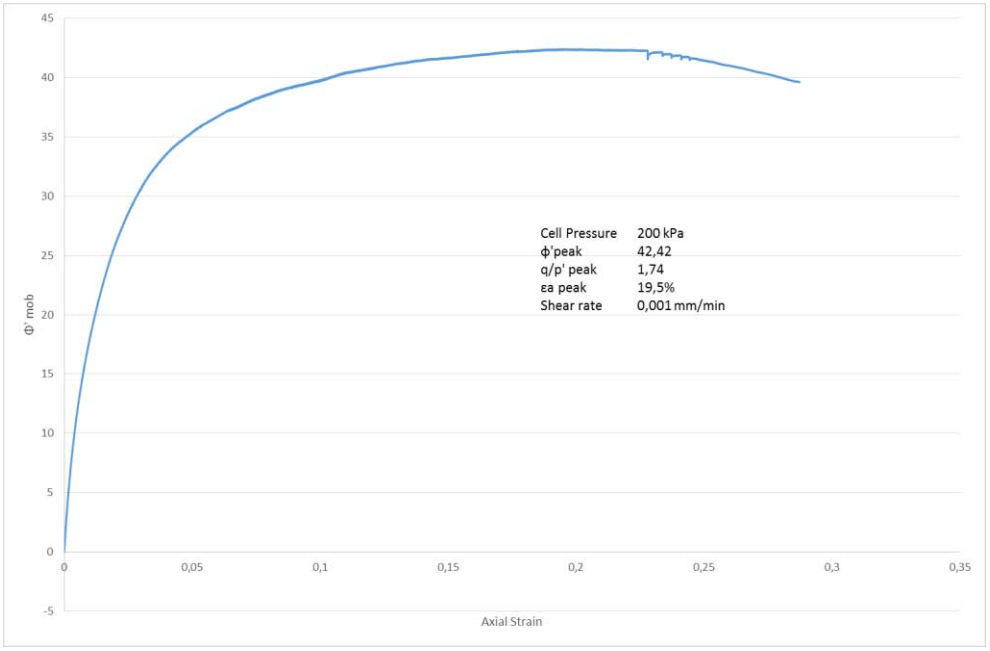

Figure 84 Mobilized angle of shearing against axial strain (Test 4)

The following Figure 85 shows the stress ratio q/p' associated with a given degree of dilation d. At the beginning the dilation decrease, describing the increasing rate of sample compression at the beginning of the test. After the stress ratio reached a value of ~0.7, the dilation ratio start to increase until reaching a zero value. The steady state stress ratio is achieved when the dilation rate d is nearly depleted. As we can see, the critical state when $q/p' = M$ is reached and the rate of dilation contribute reduced to zero. The specimen tested at a cell pressure of 200 kPa exhibits a more uniform deformation and it was not dilating significantly at the end of the test. For these reasons, the value of the stress ratio at the end of this test has been used as the possible critical stress ratio M. The value of dilation rate

(~0.95) is slightly lower than the value obtained for the 25 kPa test; it means that the specimen compressed with a higher rate in the first part of the shearing stage, in line with the lower stiffness value observed in the previous graphs. The rate of compression, connected with the dilation rate d, after reaching a negative peak, increases until becoming zero at the end of the test; at this point the specimen has reached the critical state condition when the volumetric strain does not change with increasing of axial strain.

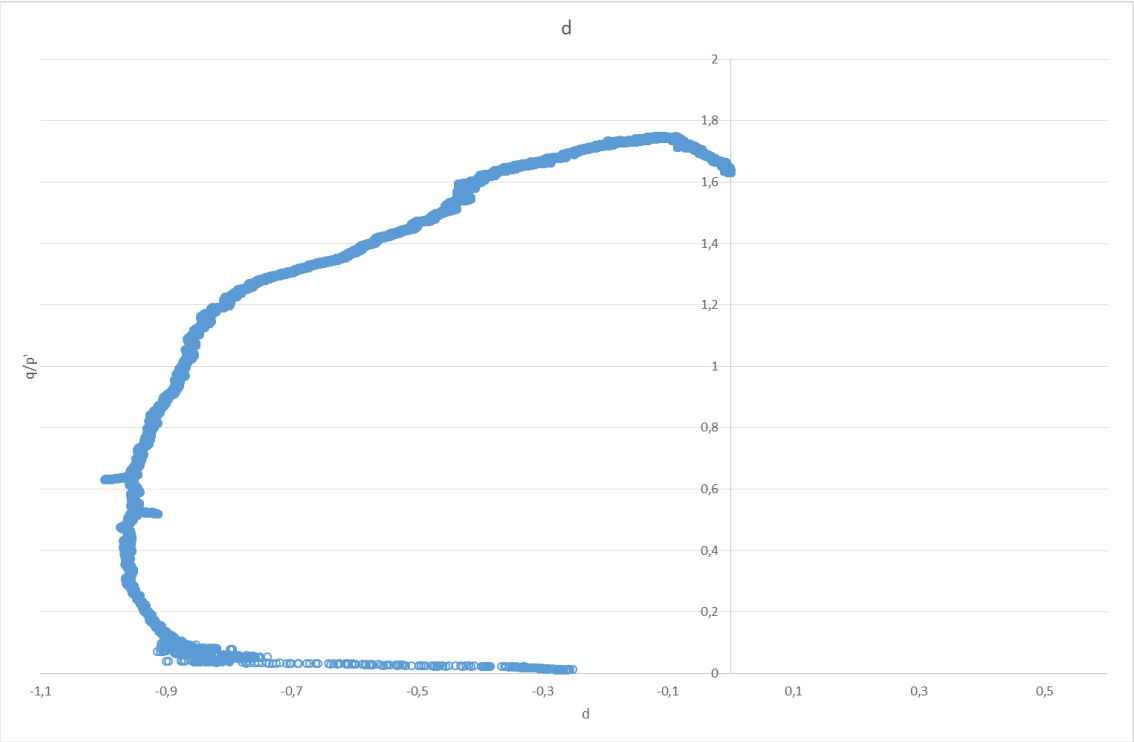

Figure 85 Stress ratio against dilation rate (Test 4)

The consideration about the different behaviour shown by the specimen once tested at a cell pressure of 200 kPa is confirmed by the results obtained in the third test. Like in the first test, the shearing rate used was too high and the triaxial rig did not respond properly to the personal computer's commands. The average rate used was 0.112% of the initial height of the specimen per hour. The pore pressure increased until a peak of ~45 kPa (Figure 86), reducing the effective stress within the sample from 200 kPa to 160 kPa for the most of the test. However, the data can be used to illustrate the tendency to compress shown by MBT waste once subjected to a high confining stress.

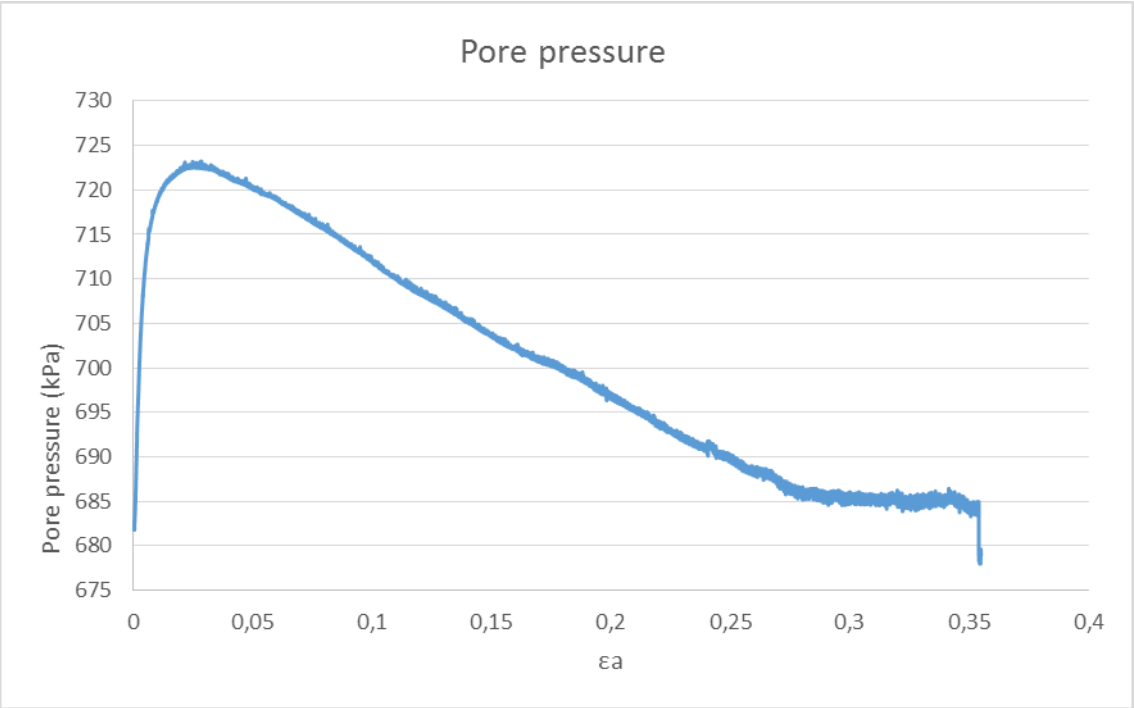

Figure 86 Pore pressure within the sample during the triaxial test 3.

The graphs obtained are shown in the following figures. The compressive volumetric strain rate is lightly smaller than what obtained in the fourth test; this fact can be explained by the impossibility for the water to flow out from the pores and the subsequent increase of its pressure. The residual stress ratio (1.76) is very similar of what obtained in the fourth test; this is because the steady state was reached at high values of axial strain, when the excess pore pressure produced at the beginning of the shear test was already dissipated. The mobilized angle of shear resistance reaches the peak value of 43°, equal to what obtained in the fourth test. The graph of the stress ratio plotted against the dilation rate d shows a similar curve, but the negative peak of d is smaller, probably because the increase of the pore pressure reduced both the volumetric strain and its increasing rate with axial strain. The rate of dilation becomes equal to zero at the end of the test, which means that the sample reached the critical state where the stress-dilatancy relationships given by Cam Clay reduced to:

$$\frac{q}{p'} = M$$

In fact, the critical stress ratio is the same of what obtained in the fourth test ($M = 1.65$). Therefore, it is possible to say that the maximum rate of dilation decreases with increasing confining pressure.

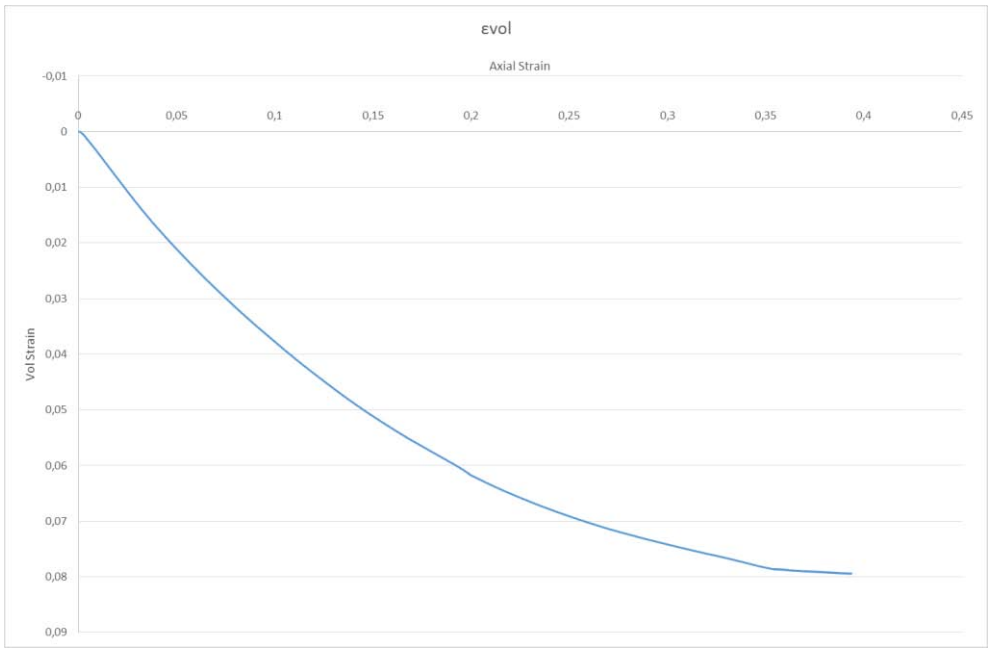

Figure 87 Volumetric strain against axial strain (Test 3)

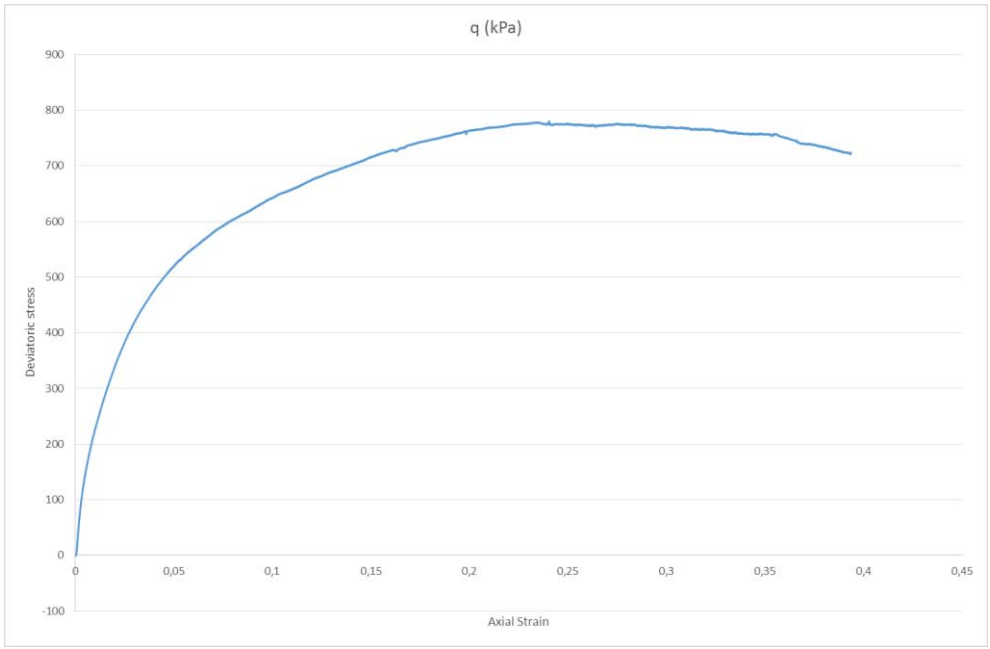

Figure 88 Deviatoric stress against axial strain (Test 3)

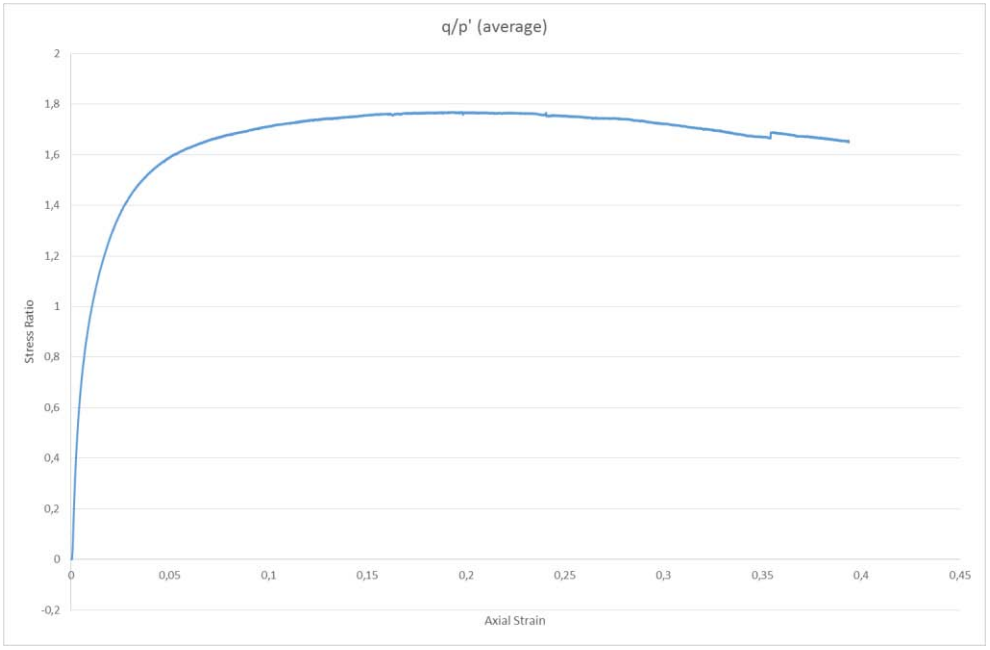

Figure 89 Stress ratio against axial strain (Test 3)

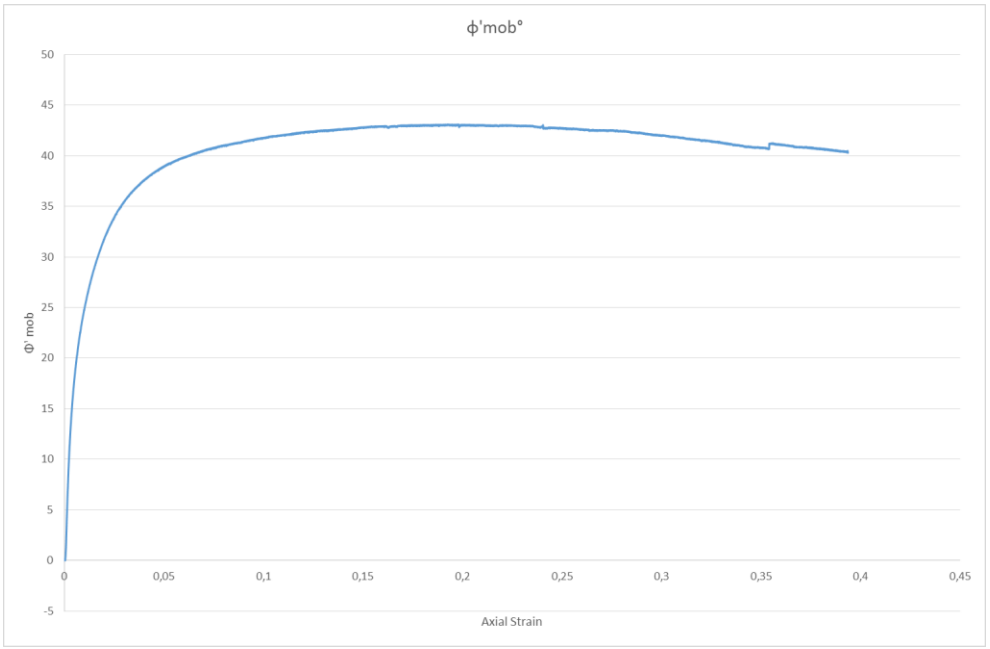

Figure 90 Mobilized angle of shearing against axial strain.

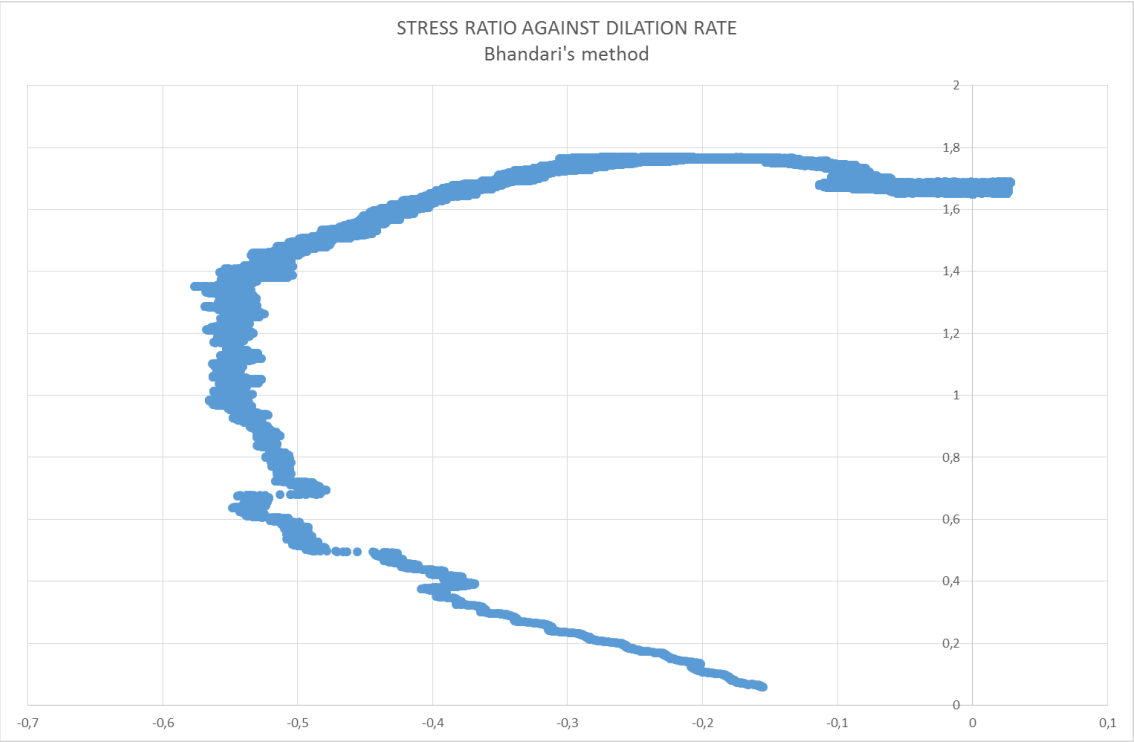

Figure 91 Stress ratio against the dilation rate (Test 3)

6.2.1 Image analysis and deformation pattern

Typical fields of displacement obtained by analysing image pairs taken at various axial strain intervals for the overconsolidated sample tested at a cell pressure of 200 kPa are shown in the following figures. The deformation fields obtained by DIC at an axial strain greater than 20% are beginning to become unreliable, owning to the folding of the membrane.

The local deformation distributions show that the main mode of deformation is one-dimensional compression because the displacement vectors are substantially vertical. However, at high axial strain values, the radial component becomes more relevant even in particular on the bottom of the specimen. The application of the deviator stress is mainly to compress the specimen one dimensionally. There is almost no lateral expansion at 4-5% axial strain values and the main effect of the shearing is a homogeneous compression and an increase of the density of the specimen. The subsequent axial strain interval shows a lightly reduction of the vertical displacement and an increment of the horizontal displacement. This trend can be observed also in the 10-11% interval of axial strain. The last graph shows

a clearly development of a symmetric bulging of the specimen. There is no evidence of clear and distinct localized failure.

At large strains (in the post peak regime) symmetric bulging and significant buckling of the specimen occur, as shown in the Figure 96. Unlike what happened at lower cell pressure, the specimen does not show any localisation of deformation.

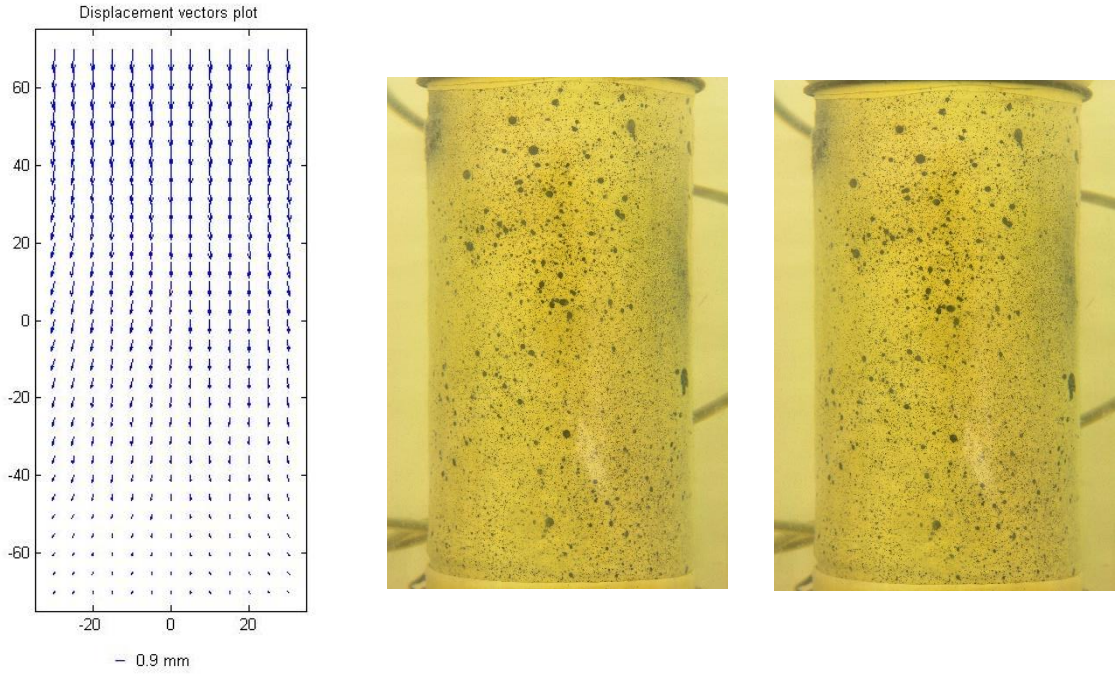

Figure 92 Displacement field at 4-5% axial strain interval (200 kPa).

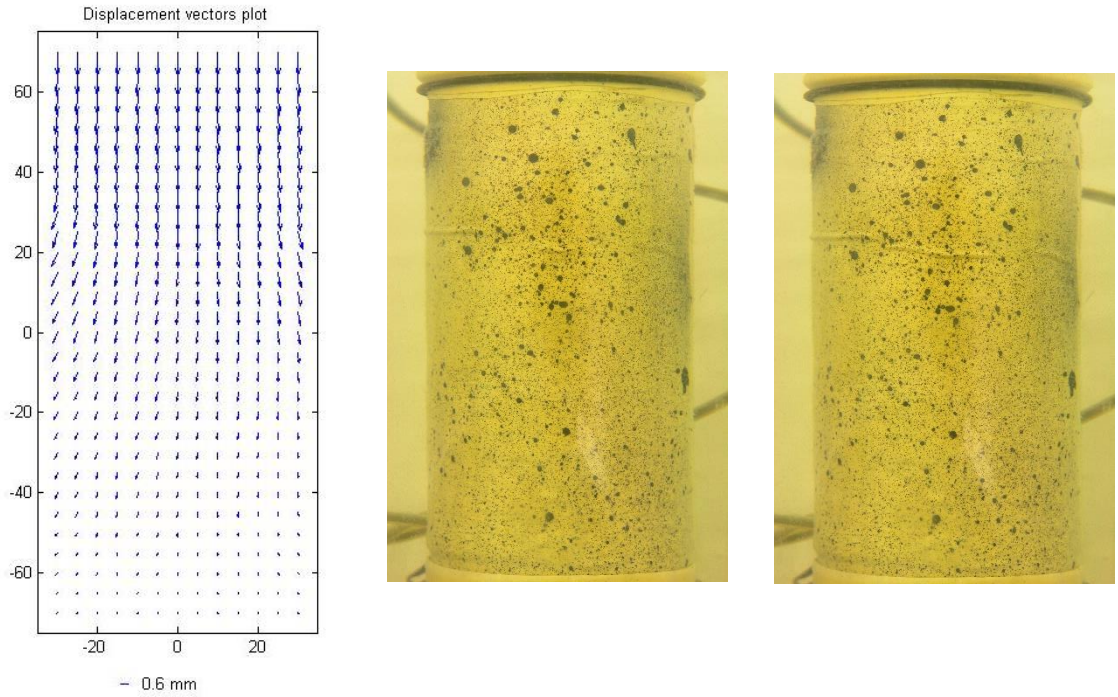

Figure 93 Displacement field at 7-8% axial strain interval (200 kPa).

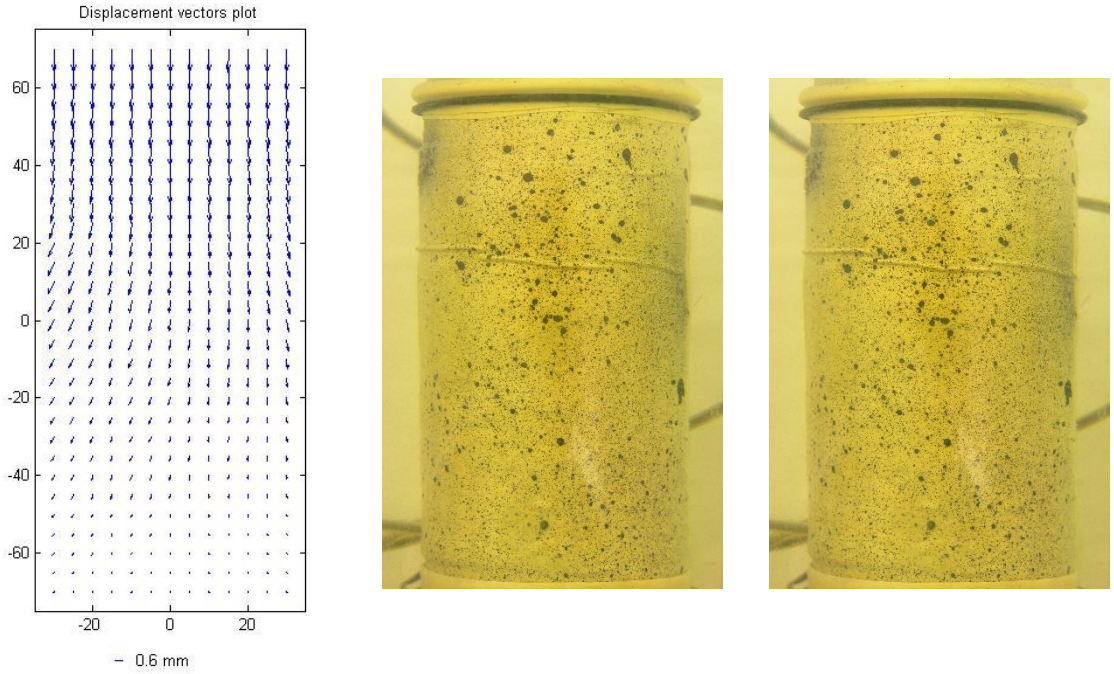

Figure 94 Displacement field at 10-11% axial strain interval (200 kPa).

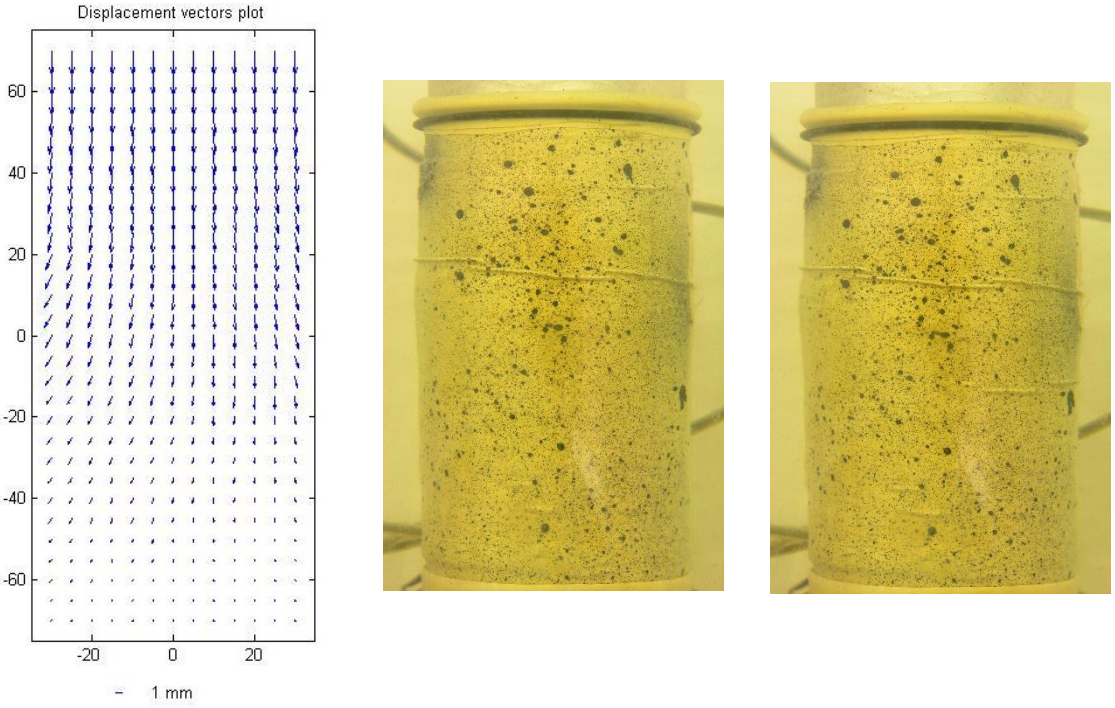

Figure 95 Displacement field at 13-15% axial strain interval (25 kPa).

Figure 96 Specimen at the end of the test at a cell pressure of 200 kPa

Figure 97 Dry specimen at the end of the test at a cell pressure of 200 kPa

6.3 State envelopes

The state paths followed during the tests in the (p', q) plane are shown in the Figure 98 and Figure 99. The graphs highlights the difference between the drained tests and the test where increase of pore pressure have been recorded. In fact, the drained condition of the triaxial test imposes that the effective stress path in (p', q) space ascends with gradient $\frac{dq}{dp'} = 3$. This fact could be easily demonstrated because the pore pressure of two subsequent instant has to be the same in a drained test. In the case of the first and third test the pore pressure was not constant during the test and that implies a curve stress path in (p', q), as could be seen in the Figure 98.

The critical state line (CSL) is defined considering a critical stress ratio M value of 1.65. The tests carried out at a radial pressure of 25 kPa do not touch this line and this fact confirms that no critical state has been reached. Another interesting aspect is the decrease of the slope of peak failure envelope.

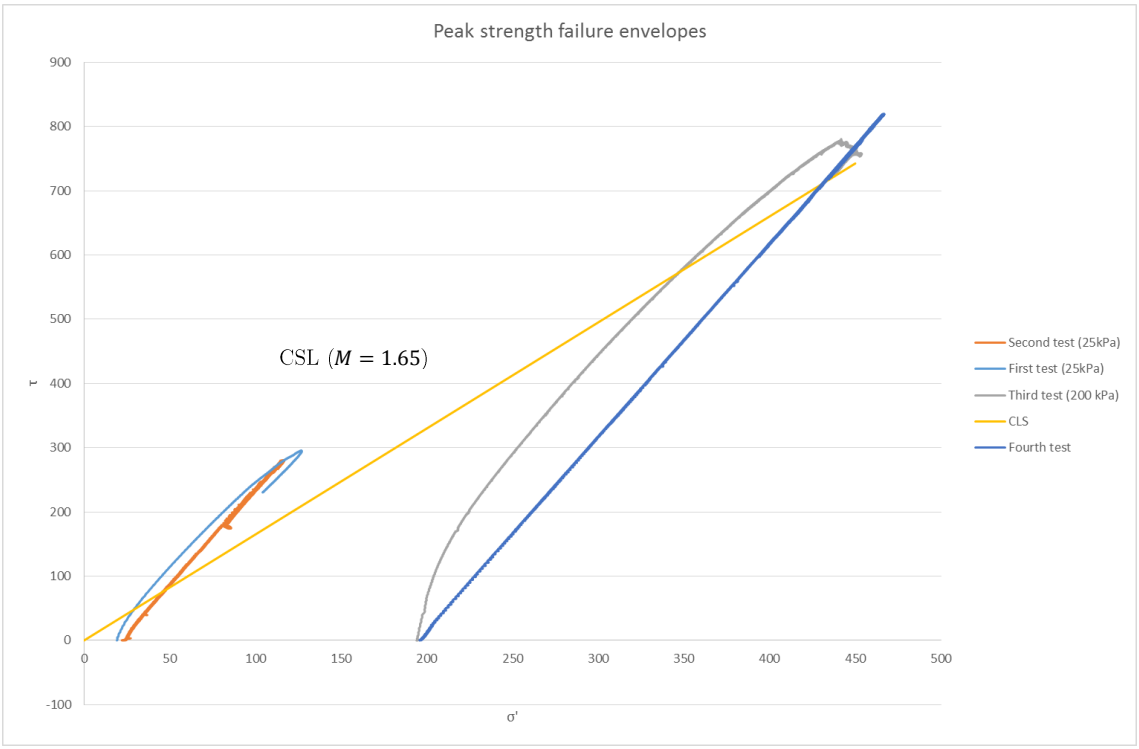

Figure 98 Critical state line in terms of q against p'

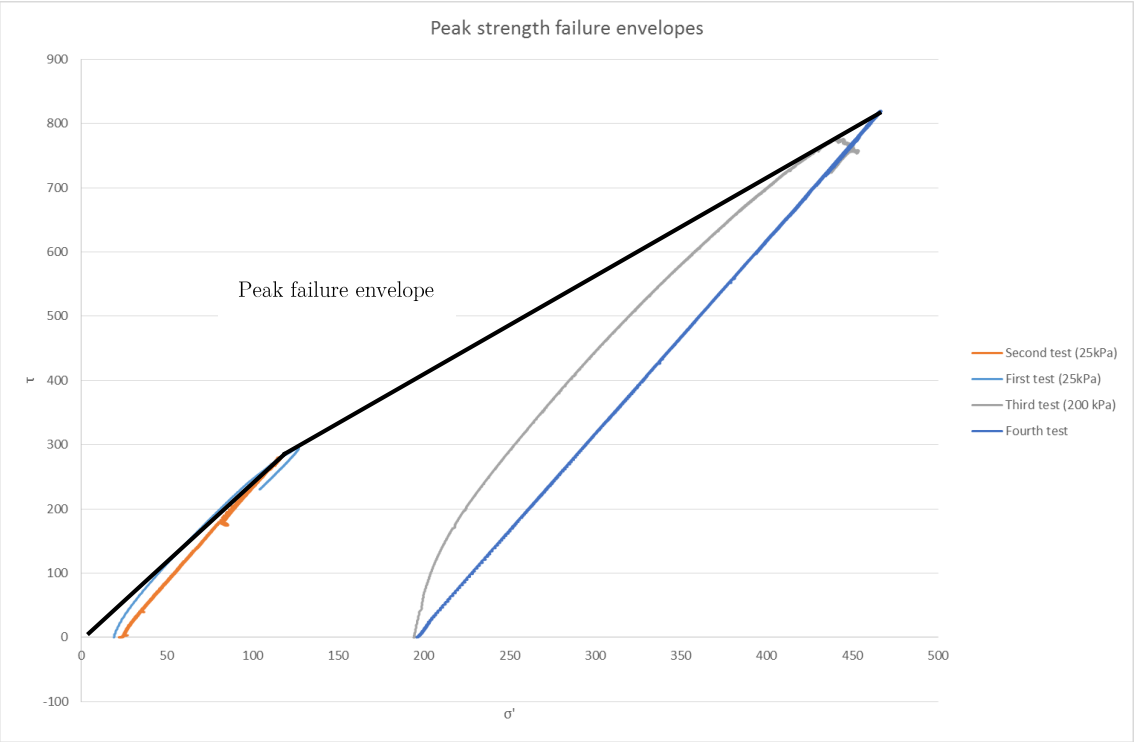

Figure 99 Peak strength failure envelope in terms of q against p'

The following Figure 100 of shearing is higher in the test carried out at lower confining pressure.

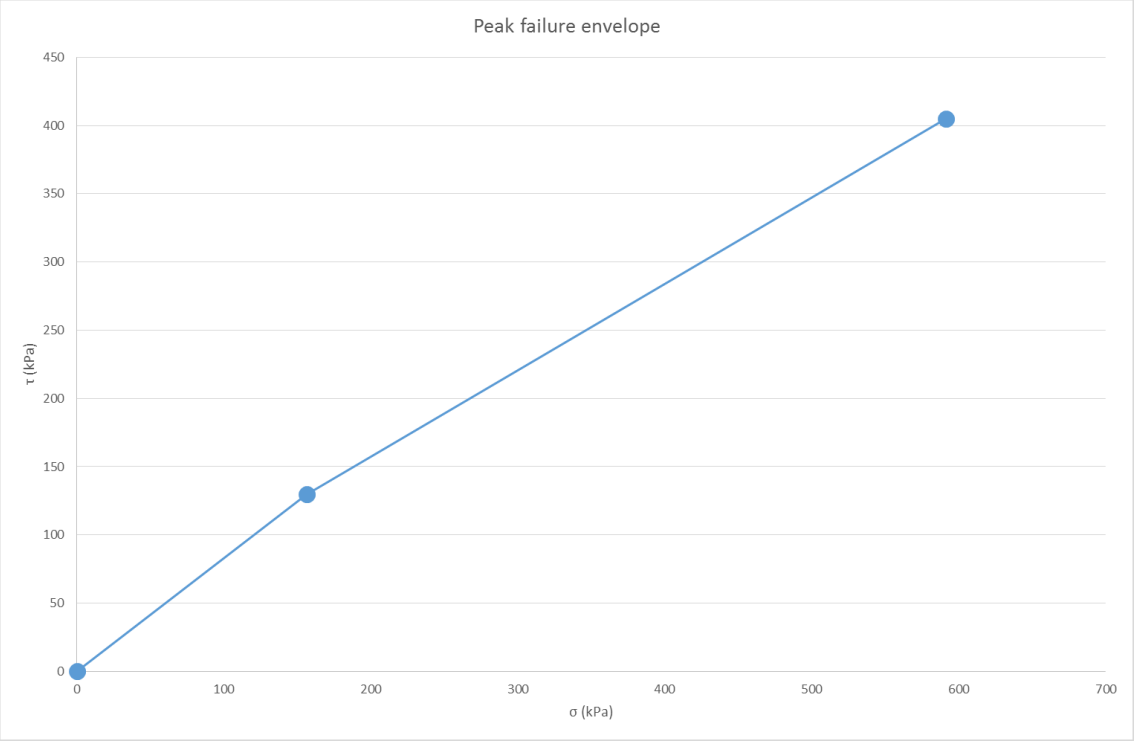

Figure 100 Peak failure envelope in terms of shear stress against normal effective stress

The values of peak stress ratio and angle of shearing resistance and axial strain at which they occurred are given in Table 26:

	Cell pressure (kPa)	**Peak stress ratio achieved**	**Axial strain at the peak stress ratio (%)**	**Angle of shear resistance at peak (°)**
Test 1	25	2.48	3.54	61.26
Test 2	25	2.29	5.48	56.09
Test 3	200	1.76	19.27	43.09
Test 4	200	1.77	19.50	43.28

Table 26 Locations of the peak stress ratios with respect to the axial strain

6.4 Discussion

The stress strain response of the sample tested at the cell pressure of 25 kPa is very similar of what obtained by Bhandari et al. (2013), using the same MBT waste material and cell pressure. The only different aspect is the partly saturation of the specimen. The peak stress ratios achieved are very similar, like the shape of the curves with a peak and a subsequent softening. The angle of shear resistance mobilised is one degree lower than what obtained by Bhandari. Even the volumetric strain is more or less the same, showing both a dilative behaviour. The volume dilatancy has been observed also by Bauer et al. (2009) after an initial volume compression.

Bhandari's triaxial results have shown that the stress ratio associated with a given degree of dilation d was much greater than that indicated by the stress-dilatancy relationship given by Cam Clay. He supposed that the generation of suction within the smaller voids might have been partly responsible for the high apparent angle of shearing resistance and stress ratios achieved by the specimen tested at low effective stress. This hypothesis can be easily rejected because the fully saturated specimen used in this research exhibited the same behaviour. The increase of strength has to be due mainly to the dilative behaviour and only a

very small amount of this increase can be considered as a consequence of the suction within the voids. This hypothesis is corroborated by the graph where the stress ratio is plotted against the rate of dilation. In fact, the peak strength corresponds to the instant at which the maximum dilation rate is achieved by the sample as in conventional soil mechanics. This trend can be seen also in Bhandari's results.

The stress ratio q/p' at peak for the test carried out at 200 kPa effective cell pressure are found to be significantly higher than those measured by Bhandari & Powrie (2013). The shape of q/p' curves, however, shows significant similarities with this study. The friction angle mobilised shows a significantly higher value at peak (+5°) comparing with those observed in the MBT waste samples tested by Bhandari but the shape of its curve is quite similar. In fact, the strain hardening behaviour can be used to describe both cases. Anyway, the residual angle of shearing is very similar to those obtained by Bauer et al. (2009) using a large triaxial compression cell. The behaviour of various MBT residues was investigated through a consolidated undrained (CU) and unconsolidated undrained (UU) triaxial compression tests at different cell pressures. The shear parameters obtained were c=14.8 kN/m^2 and φ=44.5° for the CU test and c=9.7 kN/m^2 and φ=41.8° for the UU test.

However, the strength parameters obtained in this study shows many similarities with Bhandari's results for the triaxial test carried out at 100 kPa effective cell pressure. Possible explanations for these similarities in behaviour are the effect of suctions in partly saturated sample, which are likely to lead to an effective stress higher than 100 kPa, and the problems with the strain rate control in this study, which means that the effective stress was lower than 200 kPa. Another possible cause is the differences in the MBT waste composition used to make the specimens, in particular the percentage of stiff material like plastic and glass. In fact, the material used in this study was obtained from what Bhandari & Powrie left from their previous research. Because of the small amount of MBT waste left, it is likely that the final samples used were more heterogeneous and rich of stiffer and bigger object than Bhandari's ones.

A comparison of the volumetric strains between those obtained for the partly saturated sample and for the fully saturated sample highlights an increase of the volume compression. In fact, from a value of 4.4% obtained by Bhandari, the

volumetric strain becomes the ~8% of the initial specimen volume in this study. This fact can be due to the longer test length, which means that the MBT waste was in contact with water for a long period and it probably replaced the acid solution within the specimen. In fact, the tests carried out on fully saturated specimen need at least 600 hours just for the shearing stage; meanwhile Bhandari's test was only 8 hours length. The creep and the inevitable biodegradation of the organic matter certainly have a role in the volumetric compression, leading to a volumetric strain higher than what expected.

The higher compressibility of the fully saturated specimen can be also seen in the graph where the stress ratio is plotted against the rate of dilation. In fact, the rate of dilation decreases until a value of ~0.95 before increasing. This fact suggests that the specimen reduces its volume with a higher rate comparing with the results of Bhandari & Powrie (2013). However, the shape of this curve shows significant similarities: both stress ratio peaks have been achieved when the rate of dilation was zero, in other words when the samples reached the critical state.

The possible critical stress ratio obtained from the tests carried out at a cell pressure of 200 kPa has a value of 1.65, higher than what measured by Bhandari & Powrie (2013). The possible reason for this difference in value is the different composition of MBT waste used. As said before, the residual material is usually more heterogeneous and it has a high percentage of particles usually removed during the sample preparation phase.

Figure 101 Inside of an MBT waste specimen.

Specimen state	Fraction	Cell Pressure (kPa)	Peak stress ratio achieved	Axial strain at the peak stress ratio (%)	Angle of shear resistance at peak (°)
Overconsolidated	Full	25	2.34	7.4	57.4
		50	2.11	11.5	51.3
		100	1.85	9.2	45
		200	1.54	16.2	37.8
	Fine	25	2.37	7.3	58.2
		50	2.10	10.6	51.3
		100	1.78	10.8	43.4
		200	1.32	13	32.9

Table 27 Locations of peak stress ratios with respect to axial strain (Bhandari and Powrie, 2013)

The barrelling failure form exhibited by the MBT waste specimen was already seen in Bhandari's previous work and in Bauer et al. (2009). Bauer et al. (2009) mentioned that some few specimen has exhibit a sort of failure plane like what was seen in the specimens tested at the lower radial pressure.

Chapter 7

Conclusions

This research has investigated the strength and deformation characteristics of a mechanically biologically treated waste in triaxial compression at effective stress of 25 kPa and 200 kPa. New insights were gained regarding the behaviour of MBT waste and the influence of this treatment on its mechanical characteristics, comparing the results obtained at two different confining pressure. The role of dilation with respect to the strength mobilized during the test was studied. A digital image correlation was used to analyse the images and characterise the associated deformation. The samples were consolidated using a modified oedometric apparatus, analysing the primary and secondary settlement.

The following conclusions have been drawn from this study:

1. Mechanical biological treatment deeply change the structure and the mechanical properties of municipal solid waste, decreasing the particle size and reducing the biodegradability of the organic fraction.

2. During the MBT process, where reinforcement content and particle size are reduced substantially as a result of screening and shredding, due to the changes in the material it was believed that MBT could have weak shear strength characteristics. However, the results obtained proves that treated waste is a strong material, with an angle of shearing resistance of 43° at the critical state.

3. The majority of the settlement recorded during the oedometer test are immediate compression in response to the loading and its amount decreases with increasing of normal stress. The primary settlement (consolidation) has been shown to be completed in 1 hour under a vertical stress of 1000 kPa and just 15 minutes under a vertical stress of 25 kPa, depending on the specimen density and hydraulic conductivity.

4. The secondary settlement of an MBT waste and, in particular, the impact due to the mechanical creep phenomenon seem to be influenced by the normal stress applied. In fact, the coefficient of secondary settlement $C_{\alpha\varepsilon}$ increases significantly with higher normal stress.

5. The MBT waste specimens tested at a cell pressure of 25 kPa shows a dilative behaviour and the presence of a strength peak followed by a softening. Meanwhile, the samples tested at a cell pressure of 200 kPa exhibit a compressive and strain hardening behaviour. The mobilization of the peak stress ratios is associated with dilation and its values reduced with increasing confining pressure. Both of these aspects of behaviour are qualitatively consistent with the concepts of critical state soil mechanics for specimens of the same initial density.

6. The high apparent angles of shearing resistance and stress ratios achieved by the specimen tested at 25 kPa effective cell pressure are likely due to the dilative behaviour exhibited and not to the suctions within the smaller voids as supposed by Bhandari & Powrie (2013) testing partly saturated sample.

7. The form of stress-strain curves obtained in this study indicates that it is quite possible to define a stress dependent strength envelope, rather than adopting a strain based failure criterion as has been proposed for unprocessed MSW. This finding is important because in most previous studies on MSW and MBT, extremely large strains were found necessary to mobilize the strength of the material and a steady (critical state) or even a peak strength was seldom observed. The MBT waste exhibited a peak angle of shearing resistance varying from 56° at a confining stress of 25 kPa to 43° at 200 kPa and an estimated critical state angle of shearing resistance of 40°. However, the specimens tested at 25 kPa confining pressure were still dilating after an axial strain of ~30% and the critical state was not achieved at the end of the test.

8. The image analysis technique used to determine whole specimen displacement fields has shown that during the initial stage of shear test,

the mode of deformation is one-dimensional compression, in other words an axial shortening with radial deformation.

9. Localization of deformation into distinct shear bands prior to barrelling or bulging has not observed. However, a probably explanation is that the triaxial stress conditions were too restrictive to allow it.

10. Mechanical biological treatment (MBT) seems to produce an output whose mechanical characteristics are much more similar to the common soil rather than raw municipal solid waste (MSW).

References

Athanasopoulos, G. A., Grizi, A., Zekkos, D., Founta, P., & Zisimatou, E. (2008). Municipal solid waste as a Reinforced soil: investigation using synthetic waste. In *Geocongress 2008* (pp. 168–175).

Bauer, J., Munnich, K., & Fricke, K. (2005). Influence of hydraulic properties on the stability of landfills. In *Proceedings Sardinia 2005, Tenth International Waste Management and Landfill symposium* (p. 1068).

Bayard, R., Araujo Morais De, J., Rouez, U., Fifi, M., Achour, F., & Ducom, G. (2008). Effect of biological pretreatment of coarse MSW on landfill behaviour: laboratory study. *Water Science and Technology*, *58*(7), 1361–1369.

Bhandari, A. R., & Powrie, W. (2013). Behavior of an MBT waste in monotonic triaxial shear tests. *Waste Management*, *33*(4), 881–891.

Bhandari, A. R., Powrie, W., & Harkness, R. M. (2012). A digital Image-Baseed Deformation Measurement System for Triaxial Tests. *Geotechnical Testing Journal*, *35*(2), 209–226.

Borgatto, A. V. A., R.L., I., & Bauer, J. (2009). Influence of soft plastics on MSW geomechanical behaviour. In *Third International Workshop "Hydro-Physico-Mechanics of Landfills."*

Caicedo, D. M., Sandoval, J. J., Watson, G. V., Siddiqui, A. A., Richards, D. J., & Powrie, W. (2010). Exploring the use of modified dye-adsorption method for a better understanding of landfilled waste structure in the context of post-closure management strategies in landfills. In *Proceedings global waste management Symposium 2010*.

Consoli, N. C., Montardo, J. P., Prietto, P. D. ., & Pasa, G. S. (2002). Engineering behaviour of a sand reinforced with plastic waste. *Journal of Geotechnical and Geoenvironmental Engineering*, *128*(6), 462–472.

Cossu, R., Diaz, L. F., & Stegmann, R. (2005). Investigation on relationship between vertical and horizontal permeabilities of mbt wastes. In *Proceedings Sardinia 2005, Tenth International Waste Management and Landfill symposium* (p. 1068).

Council, T. H. E., The, O. F., & Union, E. (1999). Official Journal of the European Communities, (10).

Dixon, N., & Langer, U. (2005). Engineering properties of municipal solid waste. *Geotextiles and Geomembranes*, *23*(3), 205–233.

Dixon, N., & Langer, U. (2006a). Development of a MSW classification system for the evaluation of mechanical properties.

Dixon, N., & Langer, U. (2006b). Development of a MSW classification system for the evaluation of mechanical properties. *Waste Management*, *26*(3), 220–232.

Edgers, L., Noble, J. J., & Williams, E. (1992). A biological model for long term settlement in landfills. In *Proceedings Mediterranean Conference on Environmental Geotechnology*.

El Fadel, M., & Al Rashed, H. (1998). Settlement in municipal soild waste landfills. *Journal of Solid Waste Technology and Management*.

Elagroudy, S. A., Ghobrial, F. H., & Abdel Razik, M. H. (2007). Effect of solid waste composition on the biodegradation of municipal solid waste in bioreactor landfills. In *Proceedings 60th Canadian Geotechnical Conference*.

Ferndando, V. (2011). *Shear strength characteristics of mechanically biologically treated (MBT) waste*.

Fucale, S. P., Juca, J. F. T., Munnich, K., & Bauer, J. (2007). Study of the mehcanical behaviour of MBT waste.

Gachet, C., Bayard, R., Singh, M., & Gourdon, R. (2003). Effects of water content and leachate recirculation on anaerobic degradation of landfilled waste. In *Proceedings Sardinia 2003, Ninth International Waste Management and Landfill symposium*.

Grisolia, M., Napoleoni, Q., & Tancredi, G. (1995). Contribution to a technical classification of MSW: the use of triaxial tests for the mechanical characterization

of MSW. In *Proceedings Sardinia 1995, Fifth International Waste Management and Landfill symposium* (pp. 703–710).

Hall, D., Drury, D., Gronow, J., Rosevar, A., Pollard, S., & Smith, R. (2006). Estimating pollutant removal requirements for landfills in the UK: I. benchmark study and characteristics of waste treatment technologies. *Environmental Technology*, *27*(12).

Heikkilä, J., & Silvén, O. (n.d.). A Four-step Camera Calibration Procedure with Implicit Image Correction.

Hudson, A. P., White, J. K., Beaven, R. P., & Powrie, W. (2004a). Modelling the compression behaviour of landfilled domestic waste. *Waste Management*, *24*, 259–269.

Hudson, A. P., White, J. K., Beaven, R. P., & Powrie, W. (2004b). Modelling the compression behaviour of landfilled domestic waste. *Waste Management*, *24*(3), 259–269.

Ivanova, L. K., Richards, D. J., & Smallman, D. J. (2008). The long-term settlement of landfill waste. *Waste and Resource Management*, *161*(WR3), 121–133.

Jessberger, H. L., Syllwasschy, O., & Kockel, R. (1995). Investigation of waste body behaviour and waste structure interaction. In *Proceedings Sardinia 1995, Fifth International Waste Management and Landfill symposium*.

Jewell, R. A., & Wroth, C. P. (1987). Direct shear test on reinforced sand. *Geotechnique*, *37*(1), 53–68.

Kavazanjian Jr, E., Matasovic, N., Bonaparte, R., & Shmertmann, G. R. (1995). Evaluation of MSW properties for seismic analysis. *Geoenvironment 2000*.

Kolsch, F. (1995a). Material values for some mechanical properties of domestic waste. In *Proceedings Sardinia 1995, Fifth International Waste Management and Landfill symposium*.

Kolsch, F. (1995b). Material values for some mechanical properties of domestic waste. In *Proceedings Sardinia 1995, Fifth International Waste Management and Landfill symposium* (pp. 711–729).

Kolsch, F. (2009). Shear strength of waste. In *Third International Workshop "Hydro-Physico-Mechanics of Landfills."*

Kuehle-Weidemeier, H., & Doedens, H. (2003). Landfilling and properties of MBP waste. In *Proceedings Sardinia 2003, Ninth International Waste Management and Landfill symposium.*

Kuehle-Weidemeier, M. (2004). Landfill properties of mechanically and biologicallt treated municipal solid waste. *The Waste Conference Limiterd.*

Landva, A., & Clark, J. (1990). Geotechnics of waste fills, theory and practice (pp. 86–103).

Langer, U., & Dixon, N. (2005). Understanding the Mechanical Behaviour of Municipal Solid Waste : The Role of a Classification System, (March), 21–22.

Machado, S. L., Carvalho, M. F., & Vilar, O. M. (2002). Constitutive model for MSW. *Journal of Geotechnical and Geoenvironmental Engineering*, *128*(11), 940–951.

McDougall, J. (2007). A hydro-bio-mechanical model for settlement and other behaviour in landfilled waste. *Computers and Geotechnics*, *34*(229-246).

Mechanical Biological Treatment of Municipal Solid Waste. (n.d.).

Michalowski, R. ., & Cermak, J. (2003). Triaxial compression of sand reinforced with fibres. *Journal of Geotechnical and Geoenvironmental Engineering*, *129*(2), 125–136.

Park, H. I., & Lee, S. R. (1997). Long-term settlement behaviour of landfills with refuse decomposition. *Journal of Solid Waste Technology and Management.*

Powrie, W. (2004). *Soil mechanics: concepts and application (2nd edition).*

Powrie, W., & Beaven, R. P. (1999). Hydraulic proprties of household waste and implication for landfills. In *Proceedings of the Instituion of Civil Engineers.*

Powrie, W., Beaven, R. P., & Harkness, R. M. (1999). Applicability of soil mechanics principles to household waste. In *Sardinia 1999, Seventh International Waste Management and Landfill Symposium.*

Powrie, W., Beaven, R. P., & Harkness, R. M. . (1995). Applicability of soil mechanics principles to household waste. In *Proceedings Sardinia 1995, Fifth International Waste Management and Landfill symposium* (pp. 429–436).

Powrie, W., Richards, D., Velkushanova, K., & Xu, X. (2009). Mechanisms of settlement in biodegradable waste. In *Third International Workshop "Hydro-Physico-Mechanics of Landfills."*

Rajan, G., Vasan, R. M., & Charan, H. D. (1996). Probabilistic analysis of randomly distributed fiber reinforced soil. *Journal of Geotechnical Engineering*, *122*(6), 419–426.

Readdy, K. R., Hettrarachchi, H., Parakalla, N., Gangatjhulasi, J., Bogner, G., & Lagier, T. (2009). Hydraulic conductivity on MSW in landfills. *Journal of Environmental Engineering*.

Shariatmadari, N., Machado, S. L., Noorzad, A., & Karimpour-Fard, M. (2009). Municipal solid waste effective stress analysis. *Waste Management (New York, N.Y.)*, *29*(12), 2918–30. doi:10.1016/j.wasman.2009.07.009

Shewbridge, S. E., & Sitar, N. (1989). Deformation characteristics of reinforced sand. *Journal of Geotechnical Engineering*, *115*(8), 1134–1147.

Shewbridge, S. E., & Sitar, N. (1996). Formation of shear zones in reinforced sand. *Journal of Geotechnical Engineering*, *122*(11), 873–885.

Siddiqui, A. (2011). *Biodegradation and settlement behaviour of mechanically and biologically treated (MBT) waste*.

Siddiqui, A. A., Richards, D. J., & Powrie, W. (2009). A preliminary analysis of mechanically biologically treated waste: Biodegradation and settlement beahviour. In *Proceedings Sardinia 2009, Twelfth International Waste Management and Landfill symposium*.

Siegel, R., Robertson, R., & Anderson, D. (1990). Geotechnics of waste fills: theory and practice, American Society for Testing and Materials Special Publication. In *Geotechnics of waste fills:theory and practice* (pp. 259–284).

Skempton, A. W. (1961). *Effective Stress in Soils* (p. 4).

Sowers, G. F. (1973). Settlement of waste disposal fills. In *Proceedingd eight international conferance on soldi mechanics and foundation engineering* (pp. 207–221).

Thomas, T., Aboura, A. A., Gourc, J. P., Gotteland, P., Billard, H., Delineau, T., … Vuillemin, M. (1999). An in situ waste mechanical experimentation on a french landfill. In *Proceedings Sardinia 1999, Seventh International Waste Management and Landfill symposium.*

Velkushanova, K., Caicedo, D., Richards, D., & Powrie, W. (2009). A detailed characterisation of an mbt waste. In *Proceedings Sardinia 2009, Twelfth International Waste Management and Landfill symposium* (p. 1190).

Wall, D. K., & Zeiss, C. (1995). Municipal landfill biodegradation and settlement. *Journal of Environmental Engineering.*

Xie, M., Aldenkortt, D., Wagner, J. F., & Rettenberg, G. (2006). Effect of Plastic Fragments on Hydraulic Characteristics of Pre-treated Municipal Solid Waste. *Canadian Geotechnical Journal*, *43*.

Xie, M., Wagner, J. F., & Rettenberg, G. (2001). Permeability characteristics of mechanical-biologically pre-treated municipal solid waste. In *Eight International Waste Management and Landfill Symposium.*

Zardava, K., Powrie, W., & White, J. (2011). Laboratory experiments for measuring the moisture retention characteristics of MBT waste. In *Fourth International Workshop "Hydro-Phsyco-Mechanics of Landfills"* (pp. 27–28).

Zekkos, D. (2013). Experimental evidence of anisotropy in municipal solid waste. In *Coupled Phenomena in Environmental Geotechnics* (pp. 69–77).

Zekkos, D., Athanasopoulos, G. A., Bray, J. D., Theodoratos, A., & Grizi, A. (2010). Large-Scale direct shear testing of municipal solid waste. *Waste Management Journal*, *30*, 1544–1555.

Zekkos, D., Bray, J. D., Athanasopoulos, G. A., Micheal, F., Kavazanjian Jr, E., Founta, P., & Grizi, A. (2007). Compositional and loading rate effects on the shear strength of municipal solid waste. In *4th International Conference on Earthquake Geotechnical Engineering.*